STUDIES ON THE SMALL G PROTEIN RAC1: INTERACTION WITH IQGAP AND THE ROLE OF Mg^{2+} DURING NUCLEOTIDE EXCHANGE

Thesis submitted in accordance with the requirements of the
UNIVERSITY OF LONDON
for the degree of
DOCTOR OF PHILOSOPHY
by

Adam Shutes
Department of Physical Biochemistry
National Institute for Medical Research
Mill Hill
London NW7 1AA
(Registered at University College, London)

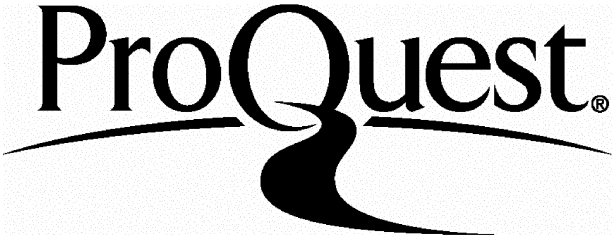

Last night I played a blank tape at full blast.

The mime artist next door went nuts.

-- *Woody Allen*

Index of Contents **Page**

Figure Number and Title **Page Number**

Chapter 3: The Self-Stimulatory Activity of Rac

Chapter 4: The Role of Mg^{2+} in Nucleotide Exchange

Abbreviations

Abbreviation	*Full Name*
E.coli	*Escherichia coli*
EDTA	Ethylenediaminetetraacetic Acid
FRET	Fluorescence Resonance Energy Transfer
GAP	GTPase Activating Protein
GDI	Guanine Nucleotide Dissociation Inhibitor
GDP	Guanosine 5'-Diphosphate
GEF	Guanine Nucleotide Exchange Factor
GMPPCP	5' Guanosine-5'-(β,γ-Methylene) Triphosphate
GMPPNP	5' Guanylylimidodiphosphate
GRD	GAP-related Domain
GTP	Guanosine 5'-Triphosphate
GST	Glutathione-S-Transferase
HPLC	High Pressure Liquid Chromatography
IPTG	Isopropyl β-D-Thiogalactopyranoside
Mant	N-methylanthraniloyl
MAPK	Mitogen Activated Protein Kinase
MBC	8-bromo-7-monoethylaminocoumarin
MDCC	N-[2-(1-maleimidyl)ethyl]-7-(diethylamino)coumarin-3-carboxamide
PBP	Phosphate Binding Protein
PCR	Polymerase Chain Reaction
pGIT2	The novel IQGAP pGEX Construct
P_i	Inorganic Phosphate
PMSF	Phenylmethylsulphonyl fluoride
S.cerevisiae	*Saccharomyces cerevisiae*
SDS	Sodium Dodecasulphate

Abstract of Thesis

This Thesis is centred around the small G-protein Rac1, and investigates: Rac's interaction with the effector protein IQGAP; the role of Mg^{2+} during Rac's nucleotide exchange; and Rac1's proposed self-stimulatory activity.

Rac1's C-terminal tail has been suggested to posses GTPase self-stimulatory activity. An investigation of this property is described. The effects on Rac's intrinsic GTPase rate were observed using full-length and C-terminal truncated forms of the protein, as well as Rac•GMPPNP forms and peptides of Rac's C-terminal tail. In contrast to the previously published data, no significant increase in rate was observed in the presence or absence of the C-terminal tail.

The role of Mg^{2+} in nucleotide exchange is examined using both novel (MBC: 7-Monoethylamino 8-bromocoumarin) and well characterised (Mant: N-methylanthraniloyl) fluorophores, covalently bound to Rac-complexed nucleotides. Fluorescent intensity measurements suggest a two step model of release of Mg^{2+} and nucleotide from Rac•nucleotide complexes during exchange. This model is supported by anisotropy data and use of Mn^{2+} as a substitute for Mg^{2+}, which allows examination of each of the two steps separately. Further work examines the Mg^{2+} binding to Rac•nucleotide complexes, and combined with the release data allows calculation of dissociation constants for Mg^{2+} from the Rac complexes.

IQGAP has been suggested to associate with Rac1 and inhibit its intrinsic GTPase activity.

These observations are confirmed in this report by measurements made on single turnover GTP hydrolysis of Rac in the presence or absence of IQGAP. The kinetics of this association are measured using fluorescent intensity and fluorescent anisotropy techniques. The use of a panel of Rac mutants provides a method to asses the importance of different Rac regions in the interaction with IQGAP. IQGAP exhibits a relatively high affinity with wild type Rac. The mutant studies suggest that the main contribution to association of Rac with IQGAP occurs via the Effector Region, with a small contribution from the Insert Loop.

Chapter 1

Introduction

1.1 Cellular Signalling

Eukaryotic cells need to respond to continuously changing extracellular or intracellular conditions and this response often requires a change of some cellular function. The flow of cellular information is not a one way process, since the cell must be able to both signal towards the extracellular environment and receive and interpret incoming signals.

The process of evolution has resulted in many different signalling pathways capable of responding to incoming signals and initiat a cellular response, such as producing changes in gene expression, cellular morphology, intracellular Calcium levels, extracellular secretion patterns, nuclear condensation levels, or even initiating apoptosis. Although these signalling pathways are diverse in function, they often share similar or related components which transmit and interpret the signal.

The very nature of a signalling pathway demands a method by which to discriminate whether the pathway is active ('On') or inactive ('Off'). The pathways found in eukaryotic cells involve different classes of proteins which can be grouped by the manner in which they differentiate between these two states. The Receptor Protein Tyrosine Kinases use the phosphorylation state of key tyrosine residues; whereas the Apoptotic pathways use the different conformations of DED Domains for this purpose.

The focus of this investigation, Rac, is a member of a protein family which uses the different forms of protein-bound Guanine Nucleotides as the indicator for the state of the pathway.

This large superfamily (Figure 1) of Guanine Nucleotide Binding Proteins (G-proteins) share a similar conserved core motif, which contains a binding and hydrolytic activity, yet the signalling G-protein members of this superfamily make up two distinct groups based upon their differing surrounding structural motifs and function.

The first of these classes, the heterotrimeric G-proteins, consist of constitutively membrane-associated proteins which are involved in signal transfer from membrane-spanning, serpentine receptors such as the β-Adrenergic system.

Monomeric G-Proteins are soluble, low molecular weight (often around 21 kDa) proteins which act as switches for a variety of effector proteins found in cells. These small G-proteins rarely exist free in the cytosol, but rather they are found tethered to a specific cellular membrane where they perform their function via a lipid anchor. This function is tightly regulated by a number of different mechanisms, suggesting that they play important roles in normal cellular function. Indeed mutations within the G-proteins themselves, or their controlling proteins can result in a constitutively active state within the cell and may cause oncogenic transformation.

Figure 1: The G-Protein Superfamily

The Superfamily classification of G-proteins is based on the presence of the conserved G Domain. In all G-protein Superfamily members this domain is involved in nucleotide binding and hydrolysis.

The Superfamily is divided up into three families based on the structure and function of the protein surrounding the G Domain. These families show further division of members into subfamilies based on structural and functional relationships.

Subfamilies can contain different classes of proteins, each showing an even greater level of specificity, as shown here by the Rho subfamily.

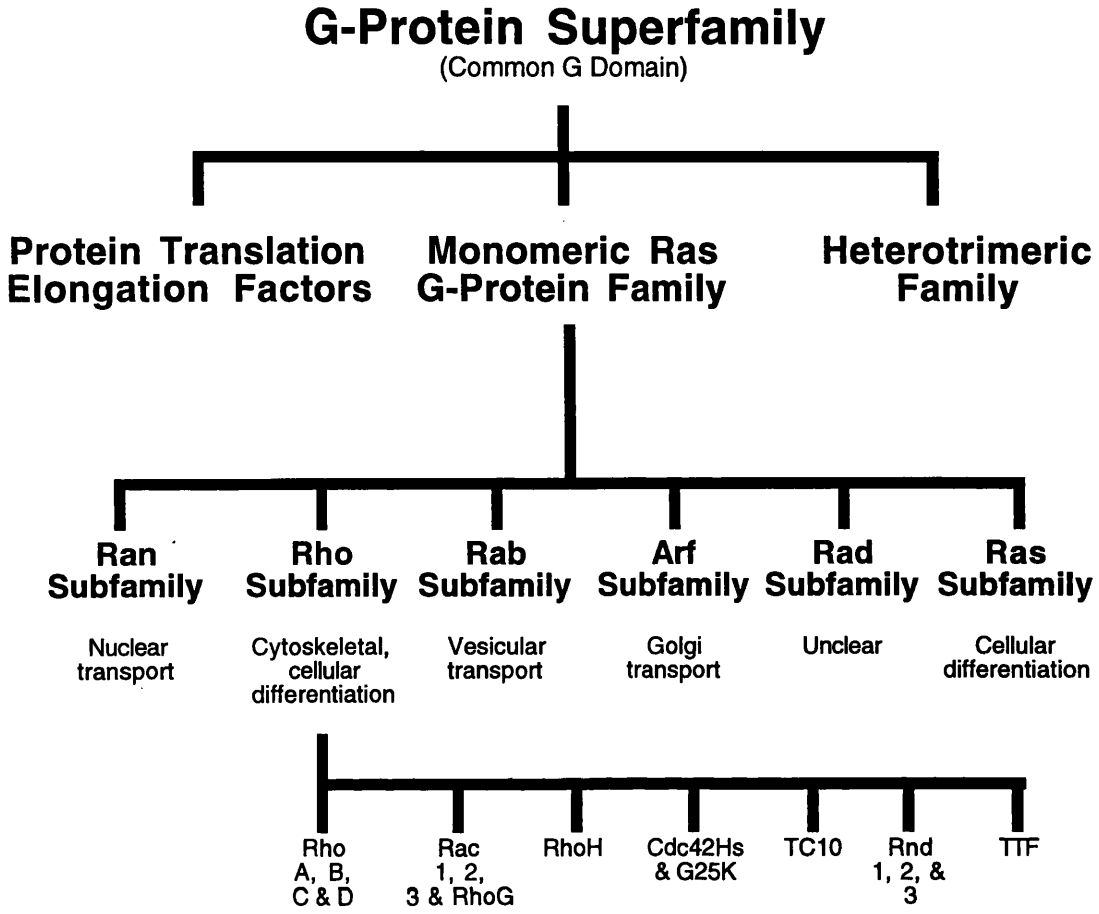
G-Protein Superfamily
(Common G Domain)
Protein Translation Elongation Factors
Monomeric Ras G-Protein Family
Heterotrimeric Family
Ran Subfamily
Rho Subfamily
Rab Subfamily
Arf Subfamily
Rad Subfamily
Ras Subfamily
Nuclear transport
Cytoskeletal, cellular differentiation
Vesicular transport
Golgi transport
Unclear
Cellular differentiation
Rho A, B, C & D
Rac 1, 2, 3 & RhoG
RhoH
Cdc42Hs & G25K
TC10
Rnd 1, 2, & 3
TTF

1.1.1 Small G-Protein Signalling

Small G-proteins are a family of proteins consisting of over 80 members in mammals alone. These proteins share a common fold in their central core (the so called 'G Domain'), while the remaining regions of the molecule are often quite varied, related to their function *in vivo*. This common core provides G-proteins with the ability to bind guanine nucleotides and to hydrolyse bound guanosine triphosphate (GTP) to guanosine diphosphate (GDP). The ability to exist in two different nucleotide bound forms [illegible] allows small G-proteins to act as cellular binary switches, the 'On' state represented by the GTP-bound form and the 'Off' state represented by the GDP-bound form. The two states are distinguished by structural differences caused by the different nucleotides bound, as will be discussed in more detail later.

The GTP- and GDP-bound forms of small G-proteins are able to associate with other molecules which have either a regulatory effect (GTPase Activating Proteins, GAPs., or Guanosine Nucleotide Exchange Factors, GEFs, or Guanosine Nucleotide Dissociation Inhibitors, GDIs), or have a downstream signalling role (p21 Associated Kinases, PI3-Kinase). The regulatory proteins are influenced by upstream signalling events, and are therefore able to control events downstream by acting upon the small G-protein, causing its inactivation (GAPs and GDIs) or activation (GEFs). The basic stages of a small G-protein's switching cycle are shown in Figure 2.

H-Ras was the first monomeric G-protein to be identified (Murayama, T. and Ui, M., 1984;

Figure 2: The Activation Cycle of Small G-Proteins

Small G-proteins are able to function as binary switches for molecular events due to their ability to bind GTP and hydrolyse it to GDP. This process is tightly controlled by a number of different proteins such as GTPase Activatory Proteins (GAPs), Guanine Nucleotide Exchange Factors (GEFs) and Guanine Nucleotide Dissociation Inhibitor (GDI).

Different subfamilies of G-proteins and different proteins within these families can have exclusive associating proteins or can share the same associating proteins. The GTP-bound form of the small G-protein is able to interact with effector proteins which then have some effect downstream in the signalling cascade.

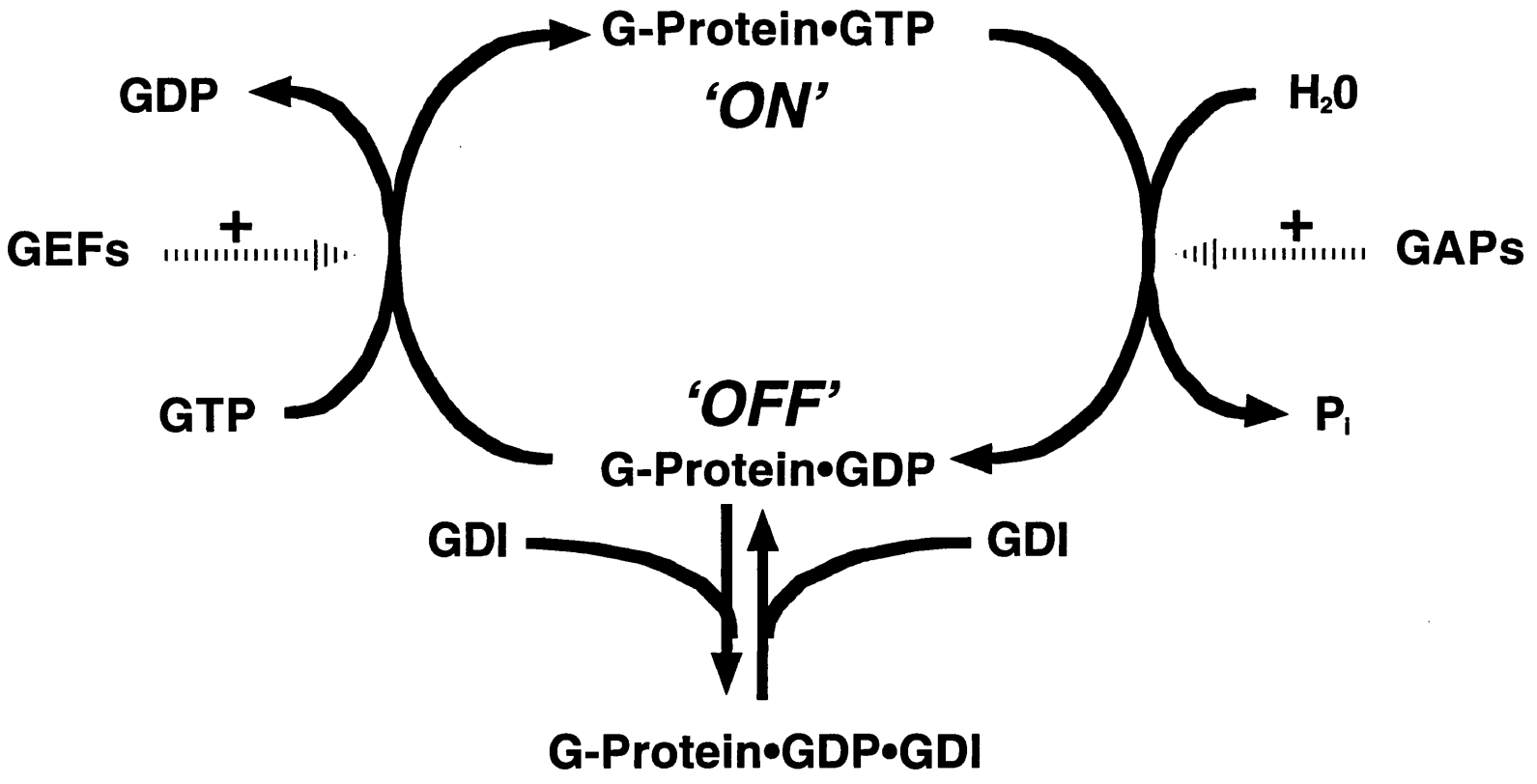
G-Protein•GTP
'ON'
GDP
H_2O
GEFs
+
+
GAPs
GTP
'OFF'
P_i
G-Protein•GDP
GDI
GDI
G-Protein•GDP•GDI

Poe, M. *et al.*, 1985), and so lends its name to the entire generic small G-protein family. The Ras family is divided up into a number of subfamilies which group together proteins sharing sequence and structural homology: Ras, Rho, Arf, Ran, Rab and Rad (Figure 1). These small G-protein subfamilies show limited structural and sequence similarity with each other, however within each of these subfamilies not only is the homology more significant, but the cellular functions of the proteins within the subfamily are also generally similar, although never exclusive. Ras subfamily proteins are generally involved in cellular differentiation and growth, Rho proteins are involved in cytoskeletal and cellular morphological rearrangements, both the Arf and Rab subfamilies are involved in intracellular trafficking – Arf being involved specifically with the Golgi apparatus and Rab being involved in many stages of the exocytic and endocytic vesicular transport, Ran proteins are involved in nuclear import processes., and the role of Rad proteins is still unclear. This Introduction will examine relevant aspects of the Ras subfamily, since it forms the basis of much of our small G-protein understanding, and the Rho subfamily on which the majority of this dissertation is centred.

1.2 Ras Subfamily Proteins

The Ras subfamily is the archetypal small G-protein subfamily, and the basis for much of our entire small G-protein knowledge, and as such will be discussed here.

The Ras subfamily consists of the four 'original' Ras proteins encoded by the three H-*ras*, K-*ras* and N-*ras* genes, as well as the R-Ras proteins (R-Ras, R-Ras2/TC21, R-Ras3/M-Ras), the Ral proteins (A and B), the Raps (1A, 1B, 2A and 2B), Rheb, Rin and Rit. The members of the subfamily are closely related by structure and sequence, and show identity (in a particular region called the 'Effector Region') ranging from 100% (H-Ras, N-Ras, K-Ras) to a minimum of 50% (Ral, Rheb, Rin and Rit).

1.2.1 Functions of Ras Proteins

A large amount of research has provided considerable insights into the functions and effects of Ras subfamily proteins, particularly those produced from the three *ras* genes. The established model for the Ras pathway begins with the reception of a signal at the cell surface (via receptors such as the Epidermal Growth Factor Receptor or the γ-chain of the T Cell Receptor) which in turn activates a single linear cascade transmitting the signal to the nucleus. The activation of Ras, mediated by Sos (its GEF), results in the activation of the Raf serine/threonine kinases, which themselves activate the Erk mitogen-activated kinases (MAPKs) and thus affect the activity of various transcription factors within the nucleus. Although this model is still valid, it is now thought that the signalling from Ras (and other small G-proteins) should not be regarded in such a linear fashion, rather each step of the signalling pathway provides a an opportunity for proliferation of interacting proteins and

therefore of the signal. The simple model with Raf as Ras's only direct effector protein, has now been expanded after the identification of other effector proteins, including other Serine/Threonine kinases (PKC-ζ, MEKK1),, Phosphoinositide 3-kinase lipid kinases and regulatory proteins such as Ras GTPase-activating proteins (p120GAP, neurofibromin) and Ral Nucleotide Exchange Factors (RalGDS, RGL, RGL2).

The pathways involving these effector proteins have been shown to involve the activation of small G-proteins from different subfamilies (such as the Rho subfamily) suggesting the possibility of cross-communication between different small G-protein subfamilies, resulting in wide ranging changes in cellular activity from just one extracellular signal event.

Since the members of the Ras subfamily are highly related, it would be easy to assume that these proteins share identical or similar functions, yet it is becoming clear that this is untrue. Even the four Ras proteins, H-Ras, N-Ras, K-Ras4A and K-Ras4B which share almost complete sequence identity, are not functionally identical. Mouse gene knock-outs have shown that K-*ras*, but not H-*ras* or N-*ras,* may be essential for normal development (Umanhoff, H., *et al.*, 1995 & Johnson, L., *et al.*, 1997), and farnysyl transferase inhibitors (which inhibit the lipid processing of Ras proteins) are effective only against oncogenic transformation of H-Ras, but not K-Ras or N-Ras (Prendergast, G., 2000). It is now apparent that individual Ras proteins differ in their trafficking and location or method of association with the plasma membrane (Apolloni, A. *et al.* 2000), thus providing a non-structural basis for functional distinctions between the proteins. Ras proteins are post-translationally modified on their C-terminal 25 amino acids, at and near a CAAX motif (a

region showing sequence divergence). This CAAX motif has been demonstrated to contain multiple signals required to target Ras proteins to cellular membranes. The CAAX signal is not enough by itself to result in Ras proteins translocation to the membrane, a secondary signal is also needed. This may be further protein sequence, such as K-Ras4B where a Lysine rich sequence upstream of CAAX provides this signal, or the secondary signal might take the form of further lipid modification, such as N-Ras and H-Ras, where a palmitate fatty acid is added to a Cysteine upstream of the CAAX motif. In this respect, Ras proteins act as the model example for the other small G-protein subfamilies, since many of these proteins also undergo such lipid modification and possess informational C-terminal tails.

1.2.2 The Structure of Ras

Initial functional analysis and subsequent structural elucidation of Ras proteins has provided insights into structure/function relationships for both Ras proteins alone and in complexes with various effectors. This information allows Ras to act as a model small G-protein for other subfamilies, and provide a comparison for the function of different structural regions of Ras family proteins.

Common to all G-proteins within the superfamily is the G Domain (or GTPase fold) (Figure 3), which high resolution structures have shown to be a variation on the classical nucleotide binding fold (La Cour, T., *et al.* 1985). This core region is made up of around 200 amino acid residues and contains a 6 stranded β-sheet surrounded by a number of α-helices. The guanine nucleotide biding site is formed by 5 polypeptide loops which are numbered G1-G5 (Bourne, H., Sanders, D., McCormick, F. 1991), and are the most highly conserved regions

Figure 3: The Conserved G Domain

The *panel opposite* shows a representation of the G Domain, the conserved core of all proteins within the GTP Binding Protein Superfamily.

The five G Loops are labelled. Loops G2 and G3 contact the Mg^{2+} (position indicated by 'Mg^{2+}')and β and γ phosphates of the nucleotide. Loops G1, G4 and G5 make contacts with the α and β phosphates and guanine ring.

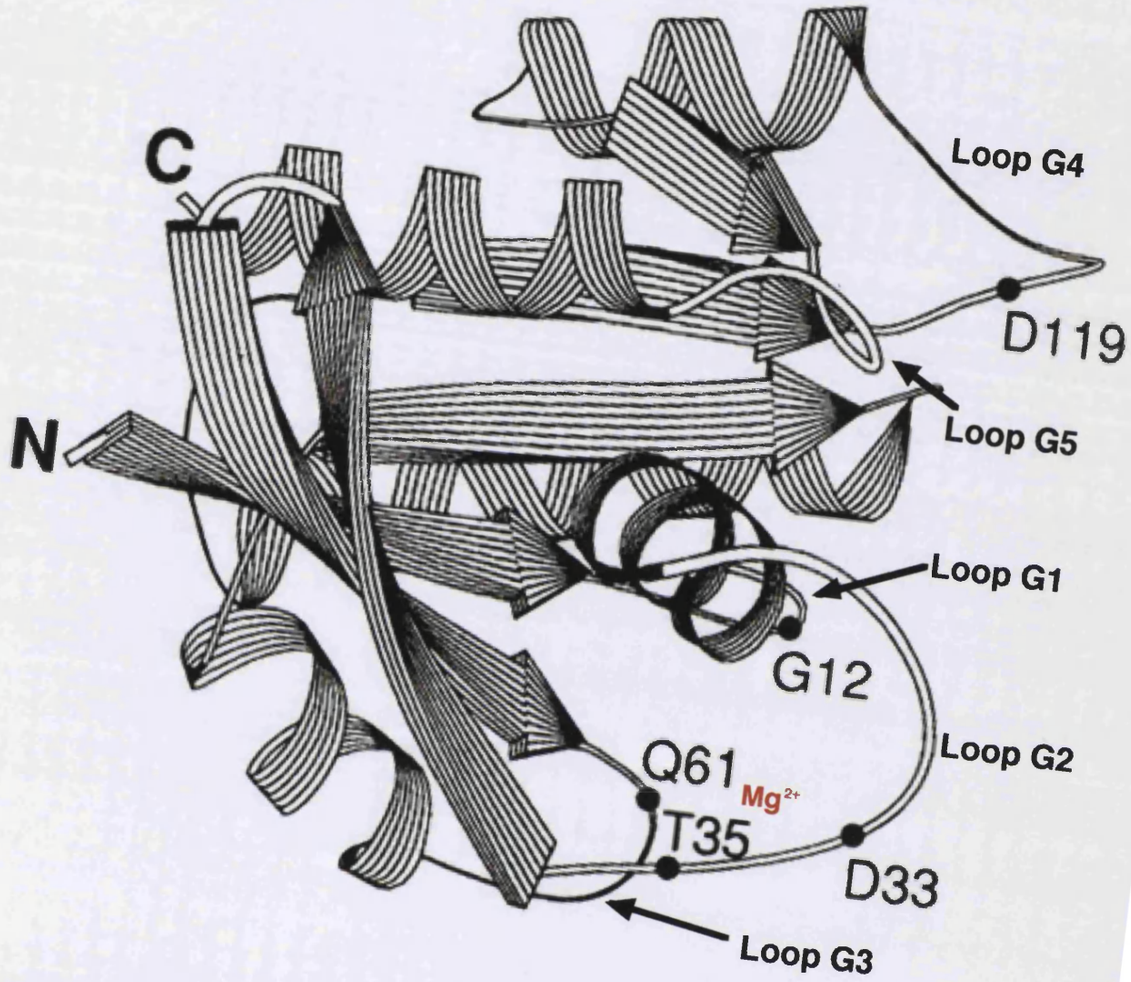

Figure 3 The Conserved G Domain of the Ras Family

From Pai, E., *et al.* (1989) *Nature* **341** , 209-214

throughout the Ras family. Indeed their homology defines the entire G-protein superfamily.

These polypeptide loops contain specific sequences which associate with the α-, β- and γ-phosphates of the bound nucleotide, the co-ordinated Mg^{2+} ion found associated with all nucleotides and the guanine.

The 'P-Loop' within G1 is involved in binding the nucleotide's α- and β-phosphates via the conserved sequence GXXXXGKS/T. The γ-phosphate and Mg^{2+} ion of the bound nucleotide associate with the DXXG motif found in the G3 loop, and the recognition of the guanine is performed by the combination of an NKXD motif in the G4 polypeptide loop and the G5-Box which contains the consensus motif (T/G)(C/S)A. The highly conserved Threonine (T35) and Tyrosine (Y32) residues found in G2 are also crucially involved in the co-ordination of the Mg^{2+} ion.

The sequence of the G Domain is highly conserved throughout the small G-protein family and the entire G-protein superfamily. The overall tertiary structure of the Ras G-protein is conserved throughout the Ras family, even though the sequence identity between two different subfamilies can be be quite low.

The crystal structures of Ras (Tong, L., *et al.,* 1989 & 1991; Krengel, U. *et al.,* 1990; Pai, E. *et al.*, 1989; de Vos, A. *et al.*, 1988) are those of a truncated form of the protein (retaining its normal GTPase function) which is expressed lacking its C-terminal tail in order to aid purification and crystallisation. In free solution this C-terminal tail is highly unstructured

(Milburn, M. *et al.*, 1990), and is not visible in crystal structures.

1.2.2.1 The Differences between GTP- and GDP-bound Ras

The structure of Ras has been elucidated in both its GDP-bound form (Tong, L., *et al.*, 1989) and in forms bound to nonhydrolysable analogues of GTP, GMPPNP (Pai, E. *et al.*, 1989), GMPPCP (Milburn, M. *et al.*, 1990) (both thought to closely resemble the GTP-bound form) and a caged-GTP form (Scheidig, A. J. *et al.*, 1999).

From these structures the differences between the GTP and GDP forms can be rationalised. On hydrolysis of GTP to GDP Ras undergoes conformational changes throughout the molecule, although these appear to be concentrated in two main regions, the 'Switch I' and 'Switch II' regions. The Switch I region is equivalent to the G2 loop (which plays a role in Mg^{2+} binding), and is often termed the Effector Loop (Pai, E. *et al.*, 1989) since it has also been shown to play a role in interaction with Ras-effector proteins. The Switch II region represents the G3 loop and the subsequent α-helix which are also implicated in Mg^{2+} binding as well as γ-phosphate association. Although these two switch regions are well defined in crystal structures suggesting that they are highly ordered states, NMR studies of the Ras protein (Kraulis, P. *et al.* 1994) have suggested that these two Switch regions should not be considered rigidly taking one or the other conformation. They possess some amount of intrinsic instability and are therefore relatively flexible within the structure.

In both GTP and GDP forms, the binding sites of the nucleotide and Mg^{2+} ion are in close communication. The α- and β-phosphates, which are both required for tight binding (GMP

binds weakly to Ras), are surrounded by the P Loop in G1, which takes on a rigid conformation (which is unchanged on GTP hydrolysis) and uses four of its backbone amides to co-ordinate the oxygens of the two phosphates. A conserved Lys in the P-Loop plays a critical role by bridging the β- and γ-phosphates of bound GTP, and a conserved Ser/Thr provides a sidegroup hydroxyl group to coordinate the Mg^{2+}.

In both the GTP- and GDP-bound form of Ras, the Mg^{2+} ion is hexacoordinated, although the groups providing this coordination are different. In the GTP-bound form, the ligands provided by the α- and β-phosphates of the nucleotide, the conserved Ser/Thr from the P loop, a conserved Thr from the G2 loop and 2 water molecules. The γ-phosphate is co-ordinated to a conserved Gly residue within the DXXG motif in the G3 loop, the conserved Ser of the G1 loop as well as the highly conserved Thr 32 and Tyr 35.

On hydrolysis and the release of the γ-phosphate as a phosphate group, the strong binding interdependence between the Mg^{2+} and the γ-phosphate is removed with the γ-phosphate's Mg^{2+}coordination contribution being replaced by a water molecule. The loss of the contacts between the conserved Gly and the γ-phosphate causes an ordered coil to helix transition in the N-terminus of the Switch II region, as well as the reorientation of Switch II's α2 helix, causing a general collapse of the effector binding site. The conformation of Switch I is also changed on hydrolysis, due in part to the loss of the γ-phosphate contact with Thr 32 and Tyr 35, causing their reorientation, and thus the conformational changes in the two regions are coupled.

The structural changes in the two nucleotide bound states have been taken further by computer modelling (Diaz, J. F. *et al.*, 1997), and it is suggested that instead of there being just two states of protein conformation (GTP or GDP bound), the pathway between the two is actually composed of a sequence of steps. The loss of the γ-phosphate causes movement to be transmitted to Switch I and Switch II, which then undergo a conformational transition relaxing Switch I and forcing Switch II into its new conformation. This model does suggest roles for a number of residues throughout the Ras protein, who's mutations cause changes in Ras's activity by an unclear route, although none of these intermediates have been observed in crystal structures.

1.3 The Rho Subfamily

The Rho subfamily of G-proteins currently consists of 16 members, grouped into 7 different classes: Rho (the isoforms A, B, C, and D), RhoH, Rac (1, 2, 3 and RhoG), Cdc42 (Cdc42Hs and G25K), TC10, Rnd (RhoE/Rnd3, Rnd1/Rho6, Rnd2/Rho7) and TTF, although the most intensively studied of these are Rac1, Cdc42, and RhoA. Each of the Rho subfamily proteins shows at least 50% identity to other subfamily members although they are only 30% related to Ras. The many similar isoforms of Rho family proteins suggest that they may share common functions, yet it is clear that *in vivo* they exhibit unique roles: RhoA, RhoB and RhoC all regulate stress fibre formation (Ridley, A., *et al.* 1992), yet they show a different subcellular localisation (Adamson, P., et al. 1992), as well as having different expression regulation (Fritz, G., Kaina, B., Aktories, K., 1995; Hunter, T. and Jähner, D., 1991) and posttranslational lipid modification (Adamson, P., et al. 1992; Lebowitz, P., *et al.* 1995). In a similar fashion, Rac1 is expressed ubiquitously, Rac2 is restricted to haematopoietic cells and Rac3 is localised to the brain (Haataja, L., *et al.* 1997).

Rho subfamily proteins are able to associate with regulatory or effector proteins, in a similar fashion to Ras. There are currently over twenty known Rho GEFs, which are either specific for a particular Rho subfamily member such as Lbc for Rho (Zheng, Y. *et al.* (1995) or specific for the Rho subfamily as a whole, such as Vav. Similarly, the Rho subfamily GAPs act either specifically (ArfGAP for Arf1 (Goldberg, J., 1999)) or nonspecifically within the Rho subfamily (p190GAP). In addition to GAPs and GEFs, some Rho subfamily proteins (Rac1, RhoA and Cdc42) are also able to interact with members of the GDP-Dissociation Inhibitor family (RhoGDI). RhoGDIs were initially identified through their ability to inhibit the dissociation

of GDP from Rho, Cdc42 and Rac. They were further shown to interfere with the intrinsic and GAP-stimulated GTP hydrolysis of Rac, and to interfere with the G-proteins' association with the cell membrane. RhoGDI therefore act to prolong the inactive state of the Rho proteins, and since 'free' cytosolic Rac, Rho and Cdc42 are found associated with RhoGDI in unstimulated cells, it is thought that RhoGDI plays an important role in sequestration and maintenance of the small G-protein in its inactive state. Disruption of this state is the initial step towards the activation of the G-protein.

The activation of Rho GTPases can occur via a number of extracellular signals, such as Platelet Derived Growth Factor (PDGF), insulin, fibronectin, bradykinin, thrombin, and bombesin, however it is becoming increasingly clear that Rho family members may also be activated by other members of both the subfamily and other Ras family members. The effects of one signal may therefore be distributed throughout a network of several Rho subfamily proteins. Indeed it is quite possible that direct activation of proteins such as Rac and Rho by receptor molecules is a rare occurrence, rather they become activated by other small G proteins (such as Ras and Cdc42) which are themselves activated directly by receptor systems.

1.3.1 Rho Subfamily Protein Function

Rho subfamily proteins have been implicated in a spectrum of cellular processes ranging from superoxide production in the NADPH Complex in Neutrophils (Heyworth, P., 1993), to Fas-induced apoptosis (Gulbins, E., *et al.* 1996), to activation of a variety of transcription factors (Hunter, T. and Jähner, D. 1991), and to their particularly well characterised role in

cytoskeletal function and cellular morphology changes (Takaishi, K. *et al.* 1997; Wójciak-Stothard, B., *et al.* 1998).

The effects of Rho subfamily proteins on cellular cytoskeletal organisation were initially used as a method by which the subfamily members' activity could be measured, and it was these studies which provided the first suggestions that the activation of various Rho proteins were interlinked. Not only were different forms of cytoskeletal arrangements associated with different forms of Rho proteins (Rac, lamellipodia formation and membrane ruffling; Rho, stress fibre formation and focal adhesions; Cdc42, filipodia formation) (Ridley, A. *et al.* 1992; Ridley, A. and Hall, A. 1992; Nobes, C. and Hall, A. 1995), but activation of Ras induced these structures through the action of Rac and Rho, as did the activation of Cdc42. Dominant negative mutational studies confirmed that both Ras and Cdc42 act upstream of Rac, which in turn is upstream of Rho, and that full cellular transformation by Ras is dependent on both Rac and Rho activity (Qiu, R-G., *et al.* 1995; Khosravi-Far, R. *et al.* 1995) (Figure 4). The method of connection between these G-proteins is unclear, although they do not contact each other directly, rather it is possible that interacting proteins, such as GAPs, GEFs and GDI proteins, which bind to several different classes of the Rho subfamily may play a role in the transfer of information between them.

This Rho family activation cascade demonstrates cell specificity which varies from the fibroblast-prototype model in which it was first established (Allen, W., *et al.* 1997). Rho's inactivation in neuroblastoma cells causes Cdc42 and Rac activation, and activated Rac does not induce stress fibre formation in MDCK cells (Ridley, A., 1995). These differing

Figure 4: Functional Connections between Ras and Rho Subfamily Proteins

Previous work has shown that Ras and members of the Rho subfamily are functionally interlinked. Ras cellular differentiation is dependent on Rac and Rho activity, and although the connection between the two pathways is not clear it is highly likely that the connection is via effector proteins which associate with both subfamilies. The GEF, Vav is a potential candidate for this role.

There is also a functional hierarchy with the Rho subfamily, with Rho action being downstream of Rac, and Rac in turn being downstream of Cdc42. This method of activation of the G-proteins is not their only pathway of activation, with each having at least one direct activatory pathway from cell stimuli. Furthermore, the functional hierarchy pictured above is subject to tissue dependency.

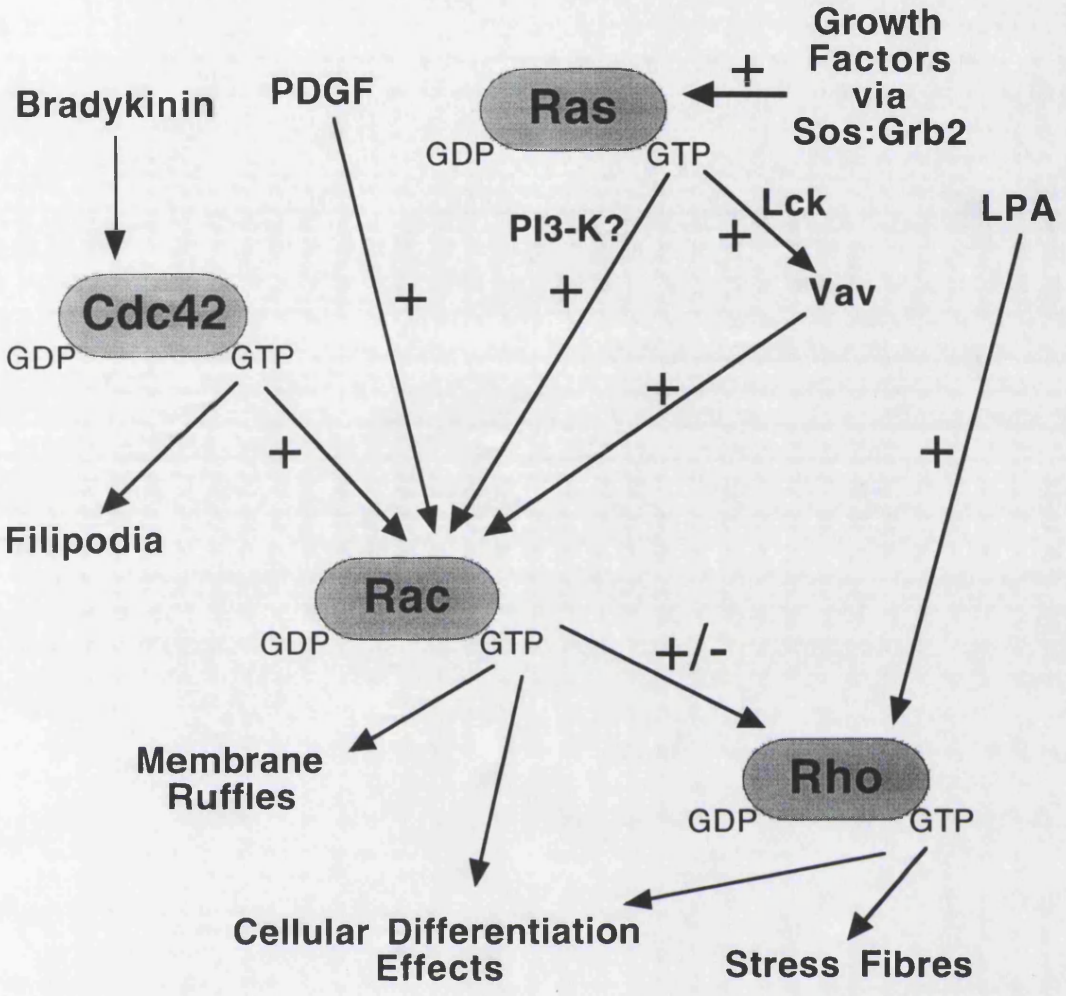
Growth
Factors
via
Sos:Grb2
Bradykinin
PDGF
Ras
GDP
GTP
PI3-K?
Lck
LPA
Vav
Cdc42
GDP
GTP
Filipodia
Rac
GDP
GTP
+/-
Membrane
Ruffles
Rho
GDP
GTP
Cellular Differentiation
Effects
Stress Fibres

observations demonstrate the inherent flexibility in Rho subfamily protein function, depending on their cellular situation.

The wide ranging and varied effects seen as a result of Rho subfamily activation is caused by their ability to associate with a wide spectrum of effector proteins (other than fellow subfamily members). These not only include their GAPs and GEFs, which often have a secondary function to that of regulating the G-protein's activity, but Rho proteins also have been shown to associate with non-kinase proteins (Wiskott-Aldrich Syndrome Protein (Symons, M., 1996), IQGAP (Weissbach, L., 1994), protein kinases (p21-activated kinase family (Abo, A., *et al.* 1998), ROK (Leung, T., *et al.* 1995), and lipid kinases (PI3K).

All Rho subfamily proteins in vivo are found posttranslationally modified on their C-terminal tail at the Cys within a CAAX motif. The Rho subfamily is geranylgeranylated at this site and this lipid modification has several biological roles. The lipid acts as an anchor in lipid bilayer membranes, thus allowing the Rho subfamily G-protein to be localised at its area of activity. The lipid attachment is also a target for the regulatory protein GDI. On binding of GDI to Rho, the C-terminal tail becomes ordered in an extended conformation reaching across the surface of GDI, where the geranylgeranylation is bound in a lipid pocket within the GDI molecule, thus preventing the G-protein associating with the membrane.

1.3.2 Rho Subfamily Structure

A number of studies have produced crystal structures for Rho subfamily members, in their GDP-bound form (Hirshberg, M., unpublished results), their GMPPNP-bound form (a

nonhydrolysable GTP analogue) (Hirshberg, M., *et al.* 1997; Ihara, K., *et al.* 1998) and in the absence of the Mg^{2+} ion (Shimizu, T., *et al.* 2000) usually associated with nucleotides *in vivo*. Together they suggest that the Rho subfamily differences between the prototype Ras proteins are a result of some significant and unique structural features (Figure 5).

The overall tertiary structure of the Rho proteins is similar to the Ras proteins. They share a core G-domain, which varies only slightly between the two subfamilies, and they share a Switch I domain which is involved in Mg^{2+} binding, and a Switch II region which is involved in the coordination of the γ-phosphate as well as containing conserved residues which play roles in catalysis and Mg^{2+} and nucleotide binding. However, all Rho proteins exhibit an Insert Region which is unique to this subfamily and shows a different character for different Rho proteins, suggesting a role in identification and specificity.

As previously discussed, the Switch I (Effector Loop) of Ras is highly exposed, and adopts different ordered conformations depending on the presence of either bound-GDP or GTP. Rho subfamily proteins are subtly different from Ras's model structure. In the GMPPNP form of Rac1 (Hirshberg, M., *et al.* 1997), the Switch I region is highly disordered and flexible, caused by several hydrophobic substitutions present, which make this region less stable and more flexible. The GDP-form of RhoA shows a Switch I region which is in a similar position to that found in the GTP structure, although more ordered. Similarly the Rac•GDP structure (Hirshberg, M., unpublished) shows that the Switch I region is more ordered than the GMPPNP structure (Figure 6). These differences between the Ras and Rho subfamilies suggest that they also differ in their method of Mg^{2+} association. In the

Figure 5: Ras and Rac Structural Comparison

The panel opposite shows both the structures of Ras (*upper*) and Rac (*lower*). The overall structural similarity between the two proteins is quite similar. The insert loop, characteristic of the Rho subfamily can be seen protruding out towards the left of the molecule. The nucleotide bound is indicated in yellow and black.

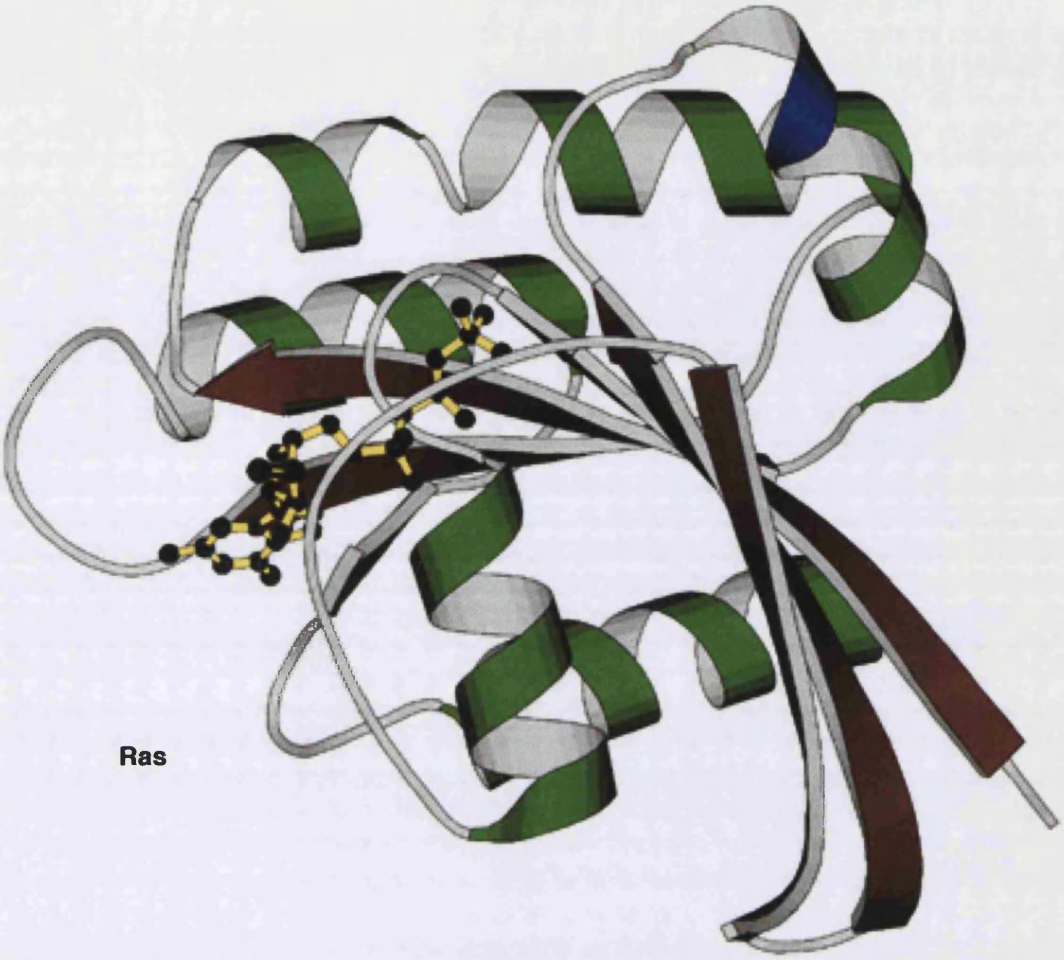

Ras

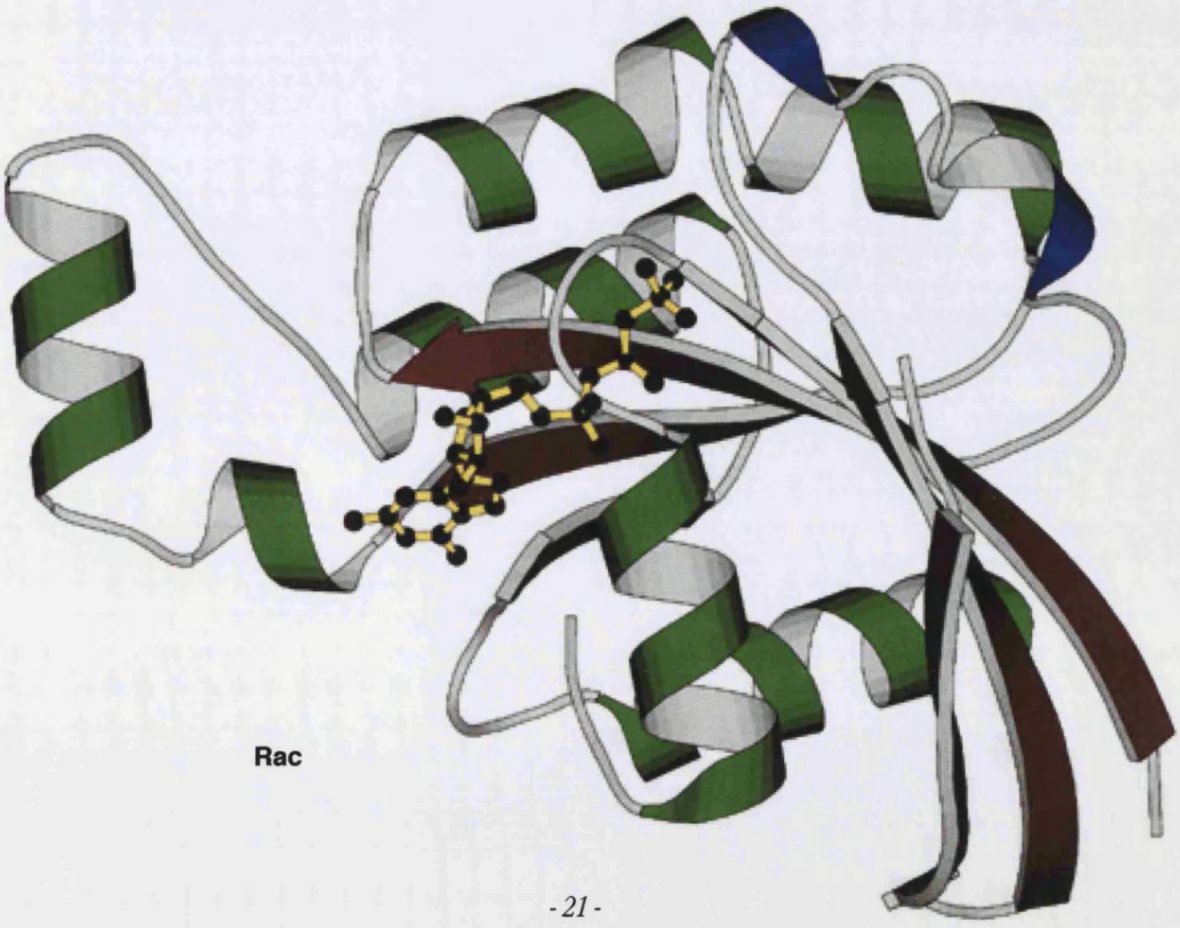

Rac

Rac•GMPPNP structure, Thr 35 co-ordinates the Mg^{2+} ion via it's hydroxyl side chain, and Thr 37 performs this role in RhoA's GDP structure, similar to the Thr 32 ligand in Ras. There are also differences in Mg^{2+} co-ordination between Ras and Rho proteins. Whereas only three H_2O molecules are co-ordinated to the Mg^{2+} (along with Thr 37, Thr 19 and the β-phosphate) in RhoA•GDP, four were required in Ras•GDP. In Rac•GMPPNP, further Mg^{2+} ligands are provided by the γ-phosphate of the bound nucleotide. The ribose ring is also bound less tightly in the Rho and Rac structures due to the greater distance between Switch I and the ring — the association is mediated through H_2O molecules (Figure 7).

The elucidation of the crystal structure of a Mg^{2+}-free form of Rho•GDP has provided insights into the mechanism of nucleotide exchange, and suggests that there is in fact significant similarity between the mechanism of nucleotide exchange fo Ras and Rho/Rac. In this case, the Switch I region showed the most significant changes from the Mg^{2+} associated structure, resembling the structure of Ras when associated with its GEF, Sos (Nimnual, A., *et al.* 1998). A large conformational change occurred so that Switch I, which normally sandwiches the nucleotide with the P Loop, had no direct or H_2O-mediated contacts with the nucleotide, and lay quite open. The loss of Mg^{2+} enhanced the mobility of the Switch I region, which was provided by and centred upon around a change in a torsion angle of Asp 28 (equivalent to Asn 26 in Ras).

This may mean that although Switch I in the Rho subfamily takes on different conformations to that found in Ras in the GTP and GDP bound state, which may be significant for specific signals downstream, they may ultimately take on a similar conformation on nucleotide and

Figure 7: Mg^{2+} Coordination with Ras

The panel opposite shows the coordination of the GTP analogue, GMPPNP, and Mg^{2+} in the active site of Ras (Pai, E., *et al.* (1989)).

Mg^{2+} (red) is hexacoordinated directly by the β and γ phosphates of the nucleotide, as well as amino acids from Ras itself (Thr 17, Thr 35,) and two H_2O. In the GDP bound form of Ras (and Rac), the contact from the γ phosphate is absent, and is replaced by one H_2O.

The α, β and γ phosphates of GMPPNP shows numerous coordinations: the Mg^{2+} ion, Ras residues (including Gln 61, Thr 35, Lys 117, Gly 60) and H_2O molecules (not shown). The GMPPNP is held less tightly than GTP, presumably since GMPPNP is not a natural nucleotide. GDP is held more tightly than GMPPNP, yet less tightly than GTP — partly due to the extra stabilisation provided by the Mg^{2+}.

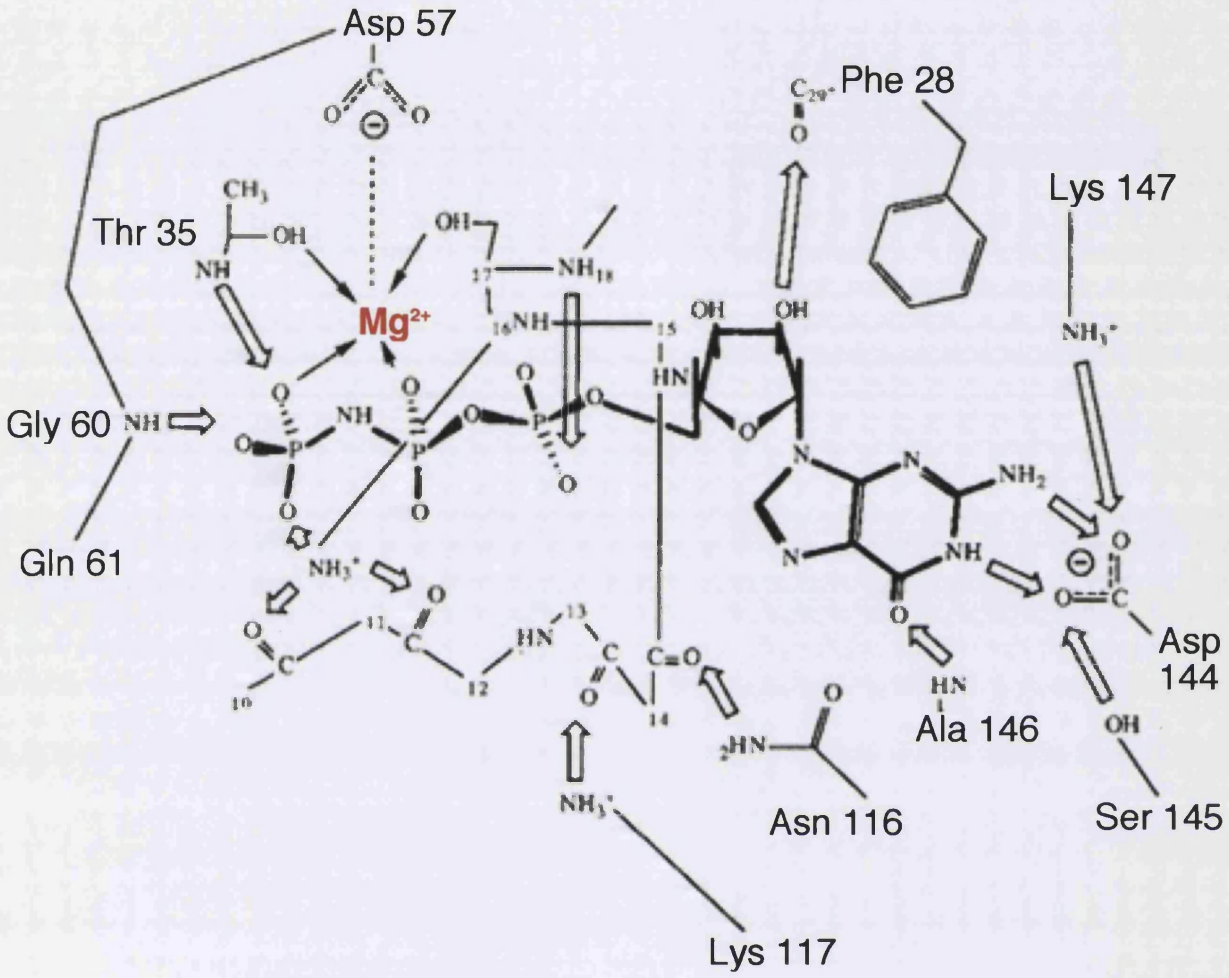

Figure 7 The Coordination of Mg $^{2+}$ and the GTP Analogue, GMPPNP

Mg^{2+} exchange.

1.3.2.1 The Rho Subfamily Insert Loop

The unique feature of the structures of Rho subfamily proteins is the Insert Loop, which runs from residues 117-137 (in Rac1). The loop is based on a conserved core of hydrophobic residues which pack together to give the loop structure, yet on the exposed face of the helix the residues are highly varied between different subfamily members. These differences in character (Rac1 exhibits a positive character, whereas as RhoA exhibits a more negatively charged nature) may play an important role in effector specificity. The insert loop has been shown to play a role in interacting with a number of effector proteins (Freeman, J., *et al.* 1996; Jin, W., *et al.* 1997;, McCallum, S. *et al.* 1996). Furthermore, when Rho is present at the membrane the Insert loop becomes unavailable to antibodies raised against it, which recognise the region in the cytosol, suggesting that it may interact with the membrane surface or effectors in this situation which cause a masking of the region.

The difference in conformation of the Insert loop, between the GDP form and GTP form of RhoA and Rac is relatively small, since it is highly mobile in both structures, suggesting that the Insert loop plays a more significant role in specificity for Rho subfamily members than activating any particular downstream signalling event. Perhaps confirming this, the Mg^{2+}-free form of Rho•GDP showed that the Insert loop was not significantly different from the Mg^{2+}-associated forms.

The Switch II region, which is implicated in both Mg^{2+} and γ-phosphate association, was

found to be more ordered in Rac•GMPPNP than RhoA•GDP, due to the extra stability provided by the terminal phosphate group. The Switch II region contains a number of conserved residues which are involved in this association (the DXXG motif), and indeed these and the overall structure and conformation of the Switch II region are conserved throughout the Ras family. In the absence of Mg^{2+}, Switch II is found with Ala 61 near the Mg^{2+} binding site, which shows similarity to Ala 59 in a Ras-Sos complex, and this change in conformation and rigidity of Switch II provides a sensitive indicator to the presence or absence of GTP.

1.3.2.2 The C-Terminal Tail

Although crystallographic studies on the GDP and GMPPNP complexes of Rho subfamily proteins have provided detailed structures of the core and surrounding regions, they have been unable to provide much information on the termini of the molecule, except that free in solution they are highly mobile and unordered. As with Ras subfamily proteins, the Rho subfamily are posttranslationally modified at their C-terminus on the Cys residue in the CAAX motif, allowing their translocation to membrane surfaces when activated. This C-terminal tail of a number, but not all, Rho proteins has also bee implicated in a self-stimulatory GTPase role (Zhang, B., and Zheng, Y., 1998; Zhang, B., *et al.* 1999). The presence of an Arg residue surrounded by positively charged Lys residues has been claimed to increase the GTPase rate of some Rho proteins to that almost equivalent of the rate in the presence of GAPs. A section of this thesis examines this supposed property with respect to Rac1.

1.4 GTP Hydrolysis by Ras and Rho Subfamilies

The lifetime of an active GTP-bound small G-protein is dependent on its GTP hydrolysis rate. Each has its own characteristic intrinsic hydrolysis rate, which tend to be similar within subfamilies, and it has been shown that the residues responsible for the varying GTPase activity lies outside the conserved G Domain, and is caused by a combinatorial effect of the residues in the two phosphate loops (Ménard, L. and Snyderman, R.., 1993). H-Ras catalyses the conversion of GTP to GDP at a leisurely 0.00033 s^{-1}, Rac1 substantially quicker at 0.003 s^{-1}, and RhoA at 0.0004 s^{-1} (at 20°C). The residues which influence the hydrolysis in Rac1, and increase its activity over H-Ras are Asp 11, Pro 29 and Gly 20 (Ménard, L. and Snyderman, R.., 1993). These rates of GTP hydrolysis are too slow to be useful for a transient signalling timescale *in vivo*, and so they associate with GAPs to increase their rate, and thus decrease their active lifetime to a more physiologically relevant level. Compared to the related heterotrimeric G-proteins, small G-proteins have extremely slow GTP hydrolysis rates. GAPs are able to increase this rate by using a method similar to that found in the intrinsic mechanism of the heterotrimeric G-proteins and this will be discussed later.

1.4.1 The GTP Hydrolysis Mechanism

The process of GTP hydrolysis in the G Domain involves an inversion about the γ-phosphate centre, with an H_2O molecule acting as the nucleophile, displacing the GDP leaving group (Feuerstein, J., Goody, R., Webb, M., 1989). The process of hydrolysis can be rationalised into a series of steps, although it is unclear as to whether they are separable kinetically, and it is also unclear which step determines the rate at which the phosphate is ultimately

generated. The hydrolysis mechanism is likely to be initiated by the polarisation of a catalytic molecule, to provided a negatively charged hydroxyl group. This polarisation is followed by its attack on the γ-phosphate, producing a transition state (the exact form of which is unclear), followed by the product formation step (Figure 8).

The character of the group responsible for the polarisation of the catalytic water molecule has been under intense investigation for some time. It was first thought that the highly conserved Glutamine residue (Gln 61 in Rac1 and Cdc42, Gln 63 in RhoA), found in the P Loop, acted as the general base by deprotonating, or polarising water so that it could then attack the γ-phosphate. Virtually all mutations at this site in Ras cause a reduction in the GTPase activity, which prevented GAP function and were oncogenic (Der, C., Finkel, T., Cooper, G. 1986). However, it became clear that not only is Gln not a strong enough base to deprotonate water, and that these mutations did not cause a change in the water's position, as would be expected if Gln 61 were to play such as role. Instead, Gln 61 may play a role in stabilising the transition state of the reaction by neutralising the excessive build up in negative charge (Privé, G., *et al.* 1992), or perhaps play a role in a proton shuttle that finally protonates the γ-phosphate of the bound GTP. An alternative model for this process involves the Mg^{2+} ion acting to polarise the γ-phosphate of the nucleotide, which then acts as the general base and polarising the water molecule. In support of this are experiments which show that the replacement of the Mg^{2+} ion with the more electronegative Mn^{2+} increases the rate of hydrolysis by increasing the basicity of the γ-phosphate, yet without changing the chemical mechanism of the reaction or the structure of the protein (Schweins,

Figure 8: The Mechanism of Small G-Proteln Catalysed GTP Hydrolysis

The figure opposite shows the current model of the hydrolysis of GTP, showing the polarised attacking water molecule, and the Mg^{2+} ion as well as the Gln 61, Gly 60 and T 35 residues. The hydrolysis of GTP is initiated by attack of a polarised water molecule on the γ-phosphate. This polarisation is thought to be caused by the Mg^{2+} in the active site. The Mg^{2+} in combination with the protein stabilises the β-phosphate of GTP, which pulls electron density towards it and thus weakens the β-γ bond, encouraging bond breakage. The bound GDP is still stabilised by Mg^{2+} and protein interactions, allowing the terminal P-O bond to be a double bond.

The form of transition state formed during the catalysis is unclear, and is examined in the main text and in Figure 9.

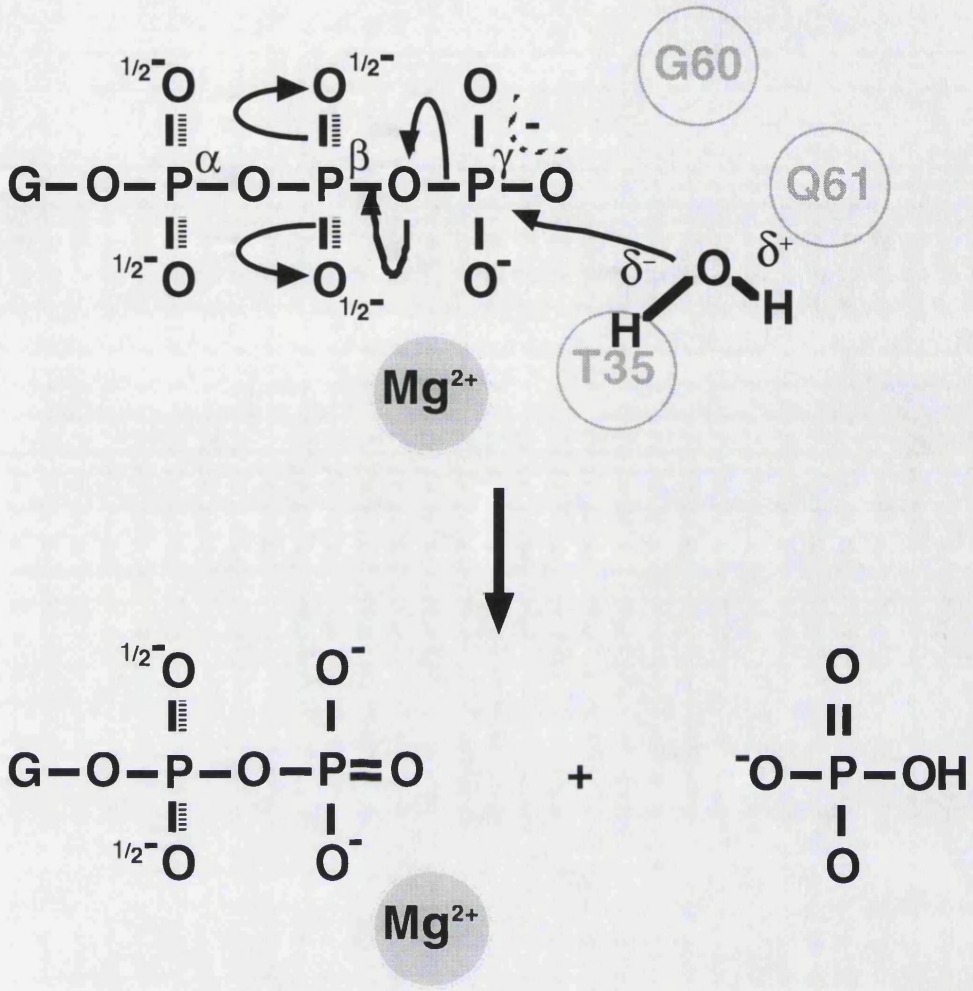
G60
Q61
T35
Mg2+
Mg2+

T., *et al.* 1997).

The polarisation of the water molecule, possibly caused by Mg^{2+} effect on the γ-phosphate, is a critical step in GTP hydrolysis, however the stabilisation of the transition state is also also of crucial importance in the catalytic process. The character of this transition state is able to determine whether the general base step is an influential step in the overall catalysis of the hydrolytic process. The current two models for the transition state in the G Domain of a small G-protein are associative or dissociative (Figure 9).

1.4.2 Transition State Character

A dissociative transition state shows a character dominated by bond cleavage between the leaving group and transition state, and in the case of GTP hydrolysis, negative charge is accumulated on the β-phosphate. The bond to the leaving group is fully or nearly broken, and the bond with the incoming nucleophile is only very small or absent. The conservation of charge is achieved by a loss of charge from the γ-phosphoryl group. In contrast to this, an associative transition state is dominated by bond formation to the attacking nucleophile, with only a small amount of bond cleavage occurring on the leaving phosphoryl group. So, there is a gain in charge on the γ-phosphoryl group. If the transition state was fully dissociative, and since there is little bond formation to the attacking nucleophile, the base catalysis step is of less overall importance. Yet, if it is of associative character, the general base step is of importance to the overall catalysis.

Experimental support exists for both classes of transition state. The associative state appears

Figure 9: The Associative and Dissociative Models of the Transition State

The two models of transition states found in GTP hydrolysis represent extremes of transition state forms. The dissociative transition state is a transition state in which is dominated by the cleavage of the bond to the phosphoryl leaving group. The bond to the outgoing group is nearly or completely broken, whereas the bond to the incoming nucleophile is hardly broken. The associative form of transition state can be contrasted from this since there is a large amount of bond formation to the incoming nucleophile with only a small amount of cleavage of the bond of the leaving group.

Evidence exists for both forms of transition state, and it is likely that the actual transition state is something in between both extremes.

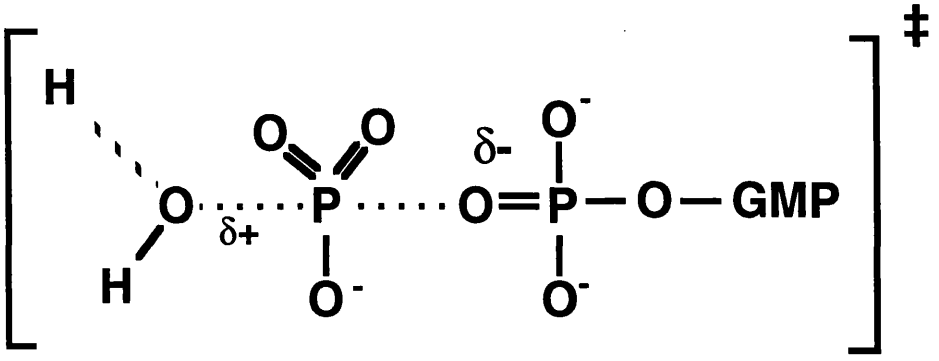

Dissociative

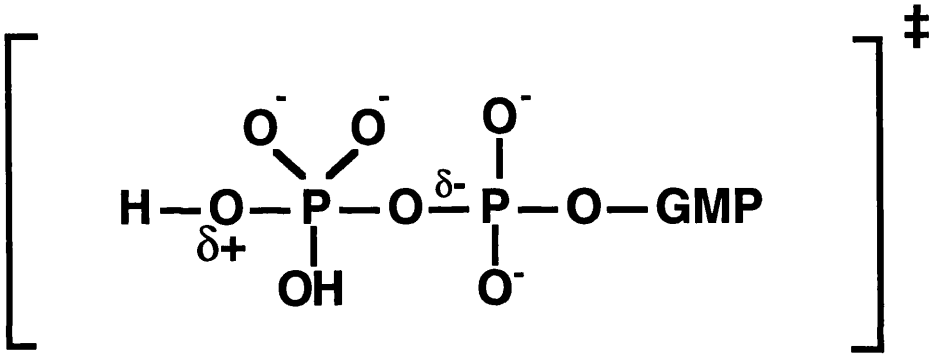

Associative

to be mimicked in a complex of Ras with GAP, GDP, ALF^{4-} and Mg^{2+} (Mittal, R., *et al.* 1996), and linear free energy relationships also support the associative model (Schweins, T., *et al.* 1997). Yet, the dissociative transition state is implicated in solution reactions of many phosphoryl-species, and fourier transform infrared spectroscopy revealed that the transition state is largely GDP-like, i.e. more dissociative in character (Du, X., *et al.* 2000; Cepus, V., *et al.* 1998). Raman spectroscopy studies show that the α-β-phosphate bond is stronger than the β-γ-phosphate bond when GTP is bound to Ras (Wang, J. H., *et al.* 1998), due to the polarisation imposed by the Mg^{2+} on the β-phosphate.

It is most likely that the transition state shares some character of both associative and dissociative transition states.

1.5 GAPs, GEFs and the Effector Protein IQGAP of the Rho Subfamily

Proteins which associate with the small G-proteins can be roughly divided into 2 groups, those which regulate the G-protein's activity, or those which are activated by the interaction and perform some downstream signalling function. These distinctions are not necessarily mutually exclusive.

This section will discuss the function and mechanisms of GAP and GEF regulatory proteins of both the Ras subfamily and the Rho subfamily, since the combined work on these has provided insight into the mechanisms of these proteins. This is then followed by an examination of an effector protein of the Rho subfamily on which sections of this dissertation

are based, IQGAP.

1.5.1 Regulators of Rho Subfamily Activity

Rho family proteins possess the potential to cause cellular malfunction, and so must be tightly regulated. Their relatively slow intrinsic GTP hydrolysis rate means that if left unattended inside the cell, they would remain in an active state for long periods of time, which is exemplified by constitutively active proteins causing oncogenic transformation. Yet, since these proteins function in signalling pathways where a rapid response is often required, their activation must occur on a rapid timescale.

Three families of proteins have evolved to allow the correct function of small G-proteins, GAPs, GEFs and GDI. GEF action exchanges a GTP for a GDP at the G-protein's active site, thus activating it. GAPs act in a way to accelerate the intrinsic hydrolysis of the G-protein and thus hurry its inactivation. GDI proteins bind to the GDP form of the G-protein and prevent both GEF binding and the G-protein's association with the plasma membrane, thus maintaining the protein in an inactive state. Each of the regulatory proteins respond to upstream signals which cause their activation and their effects on the small G-protein.

A previous section in this Introduction has highlighted the differences between the GDP-bound and GTP-bound form of the Rho subfamily proteins, and it is the differences between the two structures which are recognised by these regulatory proteins. These structural studies are complemented by functional analysis, and together they provide detailed information into the mechanism for the regulatory proteins' action.

1.5.1.1 GEFs and the Mechanism of Nucleotide Exchange

GEFs can be classified into families on their sequence and preferred small G-protein target. Most GEFs contain not only a catalytic domain, but also several protein-protein and protein-lipid interaction domains allowing the reception of upstream signals and other effector functions. The GEF-catalysed activation of Rho subfamily proteins is performed by the Dbl family, whose 30 members share a sequence of around 200 residues called the Dbl domain (DH), which is almost always followed by a 100 residue long Pleckstrin Homology (PH) domain, which associates with lipids and acts to localise the GEF to cellular membranes.

The GEF-catalysed dissociation of GDP from a small G-protein is not an active process, but GEFs act to exchange small G-protein bound-nucleotide, and that *in vivo,* GTP replaces GDP is simply a reflection of the 30-fold excess of GTP to GDP within the cell's cytosol. The kinetic barrier to GDP release from a small G-protein is still high, despite this large excess, and so the role of the GEF is to lower this barrier promoting the release of GDP. A simplified GEF reaction scheme is shown in Figure 10.

A number of structures of small G-protein GEFs have been solved, in combination with their small G-protein targets (Liu, X., *et al.* 1998; Aghazadeh, B. *et al.* 1998; Soisson, S., *et al.* 1998). These structures suggest that between GEF families there is little shared structural or sequence homology within their catalytic domains, and the families share no structural homology with any other G-protein interacting proteins, except for the RanGEF, RCC1, which resembles the propeller structure of the β-subunit of heterotrimeric proteins (which

Figure 10: The Conformational Changes During Exchange

The initial proposal of changes in conformation (Hall, A., Self, A., 1986) during nucleotide exchange (*upper panel*) suggest that an activated receptor (R*) binds to a resting Ras•GDP•Mg^{2+} complex (1), which results in the loss of bound Mg^{2+} (2). This complex now takes on a new open conformation, which can freely exchange with GTP (3). The binding of Mg^{2+} to the R*—Ras•GTP complex results in a conformational change of Ras which has high affinity for the Mg^{2+} and GTP, but low affinity for R* (4). The final complex is able to interact with effector molecules and undergo GTP hydrolysis.

Further functional and structural information has enabled a more refined model (*lower panel*), where the GDP•bound state of Ras binds to an activated GEF. The GEF causes a destabilisation of the low affinity Mg^{2+} binding coordination, allowing Mg^{2+} release followed by nucleotide release. The GEF is then able to stabilise Ras in a nucleotide-free form which represents a cation free conformation and is the structural transition between the low affinity Mg^{2+} form of Ras and the high affinity binding form as Ras. On Mg^{2+} and GTP binding with Ras, Ras takes on a high affinity conformation, which causes the release of the GEF, allowing Ras to interact with effectors and undergo GTP hydrolysis.

It is clear that this form of interaction with GEFs is a feature of the entire small G-protein subfamilies, such as Rho, Ras and Rab.

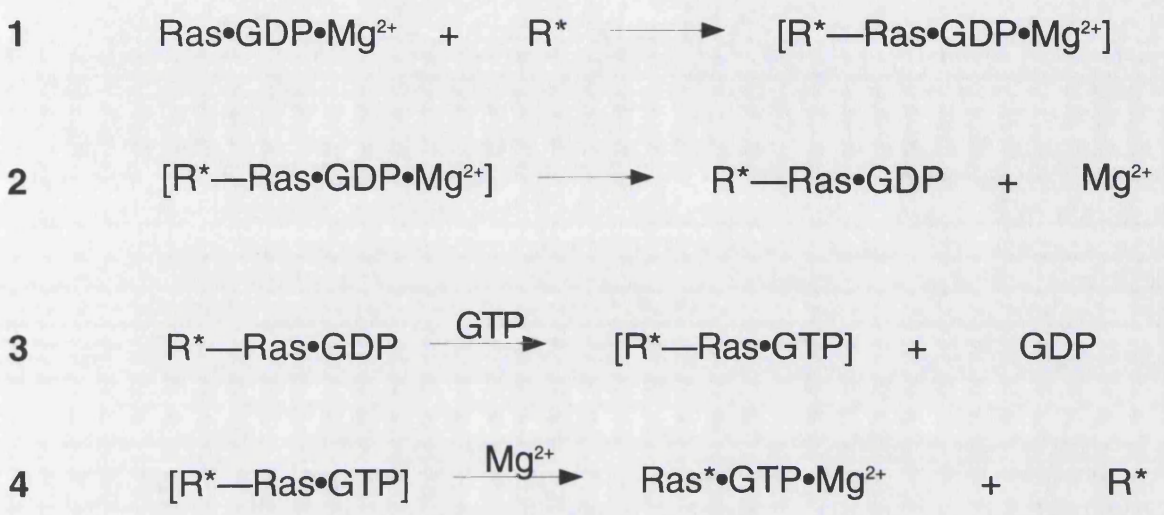

Figure 10a The simple model of GEF-mediated Nucleotide Exchange

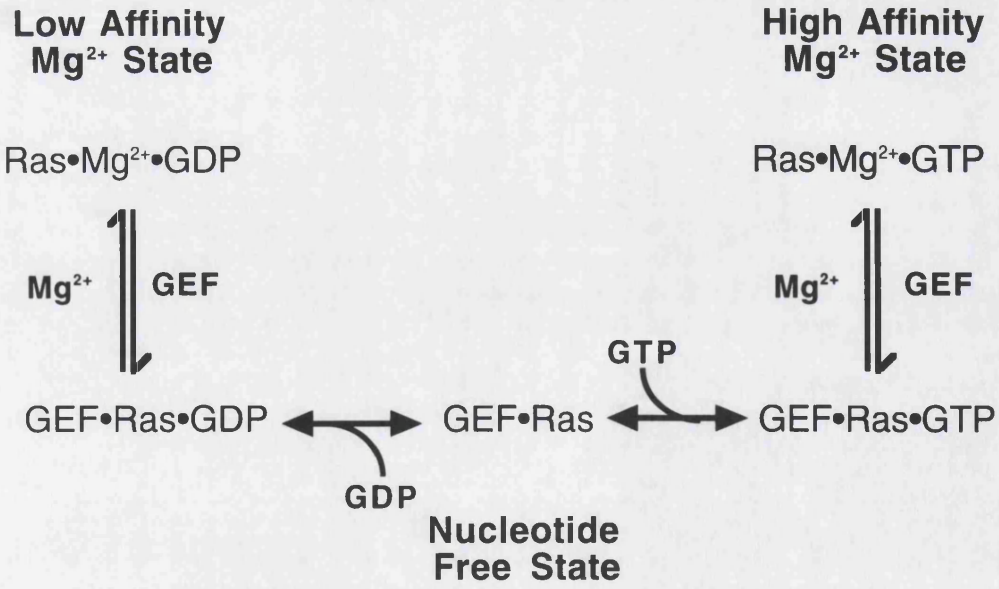

Figure 10b The refined model of GEF-mediated Nucleotide Exchange

acts as a GEF for the α-subunit). The GEF domains are all composed of α-helices, but their number and arrangement are all different (the Dbl domain contains 11 α-helices in a flattened bundle whereas the Cdc25 domain of Sos consists of 10 helices), however the mechanisms by which they induce nucleotide exchange do show some similarity.

Once again Ras subfamily proteins provide a model which can be contrasted to other members of the family, including the Rho subfamily.

The Ras-Sos complex (Corbalan-Garcia, S., *et al.* 1998) shows a large area of interaction between Sos and the P Loop, Switch I, Switch II and a short area downstream of Switch II. The interaction between Switch II and Sos causes the Switch II region to become ordered in comparison to Ras•GDP's Switch II structure. Sos forces part of its Helix H between the main body of the protein and Switch I, which pushes it away from Switch II and the active site (P Loop). A Leu, Glu and Ala residue enter the nucleotide and Mg^{2+} binding sites, salt bridges are made with Ras residues involved in nucleotide binding, and part of Switch II is restructured. The result is that the active site is no longer compatible with binding nucleotide and its dissociation is encouraged from the exposed active site. The structure of Dbl (Liu, X., *et al.* 1998; Soisson, S., *et al.* 1998) suggests that it uses a similar mechanism, by thrusting a conserved Rac/Rho binding helix in-between Switch I and the remainder of the protein, although the specific residue interactions are different. The PH domain and linker segments of Dbl have also been shown to act as part of the interface between Dbl and the G-protein, and that the presence of the PH domain increases the overall GEF activity of the protein.

Although the changes in the active site caused by the action of a GEF result in an inability to bind nucleotide, the disruption of the Mg^{2+} coordination coupled with a stabilising of the nucleotide and Mg^{2+} free state may act as the key elements to accelerating exchange.

The structure of the Mg^{2+} binding site within the G Domain have already been described, but briefly, in the GDP-bound state of Ras Mg^{2+} is coordinated by the β-phosphate of GDP, a conserved Ser/Thr residue and indirectly with other residues via four H_2O molecules. The Mg^{2+} found associated with the nucleotide in Rho subfamily members is coordinated by two Thr residues directly, the β-phosphate and three, rather than four, water molecules (Figure 7). The Mg^{2+} ion is essential for both normal nucleotide binding and hydrolysis, and mutations of the conserved Ser/Thr 17, Asp 57 and T35 (in Ras) (John, J., *et al.* 1993) show increased rates of nucleotide release in both GDP and GTPγS forms, and no longer inhibit nucleotide dissociation by high concentrations of Mg^{2+}, suggesting that the Mg^{2+} is important in both the GDP and GTP bound state. However, studies with Dbl show that GDP dissociation does occur in the absence of Mg^{2+} (Zhang, B., *et al.* 2000), suggesting that displacement of Mg^{2+} is only part of the effect RhoGEFs have on Rho proteins.

Early studies on Ras proteins (Self, A. and Hall, A., 1986) showed that nucleotide exchange in the absence of Mg^{2+} was around 40-fold slower than in the presence of Mg^{2+}. The presence of Mg^{2+} also increased the binding affinity for GTP as compared to GDP by 10-fold. These data suggested that Ras existed in at least two conformations: closed, where exchange occurred very slowly, and open allowing free exchange of nucleotides, yet having

a greater affinity for GTP. The model proposed by this study can be seen in Figure 10.

More recent studies on the protein Rab5 (Pan, J., *et al.* 1996) and the recent Mg^{2+} free structure(Shimizu, T., *et al.* 2000) have shown that Mg^{2+} binding affects both nucleotide dissociation and small G-protein conformation, suggesting that Mg^{2+}'s effect may inhibit GDP dissociation by a chemical affinity to the nucleotide and by imposing structural constraints on the protein molecule. Furthermore, the action of GEF in promoting nucleotide exchange may well be upon the Mg^{2+} rather than the nucleotide directly. The Mg^{2+} may not only impose chemical restraints on the bound nucleotide, but also it could help promote distinct nucleotide-bound structural states, which would suggest the presence of a nucleotide-free state which would lack Mg^{2+} and gain its stabilised conformation from association with a GEF molecule (Figure 10). The distinct states of bound nucleotide, GDP-bound, nucleotide-free and GTPγS-bound forms have been observed through tryptophan fluorescence (Simon, I., *et al.* 1996) in Rab 5 and Rab7, supporting this model.

Once the GEF-nucleotide free state is formed, the binding of GTP into the small G-protein is more likely than binding of GDP since not only is GTP in 30 fold excess in the cell, but the affinity of GTP-bound complexes for Mg^{2+} are at least 10 fold greater than that of the GDP-bound form (Simon, I., *et al.* 1996; John, J. *et al.* 1993; Self, A. and Hall, A. 1986). The inability of certain Rab mutants to adopt the GTP-bound form suggest that correct Mg^{2+} coordination is required to promote further structural rearrangements to reach the fully GTP-bound state.

Figure 11: IQGAP's Domain Organisation

IQGAP was initially cloned and identified due to the homology between it's GAP Related Domain (GRD) and that of other known GAPs, such as RhoGAP and Sar1 (Weissbach, *et al.* 1992). Sequencing of the protein revealed further homology with other protein domains, such as the Calponin Homology Domain, which interacts with the actin cytoskeleton; IQGAP Repeats, of unclear function; WW domain for association with Proline rich sequences; IQ motifs, which associate with Ca^{2+} binding sites; a coiled-coil domain which may play a role in IQGAP homodimerisation.

The *opposite panel* shows the two known isoforms of IQGAP, and shows their considerable domain homology. Sar1 is a GAP from yeast, consisting of mostly a GRD and is shown here to demonstrate the homology between the GRDs of IQGAP and Sar1. Although the protein is shown in a linear form, it is clear that IQGAP is heavily folded into a complex tertiary structure, enabling extensive functional contact between the N- and C-terminal domains.

The gene fragment used in this report is from amino acids 915 to 2331 of the full IQGAP protein, and this is indicated on the diagram *opposite*. The gene fragment is produced fused with a GST fusion protein (for affinity chromatography purposes).

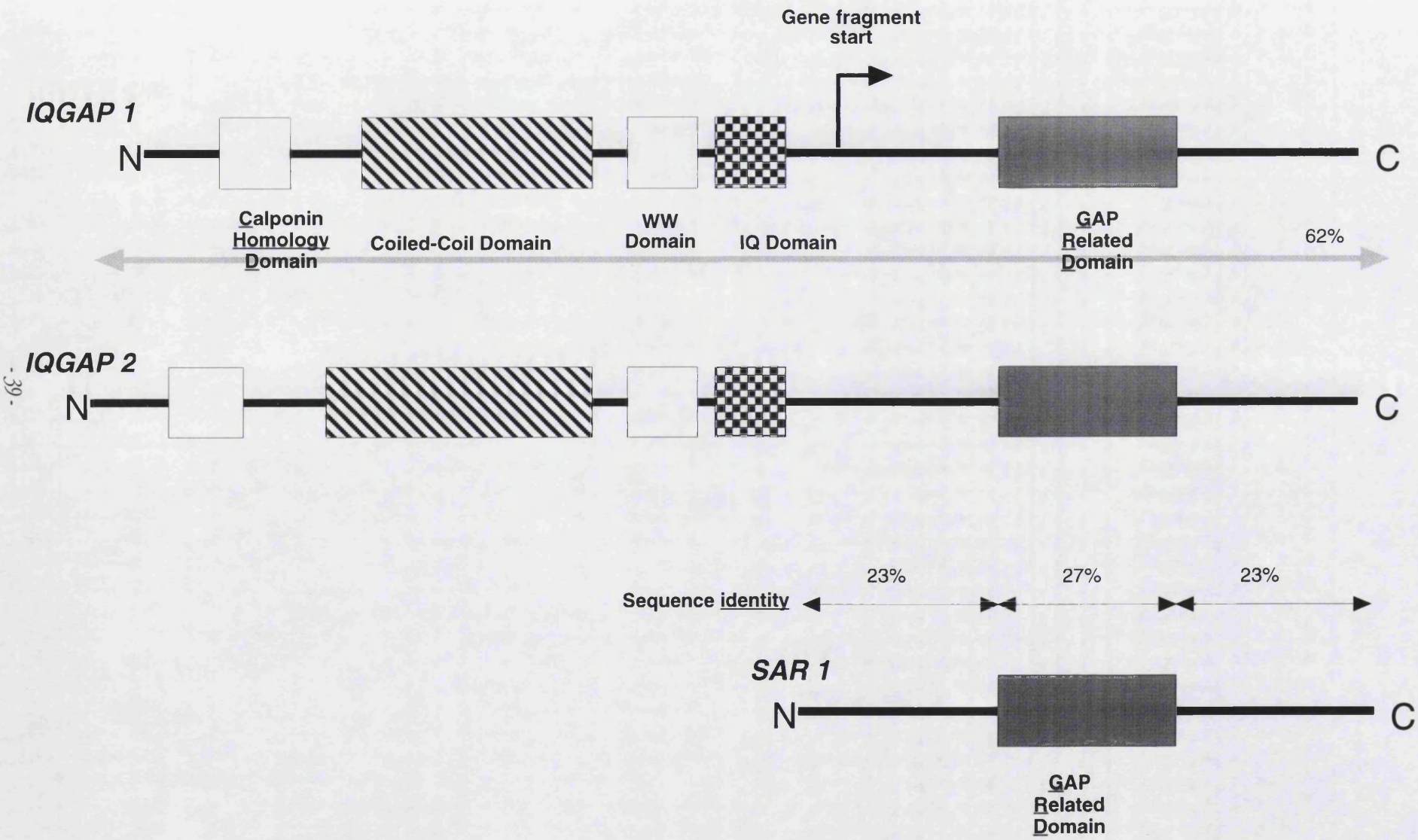
Gene fragment start
IQGAP 1
N
C
Calponin Homology Domain
Coiled-Coil Domain
WW Domain
IQ Domain
GAP Related Domain
62%
IQGAP 2
N
C
23%
27%
23%
Sequence identity
SAR 1
N
C
GAP Related Domain

1.5.2 *GAPs and GTPase Rate Acceleration*

Ras family proteins have a rate of GTP hydrolysis which varies widely between different members, but in comparison with other GTP Binding Protein Superfamily members, they hydrolyse GTP extremely slowly. Under cellular conditions the prolonged presence of GTP-bound forms of small G-proteins could cause cellular transformation, and so they require proteins to accelerate their intrinsic hydrolysis rate to provide a more transient signal. This function is performed by GTPase Activating Proteins, GAPs.

Our understanding of GAPs which act upon small G-proteins has been facilitated by the elucidation of crystal structures of a number of individual GAP molecules, or domains or small G-protein-GAP complexes. (Barrett, T. *et al.* 1997; Scheffzek, K. *et al.* 1996, 1997). There is no apparent structural similarity between RasGAPs and RhoGAPs, other than that they are α-helical bundles, although they do activate their target small G-proteins in a similar fashion.

A RasGAP, p120GAP was crystallised in the presence of Ras•GDP complexed with aluminium fluoride, which mimicked the modelled transition state of GTP hydrolysis (Scheffzek, K. *et al.* 1997). The binding interaction involves a number of residues in Ras, including the P Loop, Switch I and Switch II. Switch I interacts with p120GAP by both hydrophobic and acidic residues and becomes more structured, and Switch II is immobilised by a significant amount compared to either the GDP- or GTP-bound form of Ras. Gln 61, which is found in Switch II and implicated in transition state stabilisation is orientated towards the phosphate chain of the nucleotide and makes contacts with Arg 789 on the GAP. In this sense p120GAP

makes a H-bond network which acts to stabilise a number of Ras residues involved in catalytic steps. This is not the only means by which Ras catalysis is accelerated. Conserved throughout all Ras and RhoGAPs is the FLR motif, and the Arg in this motif has been shown to be essential for GAP's catalytic affects, but not for its binding in both Ras (Brownbridge, G. *et al.* 1993) and p50RhoGAP (Leonard, D., *et al.* 1998). This Arg 903 was shown in the Ras•p120 structure to be inserted into the active site, suggesting that it plays a role in stabilising the negative charge generated in the transition state (assuming a largely associative mechanism, as discussed previously). Crystal structures of heterotrimeric α-subunits show that this Arg is intrinsic to the catalytic site, and is one factor in the increasing hydrolysis rate found in these proteins.

The structure of a p50RhoGAP fragment complexed with the Rho subfamily member CDC42Hs•GMPPNP (a GTP analogue) (Barrett, T. *et al.* 1997) shared a similar mechanism for the increase in rate of GTP hydrolysis, although the overall structure and Rho-GAP interaction is quite different. The nine α-helical bundle exhibits one face which contains residues conserved across the RhoGAP family, and is the likely interaction site between target G-protein and GAP. Several of these conserved residues, a number of Pro and Leu, are important for the structural integrity of the molecule, and Asn 188 and Lys 122 are responsible for a H-bond network with the small G-protein. The remaining completely conserved residue is Arg 85, which is equivalent to Arg 903 in p120GAP. It is essential for high GAP activity. However, in the complex with p50RhoGAP and CDC42, the Arg was not in a correct orientation to be in any way catalytic. Subsequent elucidation of the p50RhoGAP/RhoA structure (Rittinger, K. *et al.* 1997) showed that in this context Arg 85 was

situated in RhoA's active site, forming electrostatic contacts with the transition state analogue, and resembling Arg 789 of p120GAP much more closely. In this complex, Gln 63 (RhoA's equivalent of Rac Gln 61) associated with a H_2O molecule providing stabilisation with the transition state, and Switch I was held in a more ordered conformation.

This difference in the complex of p50RhoGAP with CDC42 and RhoA demonstrates that although many members of the RhoGAP family are able to bind to members of the Rho subfamily, yet their activity towards different members varies. These differences being related to subtle differences in structure, such as in the Effector Loop (Zhang, B. and Zheng, Y. 1998a).

1.5.3 The Rho Subfamily Effector Protein: IQGAP

IQGAP1 was first isolated during a PCR screen to identify members of extracellular matrix metalloproteinases (Weissbach, L. *et al.* 1994). One of the PCR fragments produced during this screen showed homology to the catalytic domain of RasGAPs, such as p120GAP, and this was used to further isolate a complete open reading frame for the gene from human cDNA libraries. The continuous sequence of 7574 base pairs identified contained a single major open reading frame which predicted a protein of 1657 amino acids, and a molecular weight of 190 kDa. Of particular interest was a region which showed a degree of homology with residue positions conserved throughout the catalytic domain of GAP proteins (in IQGAP termed the GRD, GAP Related Domain). These initial observations suggested that IQGAP1 may bind to Ras family proteins, although the effects of its GAP domain on Ras proteins was

not certain. A high degree of homology between IQGAP and the *Schizaccharomyces pombe* protein, Sar1, was observed. Sar1 acts as a GAP for Ras in *S.pombe*, and it was therefore suggested that IQGAP1 may perform this function in mammals.

Further genetic screens in yeast, *Drosophila* and *Dictyostelium* identified other proteins which share significant homology with IQGAP, revealing that IQGAP proteins are a family grouped on the homology between their various characteristic motifs. The IQGAP family currently consists of six members: Cyk1p/Iqgp1 (*Saccharomyces cerevisiae*), GAPA, DRasGAP1, DGAP1 (*Dictyostelium discoideum*), IQGAP1 and IQGAP2 (Human).

IQGAP's initial characterisation not only predicted IQGAP to be a large cytosolic protein, but also that it contained a several protein-protein interaction motifs which indicated that IQGAP may play more roles than just that of interaction with Rho subfamily members.

On the basis of the location of IQGAP's motifs, IQGAP can be divided into two functionally distinct halves, the N-terminus and the C-terminus. The N-terminus contains protein-protein interaction motifs, whereas the C-terminus contains the GRD (Figure 11).

The very N-terminus of IQGAP's sequence contains a Calponin Homology Domain (CHD). The CHD is also present in the RasGAP Vav and actin binding proteins such as spectrin, filamin and fibrin, suggesting that IQGAP is able to bind actin structures. Following the CHD is a number of 50 - 55 residue IQGAP (IR) repeats. The IR motifs are unique and characteristic to the IQGAP family. The number present varies between IQGAP members,

IQGAP1 contains six, and IQGAP2 (an isoform identified expressed predominantly the liver (Brill, S. *et al.* 2000) contains five. The IR motifs currently have no known function. This region of the molecule also has been modelled to exhibit α-helical structure, due to a similarity with proteins such as the myosin heavy chains and intermediate filaments. The function of this putative coiled-coil, helical domain is unclear, although it has been suggested that the region plays a role in homodimerisation between IQGAP proteins. The purpose of such a homodimerisation process is unclear (Bashour, A.-M., *et al.* 1997) — perhaps it is important for intermolecular interactions. To the C-terminus of the coiled-coil/IR motif region is a single WW domain, a novel sequence motif which has been shown to associate with short Proline rich sequences, such as 'PPLP' (Kay, B. *et al.* 2000; Ermekova, K. *et al.* 1997; Macias, M. *et al.* 1996). The final protein-protein interaction domain found in the N-terminus of the protein, are one or more IQ motifs. IQ motifs are a novel Calmodulin interacting domain which have been identified in a variety of unconventional myosins (Goetinck, S. and Waterston, R. 1994; Ayme-Southgate, A., *et al.* 1989), neuromodulin (Chapman, E. R. *et al.* 1991), neurogranin (Baudier, J. *et al.* 1991), Ras-GRF (Farnsworth, C. *et al.* 1995), and IRS-1 (Munshi, H. *et al.* 1996). The IQ motif consists of 23 amino acids, which show a consensus of *IQXXXRGXXXR* (Rhoads, A., and Friedberg, F., 1997; Cheney, R., and Mooseker, M. 1992). The presence of the terminal Arginine residue dictates that Ca^{2+} is not required for the binding of IQGAP to Calmodulin (Houdusse, A. and Cohen, C. 1995). This complete IQ motif can be contrasted with the incomplete IQ motif which lacks the terminal Arginine, and requires Ca^{2+} for the binding to Calmodulin.

The C-terminal domain of IQGAP contains the GAP-related Domain (GRD), which shows

homology between IQGAP family members. The critical Arginine 'finger' used by GAPs (such as RhoGAP and RasGAP) to provided a catalytic contribution to the GTPase is modified in each IQGAP member (IQGAP1 & IQGAP2, a Threonine; DGAP1, a Lysine; GAPA, an Alanine), as well as this, the GAP '*FLR*' motif which provides further GTPase assistance is modified to '*YYR*' in all IQGAP members.

There is currently no known structure of IQGAP, and deriving functional ideas from a linear sequence is both difficult and unwise. Indeed, it is possible that IQGAP will show intra-molecular contacts between distant regions of the same molecule, suggesting a certain amount of overall molecular flexibility, as well as its ability to homodimerise.

IQGAP1 and IQGAP2 have both been shown to associate with the GTPγ-S forms of Cdc42 (McCallum, S., *et al.* 1996) and Rac1 (Kuroda, S. *et al.* 1996), in particular through the Switch I Domain of the GRD and the Insert Loop of the small G-proteins (McCallum, S., *et al.* 1996; Nomanbhoy, T. and Cerione, R. 1999), this being in contrast to proteins which interact via a CRIB motif (such as the PAK family and WASP). Although IQGAP contains a domain related to the catalytic GAP domain of RasGAPs, IQGAP does not exhibit GAP activity towards either Cdc42 or Rac1 – rather it inhibited the activity of both of these GTPases and inhibited their activation by p190RhoGAP (Hart, M., *et al.* 1996). Similarly, DGAP1 was shown to interact preferentially with Rac (although not Cdc42) in its active state (Faix, J. *et al.* 1998), yet unlike other IQGAP family members, DGAP1 neither inhibited Rac's rate of GTP hydrolysis nor activated it. The class of effector proteins which contain CRIB domains (such as WASP), bind to Rho subfamily proteins and also inhibit the rate of GTP hydrolysis.

IQGAP does not contain a CRIB domain and therefore inhibits in a different way — by the use of its GRD.

This inhibitory activity of IQGAP proteins allows them to maintain Rho proteins in their active state, and possibly localise these proteins, or the IQGAPs themselves, to an area of function. The presence of Calmodulin binding IQ motifs suggest that IQGAP may act as a cross-over point between the Rho subfamily and Ca^{2+} signalling pathways. This would presume communication between the two regions of the IQGAP molecule.

IQGAP1 has been found localised to actin structures, ruffling membranes and lamellipodia (Hart, M., *et al.* 1996), as well as associated with Calmodulin at these sites, suggesting that it may play a role in performing cytoskeletal regulation in response to active Rho subfamily members and/or Ca^{2+} levels. It was suggested that the regulation of cytoskeletal interaction with IQGAP may be caused by some form of allosteric changes (Erickson, J., *et al.* 1997), although with respect to actin binding via IQGAP's CHD domain, this interesting hypothesis has no supporting evidence.

Native IQGAP1 can be purified as homodimers and these directly bind to F-actin filaments crosslinking them in irregular bundles (Bashour, A.-M., *et al.* 1997). The binding of IQGAP to F-actin could only be achieved in the absence of Ca^{2+}, suggesting that the association of IQGAP with actin maybe be regulated by Calmodulin and Ca^{2+} levels , rather than regulation by Rho subfamily protein binding, although Cdc42 and Rac were found in these F-Actin • IQGAP complexes. Indeed, Calmodulin was shown to modulate the interaction

between IQGAP1 and Cdc42 (Joyal, J. *et al.* 1997; Ho, Y.-D., *et al.* 1999). In the absence of Ca^{2+}, Calmodulin did not interfere with the association of Cdc42 and IQGAP1, but upon the addition of Ca^{2+}, a dose-dependant inhibition of the IQGAP•Cdc42 association was observed. Since neither Ca^{2+} alone has an effect on IQGAP•Cdc42 association, nor does Calmodulin associate with Cdc42 directly, this effect was therefore mediated through Calmodulin. Ca^{2+}•Calmodulin complexes therefore regulate the interaction of Cdc42 (and Rac) with IQGAP1. On Ca^{2+}•Calmodulin binding, Cdc42 or Rac are released (in their active state) into the cell, which may be a mechanism for localising Rac and Cdc42's effects within the cell. Over expression of Calmodulin has been shown to change cell morphology and shorten the cell cycle, and these functions have also been attributed to Rac and Cdc42, which suggests that IQGAP may play a role in sequestration of the proteins in a ready, active but non-functional state, or act as a form of scaffolding protein and molecular link between the Ca^{2+}, cytoskeletal and Cdc42/Rac pathways.

The critical role of GAPA and DRasGAP1 in the completion of *Dictyostelium* cytokinesis, in which they are necessary for the severing of the midbody (via presumed regulation of the cytoskeleton), suggests a role for IQGAP proteins in such a process (Adachi, H. *et al.* (1997; Lee, S., *et al.* 1998;Gerald, N., *et al.* 1998). A similar actin fibre recruitment function was observed for Cyk1p/Iqgp1 in *S.cerevisiae*. The *Dictyostelium* DGAP1 was shown to be involved in the control of the actin polymerisation-depolymerisation cycle, affecting cell motility and levels of F-actin, rather than any cytokinesis functions (Faix, J. *et al.* 1998). Correct completion of cytokinesis also involves the activity of myosin molecules, and its aberrant function causes irregular cytokinesis in *Dictyostelium*. IQGAP was shown to bind to

myosin Essential Light Chains (ELC) (Weissbach, L., *et al.* 1998), which themselves associate with the neck region of myosin molecules, and it is therefore possible that Calmodulin may regulate IQGAP association with ELC. When IQGAP is released by Calmodulin, IQGAP's binding to ELC is possible which may lead to effects resulting in the completion of cytokinesis. These observations suggest that IQGAP plays an important role in a variety of cytoskeletal processes, depending on the cell type, the organism and the cellular localisation of the protein.

In addition to IQGAP's putative role in regulation of the activity of Rac, Cdc42 and the cytoskeleton during cytokinesis, there is also a large amount of evidence suggesting a similar role in cellular motility and cadherin-mediated cell to cell adhesion (Kuroda, S. *et al.* 1998). Both Rac and Cdc42 are found localised at E-cadherin and β-catenin sites of cell to cell contact (Fukata, M. *et al.* 1999), and IQGAP1 induces dissociation of catenins from these complexes, thus acting in a way as to downregulate cell to cell adhesion. It is the binding of IQGAP1 to β-catenin which induces the dissociation of α-catein from the cadherin-catenin complex (Fukata, M. *et al.* 1999), and thus loss of cell adhesion, presumably achieved by interfering with the helical bundle which forms the α-β-catenin interface (Pokutta, S. and Weis, W., 2000). Activated forms of Rac1 and Cdc42 prevents this IQGAP-mediated inhibition by binding to IQGAP and so promotes junction formation (Fukata, M. *et al.* 1999). In a related role, IQGAP knock-outs have shown that IQGAP1 is critical for maintaining gastric mucosal integrity (Li, S. *et al.* 2000) (Figure 12).

Little quantitative information of the association between IQGAP and Rho subfamily proteins

is known. In the studies by Zhang, B.. *et al.* 1997, it was suggested that the differences in catalytic efficiency of Cdc42, as influenced by CRIB domain containing proteins WASP and PAK1, and IQGAP1 was due to a difference in their K_m values. Furthermore, the affinity of IQGAP for Cdc42•GMPPNP was shown to be 10-fold greater than that of PAK1 and 50-fold greater than that of WASP. Neither IQGAP1, WASP or PAK1 associated with Cdc42•GDP. IQGAP was shown to associate with Rac1•GTP 4-fold less strongly than with Cdc42•GTP (Zhang, B., Chernoff, J., Zheng, Y. 1998), and these binding data confirmed that IQGAP was a potential effector for both Cdc42 and Rac1 *in vivo*. This study also demonstrated that the GAP-catalysed mechanism of hydrolysis involved a fast binding step to Rac1, followed by the rate limiting step of GTP hydrolysis, and it is at this final stage that IQGAPs are likely to inhibit.

1.6 Fluorescence

The methods used in this thesis involve the observation of molecular processes and interactions via monitoring changes in the fluorescence of particular groups (fluorophores), which are attached to the protein either directly or indirectly (such as bound to a nucleotide as part of a protein nucleotide complex). Fluorophores must be environmentally sensitive in order to provide meaningful information on the processes studied (such as conformational changes or changes in bound state), and their change in fluorescence must be of a sufficiently detectable amplitude. The two fluorophores used throughout the majority of the investigation are the well characterised Mant (N-methylanthraniloyl) fluorophore group and the novel MBC (7-Monoethylamino-8-bromocoumarin) group.

Figure 12: The Multi-Functional IQGAP

The current knowledge on IQGAP's cellular functions involves its interaction with Calmodulin and Rho subfamily proteins (Cdc42 and Rac), which have countering effects on the IQGAP molecule. Binding of IQGAP to activated Cdc42 or Rac1 causes dissociation of Calmodulin, and promotes IQGAP's activity to stimulate F-Actin bundling and to promote Cadherin-Catenin complexes leading to loss of cell to cell adhesion. The binding of a Ca^{2+}-Calmodulin complex to IQGAP causes dissociation of active Cdc42/Rac, and allows IQGAP to associate with the Essential Light Chain of myosins, which is though to encourage completion of cytokinesis.

It is clear from the diagram opposite, that IQGAP can play a number of different roles, depending on the proteins with which it is associated, and that this probably represents only the start of our IQGAP understanding.

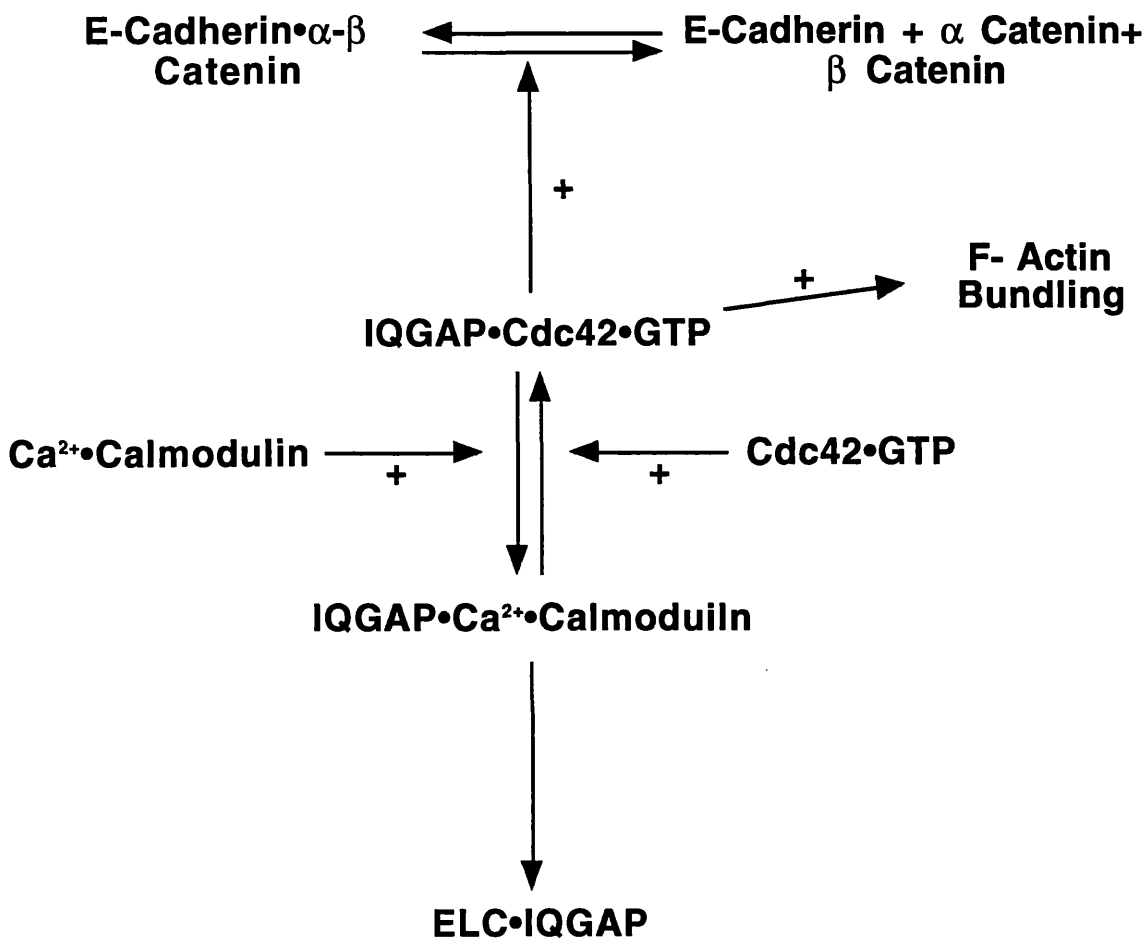
E-Cadherin•α-β Catenin
E-Cadherin + α Catenin+ β Catenin
+
F- Actin Bundling
+
IQGAP•Cdc42•GTP
Ca2+•Calmodulin
+
Cdc42•GTP
+
IQGAP•Ca2+•Calmoduiln
ELC•IQGAP

1.6.1 What is Fluorescence?

Fluorescence is a characteristic of certain molecules (often heterocyclic structures), and is the result of a three-stage process.

The first stage of the process is fluorophore excitation. The fluorophore absorbs energy from a direct source (such as a laser or lamp) or an indirect source (such as energy transferred from another nearby fluorescent group) creating an excited electronic state. This excited state has a finite lifetime, and the length of the excited period is the second stage of the fluorescent process. The excited lifetime is typically around 1 to 10 nanoseconds, and during this time the fluorophore may undergo conformational changes and is able to interact with its surrounding environment. These events result in the energy of the excited state being partially dissipated, and the state relaxes to a lower energy. Not all electrons under go this relaxation, some electrons return to the unexcited ground state through collisional quenching or energy transfer to other systems. The overall loss of energy from the fluorophore gives rise to the Fluorescence Quantum Yield, which represents the fraction of excited electrons returning to the ground state through emission, as compared to the fraction excited initially. The amount of quenching during the excited lifetime affects this value.

The third and final stage of fluorescence is emission, in which the electron in the relaxed energy state returns to the ground state. During this process energy is emitted. Since the energy of the relaxed electron at the end of the second stage, is at a lower level than before its relaxation during Stage one, the photons released have a longer wavelength than the

energy which was used for the initial excitation. The difference between the excitation and emission energy wavelengths is called the Stokes shift, and this value is fundamental to fluorescent techniques, since it allows the emission photons to be isolated from the excitation photons, providing a low background to measurements. This process is illustrated in Figure 13.

1.6.2 The Mant Fluorophore

Mant (N-methylanthraniloyl) is a small fluorophore (Figure 14) which has been widely used in fluorescent investigations with small G-proteins (John, J. *et al.* 1993). The Mant group is attached to the 3' hydroxyl group on the ribose ring of a nucleotide (such as GDP or GMPPNP). There is relatively rapid exchange of the Mant group from the 3'-OH to the 2'-OH, however small G-proteins are only able to bind 3'-OH Mant nucleotides.

The optimum excitation for Mant is by light with a wavelength of 365 nm. The peak emission for Mant is at a wavelength of 440 nm (Figure 15). This large Stokes shift makes Mant a good fluorophore for fluorescence assay in biological systems. The lifetime of Mant is also usually sufficiently long to allow its use in fluorescent anisotropy techniques (Chapter 1.6.4). Mant is also environmentally sensitive to protein-bound conditions: the change in fluorescence of Mant between protein-associated and free environments is sufficiently large to be detectable. Mant is optimally excited by energy of around 365 nm, which allows the Mant fluorophore to be excited by fluorescent energy transfer from Tryptophan residues,

Figure 13: The Process of Fluorescence

The process of fluorescence is illustrated above using a Jablonski diagram. Absorption of energy occurs promoting an electron to a higher energy state (S_1') from its ground state (S_0). During its lifetime, the electron relaxes to a lower energy level (S_1), from which it returns to the ground state by emission of energy.

This emission is of a longer wavelength than the excitation energy, due to the relaxation which occurred during the electron's fluorescent lifetime. The difference between these two wavelengths is the Stokes Shift, and is represented by ($h\nu_{Ex}$ - $h\nu_{Em}$). The greater the size of the Stokes shift, the more the excitation energy can be isolated from the emission energy and therefore the recording of the emission energy can be measured with a low background contribution from the excited energy.

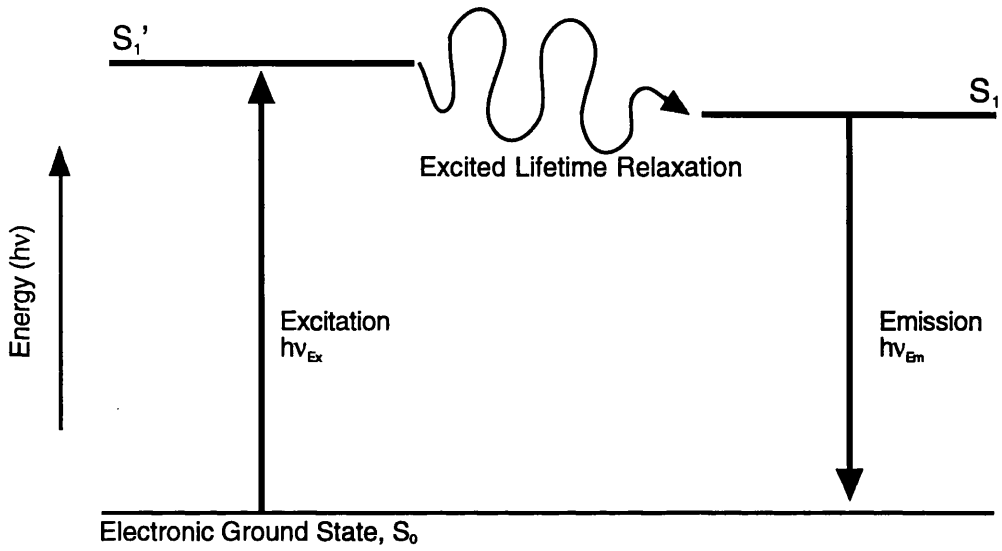

Figure 13 The electronic process of fluorescence

which emit energy at this wavelength. Tryptophan residues within Rac can be excited using energy with a wavelength of 290 nm, and Trp residues proximal to the bound Mant-labelled nucleotide emit energy at 365 nm and are able to excite the nearby Mant group. The considerable difference between the excitation and emission wavelengths for this overall process (excitation at 290 nm and emission at 440 nm) is clearly beneficial for fluorescent measurements.

The presence of Mant bound to a nucleotide does not affect the normal function of the small G-protein. Mant is attached to the ribose ring and this allows it to lie relatively exposed at the mouth of the catalytic site. This location does not interfere with the hydrolysis process, nor with nucleotide exchange. Rac-bound Mant-labelled nucleotides have been shown to exhibit similar kinetic properties to unlabelled nucleotides (Neal, S. *et al.* 1990).

The exposed position which the Mant group is thought to take up on the binding of a labelled nucleotide to a small G-protein, provides a potential method of monitoring proteins which associate with the nucleotide binding region of Rac, such as GEFs and GAPs. A change in the local environment around the Mant (such as on effector binding) causes a change in the overall fluorescence of the group by altering its fluorescent lifetime. This fluorescent change can be measured and related to protein-protein interaction.

1.6.3 The MBC Fluorophore

The 8-bromo-7-monoethylaminocoumarin (MBC) group (Figure 14) is a novel fluorophore,

Figure 14: The Structures of Mant and MBC

The *upper panel* opposite shows the Mant fluorophore attached to the 3'-OH of GMPPNP, the nonhydrolysable GTP analogue. Although the labelled nucleotide is labelled on the 3'-OH during synthesis, there is a certain amount of exchange with the 2'-OH. Small G-proteins do not bind the 2'-OH form of labelled nucleotide. N-methyanthraniloyl (Mant) is a fluorophore of low molecular weight, and its small size of the fluorophore minimises the amount of steric hinderance with the function of the attached nucleotide.

The *lower panel* shows the structure of MBC-GDP, the MBC being attached to the 3'-OH of the ribose ring. Exchange between the 2'-OH and 3'-OH does not appear to occur with the MBC fluorophore, since the fluorophore is attached via an amide bond, [illegible], rather than a carboxyl bond as seen in the MantGMPPNP structure. The fluorophore is larger than the Mant fluorophore, and it is possible that its size may cause steric hinderance.

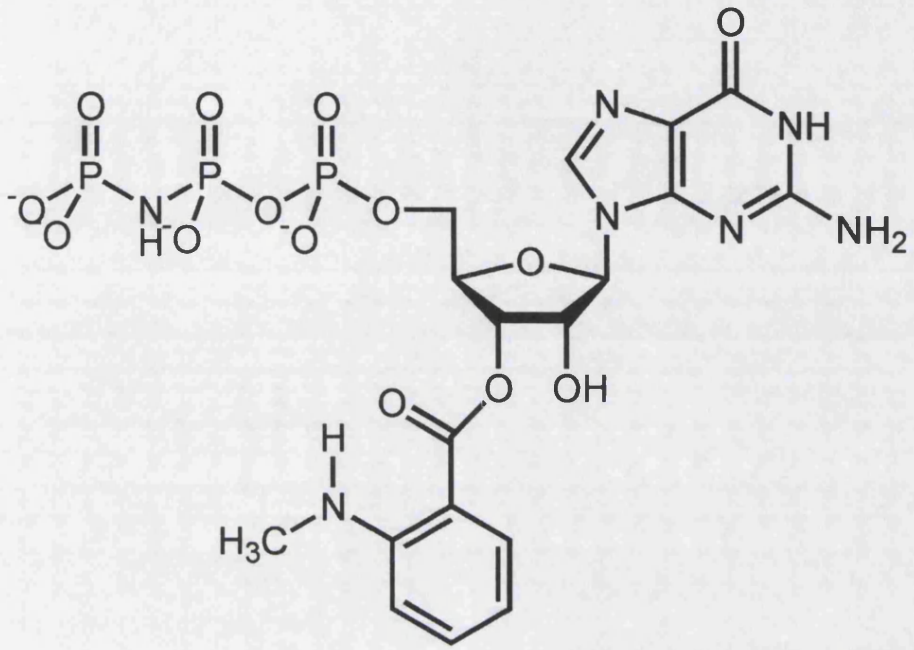

N-methylanthraniloyl GMPPNP (MantGMPPNP)

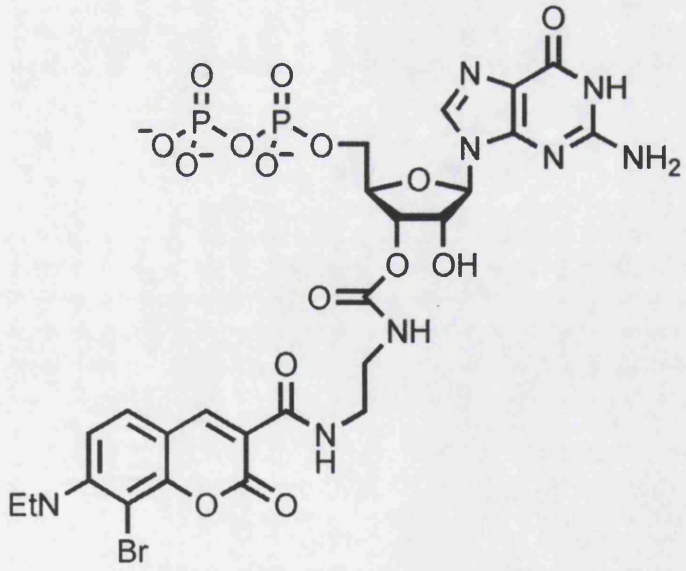

8-bromo-7-monoethylamino GDP (MBCGDP)

Figure 15: The Spectra of Mant and MBC

The Mant group is excited directly by light of 360 nm and emits light at a maximum of 440 nm. However, when the Mant group is attached to a Rac-bound nucleotide it is possible to excite tryptophan residues (belonging to Rac) around the nucleotide binding site. This energy is then transferred to the Mant group by Fluorescence Resonance Energy Transfer (FRET) and the energy emitted at 440 nm. FRET is an interaction which acts in a distance dependent fashion between excited states of two neighbouring molecules. Not only must the two molecules be sufficiently close to allow for FRET, but they must also have an overlapping emission and excitation spectrum.

The *upper panel* shows the emission spectrum of Mant, the excitation spectrum of Rac's tryptophans, and the excitation spectrum of the Mant group directly. The overlap of the two excitation spectra due to FRET is clearly visible.

The *lower panel* shows the maximum and minimum of Rac•MBCGDP fluorophore excitation. It's peak excitation occurs at 406 nm, and peak emission at 460 nm.

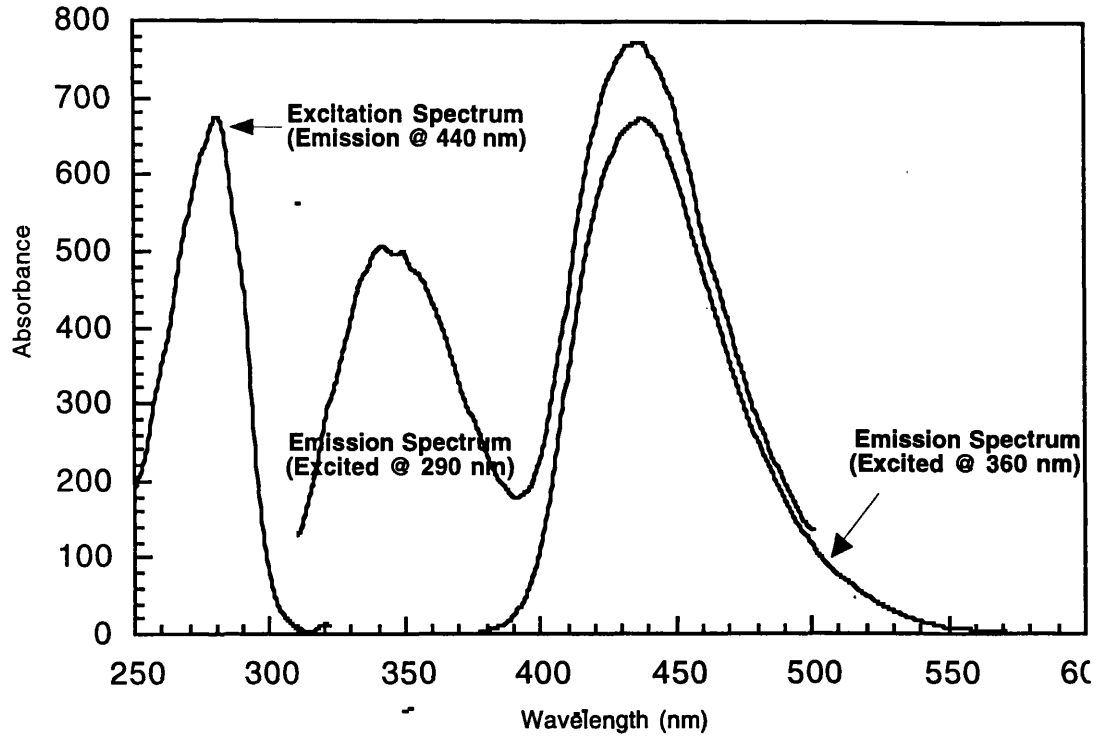

Figure 15a The Excitation and Emission Spectra of Mant

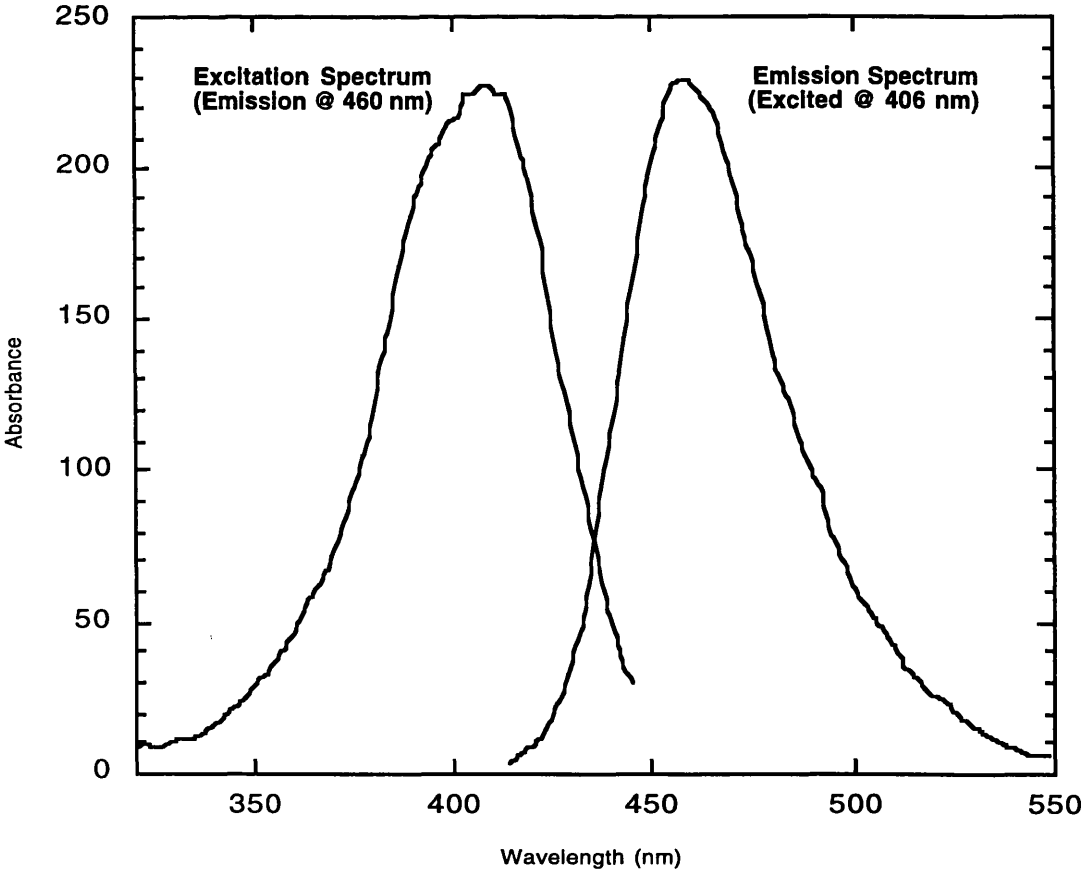

Figure 15b The Excitation and Emission Spectra of MBC

which was synthesised as a potential fluorescent labelling reagent for proteins (Corrie, J., *et al.* 2000). MBC is attached to the 3'-OH group of the ribose ring of nucleotides, in a similar fashion to Mant but shows very slow exchange with the 2'-OH position. The 2'-OH form does not bind to small G-proteins. Little information is known about the MBC fluorophore. It has a high Quantum Yield, and a relatively long fluorescent lifetime, compared to other coumarins, and has a maximum excitation occurs at 406 nm and maximum emission at 460 nm, the Stokes Shift of around 60 nm being characteristic of coumarins. MBC is part of a series of coumarin-nucleotides which are being used to investigate the mechanism and properties of small G-proteins.

The observations of MBC in this thesis suggest that it will be of use in further investigation of small G-protein associations, GTP hydrolysis and nucleotide and Mg^{2+} exchange.

1.6.4 Fluorescent Anisotropy

Light can be considered to be made up of a mix of parallel and perpendicular vectors, which are perpendicular to the direction of propagation. When passed through a polarising crystal the resulting light becomes polarised in a single plane. A fluorophore is able to absorb this polarised light if it is aligned with the polarised light, and be raised to an electronic excited state. During the lifetime of this excited state, the fluorophore rotates, which causes a change in the intensities of the vectors of the emitted light (parallel or perpendicular), and the more random the rotation, then the greater the loss of polarisation The emitted light at these vectors can be measured and used to calculate a value representing a ratio of the light emitted at each of these vectors. This ratio is called Anisotropy, and is calculated using the

equation:

$$r = \frac{(\| - \perp)}{(\| + 2\perp)}$$

Equation 1

Where | | represents the emitted fluorescence of the parallel vector, and ⊥ represents the emitted fluorescence of the perpendicular vector. Anisotropy has two main advantages: it is concentration independent since it is an intrinsic property of the fluorophore; and anisotropy does not rely on catalytically active complexes.

Anisotropy therefore reflects the rotational motion of the fluorophore. If the fluorophore has restricted local motion when bound to a protein, its fluorescent anisotropy will reflect the overall size of the complex, however local motion of the fluorophore, separate from that of the global rotation, can affect the measured anisotropy of a complex. An increase in fluorescent anisotropy represents a decrease in fluorophore rotation, and indicates an increase in complex size. Free Mant-labelled and MBC-labelled nucleotides (GDP or GMPPNP) show an anisotropy value of 0.08. When bound to Rac, these labelled nucleotides show an anisotropy value of 0.16 to 0.18. Binding of Rac complexes to associating proteins causes the anisotropy to increase further as the complex size increases.

Anisotropy is used throughout this thesis to provide a measure of fluorophore complex size, associated or otherwise, to Rac alone or a Rac/IQGAP . It is used to monitor the binding of Rac-labelled nucleotide complexes to IQGAP (Chapter 4), and it is used to provide

information on the movements of fluorescently labelled nucleotides during nucleotide exchange (Chapter 5).

1.7 Aims of this Study

This thesis is centred around the small protein Rac, and investigates a number of aspects of its interaction with the effector protein IQGAP, the process of nucleotide exchange, and a purported self-stimulatory activity.

Using both a novel (MBC: 7-Monoethylamino-8-bromocoumarin) and well characterised (Mant: N-methylanthraniloyl) fluorophore groups attached to Rac-bound nucleotides, the process of nucleotide exchange is explored. Direct fluorescent and fluorescent anisotropy methods provide a method for measuring the release and binding of Mg^{2+} and nucleotides (GDP or GMPPNP) to Rac's active site. Mn^{2+} is used to provide a comparison for the effects observed with Mg^{2+}. Together, the data gathered from these experiments suggest a new model of the process of nucleotide and Mg^{2+} association. This may be of significance for GEF action, but also suggests that MBC may be a productive fluorophore for protein investigations.

A brief investigation of Rac1's C-terminal self-stimulatory ability is described. The effects on Rac's intrinsic GTPase rate was observed using full-length and C-terminal truncated forms of the protein as well as Rac•GMPPNP forms and peptides of Rac's C-terminal tail. In contrast to the previously published data, no significant increase in rate was observed in the presence or absence of the C-terminal tail.

IQGAP has been suggested to associate with Rac1 and inhibit its intrinsic GTPase activity. These observations are investigated in this report. The kinetics of this association are measured using fluorescent and fluorescent anisotropy techniques. The use of a number of Rac mutants in the

potential area of IQGAP association with Rac is assessed. IQGAP exhibits a tight but slow binding with wild type Rac. The mutant studies suggest that IQGAP associates via the Insert Domain and the Effector Loop, and that differently charged amino acids influence this association.

Chapter 2

Materials & Methods

2.1 Cloning of IQGAP from pGEX1 system into pGEX-2T system

The C-terminal domain of IQGAP1 (amino acids 862 to 1658) was initially provided as a GST-tagged fusion protein in the pGEX1 expression system of *Escherichia coli*. For purification purposes, the pGEX1 system only includes a GST-tag at the N-terminus of the fusion protein. In order to obtain protein preparations of greater purity, it was necessary to reclone the gene into a suitable vector containing a Thrombin cleavage site, such as pGEX2T.

2.1.1 Insert and Vector Excision and Ligation

Initial digestion of IQGAP-pGEX1 (0.5 μg) by Xba I (Boehringer) and the pGEX-2T vector (0.5 μg) (Pharmacia) by EcoR I (Boehringer) (2 hours at 37°C in appropriate buffers). These single cut plasmids were blunt-ended by incubation in their respective buffers with the Klenow fragment (Boehringer) (1 hour at 37°C) and $^1/_{10}$ volume of Klenow Buffer (0.5 M Tris.HCl pH 7.6, 0.1 M $MgCl_2$) in the presence of 1 mM deoxynucleotides.

0.1% volume of 3M NaOAc (pH 4.8) and 2x volume of ice cold 100% ethanol was added to the solutions containing the blunt-ended, single-cut fragments, and left for 5 minutes on ice. The fragments were centrifuged for 5 minutes at 13,000 rpm on a Heraeus Biofuge to pellet the DNA. The supernatant was removed and the pellet dried at 50° C for 15 minutes. The pellet was then resuspended in a buffer containing BamH I (Boehringer), and incubated at 37 °C for 2 hours.

50 mM $MgCl_2$, 50 mM dithiothreitol, 1 mM ATP) (Boehringer). The ligation mixture was left overnight at room temperature, and then used to transform XL1 Blue *E.coli* cells (Stratagene).

2.1.2 E.coli Cell Transformation

5 μl of ligation mixture was added to 50 μl of XL1 Blue cells, and left for 20 minutes on ice. The cells were then heat-shocked at 37 °C for 45 seconds, and placed on ice for 2 minutes before addition of 400 μl of warm L-broth and agitated incubation at 37 °C for 30 minutes. 100 μl of the cell suspension was plated on a 10% ampicillin/L-Agar plates in order to screen for transformed colonies. The plates were incubated overnight at 37 °C, and colonies which had grown on the plates the following morning were picked into 30 ml L-broth and further incubated at 37 °C overnight. 10 ml of the cell suspension produced from these starter cultures was centrifuged at 1,400 x g for 20 minutes, and the resulting cell pellet resuspended in 300 μl fresh L-Broth with 50 $\mu g\ ml^{-1}$ ampicillin and 300 μl glycerol. These cell stocks were frozen on dry ice and stored at -80 °C.

2.1.3 Modification of pGIT2 to correct open reading frame

Due to the positioning of the BamH I site in the original vector and gene fragment, the gene insert was out of reading frame with the GST-fusion protein (confirmed by DNA sequencing) preventing the gene's expression.

Two base pairs (cytosine-cytosine) were inserted into the BamH I site region, so as to

maintain both the Thrombin cleavage site and the BamH I site.

Plasmid was purified from the colonies produced in the previous manipulation step, as described below (section 2.1.5). PCR primers were designed complimentary to the Bgl II site in the pGIT2 plasmid [5'—GGGGCCAAGATCTGTCTCAGGGC—3'] and the BamH I site [5'—GGTTCCGCGTGGATCCCCTCCTATGGTTGTGG—3'] containing the correcting insertions (underlined type). The 900 bp stretch of DNA between the two primers was PCRed thus: 10 ng of plasmid, 125 ng of both primers, 200 μM deoxynucleotides mix, 10% Pfu buffer (50 mM KCl, 10 mM Tris.HCl (pH 8.3), 1.5 mM $MgCl_2$) were subjected to 28 cycles of 95 °C (30 seconds), 55 °C (1 minute) and 68 °C (2 minutes). The original plasmid was digested by addition of 1 μl Dpn I to the PCR mixture.

The PCRed fragment containing the mutation and with BamH I and Bgl II sticky ends was then ligated into a BamH I/Bgl II cleaved pGEX2T vector (using the method as described above) and transformed into XL1 Blue *E.coli* cells (as described above). The final construct was called pGIT2 (GAP-IQ-Thrombin-2).

1 μl of PCR mixture was used to transform XL1 Blue *E.coli* cells, and successful colonies were picked to create glycerol stocks (as described in section 2.1.2). These clones were subjected to restriction enzyme digestion tests, protein expression tests and DNA sequencing, to confirm the presence of the vector and insert in the correct orientation and location in the plasmid.

2.1.4 Protein Expression Testing

The predicted size of the GST-IQGAP protein from the DNA sequence is 116 kDa, and is found in post-induction cell lysate and not pre-induction cell lysate of correctly transformed cells. Colonies produced from the final transformation were picked into L-Broth containing 50 μg/ml ampicillin and grown overnight at 37 °C with vigourous shaking. 3 ml of this cell suspension was added to fresh L-Broth, and incubated at 37 °C until the absorbance at 600 nm was equal to 0.8 units. At this point the cells were induced with IPTG to a final concentration of 1 mM and the cell suspension was incubated for a further 4 hours. Samples of pre- and post-induction cell lysate were run on an SDS-PAGE gel to compare the induced proteins of the clones.

The gel produced from a negative and positive (including the clone which was used for subsequent protein preparations) expression test can be seen in Figure 50.

2.1.5 Restriction Digest Testing of Clones

Clones produced from the transformation procedure in Section 2.1.3, were picked into 100 ml L-Broth containing 50 μg/ml ampicillin and grown overnight at 37 °C with vigourous shaking.

10 ml of the resulting cell suspension was centrifuged at 1,400 x g for 20 minutes, the supernatant removed and the cell pellet was resuspended in 200 μl of Solution 1 (50 mM

Tris.HCl pH 7.5, 10 mM EDTA, 100 μg/ml RNase). In order to lyse the cells, 200 μl Solution 2 (200 mM NaOH, 1% SDS) was added and gently inverted for 2 minutes. This solution was neutralised by Solution 3 (1M KOAc pH 4.8), and left for 5 minutes at room temperature. The precipitated protein and genomic DNA was pelleted by microcentrifugation for 5 minutes at 10,000 x g.

The supernatant was passed through a DNA-affinity column, to which the DNA remained bound. The column was washed in 2 ml of Solution 4 (80 mM KOAc, 8.3 mM Tris.HCl pH 7.5, 40 μM EDTA, 55% Ethanol), and then centrifuged at 10,000 x g to remove excess wash solution. 50 μl of H2O was placed in the top of the column, and this was centrifuged at 10,000 x g for 20 seconds to centrifuge the water as it passed through the column and redissolved the DNA. The concentration of the DNA was calculated by measuring the DNA solution's absorbance at 260 nm and 280 nm. This plasmid purification process was performed using the Wizard MiniPrep System (Promega).

Plasmids from successful colonies were subjected to a digestion test of the restriction enzymes, BamH I, Bgl II, Hind III, EcoR I and Nhe III (Boehringer), to test the presence of the correct insert in the correct orientation 0.5 μl of these enzymes were incubated in the presence of their respective buffers and 5 ng of plasmid DNA, in such a way as to reveal digestion patterns which could be related to the predicted digestion patterns of the correct plasmid.

2.1.6 Plasmid Sequencing

The plasmid of a clone which showed both correct digestion patterns and correct protein expression, was subject to DNA sequencing, which was performed by the dye-terminated cycle sequencing method as described previously using primers designed complementary to a sequence upstream of the BamH 1 site. The sequence can be seen in Appendix 1.

2.2 Protein Preparation of C-Terminal IQGAP Fragment

Recombinant C-terminal IQGAP1 was expressed in *E.coli* as a GST-tagged fusion protein using the novel pGIT2 expression system (described above), and induced by IPTG. Thrombin (Calbiochem) cleavage (100 units) of GST-protein bound to a Glutathione-Sepharose (Pharmacia) affinity column allowed the purification of recombinant protein.

Cleaved C-terminal IQGAP preparations did not produce protein large amounts of protein, although the purity of the preparation was increased from the initial clone in the pGEX1 vector (Figure 47).

An overnight starter culture of 100 ml L-Broth (including 50 μg/ml ampicillin) provided the starter cell suspension for the protein preparation. 10 ml of the starter culture was added to 500 ml of L-Broth (containing 50 μg/ml ampicillin, and a total of 8 flasks) at 37 °C. The cells were incubated in a shaking incubator (Brunswick Scientific, 220 rpm) at 37 °C, and on reaching an optical density of 0.8 units at 600 nm, the cells were induced to express the

GST-IQGAP fusion protein, with 1 mM IPTG (Sigma) for a further 4 hours. The induced cells were centrifuged at 4,000 rpm, 4°C for 20 minutes (Beckman JC-HC) and resuspended in 30 ml STE buffer (50 mM Tris.HCl, 100 mM NaCl, 1 mM EDTA, pH 8.0, 1 mM PMSF, 0.5% Triton 100). These cells were subjected to vigourous sonication on ice (180s at 4 kW increasing to 6 kW followed by 50% duty-cycle at 6 kW) and the cell lysate centrifuged at 40,000 rpm for 30 minutes at 4°C (Beckman L-70 Ultracentrifuge, 45 Ti rotor). The supernatant was loaded onto a Glutathione-column (pre-equilibriated with 20 mM Tris.HCl, 50 mM NaCl). The loaded column was washed with a low (20 mM Tris.HCl, 50 mM NaCl) and high (20 mM Tris.HCl, 450 mM NaCl) salt wash. Thrombin cleavage of the column-bound protein was performed in 20 mM Tris.HCl, 200 mM NaCl, and 2.5 mM $CaCl_2$. The protein passing through the column both during loading and cleavage was monitored at 280 nm. The fractions containing the cleaved protein were collected and dialysed into 2 litres of 20 mM Tris.HCl pH 7.6, 100 mM NaCl.

The dialysed solution was concentrated under pressure using an Amicon 10 ml Concentrator and ultrafiltration membranes (Diaflo), with a cut off of 20 kDa. The resulting protein solution was separated into 100 μl aliquots and stored at -80 °C.

The concentration of final protein produced was calculated from Beer-Lambert's law:

$$A = \varepsilon c l$$

where A was the measured absorbance at 280 nm (Beckman DU640 spectrophotometer), ε was the extinction coefficient of IQGAP at 280 nm (calculated from its sequence to be 40,500 M^{-1} cm^{-1}), and l was the cell path length of 1 cm.

2.2.1 SDS-Polyacrylamide Gel Electrophoresis Analysis of Protein Preparation

Samples of pre-induction cell lysate, post-induction lysate, the fast-spin supernatant and cleaved, concentrated protein were added to 50 μl of gel loading buffer (50 mM Tris.HCl pH 6.8, 100 mM dithiothreitol, 2% Sodium Decasulphate, 0.1% Bromophenol Blue, 10% Glycerol). The samples were boiled for 5 minutes at 95 °C and loaded onto a 15% resolving gel. The gel was run in Tris-glycine electrophoresis buffer (25 mM Tris.HCl pH 8.3, 250 mM Glycine, 0.1% SDS) and run a t 18 mV for 1 hour. When complete, the gel was stained in Coomassie Brilliant Blue Dye (0.25 g Coomassie Brilliant Blue R250, 10 ml glacial acetic acid, 45 ml methanol, 45 ml water) for 4 hours with gentle agitation. The gel was destained by soaking it in 50% Methanol:50% Water for 4 hours with gentle agitation, and finally the gel photographed to make a permanent record.

2.3 Rac1 Recombinant Protein Preparation

Rac1 was prepared as described in (Hirshberg, M., *et al.*, 1997), and these preparations were sufficiently pure (Figure 16) for experimentation. The Rac1 protein prepared in this way contains some differences from the wild type protein: the Proline at position 1 is preceded by a Glycine and Serine; and a Phenylalanine is present at position 78 instead of a

Serine. These make no difference to the activity of the protein (Hirshberg, M., *et al.*, 1997). The Rac protein is expressed in a truncated form – the C-terminal tail is missing the last 8 residues after Lysine 184, and the significance of these are alluded to in Chapter 3 of this dissertation.

2.4 Preparation of Rac Nucleotide Complexes

A variety of Rac complexes are used in this study: complexes with different associated nucleotide (GTP, GDP or GMPPNP) or with a different fluorescent label attached to the nucleotide (Mant, the but-eda-coumarin or MBC).

Unlabelled Rac•GTP was used in the assay to measure the effect on Rac's GTP hydrolysis, the measurement being monitored by Phosphate Binding Protein (see Chapter 3). The MBC-labelled complexes, Rac•MBCGTP, Rac•MBCGMPPNP, and Rac•MBCGDP are used to examine the GTP hydrolysis and the binding and release of Mg^{2+} and nucleotide from the respective Rac complexes. These complexes were used in both direct fluorescent measurements and via fluorescent anisotropy. Rac•MantGMPPNP and Rac•MantGDP are used in measuring interactions between IQGAP and Rac via direct fluorescent measurements and fluorescent anisotropy, as well as acting as a second fluorophore system used to monitor the binding and release of Mg^{2+} and nucleotide from the Rac complexes. Rac•CoumarinGMPPNP was prepared and used to examine the interaction of IQGAP with the Rac complex.

The conditions used for complex preparation, involve the presence of excess nucleotide, EDTA and $(NH_4)_2SO_4$. These conditions act to accelerate nucleotide exchange and lower levels of hydrolysis, by lowering the levels of Mg^{2+}. To terminate the exchange process excess Mg^{2+} is added, which complexes with free EDTA and stabilises the bound nucleotide (as described in Chapter 1).

2.4.1 Rac•GTP Complex Preparation

Rac•GTP preparation involved incubating 50 nmol Rac with 500 μM fresh GTP (Sigma), 200 mM $(NH_4)_2SO_4$, 20 mM Tris.HCl (pH 7.6) and 40 mM EDTA. This reaction mixture was incubated for 2 minutes at 30 °C. The exchange reaction was terminated by the addition of ice cold 50 mM $MgCl_2$. The mixture was then passed down a PD10 column (Pharmacia) pre-equilibriated in 1 mM $MgCl_2$ and 20 mM Tris.HCl (pH 7.6) at 4 °C to remove excess nucleotide. Fractions collected were assayed for protein content at 280 nm and frozen in aliquots at -80 °C.

2.4.2 Rac•GDP Complex Preparation

The two Rac•GDP complexes of Mant and MBC were prepared by incubating Rac in the presence of 50- to 100- fold excess nucleotide (MantGDP or MBCGDP), 200 mM $(NH_4)_2SO_4$, 20 mM Tris.HCl (pH 7.6) and 40 mM EDTA at 30 °C for 30 minutes. Excess $MgCl_2$ was then added to the mixture, and the nucleotides passed down a PD10 column and fractions

collected and assayed for protein content and stored at -80 °C.

In some cases Rac•MBCGDP was created by the hydrolysis of Rac•MBCGTP. 50 nmol Rac was incubated in the presence of 200 mM $(NH_4)_2SO_4$, 20 mM Tris.HCl (pH 7.6), 40 mM EDTA and 50-fold excess MBCGTP. This mixture was left at 30 °C for 2 hours to allow all the MBCGTP present to be hydrolysed to MBCGDP. The nucleotide content could be analysed by both HPLC and fluorescence (using the MBC fluorophore itself, see Chapter 1).

HPLC of MBC complexes required 10 μl sample loading in 90 μl of Buffer (75% 0.4 M HPO_4^-, 25% MeOH), onto a PartiSphere HPLC column (Pharmacia) and run on a Waters HPLC system at 1 ml min^{-1}.

2.4.3 Rac•GMPPNP Complex Preparation

The creation of Rac•GMPPNP, Rac•MantGMPPNP and Rac•MBCGMPPNP all followed the same protocol. 100 nmol of Rac was mixed with 5-fold excess of nucleotide (Sigma) in the presence of 20 mM Tris.HCl (pH 7.6) and 12 unit of alkaline phosphatase linked to agarose beads (Sigma). This mixture was rotationally incubated at room temperature for 2 hours, and after completion of the reaction, the mixture was passed down a PD10 column equilibrated in 1 mM $MgCl_2$ and 20 mM Tris.HCl at 4 °C. Samples of the final complex were taken and analysed by HPLC. 10 μl samples were added to 90 μl of running buffer (75% 0.4 M HPO_4, pH 4.0, 25% MeOH buffer (MeOH was not present for Rac•GMPPNP analysis)), centrifuged at 13,000 rpm for 2 minutes, and then run on a PartiSil SAX-10 column

(Whatman) which had been pre-equilibriated with running buffer, at 1 ml min^{-1}. The fractions containing Rac•GMPPNP (labelled or otherwise) were collected and assayed for protein content and frozen in aliquots at -80°C.

2.4.4 Mn^{2+} Rac•GDP and Rac•GMPPNP Complex Preparation

Rac nucleotide complexes in the presence of Mn^{2+} were prepared by substituting $MgCl_2$ for $MnCl_2$ throughout the relevant steps of the complex preparation. The PD10 columns were pre-equilibrated in the presence of 1 mM $MnCl_2$, rather than $MgCl_2$, and experiments were performed in the presence of 1 mM $MnCl_2$ and 20 mM Tris.HCl pH 7.6.

2.5 Single Turnover Rac GTPase Hydrolysis Assay

Single turnover Rac GTPase hydrolysis activity was measured by monitoring the change in fluorescence of labelled Phosphate Binding Protein (MDCC-PBP) (Brune, M., *et al.*, 1994) on binding of free phosphate in solution, as described in Chapter 3.2.

The hydrolysis solution (total volume 200 μl) contained Rac•GTP complex (added last), 15 μM MDCC-PBP, 20 mM Tris.HCl pH 7.6, 1 mM $MgCl_2$ at 30°C. The solution also contained varying amounts of effector or other protein (*e.g.* IQGAP, Rac•GMPPNP, C-terminal peptides) if required. The MDCC-PBP complex was excited at 425 nm and the emitted light was collected at 465 nm on a Perkin Elmer LS-50 fluorimeter. The fluorescence of MDCC-PBP is linear over the first 60% of its saturation by phosphate, and beyond this level data

was not used for analysis. It was therefore beneficial to maintain as little free phosphate in the pre-reaction solution as possible, which was achieved by using a phosphate free buffer composed of both phosphate-free Tris.HCl and water. Rac•GTP and effector proteins were the sole source of free P_i. The data collected during the hydrolysis experiments were fitted to a single exponential curve.

After each set of experiments, known amounts of P_i were added to a solution containing the experimental concentrations of MDCC-PBP, in order to confirm that the decrease in fluorescence observed was due to the decrease in P_i release rate, rather than a capacity limit of MDCC-PBP.

2.6 Fluorescent Measurements of Rac/IQGAP Interaction

The use of fluorescently labelled nucleotide-Rac complexes allows the monitoring of events occurring at the nucleotide binding site and surrounding region. The GMPPNP and GTP labelled forms provide information on the protein when it is in its active state, and the GDP complex provides information on the inactive state. Proteins which associate with Rac proximal to the nucleotide binding site — the location of the fluorescent label — may cause a change in the fluorescence due to the change in the character of the environment, and this change can be monitored on a fluorimeter.

2.6.1 Rac•Mant, Rac•Coumarin Fluorescence and IQGAP

Rac•Mant nucleotide complexes can be excited either directly or indirectly via Fluorescent Energy Transfer. Direct Mant excitation occurs with light of wavelength 365 nm, with emission recorded at 440 nm. Fluorescent energy transfer requires excitation at 290 nm, which excites at least one of Rac's nucleotide proximal tryptophan residues to the Mant group. The overlapping Tryptophan emission and Mant excitation spectra allows FRET to occur, and emission from the Mant group was measured at 440 nm (Figure 15). The but-edaGMPPNP complex was excited at 448 nm and the emission recorded at 491 nm. In both sets of experiments, the complex required 5 minutes to equilibrate with the surrounding solutions.

IQGAP was titrated into a solution of 1 μM Rac•MantGMPPNP or Rac•CoumarinGMPPNP, 1 mM $MgCl_2$, 10 mM $(NH_4)_2SO_4$, and 20 mM Tris.HCl pH 7.6 at 20 °C, and the fluorescence changes measured over time, by exciting at 290 nm, 360 nm, or 448 nm. The data was recorded on a Perkin Elmer LS-50 Spectrofluorimeter.

2.6.2 Labelling of IQGAP with MDCC and IDCC

The C-terminal fragment of IQGAP which is used in this study contains only two Cys residues at fragment positions 414 (immediately after the GRD, which ends at 411) and 678 (124 residues away from the end of the fragment) (see Appendix for sequence). It is unknown where these Cys residues reside in the tertiary structure, however the proximity of Cys 414 to the GRD may prove of use. It is possible to label reactive Cys residues with a

coumarin, such as MDCC as used in the Phosphate Binding Protein, which may then provide a change in fluorescence on molecular interaction. This relies on the Cys being reactive and available for labelling, not buried or involved in a Cys-Cys bridge or other structural interactions. To report on molecular interaction, the labelled Cys must be proximal to the area of binding, so that it undergoes a change of environment leading to a change in fluorescence.

The reactivity of molecular Cysteines can be measured by use of the DTNB Assay. In this process, any reactive Cysteines present on the protein under test react with a DTNB molecule (5,5'-Dithio-bis-(2-Nitrobenzoic Acid) (Sigma), to produce two molecules of nitrophenol. The production of nitrophenol can be observed by measuring the increased absorbance at 412 nm (ε_{412} = 18.8 x 10^3 M^{-1} cm^{-1}). DTNB shows slow self-hydrolysis in solution.

5 μM of IQGAP was incubated in 100 mM Tris.HCl (pH 8.0) in the presence of 2.5 mM DTNB for 5 minutes, and the absorbance at 412 nm then measured against an air blank. A control lacking IQGAP was performed (DTNB hydrolyses slowly by itself at room temperature) and this value was subtracted from the value in the presence of IQGAP. A positive control was performed using NDPK (known to contain 1 reactive Cys residue, kindly supplied by Martin Brune).

To label IQGAP's reactive Cys residue, 25 μM IQGAP was incubated with 5-fold excess (125

μM) of the fluorophore (MDCC or IDCC) in 20 mM Tris.HCl (pH 8.0) for two hours at room temperature. The mixture was then run down a PD10 column pre-equilibriated with 20 mM Tris.HCl (pH 8.0) to separate the free label from the labelled-IQGAP. The fraction containing the labelled protein was collected and assayed for protein and label content. The label concentration and protein concentration were in an approximate 1:1 ratio, suggesting that any available protein had labelled successfully.

2.6.3 Interaction of MDCC-IQGAP with Rac•GMPPNP

Although it is unclear which Cys is labelled in the IQGAP molecule, it is possible that the Cys and label may be proximal to the IQGAP/Rac•GMPPNP interaction site and provide information on the interaction between the two proteins.

The interaction between the two proteins could be followed in a time-resolved fashion on a spectrofluorimeter by following fluorescent changes by exciting at 420 nm and monitoring emission at 468 nm. Excitation of Tryptophan residues at 290 nm, and emission at 468 nm was also followed to observe if any Fluorescent Energy Transfer could occur.

Rac•GMPPNP was added in 0.5 μM aliquots to 2 μM IQGAP in 20 mM Tris.HCl (pH 7.6) and 1 mM $MgCl_2$ buffer at 20 °C, and the fluorescence changes observed by exciting at 420 nm and 290 nm and collecting emission at 468 nm.

2.7 Measurement of Rac/IQGAP Interaction by Anisotropy

A method to measure interaction of RasGAP with Ras by fluorescent anisotropy has been described previously (Brownbridge, G., *et al.* 1993), and a similar method has been utilised here. The principles of fluorescent anisotropy have been described previously, but in essence, changes in anisotropy reflects a decrease in fluorophore rotation which can be related to the complex size to which the fluorophore is bound. On binding of one protein, such as IQGAP, to another, such as Rac, will increase the anisotropy as the rotation rate decreases on complex size.

Two approaches to anisotropy are used to study IQGAP's interaction with Rac — titrations and time-resolved stopped flow experiments.

2.7.1 IQGAP Titrations

Titration of IQGAP into Rac•MantGMPPNP was performed on an Aminco SLM Instrument. Additions of IQGAP on a microlitre scale, using a Hamilton Syringe, into 0.2 μM of Rac•MantGMPPNP complex (20 mM Tris.HCl pH 7.6, 1 mM $MgCl_2$ at 20 °C, total volume of 400 μl) were made every three-minutes. The IQGAP solution was 'spiked' with 0.2 μM Rac•MantGMPPNP, so that dilution of the Rac complex did not occur during the titration. The Mant fluorophore was excited at 366 nm, and the changes in fluorescence on addition of IQGAP to the Rac complex recorded in both the perpendicular and parallel vectors. From the readings of these two channels, anisotropy could be measured.

The anisotropy was calculated as described previously, using the equation:

$$r = \frac{(\parallel - \perp)}{(\parallel + 2\perp)}$$

Equation 1

where r represents anisotropy, $\parallel$ the parallel vector, and $\perp$ the perpendicular vector. Anisotropy is discussed in more detail in Chapter 4.2. The data was recorded manually, and entered into a spreadsheet which calculated the values for r at each titration point. These data were then plotted and fitted to a single binding quadratic curve, and this was used to calculated a K_D for the interaction.

2.7.2 Time-Resolved Stopped Flow Anisotropy

Stopped flow apparatus allows measurement of changes in fluorescence and anisotropy on a rapid time scale. The interaction process of IQGAP and Rac can therefore be monitored directly, and permit calculation of a rate constant for the interaction. A HiTech Scientific SF-61MX Stopped Flow Spectrophotometer was used in the T-formation, allowing data collection from the parallel and perpendicular vectors. The Mant fluorophore was excited at 363.4 nm through 320 nm filters, and data recorded of both parallel and perpendicular vectors by the HiTech software.

Using this technique it is possible to measure both the association and dissociation rates of

the IQGAP/Rac interaction.

Before collection of actual anisotropy data could occur, the anisotropy correction factor (see Chapter 4) must be equivalent to zero. It is possible to balance the parallel and perpendicular vectors (to achieve a correction factor of zero) recorded on the HiTech instrument, by equalising the two readings when the fluorophore is excited by perpendicularly-polarised light. In order to do this, the Rac complex (in one chamber)is pushed against a blank (20 mM Tris.HCl pH 7.6, 1 mM $MgCl_2$, and 20 mM $(NH_4)_2SO_4$) in the other chamber. The voltages across the photomultipliers adjusted until the two readings are equal.

To measure the association rate of the complex, the exciting light is polarised in a parallel direction, and the parallel and perpendicular vectors recorded. The two stopped-flow reservoirs contained: 2 μM Rac complex, 20 mM Tris.HCl pH 7.6, 1 mM $MgCl_2$, 20 mM $(NH_4)_2SO_4$; and 20 μM IQGAP, 20 mM Tris.HCl, 1 mM $MgCl_2$, 20 mM $(NH_4)_2SO_4$ respectively. The solutions were allowed to equilibrate to 20 °C before use.

On rapid mixing the changes in the fluorescence of the parallel and perpendicular vector recorded over varying time frames, and used to calculate anisotropy. The data recorded by the HiTech instrument was processed and the resulting changes in anisotropy plotted against time, and fitted to a single or double exponential.

2.8 Fluorescence Measurement of GTP Hydrolysis, Nucleotide and Mg^{2+} Binding and Release from Rac

Fluorescent techniques have been used to study the exchange of both the Mg^{2+} found associated with nucleotides and the nucleotides themselves from Rac complexes. Fluorescent measurements provided initial observations for the changes in fluorescence for the novel MBC fluorophore, as well as allowing direct observation of MBC's change in fluorescence during the process of GTP hydrolysis. Changes in the fluorescence of the Mant group were too small to be observed under these conditions, however by using the HiTech Stopped Flow fluorimeter, measurement of the changes in fluorescence of both the Mant and MBC were possible.

Stopped Flow fluorescent techniques were used to observe the changes in both MBC and Mant fluorescence, on the binding or release of Mg^{2+} as well as loss of nucleotide from the Rac complex. Not only was direct fluorescence used but, in a similar fashion to IQGAP, fluorescent anisotropy was employed which provided information as to the release of nucleotide from the Rac complex.

2.8.1 Nucleotide, Mg^{2+} Release and Binding

To investigate whether Rac•MBC complexes gave a change in fluorescence on binding or release of nucleotide or Mg^{2+}, the fluorescence of the MBC group was followed over time on a Perkin Elmer LS-50 fluorimeter.

Release of nucleotide and Mg^{2+} was studied in the presence of excess Mg^{2+} in the reaction solution. This ensured that all the Rac was complexed with Mg^{2+}. 2 μM of the Rac•MBC complex (GDP or GMPPNP) was incubated with 20 mM Tris.HCl pH 7.6, 20 mM $(NH_4)_2SO_4$, and 1 mM $MgCl_2$ at 30 °C. Micromolar concentrations of EDTA (to remove both free and complex-bound Mg^{2+}) were titrated into the Rac solution, and 200 μM GDP was added to commence nucleotide exchange as the final step in the titration. Changes in fluorescence of the MBC group were followed by exciting at 406 nm and emission at 460 nm

Changes in MBC fluorescence on Mg^{2+} binding to a Mg^{2+}-free Rac•MBC complex were also measured under similar conditions. 0.5 μM Rac•MBCGDP or Rac•MBCGMPPNP complex was incubated at 30 °C in the presence of 20 mM Tris.HCl pH 7.6, 20 mM $(NH_4)_2SO_4$ and 1 mM EDTA. Changes in MBC fluorescence on Mg^{2+} titration into this solution were measured by excitation at 406 nm and emission at 460 nm.

2.8.1.1 Comparison of Affinity of Binding between MBCGDP and GDP

This study examines the role of Mg^{2+} in the process of nucleotide exchange, using the novel MBC fluorophore. To validate the experiments described, it is necessary to confirm that both MBCGDP and GDP bind to Rac with equal affinity. This was accomplished by use of the stopped-flow apparatus. One reservoir contained 0.2 μM Rac•GDP (in 20 mM Tris.HCl pH 7.6, 10 mM EDTA, and 20 mM$(NH_4)_2SO_4$), and the other contained a concentration ratio of MBCGDP and GDP with a total concentration of 1 μM (in 20 mM Tris.HCl pH 7.6, 10 mM

EDTA, and 20 mM$(NH_4)_2SO_4$). A range between 1 μM MBCGDP: 0 μM GDP and 0.025 μM MBCGDP: 0.975 μM GDP was used. On rapid mixing, the amplitude of the change in fluorescence was observed (excitation at 403.4 nm, using 435 nm filters). The change in fluorescence can be plotted (as a fraction of the change at 1 μM Rac•MBCGDP) against the MBCGDP:GDP ratio, and the data fitted to a simple binding curve.

If equal binding between the two nucleotides occurs, then a 50% fluorescent amplitude change will occur when the MBCGDP:GDP ratio is to 1.

2.8.2 Monitoring of GTP Hydrolysis by MBC Fluorescence, MDCC-PBP Fluorescence and HPLC

1 μM Rac•MBCGTP was incubated with 20 mM Tris.HCl pH 7.6, 20 mM $(NH_4)_2SO_4$ and 1 mM $MgCl_2$ at 30 °C. The change in fluorescence of the MBC fluorophore was monitored by excitation at 406 nm and collecting emission at 460 nm, on a Perkin Elmer LS-50 Fluorimeter. These represented the maxima of the excitation and emission spectrum (Figure 15). The data collected was fitted to a first order exponential, to give a first order rate constant.

This method was repeated, but in the presence of 15 μM MDCC-PBP and by exciting the MDCC bound to the MDCC-PBP with 450 nm light and collecting the emission at 470 nm. This allowed the rate of GTP hydrolysis to be monitored by following the fluorescent

changes in MDCC-PBP. In order to see what magnitude of fluorescence MBC contributed to the changes of fluorescence at these wavelengths, the same experiment was performed in the absence of MDCC-PBP. In both cases date was collected and fitted to a first order exponential to give a first order rate constant.

The progress of GTP hydrolysis of Rac•MBCGTP was also followed by HPLC. 1 μM Rac•MBCGTP was incubated in the presence of 20 mM Tris.HCl pH 7.6, 20 mM $(NH_4)_2SO_4$, 1 mM $MgCl_2$ at 30 °C (total volume of 200 μl), and 10 μl samples taken at various time points. The samples were added to 90 μl of running buffer (75% 400 mM HPO_4 (pH 4.8), 25% CH_3OH) and injected onto a PartiSphere HPLC column (Whatman), pre-equilibriated in running buffer, running at 1 ml min^{-1}. The levels of GTP or GDP present were calculated by integration of the respective peaks on the HPLC trace. These values could be plotted against their sampling time and a single exponential curve fitted.

2.8.2.1 Mg^{2+} and Nucleotide Release Measured by Stopped Flow Fluorescence and Fluorescent Anisotropy

In order to observe the exchange processes of the Mg^{2+} and nucleotide bound to Rac, Rac•GDP and Rac•GMPPNP complexes were required in Mg^{2+} bound and Mg^{2+} free states. These separate conditions were created in the reservoirs of the HiTech device.

2 μM Rac•GMPPNP or Rac•GDP (MBC or Mant labelled) was incubated in one chamber with 20 mM Tris.HCl pH 7.6, 20 mM $(NH_4)_2SO_4$, at 30 °C. If Mg^{2+} free conditions were

desired, 10 mM EDTA was present, whereas if Mg^{2+} bound form of Rac complexes were required, 0.5 mM $MgCl_2$ was present.

In the second chamber of the stopped flow device, 200 μM GDP, 20 mM Tris.HCl pH 7.6, 20 mM $(NH_4)_2SO_4$, and 10 mM EDTA were incubated at 30 °C. The instrument setup is illustrated in Figure 17. If necessary the EDTA concentrations in either of the reservoirs could be changed. For experiments involving Rac•MBCGMPPNP in its Mg^{2+}-free state, concentrations of EDTA were increased to 40 mM and 60 mM. The reason for this is explained in a later section.

Single pushes of these solutions were recorded over varying time scales to provide data on both short and long time scales. The MBC fluorophore was excited by light at 403.4 nm (using 435 nm filters), and Mant fluorophore at 363.4 nm (385 nm filters). Data was recorded by the HiTech software and data fitted to either single or double exponential fits by this software.

The HiTech instrument also allowed observation of anisotropy changes under the conditions described above. The instrument was used in T-format (as described in section 2.7.3), which allowed data collection from parallel and perpendicular vectors. This data was then processed to give changes in anisotropy (as described previously and using Equation 1) on nucleotide and Mg^{2+} exchange. Anisotropy changes were recorded for both the Mant and MBC fluorophores using the same wavelength of exciting light (although polarised) and

Figure 17: Stopped Flow Analysis

The panel opposites represents the set-up for the stopped flow experiments, for observing Mg^{2+} and nucleotide exchange. The two reservoirs contain different solutions, which when rapidly mixed cause nucleotide exchange.

Reservoir 1 contains the Rac complexes. Condition 1 represents Mg^{2+}-free conditions, where excess EDTA has caused sequestered Mg^{2+}. M* represents the fluorophore, either MBC or Mant, and the associated nucleotide was either GDP or the GTP analogue, GMPPNP. Condition 2 represents the Mg^{2+}-bound form of Rac, created by ensuring Mg^{2+} excess and therefore Mg^{2+} associated with the Rac complex present.

Reservoir 2 contains excess GDP and excess EDTA.

These conditions ensured that when rapidly mixed, nucleotide exchange was observed and the changes in fluorescence during this process could be observed.

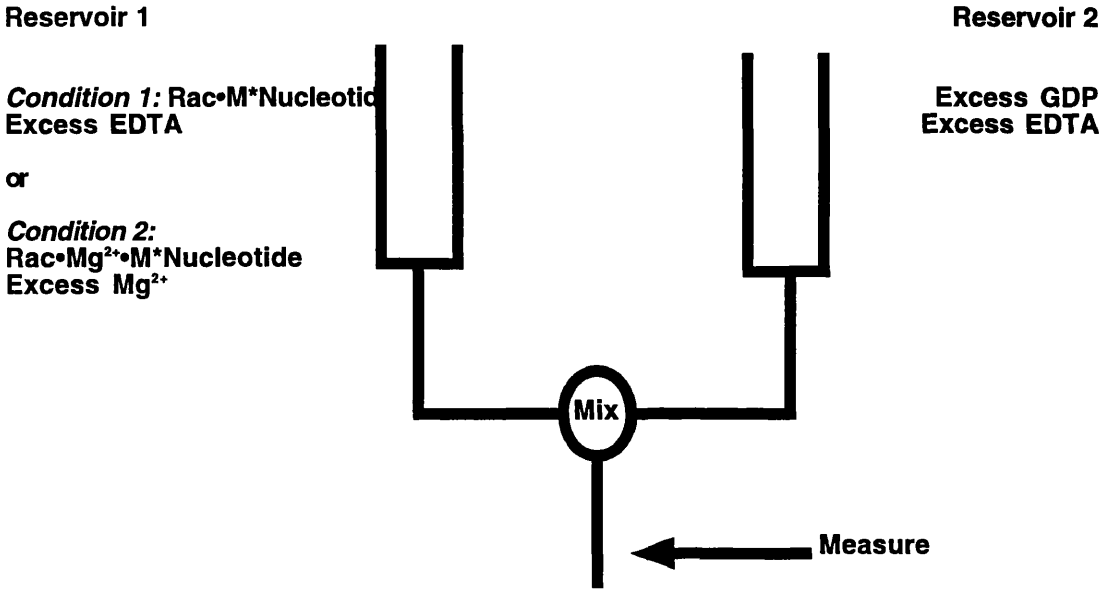
Reservoir 1
Reservoir 2
Condition 1: Rac•M*Nucleotid
Excess EDTA
or
Condition 2:
Rac•Mg2+•M*Nucleotide
Excess Mg2+
Excess GDP
Excess EDTA
Mix
Measure

filters for both the parallel and perpendicular vectors (MBC filters 455 nm). The anisotropy correction factor was zeroed using the Rac complex pushed against a buffer blank, and the two channels balanced by using light polarised in the perpendicular direction. Measurements were made using light polarised in the parallel direction.

The data recorded on the separate channels were processed and the changes in anisotropy were plotted against time.

2.8.2.2 Mg^{2+} Binding Measured by Stopped Flow Fluorescence

The apparent sensitivity of the MBC fluorophore allowed Mg^{2+} binding to be observed by direct fluorescence on a rapid time scale using the HiTech stopped flow instrument. The process of Mg^{2+} binding to Rac complexes was observed for both Rac•MBCGDP and Rac•MBCGMPPNP complexes in their Mg^{2+} free states. To produce a Mg^{2+} free state of the Rac complex, incubation with EDTA was required, however, the concentration of EDTA required for this for each of the complexes was unknown.

Titrations of EDTA into 1 μM Rac•MBCGDP or Rac•MBCGMPPNP complexes, were performed in a Perkin Elmer LS-50 fluorimeter and the fluorescent changes monitored by excitation at 406 nm and emission at 460 nm. These measurements provided the concentrations of EDTA needed to remove bound Mg^{2+} from the complexes, which were used in the stopped flow procedures.

0.5 μM Rac•GDP, 20 mM $(NH_4)_2SO_4$, 20 mM Tris.HCl pH 7.6, 15 μM EDTA were pushed against varying concentrations of $MgCl_2$ in 20 mM Tris.HCl, 20 mM $(NH_4)_2SO_4$, and the change in MBC fluorescence monitored by excitation at 403.4 nm (filter 435 nm, 30 °C). Rac•MBCGMPPNP experiments used solutions containing 0.5 μM Rac•GMPPNP, 20 mM Tris.HCl pH 7.6, 20 mM $(NH_4)_2SO_4$, 500 μM EDTA and were pushed against varying concentrations of $MgCl_2$. The changes in fluorescence monitored by excitation at 403.4 nm.

Chapter 3

The Self-Stimulatory Activity of Rac1

3.1 Introduction

3.1.1 Rac1's Self-Stimulatory Activity

The small G-protein Rac1 has an approximately 10-fold higher intrinsic rate of GTP hydrolysis in comparison to other small G-proteins, such as Ras and RhoA. Previously these differences had been attributed to residues outside of the conserved G Domain core in small G-proteins, but within proximity to the active site, as described previously in Chapter 1. Changes in these amino acids between different small G-proteins was suggested to sufficiently modify the characteristics of the active site, so as to allow for the variable intrinsic GTP hydrolysis rates (Ménard, L. and Snyderman, R., 1993). Recent investigations (Zhang, B., *et al.* 1998 & 1999), have suggested that there may be other determinants for this increased GTPase activity within the C-terminal tail.

The C-terminal tails of Rho subfamily G-proteins show an overall positively charged nature, and are the regions within the subfamily which show the most divergence between members (Figure 18). These tails are posttranslationally modified *in vivo*, by the attachment of lipids by a family of dedicated transferases. This lipid attachment provides the tail with the ability to associate with lipid bilayers, and thus localise Rho subfamily proteins to their area of action at the membrane. This lipid modification also allows certain subfamily members to interact with RhoGDI proteins (Scheffzek, K., *et al.* 2000; Hoffman, G., *et al.* 2000; Longenecker, K., *et al.* 1999). Part of the interaction between GDI and the G-protein involves the C-terminal tail, which extends over the surface of GDI, where the lipid is held within a hydrophobic pocket in the GDI molecule (Scheffzek, K., *et al.* 2000; Longenecker,

Figure 18: Rho family C-terminal Homology

Sequence comparison between a number of different small G-proteins reveals a degree of conservation for several residues in the C-terminal polybasic tail (indicated by underlined type), notably an particular arginine. The presence of this conserved arginine (marked *opposite* with an arrow) has been correlated with the self-stimulatory ability of the active forms of the GTPases.

From the *table opposite*, it can be seen that Rac1 contains this Arginine residue and was also shown to demonstrate a self-stimulatory GTPase activity (Zhang, *et al.*, 1998; Zhang, *et al.*, 1999). It is a confirmation of this self-stimulatory activity which forms the basis for Chapter 3.

		Self-Stimulatory?
RhoA	R R G K K K S G C L V L	
RhoB	S Q N G C I N C C K V L	
RhoC	R K N K R R R G C P V L	√
RhoG	T P I K R G R S C I L L	√
TC10	I G S R C I N C C L I T	
Rac1	P V K K R K R K C L L L	√
Rac2	P T R Q Q K R A C S L L	√
Cdc42H	P E P K K S R R C V L L	√
N-Ras	T Q G C M G L P C V V M	

Adapted from Zhang, B., *et al.* (1999) *J.Biol.Chem.*, **274** 2609-2612

K., *et al.* 1999). This keeps the C-terminal tail in an extended and ordered form. Both crystal and NMR structures have shown that the C-terminal tail is generally unordered and mobile when the protein is not complexed with other proteins.

The work by Zhang, B., *et al.* suggests that the C-terminal tail of specific Rho subfamily proteins may have another role conferring an ability to dimerise and stimulate the activity of the intrinsic GTPase

GTPγS forms of Cdc42, Rac2 and RhoA were isolated by gel filtration as both monomeric and homodimeric complexes, whereas N-Ras•GTPγS and C-terminal deletion mutants of RhoA and Cdc42 were only eluted as monomers. This suggested that the C-terminal tail of Rho subfamily members may be important for homodimerisation. Furthermore, conformational or environmental changes in the active site of Cdc42•GDP were demonstrated by a change in Mant fluorescence on mixing ternary complexes of Cdc42•MantGDP, AlF_4^{2-} and Cdc42•GTPγS, presumably caused by its association with Cdc42•GTPγS. The presence of AlF_4^{2-} (which is thought to associate and form a transition state analogue) also enhanced the binding of GST-immobilised Cdc42•GTPγS to soluble Cdc42•GTPγS, further suggesting that homodimers could form between Rho small G-proteins, in the same nucleotide state.

A number of Rho subfamily proteins contain a conserved Arg in their C-terminal tail (equivalent position of Arg 186 in Cdc42Hs), including RhoC, Rac1, and Rac2 (Figure 18). Other Rho subfamily proteins do not, e.g. RhoA, RhoB, and TC10. This Arg residue (and

surrounding residues) was suggested to be a potential mediator of the observed homodimerisation effects. The intrinsic GTPase rates of RhoA, RhoB and RhoC were measured in order to investigate the importance of this conserved Arg residue. RhoA and RhoB were shown to have a relatively slow, concentration-independent intrinsic GTPase rate (comparable to Ras), whereas RhoC showed a drastic increase in rate constant on dose increase — a rate constant of 5×10^{-4} s^{-1} at 2 μM and a rate constant of 2×10^{-3} s^{-1} at 40 μM (at 23 °C), with a noticeable doubling by 5 μM RhoC (8×10^{-4} s^{-1}) from the rate constant at 2 μM, and a 4-fold increase at 10 μM RhoC.

Not only did RhoC show a higher basal rate of GTP hydrolysis than RhoA and RhoB, but it also demonstrated a 1.5-fold increase in rate in the presence of RhoC•GTPγS, which was not observed for in similar experiments for RhoA and RhoB.

The GTPase activity of Cdc42 proteins from *Homo sapiens*, *Drosophila melanogaster* and *Caenorhabditis elegans* were examined due to their differing inherent C-terminal sequences. Cdc42Hs and Cdc42Dm both contain Arg 186, whereas Cdcd42Ce contains Lys at this position. As predicted, Cdc42Hs and Cdc42Dm showed a higher basal rate (3-fold) of GTP hydrolysis compared to Cdc42Ce, as well as being affected by the presence of Cdc42•GTPγS. The geranylgeranylation of the C-terminal tail at the CAAX motif, as found *in vivo*, did not affect the stimulatory effect.

These data support a model for the increased GTPase rate of Rac1 and other Rho subfamily

proteins, involving the C-terminal tail providing an Arg finger to aid catalysis. These studies do not mention the biological significance or relevance of the reported self-stimulatory activity. In resting cells, Rho subfamily proteins such as Rac1, Rac2 and Rho are found associated with GDI in their GDP-bound form. It is possible that IQGAP proteins may also bind to these Rho proteins and hold them in their GTP-bound form. As soon as they are released it is almost certain that they interact with other effectors such as GAPs and GEFs. Interaction between two similar Rho members may be feasible, but it is unclear as to the function this process could have. A study into the strength of Rho subfamily dimerisation might clarify the kinetically favoured binding partner.

This Chapter presents a brief investigation of Rac1's putative self-stimulatory activity, by monitoring its GTPase activity *in vitro* by fluorescent methods. The use of a full length Rac1 expression system and a truncated Rac1 expression system (missing the last 12 C-terminal amino acids) to produce full length and truncated versions of Rac1 allows a direct comparison of the importance of the C-terminal tail in this activity. Peptides mimicking the C-terminal sequence are also used to assess any increased GTPase activity in their presence, as are nonhydrolysabe GTP analogues (GMPPNP) used to mimic the overall Rac1•GTP bound form.

Throughout this Chapter, observations of GTP hydrolysis in the presence of full length or truncated Rac or C-terminal peptides showed no significant increase on Rac's intrinsic GTPase rate, contrary to the results suggested previously by (Zhang, B., *et al.* 1998, 1999).

3.1.2 Phosphate Binding Protein

The ability to measure the rate of GTP hydrolysis in a solution in real-time without interfering with the hydrolysis reaction itself, is provided by a fluorescently labelled Phosphate Binding Protein (MDCC-PBP) (Brune, M. *et al.* 1994, 1998). PBP is an *E.coli* protein, which is expressed under conditions of low levels of inorganic phosphate (P_i), and scavenges for free P_i, transporting it to the cytoplasm. PBP has an overall clam-like fold resembling two hinged domains forming a binding cleft between them. The P_i binds within this cleft causing a large conformational change as these two domains close to bind the P_i between them. A single Cysteine residue was introduced into PBP at position 197, on the lip of one of the hinged domains, which allowed selective labelling with a fluorophore, N-2[2-(1-maleimidyl)ethyl]-7-(diethylamino)coumarin-3-carboxamide (MDCC) at this position. The resulting labelled MDCC-PBP gives an approximate 7-fold increase in fluorescence at 465 nm on saturating levels of P_i. The binding of P_i to MDCC-PBP is both fast, 1.36×10^8 M^{-1} s^{-1}, and tight, K_D around 100 nM. These properties make MDCC-PBP excellent for studying GTP hydrolysis, since it is able to bind to free P_i released at low levels (sensitive to nanomolar ranges), rapidly and in an, effectively, unidirectional manner. The binding also provides a large, detectable increase in fluorescence.

MDCC-PBP is used in GTP hydrolysis assays through this thesis.

3.2 Materials and Methods

Rac1•GTP and Rac•GMPPNP complexes of both truncated and full length Rac1, were prepared as described in Chapters 2.4.1 and 2.4.3 respectively.

The method of measuring the rate of GTP hydrolysis is described in Chapter 2.5, and was performed here by monitoring the change in the fluorescence of PBP by excitation at 425 nm and recording the emission at 464 nm at 30 °C. As the method used measures the amount of P_i produced by the GTP hydrolysis, the levels of free P_i were kept to a minimum by using phosphate-free Tris.HCl buffer (pH 7.6) and a P_i free water source. Rac1•GTP complexes were stored at -80 °C after their preparation in small aliquots since Rac-mediated GTP hydrolysis was observed to occur throughout a day's experimentation even if the complex was kept on ice.

3.2.1 Rac•GTP Titration Experiments

The model proposed by Zhang, B., *et al.* suggests that increasing the concentration of Rac1 present in solution will show an increase in the GTP hydrolysis rate constant, as long as the C-terminal tail is present. In normal situations the rate constant of hydrolysis would not increase as the concentration (of enzyme) is increased, rather the observed rate of hydrolysis would increase.

Varying concentrations of full length and truncated Rac1 were incubated in 20 mM Tris.HCl

(pH 7.6), 1 mM $MgCl_2$ and 15 μM of PBP at 30 °C. The increases in fluorescence produced were recorded and analysed by fitting them to a single exponential. The data produced is an average of at least three separate experiments.

3.2.2 Rac•GMPPNP Stimulated Rac•GTPase Activity

The presence of nonhydrolysable analogues (GTPγS) has been shown to increase the GTP hydrolysis rate constant (Zhang, B. *et al.*, 1999). The use of Rac•GMPPNP forms can be used to investigate this. Full length Rac•GMPPNP should provide the correct determinants to increase the rate of both truncated Rac1•GTP and full length Rac1•GTP complexes, whereas a truncated Rac•GMPPNP complex should not be able to provide these C-terminal determinants and so not cause an increase in rate constant.

Varying concentrations of full length or truncated Rac1•GTP were incubated with equimolar or excess of full length or truncated Rac•GMPPNP in the presence of 20 mM Tris.HCl (pH 7.6) and 1 mM $MgCl_2$ and 15 μM PBP (30 °C). The increases in fluorescence produced were recorded and analysed by fitting them to a single exponential. The data produced is an average of at least four separate experiments.

3.2.3 Rac•GTP Hydrolysis in the Presence of C-terminal Peptides

Whole Rac molecules locked in a GTP-bound state by the GMPPNP analogue, were examined to see if they could provide the necessary determinants which are supposed to provide stimulatory determinants. Incubation of Rac1•GTP complexes, both truncated and

full-length, with peptides of the C-terminal residues will demonstrate whether these peptides alone are sufficient for an increase in Rac1's GTPase activity.

Two peptides were used to mimic the C-terminal tail, a '9-mer' PVKKRKRKC, and a '12-mer' PVKKRKRKCLLL. 1 μM Rac1•GTP (full length or truncated) was incubated in 20 mM Tris.HCl (pH 7.6), 1 mM $MgCl_2$ and 15 μM PBP with 1 μM or 10 μM of peptides. The increases in fluorescence produced were recorded and analysed by fitting them to a first order exponential fit. The data produced is an average of at least three separate experiments.

3.3 Results

3.3.1 Rac•GTP Titrations: Truncated and Full Length Rac

Analysis of the hydrolysis rate constant of increasing Rac•GTP concentrations, both of the truncated and full length forms, allow the self-stimulatory activity mediated by the C-terminal tail to be examined. If the C-terminal tail plays a role in self-simulation of Rac's GTPase then increasing concentrations of Rac•GTP should show an increase in the GTP hydrolysis rate constant.

Figure 19 shows a typical curve obtained from data from the GTPase assay. The increase in fluorescence is due to the binding of free P_i by Phosphate Binding Protein. This P_i being produced from Rac-mediated GTP hydrolysis. Table 1 shows the concentrations of truncated

Figure 19: Rac•GTP Hydrolysis Curve

The *figure opposite* shows a typical data set produced from the Rac•GTPase assay using Phosphate Binding Protein, as described in Chapter 2.

In the example, 5 μM of truncated Rac•GTP was incubated with 15 μM Phosphate Binding Protein at 30 °C in the presence of 20 mM Tris.HCl pH 7.6, 1 mM $MgCl_2$. The increase in fluorescence observed here is due to the binding of free P_i (produced from GTP hydrolysis) to free PBP in solution. The data was collected on a Perkin Elmer LS50B fluorimeter and then fitted to a single exponential curve to produce a rate of reaction, k_{obs} = 3.0 x 10^{-3} s^{-1}.

The trace begins here at 200 fluorescent units due to P_i already present in solution being bound by PBP before the initiation of GTP hydrolysis.

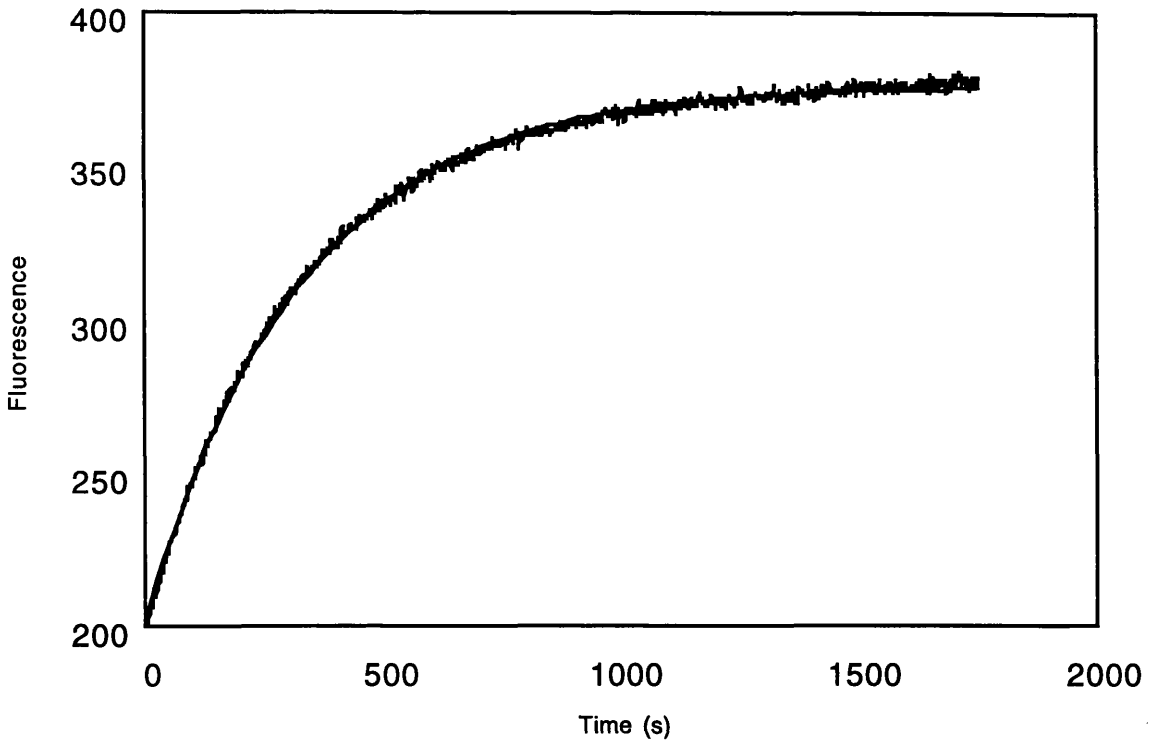

Figure 28 Fluorescent Increase on Rac•GTP Hydrolysis

Table 1: Full Length and Truncated Rac1GTP Hydrolysis Rates

Full Length Rac1•GTP

[Rac1•GTP] μM	k_{Obs} s^{-1}
0.5	3.0×10^{-3}
1.0	2.9×10^{-3}
2.5	2.9×10^{-3}
5.0	3.5×10^{-3}
7.0	4.0×10^{-3}
25	8.0×10^{-3}

Truncated Rac1•GTP

[Rac1•GTP] μM	k_{Obs} s^{-1}
0.2	1.8×10^{-3}
1.0	2.6×10^{-3}
2.5	3.0×10^{-3}
3.0	3.0×10^{-3}
5.0	3.0×10^{-3}
10	3.4×10^{-3}

Data are averages of at least 3 separate experiments.
Data was collected at 30 °C, in the presence of 20 mM Tris.HCl, 1 mM $MgCl_2$, 15 μM PBP.

Rac2•GTP*

[Rac2•GTP] μM	k_{Obs} s^{-1}
3	0.5×10^{-3}
6	0.9×10^{-3}
9	1.2×10^{-3}
15	1.5×10^{-3}
20	1.83×10^{-3}
40	2.2×10^{-3}

* Data from: Zhang, B., Zheng, Y. *J. Biol. Chem.* (1998) **273**, 25728-25733

RhoC•GTP§

[RhoC•GTP] μM	k_{Obs} s^{-1}
2	0.2×10^{-3}
5	0.8×10^{-3}
10	1.2×10^{-3}
20	1.7×10^{-3}
40	2.0×10^{-3}

§ Data from: Zhang, B., Zheng, Y. *J. Biol. Chem.* (1999) **274**, 2609-2612

and full length Rac•GTP with the rate constants observed (k_{Obs}) at their respective concentrations, and also shows the rate constants found in previous studies (Zhang, B., *et al.* 1998, 1999) as a comparison (Rac2 and RhoC).

The rate constants of GTP hydrolysis observed for truncated Rac•GTP shows no significant increase from 1 μM to 10 μM Rac•GTP (2.6×10^{-3} s^{-1} and 3.4×10^{-3} s^{-1} respectively). The rate constant of 0.2 μM truncated Rac•GTP is approximately 50% of the rate observed at 10 μM (1.8×10^{-3} s^{-1} and 3.4×10^{-3} s^{-1} respectively). Full length Rac•GTP titrations show little increase of GTP hydrolysis rate constant over concentrations of Rac from 0.5 μM to 7 μM (3.0×10^{-3} s^{-1}), yet 25 μM Rac•GTP is almost 3-fold greater than the GTPase rate constant at a Rac•GTP concentration of 0.5 μM (8.0×10^{-3} s^{-1} and 3.0×10^{-3} s^{-1} respectively).

The data does not indicate significant increases in rate constants with an increase in Rac•GTP concentration.

3.3.2 *Rac•GMPPNP Stimulated Rac•GTPase Activity*

Incubation of full length Rac•GTP with full length Rac•GMPPNP, a non-hydrolysable Rac•GTP analogue, would be expected to increase the rate of GTP hydrolysis on increasing concentrations of Rac•GMPPNP, since more C-terminal tail determinants are available to aid hydrolysis — in a similar fashion to increasing Rac•GTP concentrations as described in 3.4.1, but titrations of Rac•GMPPNP into a single Rac•GTP concentration should show an increase in rate constant.

Table 2 shows the rate constants of GTP hydrolysis of 5 μM full length Rac•GTP in the presence of varying concentrations of full length Rac•GMPPNP. With no Rac•GMPPNP present, 5 μM full length Rac•GTP has a rate constant of 3.5 x 10^{-3} s^{-1}. In the presence of 1 μM Rac•GMPPNP (full length), the rate constant is 3.2 x 10^{-3} s^{-1}, 5 μM Rac•GMPPNP the rate constant is 2.9 x 10^{-3} s^{-1}, 10 μM Rac•GMPPNP the rate constant is 2.6 x10^{-3} s^{-1}, and 15 μM Rac•GMPPNP the rate constant is 2.6 x 10^{-3} s^{-1}. These data show that in the presence of full length Rac•GMPPNP, the rate constants of hydrolysis by full length Rac•GTP drops 20% (3.2 x 10^{-3} s^{-1} to 2.6 x 10^{-3} s^{-1}).

5 μM truncated Rac•GTP was incubated with 5 μM and 10 μM full length Rac•GMPPNP, and the rate constant of GTP hydrolysis measured as described. In the absence of any Rac•GMPPNP, truncated Rac•GTP hydrolysed GTP with a rate constant of 3 x 10^{-3} s^{-1}. In the presence of 5 μM full length Rac•GMPPNP this rate constant was 2.5 x 10^{-3} s^{-1}, and in the presence of 10 μM full length Rac•GMPPNP the rate constant was also 2.5 x 10^{-3} s^{-1}. In a similar fashion to that shown by full length Rac•GTP, the presence of truncated Rac•GMPPNP causes the rate constant of GTP hydrolysis to drop by around 16%.

Two peptides representing the terminal 9 (9-mer) and 12 (12-mer) amino acids of the C-terminal tail were also incubated in the presence of 1 μM full length Rac•GTP, at varying peptide concentrations. In the presence of equimolar concentrations of 12-mer, the rate constant of GTP hydrolysis was 3.3 x 10^{-3} s^{-1}, and 9-mer, the rate constant was 2.5 x 10^{-3} s^{-1}. 1

Table 2: Titrations of Rac1•GTP with Rac1•GMPPNP

5 µM Full Length Rac1•GTP

Full Length [Rac•GMPPNP] µM	k_{Obs} s^{-1}
1	3.2×10^{-3}
5	2.9×10^{-3}
10	2.6×10^{-3}
15	2.6×10^{-3}
0	3.5×10^{-3}

5 µM Truncated Length Rac1•GTP

Full Length [Rac•GMPPNP] µM	k_{Obs} s^{-1}
5	2.5×10^{-3}
10	2.5×10^{-3}
0	3.0×10^{-3}

Data is an average of at least 3 separate experiments.
Data was collected at 30 °C, in the presence of 20 mM Tris.HCl, 1 mM $MgCl_2$, 15 µM PBP.

μM full length Rac•GTP was incubated in 10-fold excess of peptide, and for the 12-mer this gave a rate constant of 3.2 x 10^{-3} s^{-1}, and for the 9-mer the rate constant was 3.5 x 10^{-3} s^{-1}.

Titration experiments with increasing Rac•GTP concentrations, incubation with Rac•GMPPNP and C-terminal peptides do not show any major trend in an increase of GTP hydrolysis rate constant. The increasing concentrations of full length Rac•GTP show only a small increase in GTP hydrolysis rate constant, as does increasing concentrations of truncated Rac•GTP. The presence of full length Rac•GMPPNP caused a slight decrease in the rate constants of both full length and truncated Rac•GTP, and the presence of peptides representing the C-terminal tail showed no stimulatory effect on the GTP hydrolysis rate constant.

3.4 Discussion

The evidence presented by Zhang *et al.* suggests a model for the relatively higher intrinsic rate constants for some Rho subfamily members over other members and other subfamilies. The involvement of the C-terminal tail which provides both a catalytic determinant, to cause an increase in hydrolysis, and a structural determinant, to allow protein-protein homodimerisation is a compelling one for the Rho subfamily members they investigate (RhoC, Cdc42, Rac2, RhoA and RhoB), since it seems to concur with details known about the action of GTPase Activating Proteins. The conclusions they draw suggest an important activity for the C-terminal tail of Rho subfamily proteins, and this chapter describes an

investigation into the significance of the C-terminal tail of Rac1.

The results described in section 3.4.1 and summarised in Table 1, show that similarly to the results presented by Zhang *et al.*, Rac1 shows little increase in rate constant as the concentration of either truncated Rac1 or full length Rac1 is increased. The increase observed in previous reports (up to 8-fold increase) is of a greater magnitude over measured concentrations, than observed in this report (up to 2.5-fold increase). These two sets of data presented both in this report and by Zhang, B., *et al.*, show no significant kinetic differences.

The presence of Rho subfamily GTP-analogues, such as Cdc42•GTPγS was shown to increase the GTP hydrolysis rate constant and to allow the formation of homodimers (Zhang, B., *et al.* 1999). The C-terminal tail was suggested to be of importance in these activities. In this report GTP-analogues (Rac1•GMPPNP) of both the truncated Rac1 and full length Rac1 protein were used to investigate this property of Rho subfamily proteins in their active states. Incubation of truncated forms of Rac1•GMPPNP and Rac1•GTP, would not be expected to show an increase in rate constant, since they lack the C-terminal tail necessary for any increase in GTP hydrolysis. On the other hand, full length forms of Rac1•GMPPNP and Rac1•GTP, which contain the C-terminal tail, would be expected to show some form of increased GTP hydrolysis as the concentrations of Rac•GMPPNP were increased. The results presented in section 3.4.2 show that, both truncated and full length Rac•GTP do not show any increase in rate constant on the addition of truncated or Rac•GMPPNP full length

The incubation of the C-terminal peptides, as described in section 3.4.2, with full length

Rac•GTP would also be expected to provide the C-terminal determinants (as suggested by Zhang, B., *et al.*) and show an increase in GTP hydrolysis — only if the C-terminal tails are necessary and sufficient for the stimulatory activity. The presence of these peptides made a negligible difference on the rate constants observed for full length Rac1.

The investigations described in this report, using Rac1, show that the measured GTPase rates do not differ significantly from those measured by Zhang, B., *et al.*

The rate constants observed in this study for Rac1 and those measured in Zhang, B., *et al.*, are shown in Table 1. This table of data shows that for related proteins, such as Rac1 and Rac2, the difference in rate constants is not significant. Although small differences between the data exist, the overall data is within an order of magnitude and therefore consistent with each other. The differences that are present in the data could be due to temperature effects — this study measures at 30 °C, Zhang, B., *et al.* at 23 °C — or due to the different methodology used to measure the GTP hydrolysis. Previous measurements of Rac1's intrinsic GTP hydrolysis at different temperatures, show rate constant for GTP hydrolysis of 4.8×10^{-3} s^{-1} (20 °C) and 6.5×10^{-3} s^{-1} (37 °C) (Bernard, A., *et al.* 1992), which is consistent with the data presented here. The MESG system used by Zhang, B., *et al.* has been used previously (Webb, M., and Hunter, J., 1992) and provided data that is also consistent with

the data presented here and in Zhang, B., *et al.* The slight differences between the data presented here and in Zhang, B., *et al.* may be due to variations in the actual protein concentrations present, or variations in the active protein concentration, as well as variations in the efficiency of the GTP nucleotide loading onto Rac. From the data presented here Rac1 does indeed have a higher GTPase hydrolysis compared to other Rho subfamily proteins, although the importance of the C-terminal tail in this process is unclear.

Zhang, B., *et al.* have suggested that it is a specific Arg residue involved in this stimulation of catalysis, in a similar fashion to the process used by GAPs to promote catalysis. It has been shown that this 'Arg finger' is not the only residue involved in stimulation of GTP hydrolysis by GAPs (Sermon, B., *et al.* 1988) and so the ability of a single Arg residue, present in the C-terminal tail, to stimulate GTP hydrolysis to levels similar achieved by a complete GAP molecule would be quite unlikely.

The presence of bound nonhydrolysable GTP analogues, such as GTP-γS, were shown to increase the rate of hydrolysis of RhoC, Rac2 and Cdc42 to that almost equivalent to the rate of G-proteins in the presence of an active GAP (8-fold), and this current study demonstrated GTP hydrolysis levels which were consistent with previous work. The hypothesis that Rho subfamily-bound GTP analogues are activatory via their C-terminal tail, suggests that the C-terminal tail becomes activated in some way in the active state. It is possible that in a GDP-bound form the C-terminal tail is sequestered by the G-protein

preventing its activatory ability. In the GTP-bound form the C-terminal tail somehow becomes active, and is able to perform its putative role. Both crystal and NMR structures have shown that in both GDP- and GTP- forms of Rho subfamily proteins, the C-terminal tail is essentially very mobile and unstructured. This suggests that there can be little or no change in C-terminal tail structure or molecular-associations between the two states of the proteins. This further suggests that both GDP-bound and GTP-analogue-bound forms of Rho subfamily proteins would be able to stimulate GTP hydrolysis of susceptible Rho subfamily proteins (such as Rac2). The GDP forms of the proteins were not observed to have this ability by Zhang, B., *et al.*

The presence of the C-terminal peptides had no effect on the rate of GTP hydrolysis, which may be expected if the C-terminal tails are not directly involved in the dimerisation process (but are involved in hydrolysis acceleration), or if certain structural characteristics are required in the C-terminal tail, which would almost certainly not be present in isolated peptides in solution.

It is possible that both active and inactive forms of certain Rho subfamily proteins are able to homodimerise through a separate region of the protein, which brings the C-terminal tail into proximity of the catalytic site. Indeed, the Cdc42•GDP form is able to homodimerise as shown by column immobilisation studies, although shows no activatory activity suggesting that the dimerisation and activatory characteristics may be separate regions of the protein.

Observations in this laboratory (Webb, M., personal communication) have suggested that truncated Rac1•GDP is able to exist in both monomeric and homodimeric forms, possibly in some form of conformational equilibrium. The observation of Rac1•GDP being able to dimerise, without a C-terminal tail, further suggests that the C-terminal tail may not play a significant role in Rac dimerisation. However, the C-terminal tail's role in accelerating the GTP hydrolysis of Rac1 cannot be discounted from the work presented in this present study.

Chapter 4

The Role of Mg^{2+} in Nucleotide Exchange

4.1 Introduction

The exchange of GTP for GDP in the nucleotide binding site of small G-proteins is an essential step in their activation and subsequent effects. Although GTP is in 10-fold excess over GDP *in vivo*, an inactive GDP-bound small G-protein will only exchange GDP for GTP slowly in the absence of GEFs, which are required for the catalysis of the exchange process. As an increasing amount of information is published on GEFs, it appears that they share a common mechanism of action despite their structural diversity.

As alluded to in Chapter 1, one current model of GEF action involves destabilisation of Mg^{2+} within the nucleotide binding site (Figure 10)(Pan, J. and Wessling-Resnick, M., 1998). Disruption of the Mg^{2+} coordination to both the nucleotide and the protein by the GEF, permits the loss of Mg^{2+}. Stabilisation of the Mg^{2+}-free state by the bound GEF, where the bound nucleotide is released and the natural *in vivo* excess of GTP over GDP causes GTP to enter the active site. Subsequent reassociation of Mg^{2+} to the bound-GTP with a higher affinity than with the GDP, causing the GEF's dissociation and stabilisation of the GTP-bound state. It has been suggested that the conformational changes between the two nucleotide-bound states may be a direct result of the influence of the Mg^{2+} (Shimizu, T., *et al.* 2000). In some aspects, therefore, the role of the Mg^{2+} in exchange can be regarded as a gatekeeper for the release and binding of nucleotide — the release of the nucleotide is dependent on the weakening of the affinity for the associated Mg^{2+}, which occurs subsequent to the hydrolysis of GTP.

In this study two nucleotide-bound fluorophores, Mant and the Coumarin MBC, are used in the examination of the mechanism of nucleotide exchange in the absence of a GEF, which may provide insights into the possible mechanism for GEF-mediated exchange. Current models suggest an important role for the associated Mg^{2+} in the control of nucleotide exchange, and it is this which is investigated in this study using both Mg^{2+} bound and Mg^{2+} free forms of the Rac nucleotide complex. The Mg^{2+}-bound form is produced by incubation of micromolar Rac•GDP or micromolar Rac•GMPPNP (used to mimic GTP) in the presence of millimolar Mg^{2+}, whereas the Mg^{2+}-free form is produced by incubation of Rac in the presence of millimolar EDTA, which sequesters Mg^{2+}. In both the Mg^{2+}-bound and Mg^{2+}-free states, nucleotide binds tightly to the Rac protein. Initially the exchange process is examined using the MBC fluorophore in titration experiments. Stopped flow fluorescent intensity and fluorescent anisotropy techniques provide direct information on the rates of Mg^{2+} release and binding. They also give information on the loss of nucleotide from the different nucleotide bound forms of Rac.

The experiments presented in this thesis show that MBC responds to the three separate processes: Mg^{2+} release, nucleotide release, and GTP hydrolysis. The Mant fluorophore however, is sensitive only to the release of nucleotide from Rac. The results for the Rac•MBCGDP and Rac•MBCGMPPNP forms (allowing a comparison of the exchange mechanism between the active and inactive states of Rac) suggest that they share similar mechanisms for the release and binding of Mg^{2+}, but with very different kinetics. The rates for the various processes are analysed and they provide a kinetic model for the process of

Mg^{2+} release and binding to both the GDP and GMPPNP states of Rac. Mg^{2+} binds approximately 1000-fold tighter in the presence of GMPPNP compared to GDP.

Mn^{2+} is used as a analogue of Mg^{2+}, to provide confirmation as to changes in MBC fluorescence resulting from metal ion release. Due to Mn^{2+}'s similar size and coordination to Mg^{2+}, it is able to act as a valid analogue in Rac. Mn^{2+} has been used as a Mg^{2+} analogue previously: in Ras, Mg^{2+} was replaced with Mn^{2+} and shown to have a similar structure to the Mg^{2+} complexed protein, and similar mechanism for GTP hydrolysis although it is accelerated by 4-fold (Schweins, T., *et al* 1997). Other investigations have demonstrated the validity of Mn^{2+}/Mg^{2+} replacement in a variety of molecular systems (Leupold, C., *et al.*, 1983; Ivell, R., *et al.*, 1981).

The data is explained by a two-step model, the first step being Mg^{2+} release followed by nucleotide release:

$$\text{Rac•MBCGXP•Mg}^{2+} \underset{+Mg^{2+}}{\overset{-Mg^{2+}}{\rightleftharpoons}} \text{Rac•MBCGXP} \rightleftharpoons \text{Rac + MBCGXP}$$

Equation 2

4.2 Results

4.2.1 Changes in MBC Fluorescence on Mg^{2+} and MBC Nucleotide Release from Rac

As this study was the first biochemical investigation using the MBC fluorophore, it was

necessary to establish its fluorescent behaviour on nucleotide and Mg^{2+} binding or release. To achieve this, experiments were performed as described in section 2.8.1. The data from these experiments for both Rac•MBCGMPPNP and Rac•MBCGDP complexes, indicated that the changes in MBC fluorescence occurred both on the release of Mg^{2+} as well as the subsequent release of MBC nucleotide (Equation 2). Justification for these interpretations will be demonstrated later in the Chapter.

To provide initial observations of the changes in fluorescence on Mg^{2+} release or Mg^{2+} binding, sequential additions of either EDTA or Mg^{2+} to Mg^{2+}-bound Rac•MBC-Nucleotide complex were made(EDTA sequesters free Mg^{2+} and therefore prevents Mg^{2+} rebinding to Rac creating Mg^{2+}-free Rac forms). A final excess addition of GDP allowed the MBC fluorescence changes during MBC-nucleotide release to be measured. This was performed with both Rac•MBCGDP and Rac•MBCGMPPNP complexes.

Figure 20 shows the changes in MBC fluorescence on addition of EDTA to Rac•MBCGDP•Mg^{2+}. A large decrease in fluorescence accompanies addition of EDTA to the complex (Figure 20a), presumably due to the release of Mg^{2+}. The subsequent addition of excess GDP to the now Mg^{2+}-free complex causes a relatively small increase in fluorescence as the MBCGDP is displaced from Rac into solution. A rate of 0.007 s^{-1} could be measured for this exchange process by fitting a single exponential to this section of the data.

Figure 20b shows the changes in MBC fluorescence for the Rac•MBCGMPPNP•Mg^{2+}

Figure 20: Mg^{2+} Release from Rac•MBCGDP & Rac•MBCGMPPNP

The panels opposite show the changes in fluorescence on Mg^{2+} release from Rac•MBCGDP (*upper*) and Rac•MBCGMPPNP (*lower*) complexes, as measured on a fluorimeter, (Perkin Elmer LSB50) at 30 °C (Chapter 2). The excitation wavelength was 406 nm and emission was recorded at 460 nm. The graphs opposite are shown as changes in fluorescence in arbitrary units.

The upper Rac•MBCGDP panel shows on addition of EDTA (i) to a final concentration of 5 mM, there is a rapid and large decrease in fluorescence (=85%), whose rate is too fast for analysis by this method. A subsequent addition of EDTA (ii) causes a further small decrease in fluorescence, suggesting that most of the Mg^{2+} has already been released from the Rac complex. A final addition of 200 µM GDP (iii) causes a slight increase in fluorescence, which can be fitted to a single exponential to give a rate of 0.007 s^{-1}.

The lower panel represents Mg^{2+} release from Rac•MBCGMPPNP. Initial addition of EDTA (i) (5 mM) causes a large, slow decrease in fluorescence, which can be fitted to a single exponential to give a rate of 0.004 s^{-1}. Subsequent additions of EDTA (ii) and (iii) causes only a small change in fluorescence, suggesting the majority of Mg^{2+} has been released. Addition of 200 µM GDP (iv) shows a fast decrease in fluorescence, which is too fast to be analysed by this method.

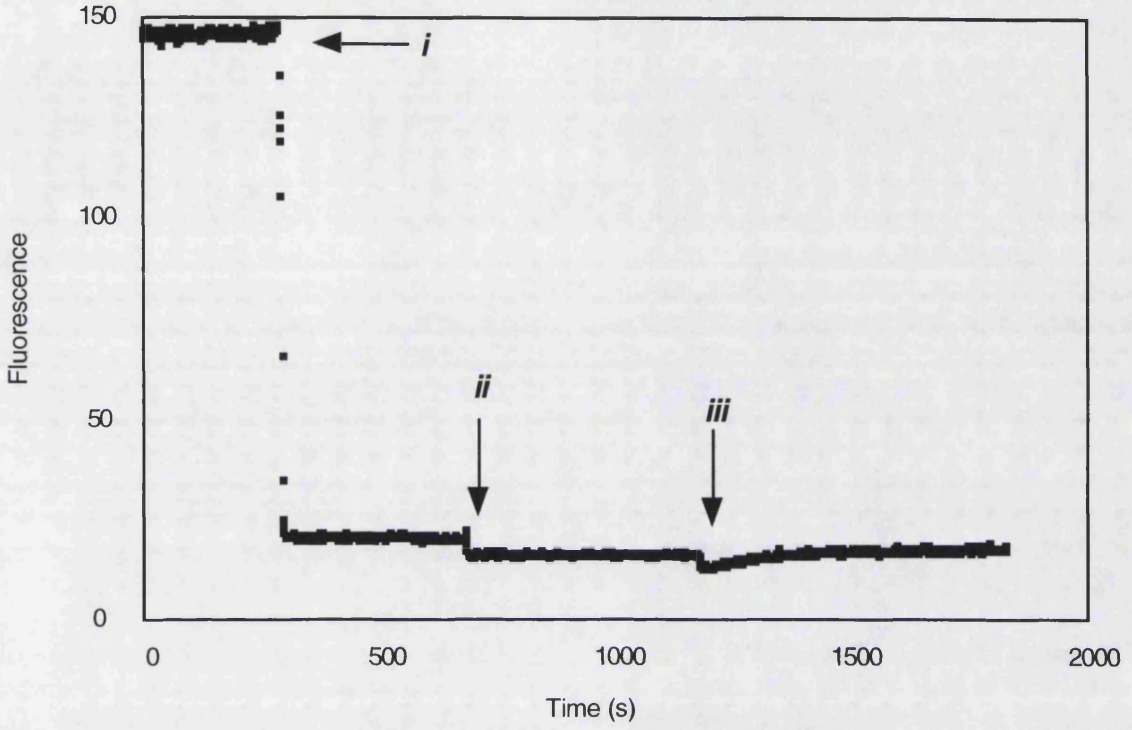

Figure 20a Loss of Mg^{2+} from Rac•MBCGDP show a decrease in fluorescence, but GDP exchange shows an increase

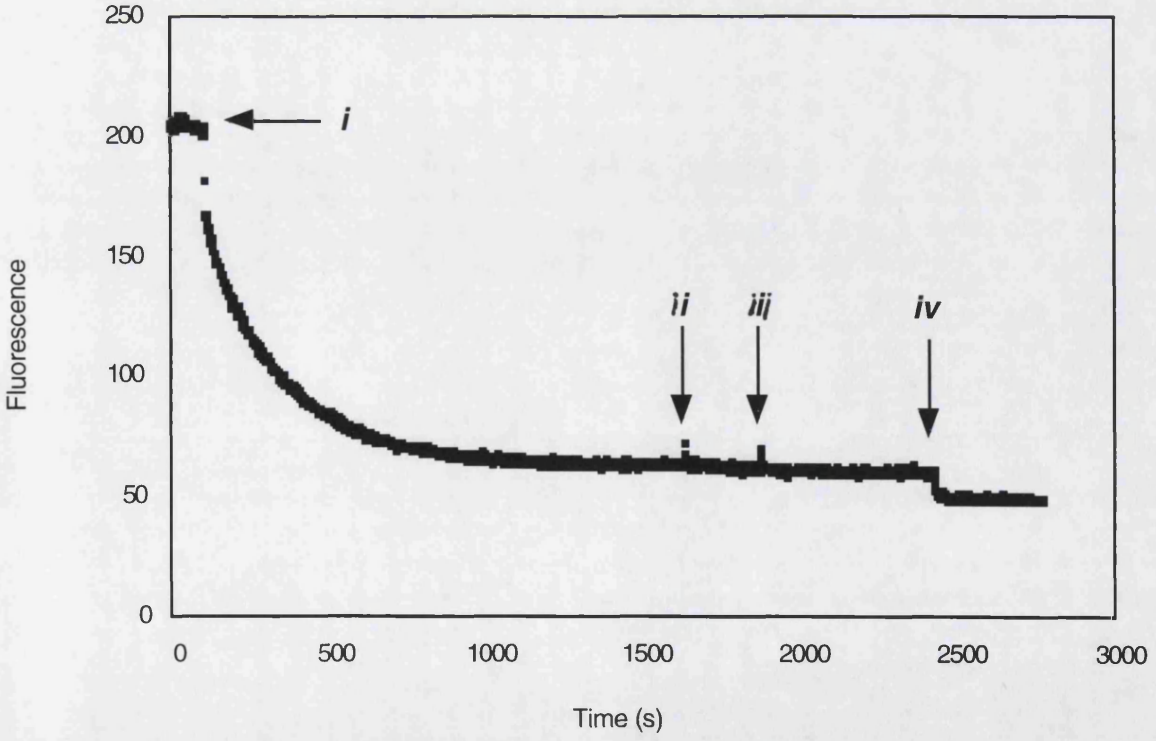

Figure 20a Both loss of Mg^{2+} and nucleotide from Rac•MBCGMPPNP shows a decrease in fluorescence

complex on release of bound Mg^{2+}. Addition of EDTA again causes a large decrease in fluorescence, presumed to be caused by Mg^{2+} release similar to that observed with Rac•MBCGDP. The release is slow; fitting a single exponential to this curve gives a rate of 0.004 s^{-1}. Addition of GDP to the now Mg^{2+}-free Rac•MBCGMPPNP complex causes a further rapid yet small decrease in fluorescence as MBCGMPPNP is released into solution.

Fluorescence increases on Mg^{2+} binding to Rac•MBC nucleotide complexes were followed on addition of Mg^{2+} into a solution containing Mg^{2+}-free Rac•MBCGDP or Rac•MBCGMPPNP (Figure 21).

The data from these initial experiments suggest that the MBC fluorophore is both sensitive to the presence of Mg^{2+} bound to the Rac complex, and to the exchange of the nucleotide. The changes in fluorescence differ with the form of nucleotide bound. A large decrease in fluorescence is observed on release of Mg^{2+} from both MBCGDP and MBCGMPPNP complexes, whereas a fluorescent increase occurs on Mg^{2+} binding. On MBCGDP release a small increase in fluorescence occurs whereas the MBCGMPPNP nucleotide conversely shows a decrease in fluorescence. These data also suggest that the Mg^{2+} is released more slowly from Rac•MBCGMPPNP than Rac•MBCGDP.

These experiments also suggest that the fluorescence of Rac•MBCGMPPNP is higher than that of Rac•MBCGDP, in both the presence and absence of bound Mg^{2+}. When free in solution, the fluorescence of MBCGDP and MBCGMPPNP are equal.

Figure 21: Mg^{2+} Binding to Rac•MBCGDP & Rac•MBCGMPPNP

The panels opposite show data of Mg^{2+} binding to Rac•MBCGDP (upper) and Rac•MBCGMPPNP (lower) complexes, in the absence of Mg^{2+}, in the presence of 10 mM EDTA and 20 mM $(NH_4)_2SO_4$, at 30 °C. The fluorescence scale represents arbitrary units.

On addition of Mg^{2+} to Mg^{2+}-free Rac•MBCGDP (upper panel), each addition marked by an arrow, there is an approximate two fold increase in fluorescence. The increase in fluorescence reaches a saturated level.

On addition of Mg^{2+} to Mg^{2+}-free Rac•MBCGMPPNP there is an approximately two fold increase in fluorescence, which also reaches a saturated level.

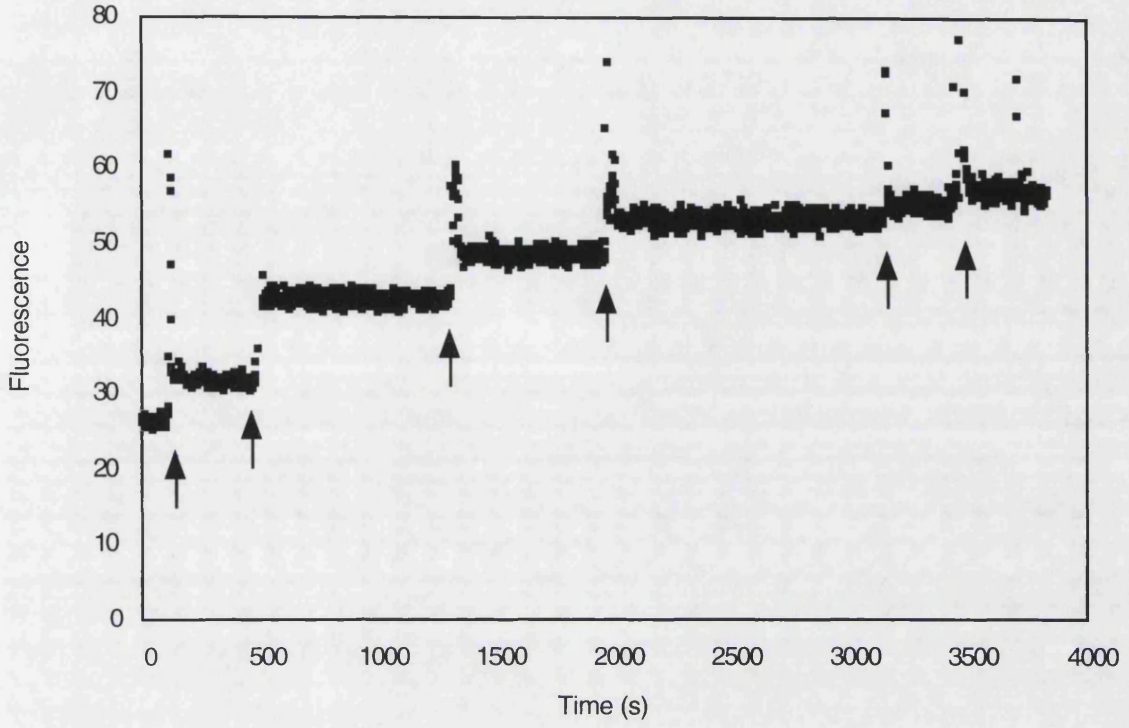

Figure 21a Binding of Mg^{2+} to Rac•MBCGDP shows an increase in fluorescence

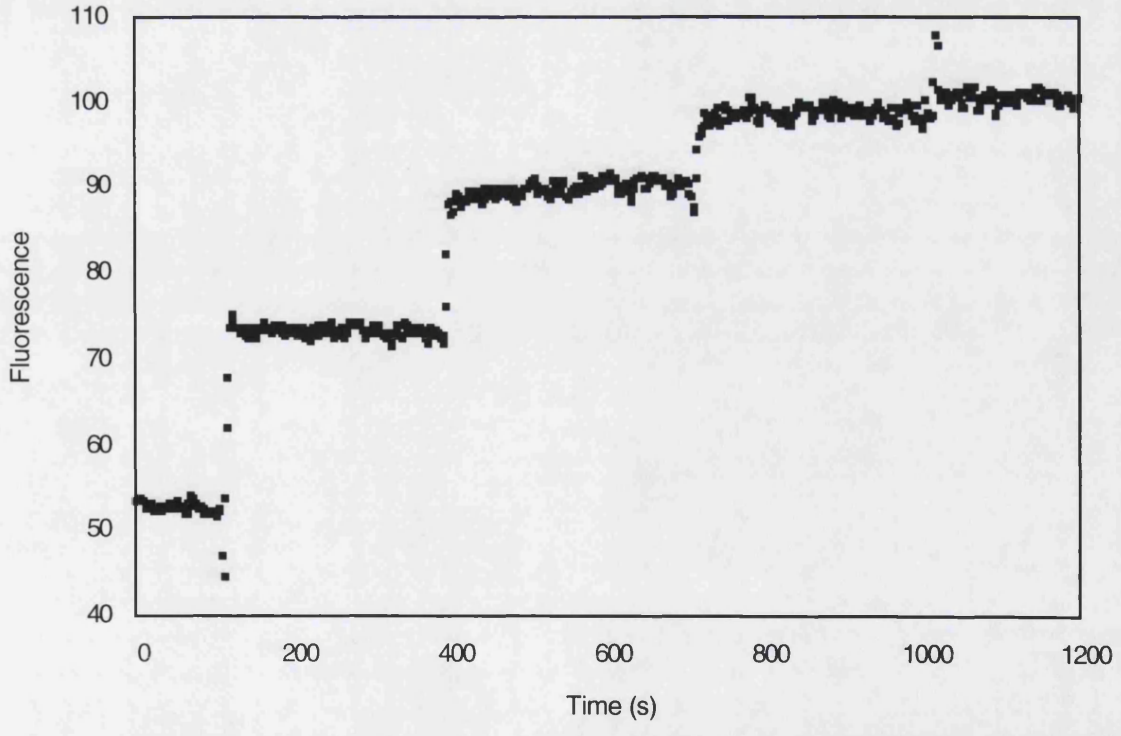

Figure 21b Binding of Mg^{2+} to Rac•MBCGMPPNP shows an increase in fluorescence

4.2.2 MBC and Unlabelled Nucleotides Bind to Rac with Approximately Equal Affinity

To confirm that the MBC fluorophore makes no difference to the binding of nucleotide to Rac, nucleotide exchange reactions were performed in the presence of different concentrations of MBCGDP and GDP. The amplitude of the MBC fluorescent change at the different ratios of labelled to unlabelled nucleotide was then measured. Figure 22 shows the plot of the ratio of concentrations of MBCGDP:GDP against the amplitude of fluorescent change (as a fraction of the maximum fluorescent change). The ratio of the K_d between MBCGDP and GDP is 0.96, which suggests that Rac's affinity for MBCGDP and GDP is approximately equal.

This suggests that the MBC-bound nucleotides show similar affinity for Rac as the unlabelled nucleotide, and is, therefore consistent with the MBC fluorophore having no effect on nucleotide binding.

4.2.3 Rac•GTP Hydrolysis can be Monitored Using Changes in MBC Fluorescence

The fluorescence of MBCGTP and MBCGDP have been shown to differ in the previous section, and so a change in fluorescence on hydrolysis of Rac•MBCGTP might be expected, assuming that MBCGMPPNP and MBCGTP have a similar fluorescence. Different methods of measuring Rac•MBCGTP hydrolysis showed that hydrolysis measured by changes in MBC fluorescence and increases in free P_i were similar, and these were slightly lower than the

Figure 22: MBCGDP and GDP Bind with Equal Affinity

0.2 μM Rac•GDP was mixed with varying concentrations of MBCGDP and GDP (the total of which was equal 1 μM) in the presence of 20 mM Tris.HCl (pH 7.6) 10 mM $(NH_4)_2SO_4$.

The plot opposite shows the amplitude of the change in fluorescence against the ratio of the concentrations of MBCGDP and GDP present in solution ([MBCGDP]/[GDP]). When 1 μM MBCGDP was present the only unlabelled GDP present was from the Rac•GDP (0.2 μM). The data isf fitted to a simple binding curve.

The reference point taken for where the change in fluorescence was equal to 1, was when [MBCGDP] = 1 μM, [GDP] = 0.2 μM (contributed by the 0.2 μM Rac•GDP present), and so ([MBCGDP]/[GDP] = 5.

At 50% saturation, the ratio of [MBCGDP]:[GDP] is equal to 0.96, which suggests that the binding affinity of the nucleotides is very similar, with MBCGDP binding very slightly more tightly.

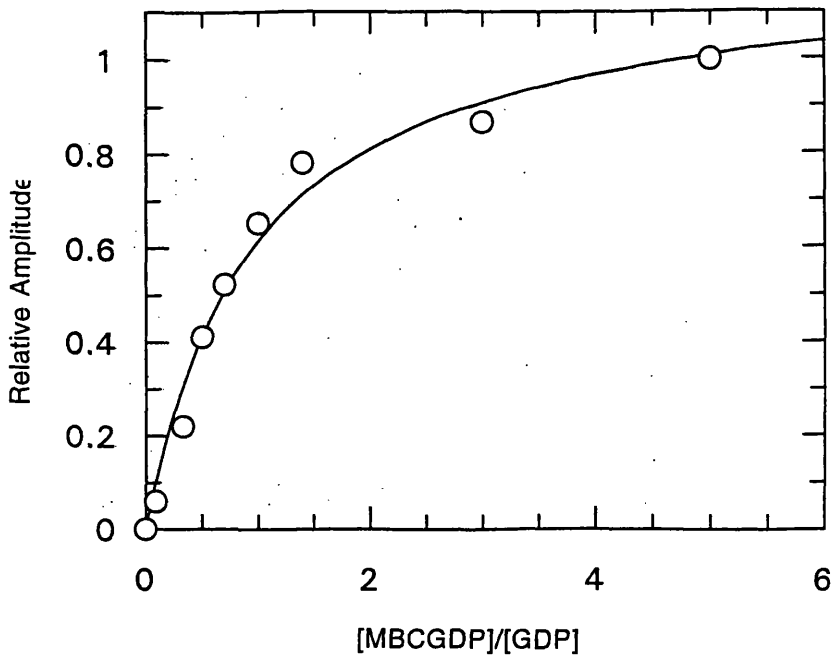
Relative Amplitude
1
0.8
0.6
0.4
0.2
0
0
2
4
6
[MBCGDP]/[GDP]

rate of β-γ phosphate bond cleavage (by HPLC).

The changes in MBC fluorescence during Rac•MBCGTP hydrolysis, are shown in Figure 23a. The data fits a single exponential, and the fluorescence decreases with a rate of 2.0×10^{-3} s^{-1}. This was repeated in the presence of MDCC-PBP which measures the increase in P_i levels derived from MBCGTP hydrolysis . The fluorescence of MDCC-PBP, as shown in Figure 23b, increased (as MDCC-PBP bound free P_i) at a rate of 2.0×10^{-3} s^{-1}.

Excitation of MDCC-PBP was at 450 nm (max. 425 nm), so that excitation of the MBC fluorophore was minimised. This was confirmed by following the fluorescence time course in the absence of MDCC-PBP using the same conditions. The amplitude of this fluorescent change is very small in comparison to the change in the presence of the MDCC-PBP, and therefore the contribution of MBC to the MDCC-PBP data (Figure 23b) is negligible.

The rate of MBCGTP hydrolysis by Rac was also monitored using HPLC (as described in Chapter 2.8.1). Samples were taken at time intervals and analysed for their relative levels of MBCGDP to MBCGTP (Figure 24). These data fitted a single exponential with a rate of MBCGTP hydrolysis, monitored by GTP decrease is 5.0×10^{-3} s^{-1}.

These data from Rac•MBCGTP hydrolysis measured by changes in MBC fluorescence, MDCC-PBP fluorescence show similar rate constants for the GTP hydrolysis ($2.0 \times 10^{-3} s^{-1}$ and 2.0×10^{-3} s^{-1} respectively). The rates also agree with those found in Chapter 3. Hydrolysis

Figure 23: Rac•MBCGTP Hydrolysis: MBC and MDCCPBP

The two panels opposite show data produced from Rac•MBCGTP hydrolysis, when monitoring the changes in fluorescence of either MBC or Phosphate Binding Protein, in the presence of 20 mM Tris.HCl (pH 7.6) 20 mM $(NH_4)_2SO_4$ at 30 °C.

The *top panel* (*23a*) shows the decrease in fluorescence of the MBC group (excitation at 406 nm, emission at 460 nm) during the process of hydrolysis. This data can be fitted to a single exponential to give an observed rate, k_{obs} of 0.002 s^{-1}.

The *lower panel* (*23b*) shows two data sets for Rac•MBCGTP hydrolysis, both with excitation at 450 nm, emission at 470 nm. The upper set (*i*) represents data collected in the presence of 15 μM Phosphate Binding Protein. The increase in fluorescence is due to the binding of free P_i (produced by GTP hydrolysis) to the MDCC-PBP causing a subsequent increase in fluorescence of its associated fluorophore. The rate of increase of the MDCC-PBP's fluorescence can be fitted to a single exponential curve with a rate of 0.002 s^{-1}. The lower trace (*ii*) shows the changes in fluorescence of the MBC group during GTP hydrolysis, in the absence of MDCC-PBP, using excitation at 450 nm and emission at 470 nm, which minimises the fluorescent contributaion from the MBC fluorophore. The amplitude of the change in fluorescence is sufficiently small as for its effect to be negligible, with respect to the data in the presence of MDCC-PBP. The rate of this small change in fluorescence can be fitted to a single exponential, with a rate of 0.002 s^{-1}.

The similar rate constants, but different amplitudes of change, between the fluorescent changes of the MBC group when excitation and emission are monitored at different wavelengths suggests that the same process (that of GTP hydrolysis) is being observed. Since MDCC-PBP is known to show an increase in fluorescence on GTP hydrolysis due to increasing P_i levels, the trace including MDCC-PBP (*i*) confirms that MBC is reflecting GTP hydrolysis and not some other process.

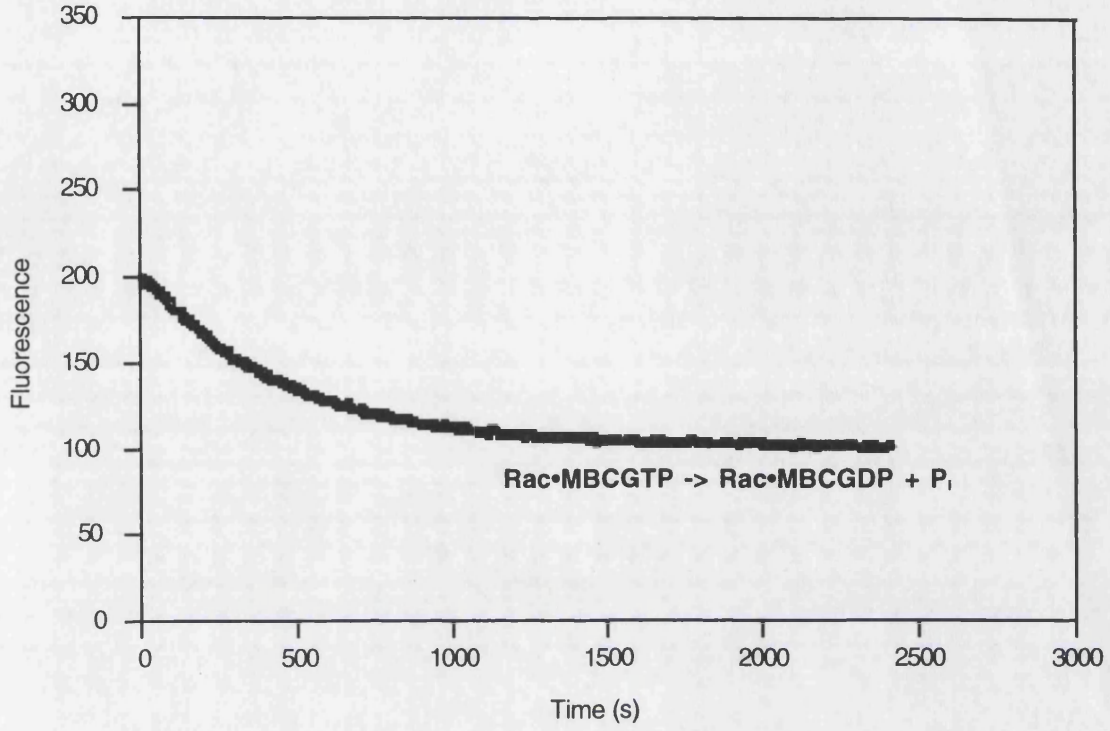

Figure 23a Hydrolysis of MBCGTP demonstrates a decrease in fluorescence. (Ex. 406 nm, Em. 460 nm)

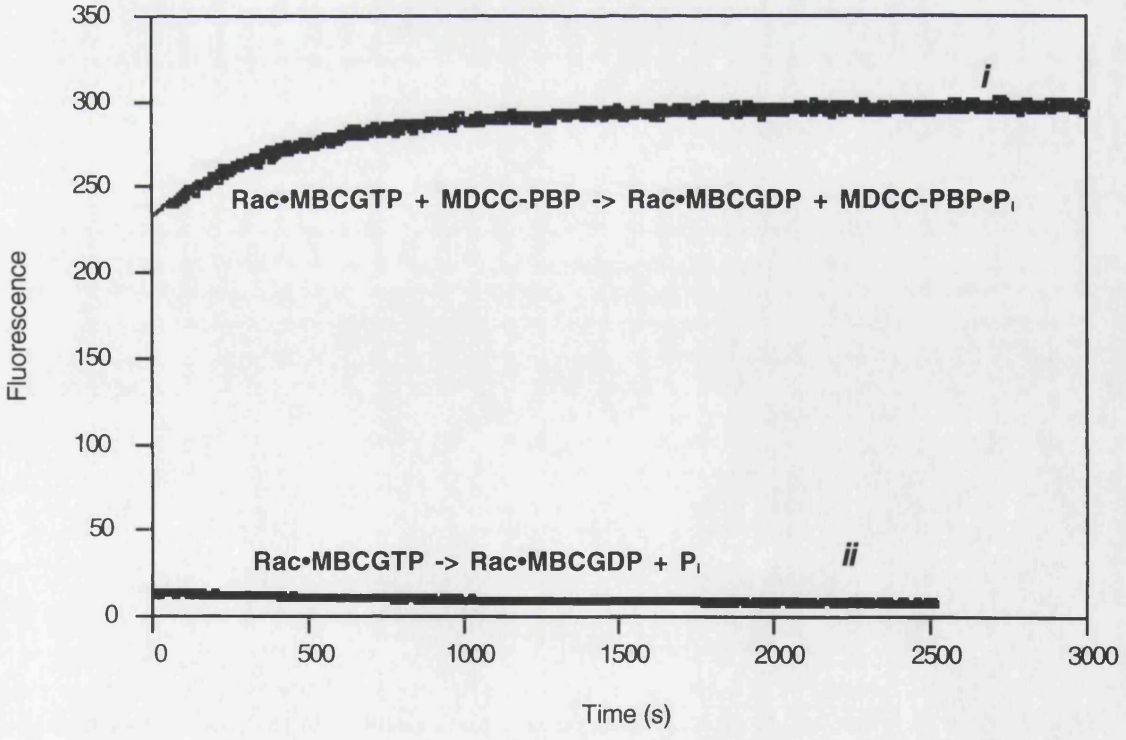

Figure 23b GTP Hydrolysis Shows an Increase in Fluorescence when measured using MDCC-PBP. The change in is MBC fluorescence is negligible. (Ex. 450 nm, Em. 470 nm)

Figure 24: Rac•MBCGTP Hydrolysis: HPLC

The *panel opposite* represents data collected during the analysis of Rac•MBCGTP hydrolysis using HPLC to assess the amount of GTP or GDP present bound to Rac, described in Chapter 2.

The curve opposite shows the best fit single exponential to the data recorded — the amount of MBCGTP present bound to Rac at a particular time point. The amount of MBCGTP bound decreases as the MBCGTP is hydrolysed to MBCGDP + P_i by Rac. The data has an observed rate of 0.005 s^{-1}.

The initial amount of Rac•MBCGTP present in solution is approximately 50%, due to the method of its preparation. During this process, GTP hydrolysis is still occurring, and so at any one time, a maximum of 50% of Rac is bound to GTP (pre-hydrolysis) and 50% to GDP (post-hydrolysis).

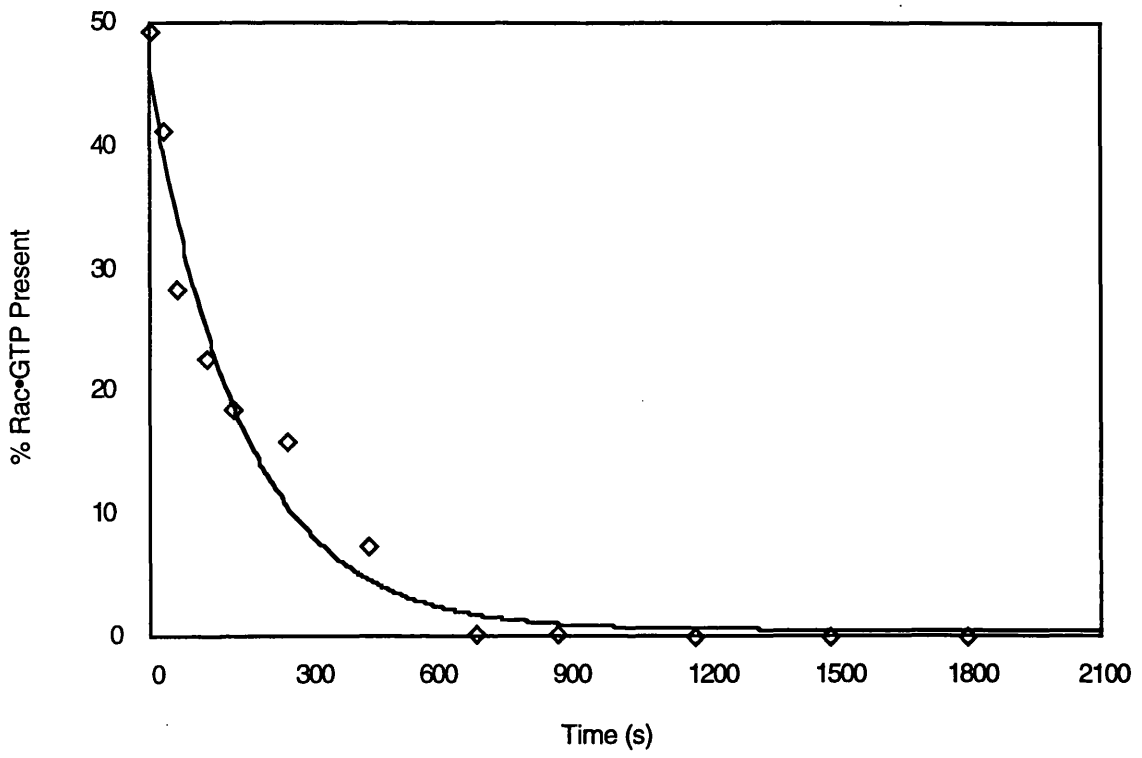

Figure 24 HPLC shows a decrease in GTP bound to Rac as GTP hydrolysis occurs

measured by HPLC gave a slightly different value (5.0×10^{-3} s^{-1}). The significance of which is discussed later. These data suggest that the MBC fluorophore is therefore sensitive to GTP hydrolysis.

4.2.4 Rapid Reaction Analysis

The use of stopped flow techniques allows the observation of the fluorescent changes of the MBC and Mant fluorophores in a time resolved fashion. In this thesis, stopped flow techniques were used to measure the kinetics of Mg^{2+} and nucleotide release from Rac complexes as well as the binding of Mg^{2+} to Mg^{2+}-free Rac complexes. Fluorescent intensity measurements provide information on the involvement on both Mg^{2+} and nucleotide release and binding.

The methods for the stopped flow experiments have been described in section 2.8.2.1 and are illustrated in Figure 17. The traces shows the changes in fluorescent intensity on Mg^{2+} or nucleotide release or binding, and each trace shown is representative of at least three separate experiments.

4.2.4.1 Fluorescent Changes on Mg^{2+} and Nucleotide Release from Rac•MantGDP and Rac•MantGMPPNP

Previous work (John, J. *et al.* 1990) has shown that Mant labelled nucleotides demonstrate a change in fluorescence on nucleotide release but not on Mg^{2+} release. The Mant

fluorophore is sensitive to Mant nucleotide release from Rac and not Mg^{2+} release. Figure 25 shows traces derived from nucleotide exchange experiments for Rac•MantGDP, in both Mg^{2+}-free and Mg^{2+}-bound forms. On rapid mixing of Mg^{2+}-free Rac•MantGDP with an excess of GDP, a single exponential decrease in fluorescence is observed (Figure 25a) with a rate of 0.17 s^{-1}. The rapid mixing of Rac•MantGDP (in the presence of Mg^{2+}) with GDP and EDTA to initiate exchange, shows a biphasic trace (Figure 25b). An initial small increase in fluorescence, with an observed rate of 1.8 s^{-1}, is followed by a large exponential decrease in fluorescence with a rate of 0.17 s^{-1}. This second phase is similar to the decrease in fluorescence observed in the absence of Mg^{2+} (Figure 25a).

These changes in fluorescence are interpreted as reflecting two steps during nucleotide exchange (Equation 2): the initial, rapid release of Mg^{2+} (present only with Rac complexed Mg^{2+}) followed by a slower release of nucleotide.

These experiments were repeated using MantGMPPNP. Figure 26 shows the changes in fluorescence observed with Rac•MantGMPPNP in both Mg^{2+}-free (Figure 26a) and Mg^{2+}-bound (Figure 26b) forms. On nucleotide exchange with Mg^{2+}-free Rac•MantGMPPNP and GDP, there is a rapid exponential decrease in fluorescence, followed by a slower, subsequent exponential decrease in fluorescence. These data were fitted to two exponentials, with a rate of 3.2 s^{-1} and 0.020 s^{-1}. The rapid phase was of a significantly greater amplitude than the slower phase. On rapid mixing of the Rac•MantGMPPNP•Mg^{2+} complex with excess EDTA and excess GDP, an exponential decrease in fluorescence is

Figure 25: Changes in Fluorescence on Rac•MantGDP Exchange

The panels opposite show the changes in fluorescence on nucleotide exchange with Rac•MantGDP in the presence and absence of Mg^{2+}. The data produced from the instrument are measured in Volts, which is inversely related to fluorescence. The traces shown are y-axis inverted to demonstrate the changes in fluorescence.

The *upper panel*, *25a*, shows the changes in fluorescence on rapid mixing of Mg^{2+}-free Rac•MantGDP against excess GDP and EDTA. The decrease in fluorescence is immediate, and fits to a single exponential, with a rate of 0.17 s^{-1}.

The changes in fluorescence observed when mixing Rac•MantGDP•Mg^{2+} can be seen in the *lower panel, 25b*. This data shows a slight increase in fluorescence (with a rate of 1.8 s^{-1}) before a decrease in fluorescence which is identical to that observed in the upper panel (rate 0.17 s^{-1}). The graph itself is formatted so that the initial increase is visible, rather than the entire decrease in fluorescence.

The initial increase is seen only in the presence of Mg^{2+}, which suggests that this fluorescence effect may represent the rapid release of Mg^{2+} occurring before the release of nucleotide. The release of nucleotide is identical in both conditions, and approximately 10-fold slower than the release of Mg^{2+}, although the amplitude of the change in fluorescence is much greater.

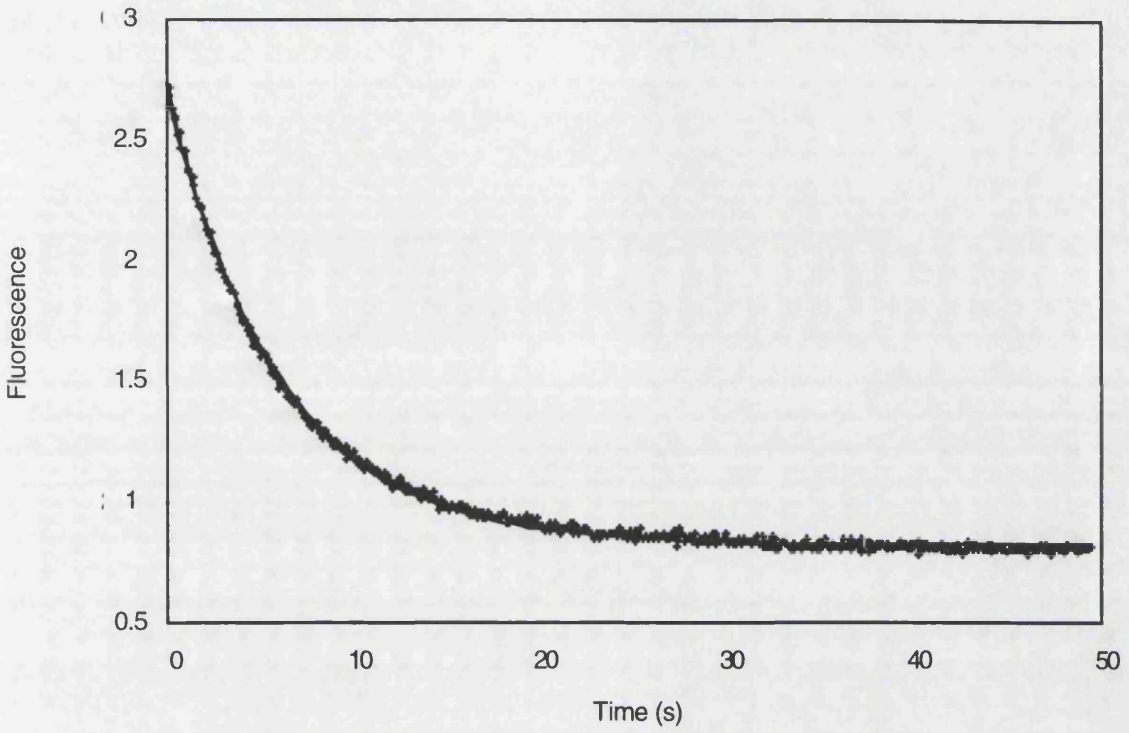

Figure 25a Rac•MantGDP exchange in the absence of bound Mg^{2+} shows a decrease in fluorescence

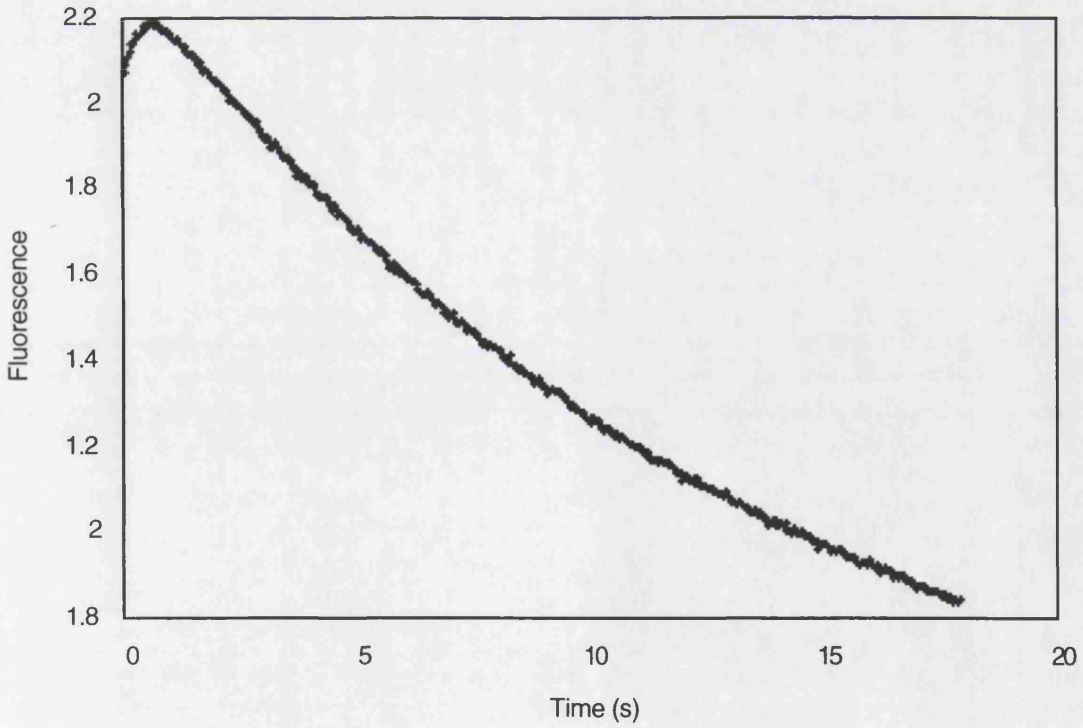

Figure 25b Rac•MantGDP exchange in the Presence of Bound Mg^{2+} shows an initial increase then a decrease in fluorescence

Figure 26: Fluorescent Changes on Rac•MantGMPPNP Exchange

The panels opposite show the changes in fluorescence on nucleotide exchange with Rac•MantGMPPNP in the presence and absence of Mg^{2+}. The data produced are measured in Volts which is inversely related to fluorescence. The traces shown are y-axis inverted to demonstrate the changes in fluorescence.

The *upper panel, 26a*, shows the changes in fluorescence on rapid mixing of Mg^{2+}-free Rac•MantGMPPNP against excess GDP and EDTA. The figure represents only the first 5 seconds of the exchange, which shows an inital phase of 2.8 s^{-1}. A second phase was observed (not shown) with a much slower rate of 0.02 s^{-1}.

The data from Rac•MantGMPPNP exchange in the presence of Mg^{2+} is shown in the *lower panel, 26b*. The decrease in fluorescence observed shows no lag, but can be fitted to a single exponential. The rate of change is slow, 0.015 s^{-1}.

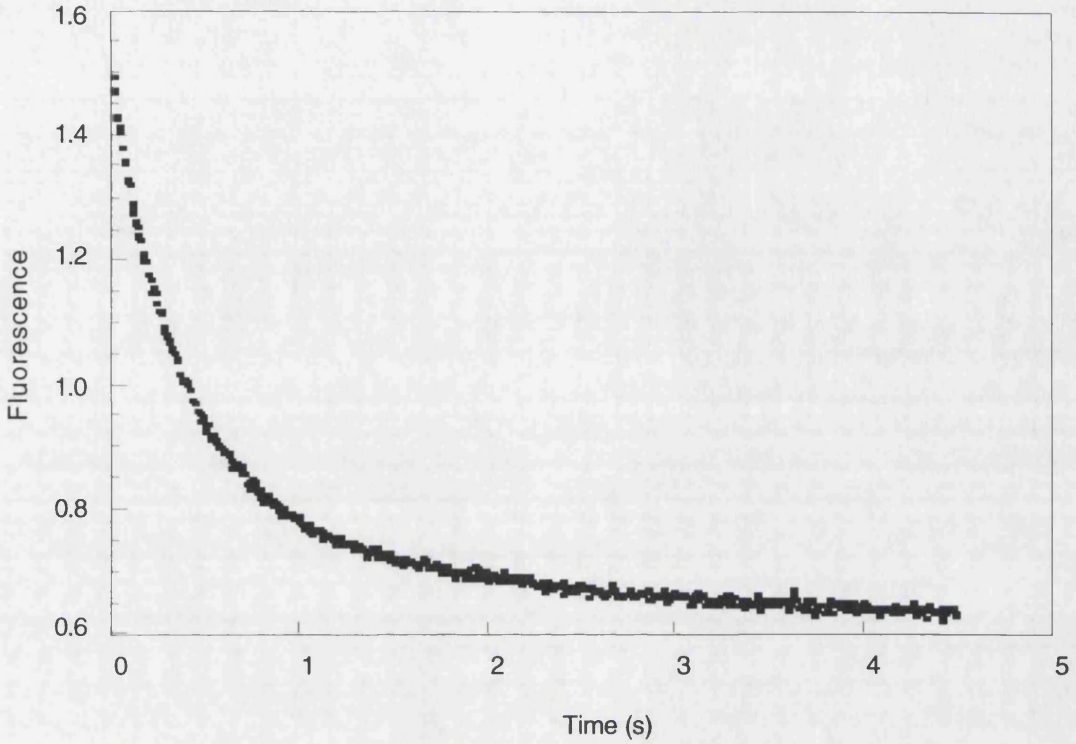

Figure 26a Rac•MantGMPPNP exchange in the absence of bound Mg^{2+} shows a two phase decrease in fluorescence

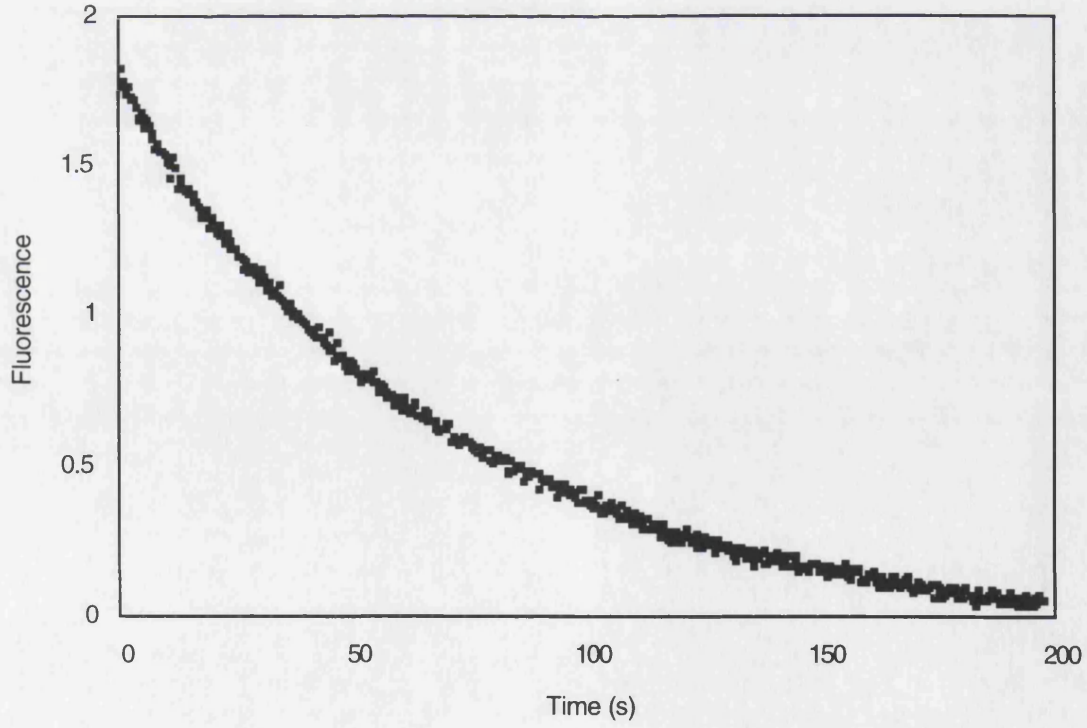

Figure 26b Rac•MantGMPPNP exchange in the presence of bound Mg^{2+} shows a decrease in fluorescence

observed with a rate of 0.015 s^{-1} with an amplitude similar to that of the slow phase observed in the absence of Mg^{2+}.

The data for the Rac•MantGMPPNP is different from that observed for the Rac•MantGDP complex and shows that the kinetics for the process of Mg^{2+} and nucleotide release is different between the two nucleotide forms (Table 3). The data can be interpreted in a two-step model as described in Equation 2. Step One is represented by the slow decrease in fluorescence observed in the presence of Mg^{2+}, and Step Two (nucleotide release) is demonstrated by the rapid decrease in fluorescence in the absence of Mg^{2+}. The slower secondary phase observed may suggest that a conformational change is required for a fraction of the molecules to release nucleotide, or that not all the Mg^{2+} had been removed because it is too tightly bound. In the presence of Mg^{2+} the slower exponential decrease suggests that, in this case, the Mg^{2+} release is slow and limits the nucleotide release.

4.2.4.2 Fluorescent Changes on Mg^{2+} and Nucleotide Release from Rac•MBCGDP and Rac•MBCGMPPNP

Section 4.2.1 suggested that the fluorescence of MBC is sensitive to both Mg^{2+} and nucleotide release. The use of stopped flow techniques allows a time-resolved examination of these processes.

In the absence of Mg^{2+}, release of MBCGDP shows an exponential increase in fluorescent

Table 3: Summary of Fluorescent Intensity and Anisotropy Data

		Intensity Data		Anisotropy Data *
		k_{+1}	k_{+2}	k_{+2}
GDP	**Mant**	Small lag	0.17	0.076, 0.060
	MBC/Mg^{2+}	1.4	0.010	0.020, 0.020
	MBC/Mn^{2+}	24	0.018	0.030, 0.030
GMPPNP	**Mant**	0.015	1.8, 0.02	0.0070, 0.85
	MBC/Mg^{2+}	0.010	3.2, 0.008	0.0040, 0.36
	MBC/Mn^{2+}	0.017	4.0, 0.005	0.030, 0.40

* The Anisotropy dataareis presented here in the form of 'Rate in the presence of metal ion, Rate in the absence of metal ion'.

All rates shown are s^{-1}.

intensity with a rate of 0.017 s^{-1} (Figure 27). In the presence of Mg^{2+}, the changes in fluorescence intensity on MBCGDP release demonstrate a large exponential decrease in fluorescence (rate of 1.4 s^{-1}) (Figure 28b) followed by a slower increase in fluorescence (0.017 s^{-1}) (Figure 28a). This increase in fluorescence is similar to that observed in the absence of Mg^{2+} (Figure 27). The short time scale in Figure 28b illustrates that while in the presence of Mg^{2+} a large decrease in fluorescence is observed, in the absence of Mg^{2+} this is absent — only a slow increase in fluorescence is observed.

These data are interpreted as representing an initial, rapid release of Mg^{2+}, followed by a slower release of MBCGDP (Equation 2).

These experiments were repeated with MBCGMPPNP (Figure 29). On mixing Mg^{2+}-free Rac•MBCGMPPNP with excess GDP and EDTA (Figure 29a), there is an initial rapid exponential decrease in fluorescence (rate of 3.2 s^{-1}), followed by a very slow exponential phase (rate of 0.0080 s^{-1}). It is possible that this slow phase is due to Mg^{2+} remaining bound to the Rac complex. In order to examine this, the concentration of EDTA present in the mixing chamber of the stopped flow instrument was increased. Such changes did not significantly affect the rate of this second phase (data not shown). On mixing Rac•MBCGMPPNP•Mg^{2+} with excess GDP and EDTA (Figure 29b), nucleotide exchange showed a slow, single exponential decrease in fluorescence with a rate of 0.010 s^{-1}. On rapid mixing of Rac•MBCGMPPNP•Mg^{2+} with EDTA, but no GDP, a single exponential decrease was observed, with a rate of 0.011 s^{-1} (Figure 30).

Figure 27: Fluorescent Changes on Rac•MBCGDP Exchange

The panel opposite shows the changes in fluorescence on nucleotide exchange with Rac•MBCGDP in the absence of Mg^{2+}. The data produced are measured in Volts which is inversely related to fluorescence. The traces shown are y-axis inverted to demonstrate the changes in fluorescence.

The *panel*, shows the changes in fluorescence on rapid mixing of Mg^{2+}-free Rac•MBCGDP against excess GDP and EDTA. The data produced shows an exponential increase in fluorescence, with a rate of 0.01 s^{-1}. There is a slight lag during the first few seconds of the data, which is not visible on the panel opposite, but can be seen in Figure 28b.

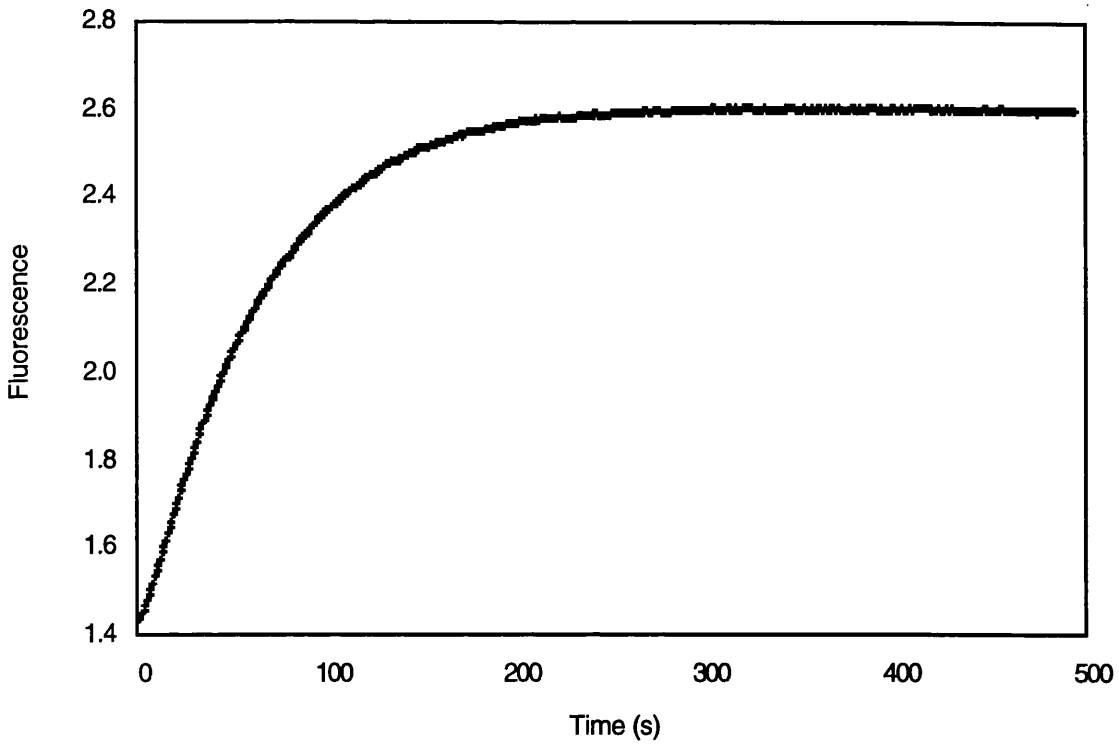

Figure 27 Rac•MBCGDP exchange in the absence of bound Mg^{2+} shows an increase in fluoresence

Figure 28: Fluorescent Changes on Rac•MBCGDP Exchange

The data from Rac•MBCGDP exchange in the presence of Mg^{2+} is shown in the *upper panel, 28a.* There is a large initial decrease in fluorescence (1.5 s^{-1}), followed by a slow increase in fluorescence, with a rate similar to that found in the absence of Mg^{2+}, 0.01 s^{-1}. The rapid decrease in fluorescence is shown in a greater scale on the panel below.

The *lower panel, 28b,* shows the differences in the changes of fluorescence during the first 5 seconds of the GDP exchange process. When Mg^{2+} is associated with the Rac•MBCGDP complex, initiation of exchange causes a large and rapid decrease in fluorescence, which is followed by the slower increase in fluorescence, as shown in the *upper panel.* In the absence of associated Mg^{2+}, from the Rac•MBCGDP complex the beginning of the slow increase in fluorescence can be seen.

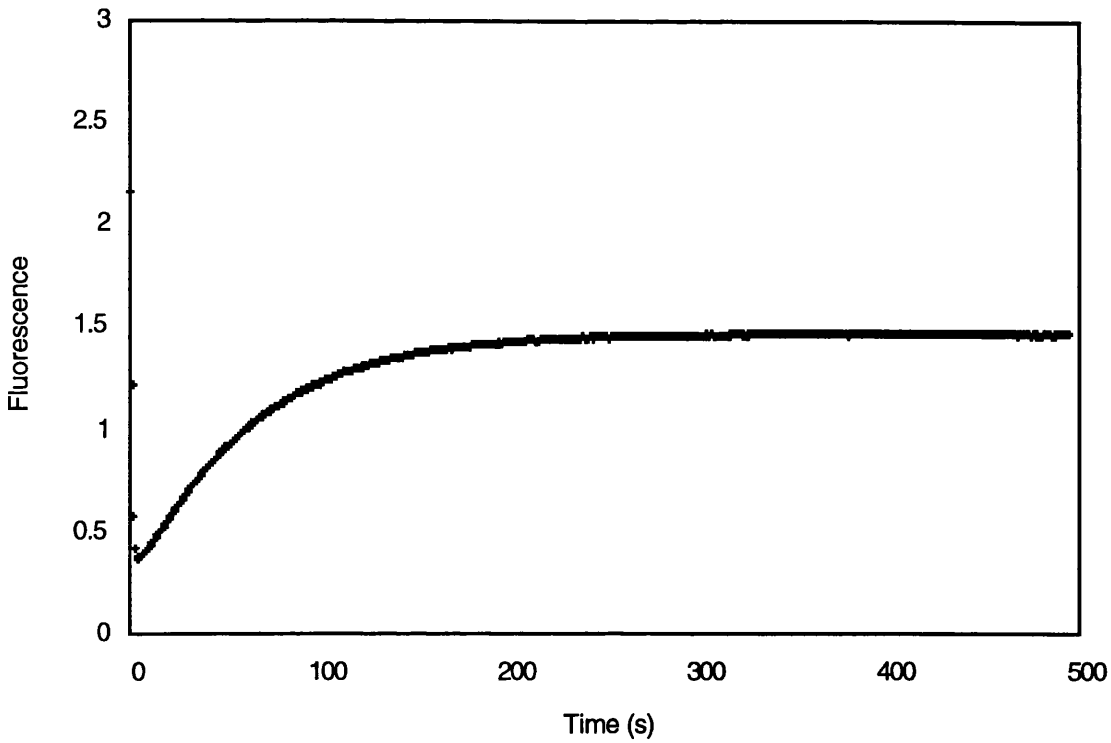

Figure 28a Rac•MBCGDP exchange in the presence of bound Mg^{2+} shows an initial large decrease in fluorescence followed by an increase in fluorescence

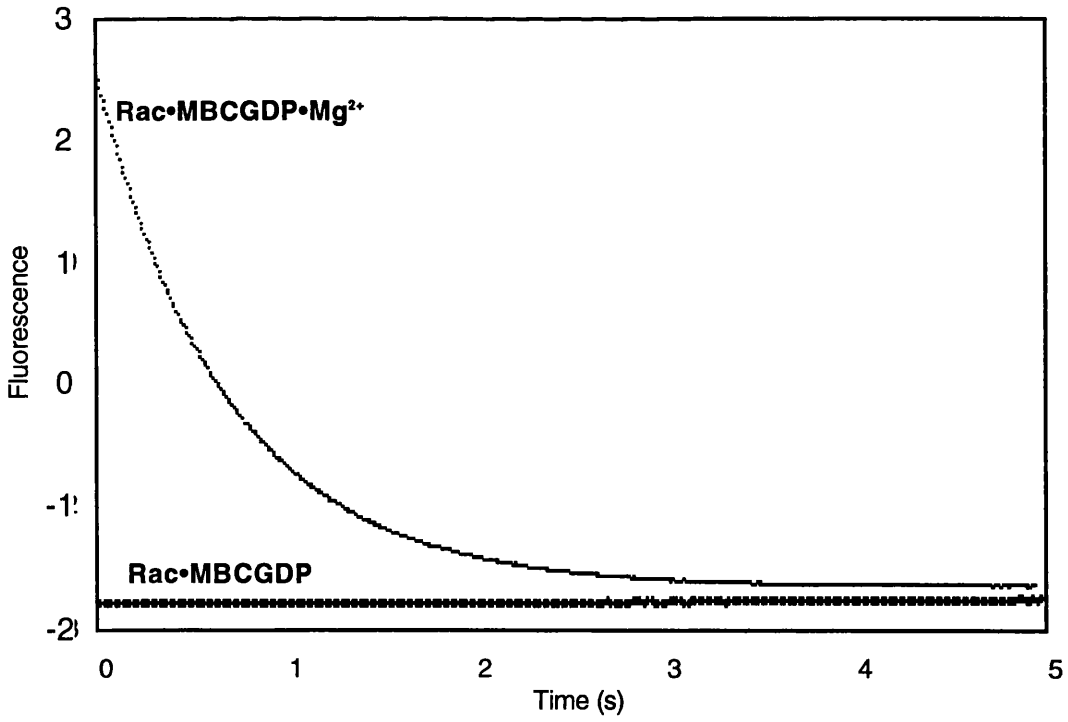

Figure 28b Short timescale of Fluorescent Changes in the Absence and Presence of Mg^{2+} for Rac•MBCGDP

Figure 29: Fluorescent Changes on Rac•MBCGMPPNP Exchange

The panels opposite show the changes in fluorescence on nucleotide exchange with Rac•MBCGMPPNP in the presence and absence of Mg^{2+}. The data produced are measured in Volts which is inversely related to fluorescence. The traces shown are y-axis inverted to demonstrate the changes in fluorescence.

The *upper panel* shows the changes in fluorescence on rapid mixing of Rac•MBCGMPPNP (in the absence of complex-associated Mg^{2+}) against excess GDP and excess EDTA, causing nucleotide exchange. The data shows the initial 20 seconds of the release. The data is biphasic [illegible], with a rapid initial decrease in fluorescence (rate 3.4 s^{-1}), followed by a slower decrease in fluorescence over a smaller amplitude (rate 0.008 s^{-1}). The rate and amplitude of this second phase does not change with increasing EDTA concentrations.

The *lower panel* shows data from Rac•MBCGMPPNP•Mg^{2+} exchange. The data shows a large, slow decrease in fluorescence which can be fitted to a single exponential with a rate of 0.010 s^{-1}.

These data suggest that with respect to Rac•GMPPNP complexes Mg^{2+} acts to limit the rate of nucleotide release and is held tightly to the complex. It also suggests that the GMPPNP nucleotide is held less tightly than GDP. The secondary phase in the absence f Mg^{2+} is not caused by Mg^{2+} being released slowly (since it is unaffected by EDTA concentrations) but may reflect some other molecular process.

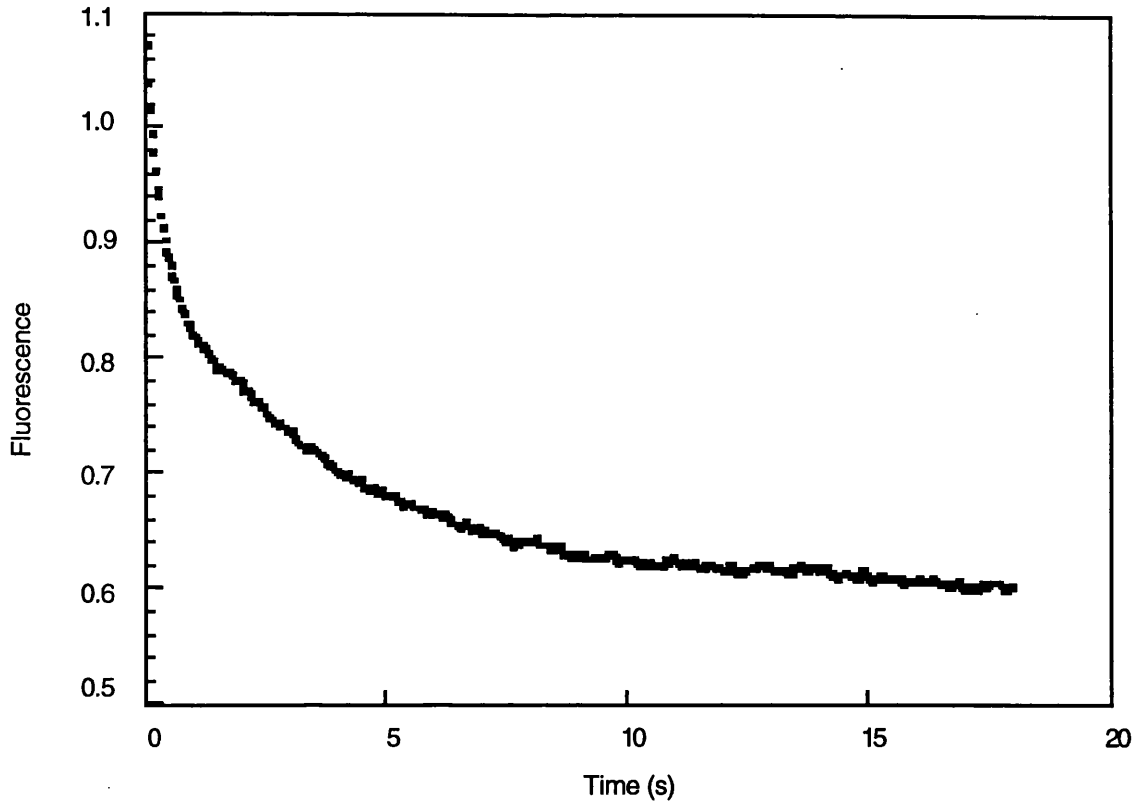

Figure 29a Rac•MBCGMPPNP exchange in the absence of bound Mg^{2+} shows a rapid decrease in fluorescence

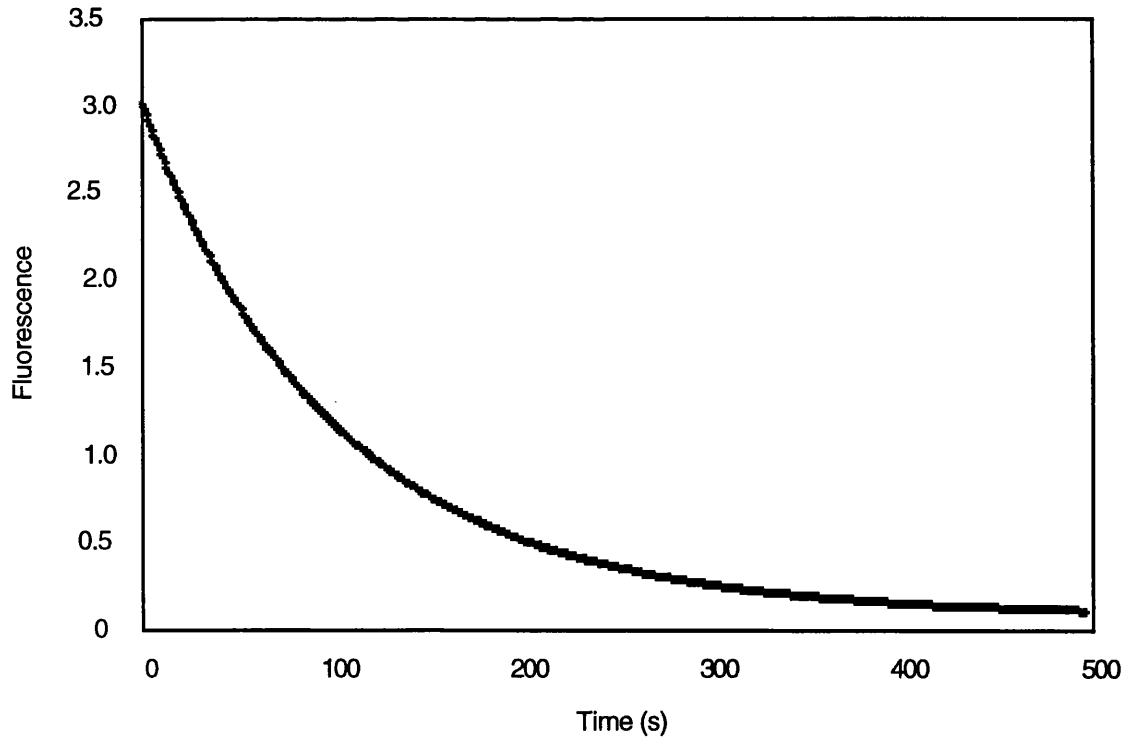

Figure 29b Rac•MBCGMPPNP exchange in the presence of bound Mg^{2+} shows a slow decrease in fluorescence

Figure 30: Fluorescent Changes on Release of Mg^{2+} from Rac•MBCGMPPNP in the Absence of GDP

The *panel opposite* shows the changes in fluorescence on rapid mixing of Rac•MBCGMPPNP (in the presence of complex-associated Mg^{2+}) with excess EDTA but no GDP. The data shows a large, slow exponential decrease in fluorescence, with a rate of 0.011 s^{-1}. This represents the release of Mg^{2+} since there is no GDP which could exchange with the bound nucleotide.

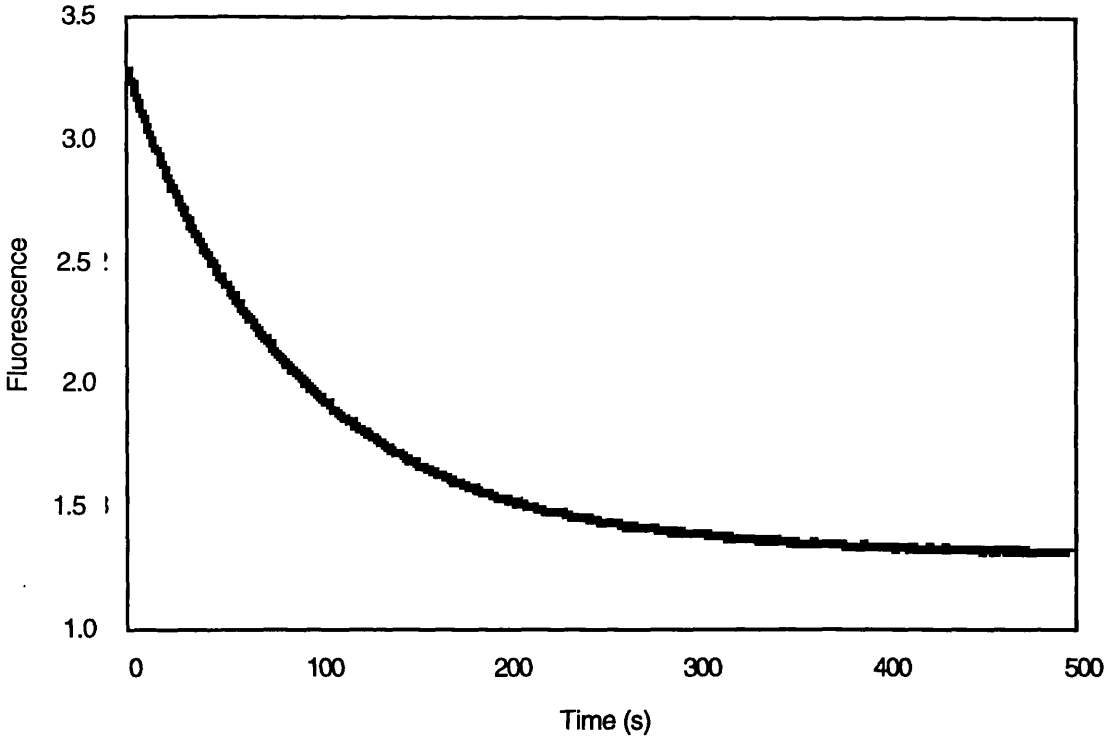

Figure 30a Rac•MBCGMPPNP•Mg^{2+} exchange in the presence of bound Mg^{2+} but in the absence of GDP shows a slow decrease in fluorescence

These release of MBCGMPPNP in the absence of Mg^{2+}, suggests that the MBC nucleotide is able to exchange rapidly with the free GDP, whereas in the presence of Mg^{2+}, this release is slowed by approximately 100-fold. This suggests that the rate of the nucleotide's release is limited by the release of Mg^{2+}. To confirm that this initial large change in fluorescence reflected loss of Mg^{2+}, Rac•GMPPNP•Mg^{2+} was mixed with excess EDTA without GDP present. A large single exponential decrease is observed, with no subsequent change in fluorescence. This confirms that this change in fluorescence is indeed Mg^{2+} release, and that any subsequent change is nucleotide release.

The data from the MBCGDP and MBCGMPPNP experiments suggest that nucleotide exchange can be rationalised as a two step process (Equation 2 & Figure 31). Initial Mg^{2+} release is followed by nucleotide release. For the different nucleotide forms different steps are rate limiting. For MBCGDP, the release of Mg^{2+} is rapid whereas the release of nucleotide is slow, and therefore rate limiting for the overall exchange process. In the case of GMPPNP, the release of nucleotide is rapid, yet in the presence of Mg^{2+}, this release is significantly slowed, which suggests that it is the release of Mg^{2+} which is rate limiting.

The changes in fluorescence observed with MBCGMPPNP show a further decrease of small amplitude in fluorescence, when in the absence of Mg^{2+}. It is possible that in preparation of the Mg^{2+}-free complexes not all the Mg^{2+} was removed by the EDTA. This subsequent decrease could therefore represent slow Mg^{2+} release. When Rac complexes were incubated

Figure 31: The Simple Exchange Model

The *upper panel* shows a simple scheme for the overall process of nucleotide exchange, as suggested by the work with the Mant and MBC fluorophores.

Release of Mg^{2+} is the initial event, followed by the release of the bound nucleotide. The rates of these steps differ as to the form of the bound nucleotide.

In the case of Rac•GDP, the inital release of Mg^{2+} (k_{+1}) is fast, 1.4 s^{-1}, whereas the release of the GDP nucleotide (k_{+2}) is slow, 0.01 s^{-1}, and rate limiting for the overall process. For Rac•GMPPNP (Rac•GTP), the initial release of Mg^{2+} (k_{+1}) is slow, 0.01 s^{-1}, whereas as the release of the nucleotide (k_{+2}) is relatively fast, 3 s^{-1}, suggesting that the release of Mg^{2+} is rate limiting for the process with respect to GMPPNP. A second slow (k_{+3}, 0.008 s^{-1}) phase may occur on release on GMPPNP from Mg^{2+}-free Rac•GMPPNP complex. (not shown).

The *lower panel* shows the rate constants for k_{+1} (step one) and k_{+2} (step two), as measured in this work, with either MBCGMPPNP or MBCGDP complexes with Mn^{2+} or Mg^{2+} as the metal ion present. This shows that by substituting Mn^{2+} for Mg^{2+}, only the step suggested to be caused by the metal ion is altered (step one — k_{+1}).

Note that the forward rates, indicated by '+', represent the release of Mg^{2+} or nucleotide. In later experiments, the reverse rates of binding are represented by '-' to maintain consistency.

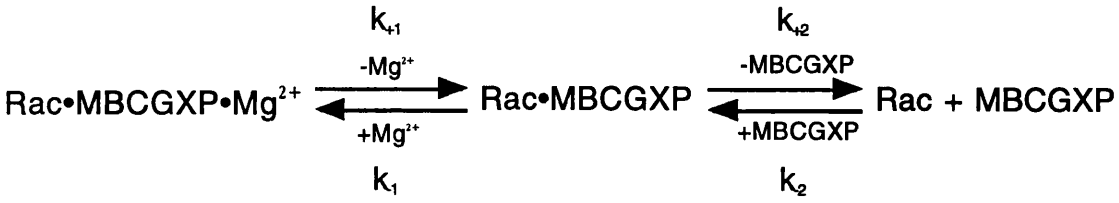

MBCGDP

Metal Ion:	k_{+1}	k_{+2}
Mg^{2+}	1.4 s^{-1}	0.017 s^{-1}
Mn^{2+}	24 s^{-1}	0.017 s^{-1}

MBCGMPPNP

Metal Ion:	k_{+1}	k_{+2}
Mg^{2+}	0.010 s^{-1}	3.2 s^{-1}
Mn^{2+}	0.090 s^{-1}	4.0 s^{-1}

with increasing concentrations of EDTA the rate of this change did not change, suggesting that Mg^{2+} was not the cause of this fluorescent change. It is possible that this change in fluorescence is due to the release of Mg^{2+}, which was not removed by the EDTA (although increased EDTA concentrations do not affect this rate). It is also possible that this secondary change in fluorescence reflects a conformational change through a fraction of Rac molecules in their GMPPNP state, perhaps releasing their nucleotide from a higher affinity bound state.

4.2.4.3 Mn^{2+} Complexed MBC Nucleotides Show Different Kinetics Compared to Mg^{2+} Complexed Nucleotides

The model was tested by the substitution of Mn^{2+} for Mg^{2+}. The main affect of this substitution is likely to be on steps that involve the metal ion. The complexes investigated were prepared in the presence of Mn^{2+} as described in Chapter 2.

Figure 32 shows the changes in fluorescence on nucleotide exchange with Rac•MBCGDP in the presence and absence of Mn^{2+} on long and short timescales. On mixing Rac•MBCGDP with excess EDTA and GDP in the absence of Mn^{2+} (Figure 32a), there is an exponential increase in fluorescence with a rate of 0.017 s^{-1}. This increase in fluorescence is similar to that found previously with Mg^{2+}. This data is also shown over a short time scale in Figure 32b, which shows the beginning of the slow exponential increase in fluorescence. The changes in fluorescence on mixing Rac•MBCGDP•Mn^{2+} with excess EDTA and GDP are

Figure 32: Fluorescent Changes on Rac•MBCGDP•Mn^{2+} Exchange

The panels opposite show the changes in fluorescence on nucleotide exchange with Rac•MBCGDP, in the presence of absence of Mn^{2+} instead of Mg^{2+}. For comparative purposes, the two graphs are shown on the same fluorescent (y) scale. The data produced are measured in Volts which is inversely related to fluorescence. The traces shown are y-axis inverted to demonstrate the changes in fluorescence.

The *upper panel*, 32a, shows the changes in fluorescence on rapid mixing of Mn^{2+}-free Rac•MBCGDP against excess GDP and EDTA. The data produced shows an exponential increase in fluorescence, with a rate of 0.017 s^{-1}. There is a slight lag during the first few seconds of the data. In the presence of Mg^{2+}, the fluorescent changes are very similar, except that over a very short timescale (see below), there is a rapid decrease in fluorescence.

Thr *lower panel,* 32b, shows the changes in fluorescent intensity over the first 0.5 seconds during the GDP exchange process. The changes in fluorescence for Rac•MBCGDP in the presence and absence of Mn^{2+} are depicted on the same graph. In the absence of Mn^{2+}, there is little increase in fluorescence during this initial 0.5 s^{-1}, however in the presence of Mn^{2+}, there is a large (3.5 unit) and rapid (24 s^{-1}) decrease in fluorescence during the time period, which represents the release of Mn^{2+}. Both data sets show very similar MBCGDP release rates, as shown in Figure 32a.

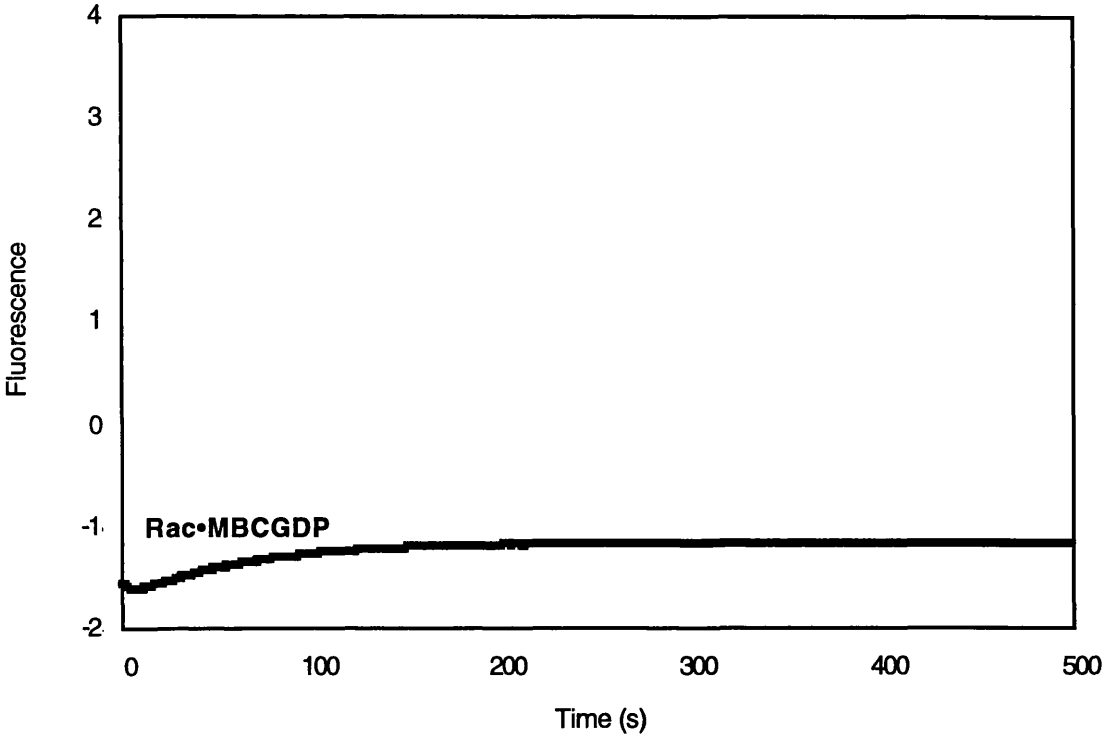

Figure 32a Rac•MBCGDP exchange in the absence of bound Mn^{2+} shows a slows increase in fluorescence

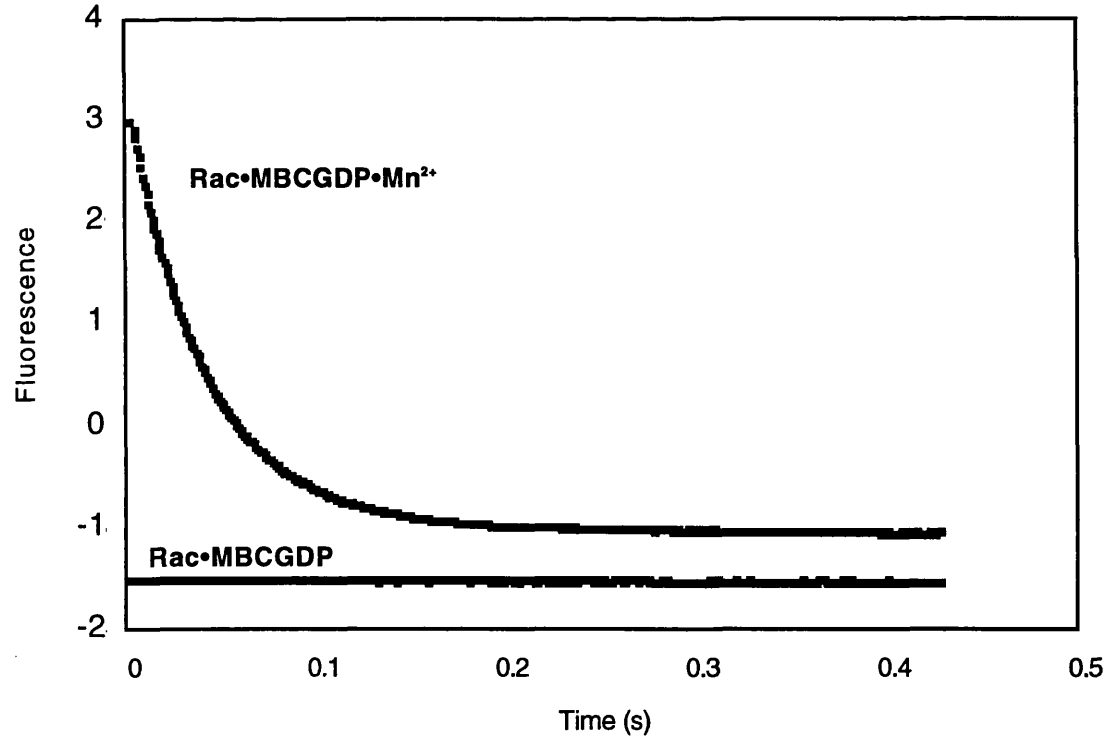

Figure 32b Fluorescent Changes in MBCGDP over 0.5 s. A large decrease in fluorescence is observed with Mn^{2+}, but a very slow increase in the absence of Mn^{2+}

shown, over a short time scale, in Figure 32b. The changes in fluorescence show two phases. The fluorescence initially decreases exponentially over a large amplitude and with a fast rate (24 s^{-1}), which is followed by a slow, relatively small increase in fluorescence (similar to Figure 32a) with a rate of 0.017 s^{-1}. The initial rate is much faster than with Mg^{2+}, whereas the rate of the second phase is very similar.

These experiments were repeated using MBCGMPPNP nucleotides. On mixing of Rac•MBCGMPPNP complexes in the absence of Mn^{2+} with excess GDP and EDTA, the fluorescence decrease occurs exponentially (Figure 33a) with a rate of 4 s^{-1}. This rate is similar to the rate observed with Rac•Mg^{2+}•MBCGMPPNP complexes (3.2 s^{-1}) On mixing Rac•MBCGMPPNP•Mn^{2+} complexes with excess GDP and EDTA, the fluorescence decreases exponentially with a rate of 0.09 s^{-1} (Figure 33b). This rate is approximately 10-fold faster than the rate observed with complexes in the presence of Mg^{2+} (0.010 s^{-1}).

The initial rapid change in fluorescence observed can be interpreted as the release of Mn^{2+}, followed by a subsequent slower release on nucleotide. These data support the model, where the phases previously attributed to nucleotide release shows an unaffected rate from the experiments with Mg^{2+}, whereas the changes in fluorescence attributed to the release of Mg^{2+} shows altered kinetics —presumably due to subtle differences between Mn^{2+} and Mg^{2+}.

Figure 33: fluorescent Changes on Rac•MBCGMPPNP•Mn^{2+} Exchange

The *panels opposite* show the changes in fluorescence on nucleotide exchange with Mn^{2+} complexes of Rac•MBCGMPPNP in the presence and absence of Mn^{2+}. The data produced are measured in Volts which is inversely related to fluorescence. The traces shown are y-axis inverted to demonstrate the changes in fluorescence.

The *upper panel*, 33a, shows the changes in fluorescence on rapid mixing of Mn^{2+}-free Rac•MBCGMPPNP against excess GDP and EDTA. The data produced is best fitted toa single exponential, with a rate of4 s^{-1}.

The data from Rac•MBCGMPPNP•Mn^{2+} exchange is shown in the *lower panel*, 33b. The decrease in fluorescence observed is immediate, and can be fitted to a single exponential. The rate of fluorescent decrease is 0.09 s^{-1}.

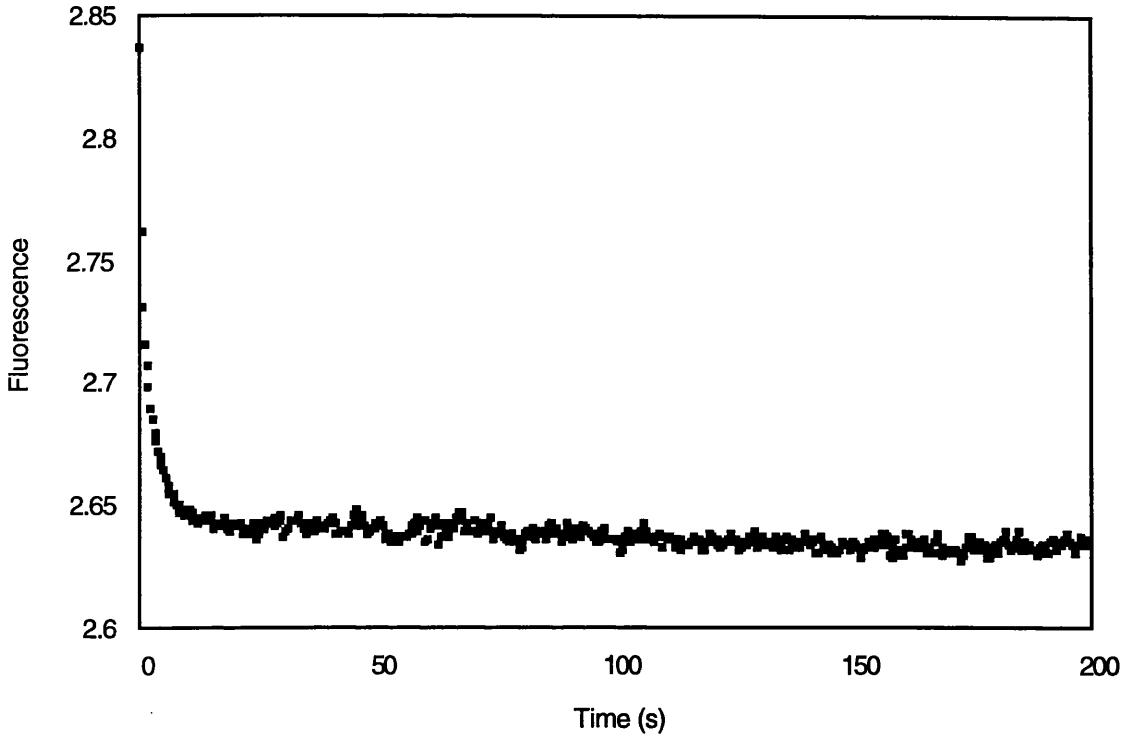

Figure 33a Rac•MBCGMPPNP exchange in the absence of bound Mn^{2+}

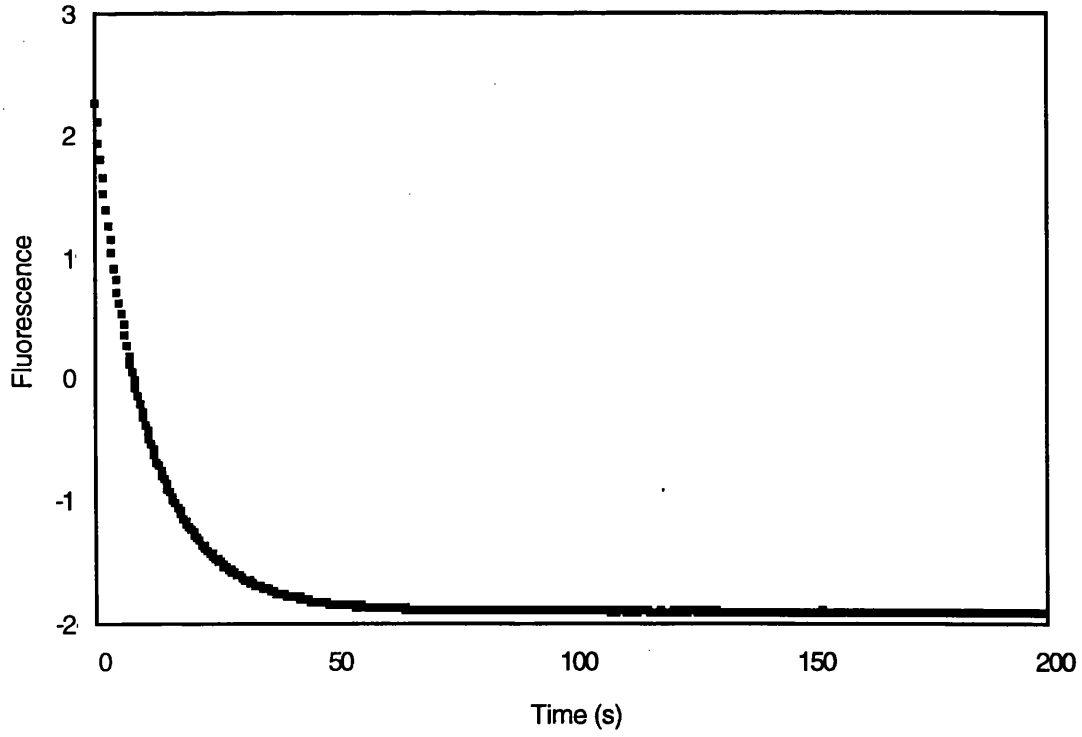

Figure 33b Rac•MBCGMPPNP exchange in the presence of bound Mn^{2+} shows a large decrease in fluorescence

4.2.5 Fluorescent Anisotropy of Mant and MBC Nucleotides Demonstrates Exchange Differences for GMPPNP and GDP Nucleotides

Another test of the proposed model, the exchange process was monitored using fluorescent anisotropy. Changes in fluorescent anisotropy of a fluorescent label may be largely determined by its rotational correlation time. The measurement of the anisotropy of Mant and MBC labelled nucleotides provides a guide as to the size of the complex to which the labelled nucleotide is bound — assuming that the rotation of the fluorophore reflects the rotation of the global complex, rather than any local rotational mobility. It follows that fluorescent anisotropy is mainly sensitive to nucleotide release, since on metal ion release there is likely to be little or no change in average global rotation. Assuming that this is the case, then fluorescent anisotropy will provide a measure for Step Two from the simple model proposed earlier (Figure 31).

Measurements of anisotropy were performed for both Mg^{2+}-bound and Mg^{2+}-free Rac nucleotide complexes as described in Chapter 2. During the nucleotide exchange experiments described in the following section, the anisotropy decreases from a value ~ 0.18 to a value of ~ 0.08.

The rate constants observed in the fluorescent intensity and anisotropy experiments are summarised together in Table 3.

4.2.5.1 Mant Nucleotide

Complexes of Rac•MantGDP in Mg^{2+}-bound and Mg^{2+}-free forms both showed a decrease in anisotropy on nucleotide exchange (Figure 34). In the absence of Mg^{2+} a single exponential decrease in anisotropy with a rate of 0.06 s^{-1} is observed. In the presence of Mg^{2+}, a single exponential decrease in anisotropy is also observed with a rate of 0.07 s^{-1}.

These rates, which reflect nucleotide release, are comparable to the rates of nucleotide release as determined by Mant fluorescent intensity — 0.017 s^{-1}. The slight initial phase observed in these anisotropy traces may represent the release of Mg^{2+}, or the effect of Mg^{2+}'s release on the local rotation of the MBC fluorophore.

These experiments were repeated using Rac•MantGMPPNP complexed nucleotides. These showed different kinetics to MantGDP complexes. The Mg^{2+}-free Rac•MantGMPPNP complex, on rapid mixing with excess EDTA and GDP, showed a single exponential decrease in anisotropy with a rate of 0.85 s^{-1} (Figure 35). In the presence of Mg^{2+}, the Rac•MantGMPPNP•Mg^{2+} complex showed a much slower rate of decrease in anisotropy, of 0.007 s^{-1}.

The previous experiments which measured the fluorescent intensity changes on nucleotide release showed a rate for Step Two of 0.01 s^{-1} in the presence of Mg^{2+} and 3 s^{-1} in the absence of Mg^{2+}. The anisotropy data for the release of GMPPNP in the presence of Mg^{2+} is in approximate agreement with the fluorescent intensity data, however, in the absence of

Figure 34: Changes in Anisotropy on Rac•MantGDP Exchange

The panels opposite show the changes in anisotropy on nucleotide exchange with Rac•MantGDP in the presence and absence of bound Mg^{2+}.

The *upper panel*, 34a, shows the changes in anisotropy on rapid mixing of Mg^{2+}-free Rac•MantGDP against excess GDP and EDTA. The data shows a decrease in anisotropy from 0.17 to 0.07, representing MantGDP exchange into solution and an increase in rotational freedom. This decrease can be fitted to a single exponential with a rate of 0.06 s^{-1}.

The *lower panel*, 34b, illustrates Rac•MantGDP•Mg^{2+} exchange. The data shows a decrease in anisotropy, as in the *upper panel*, also with a slight lag in the initial few seconds of exchange. The large decrease in anisotropy can be fitted to a single exponential with a rate of 0.06 s^{-1}.

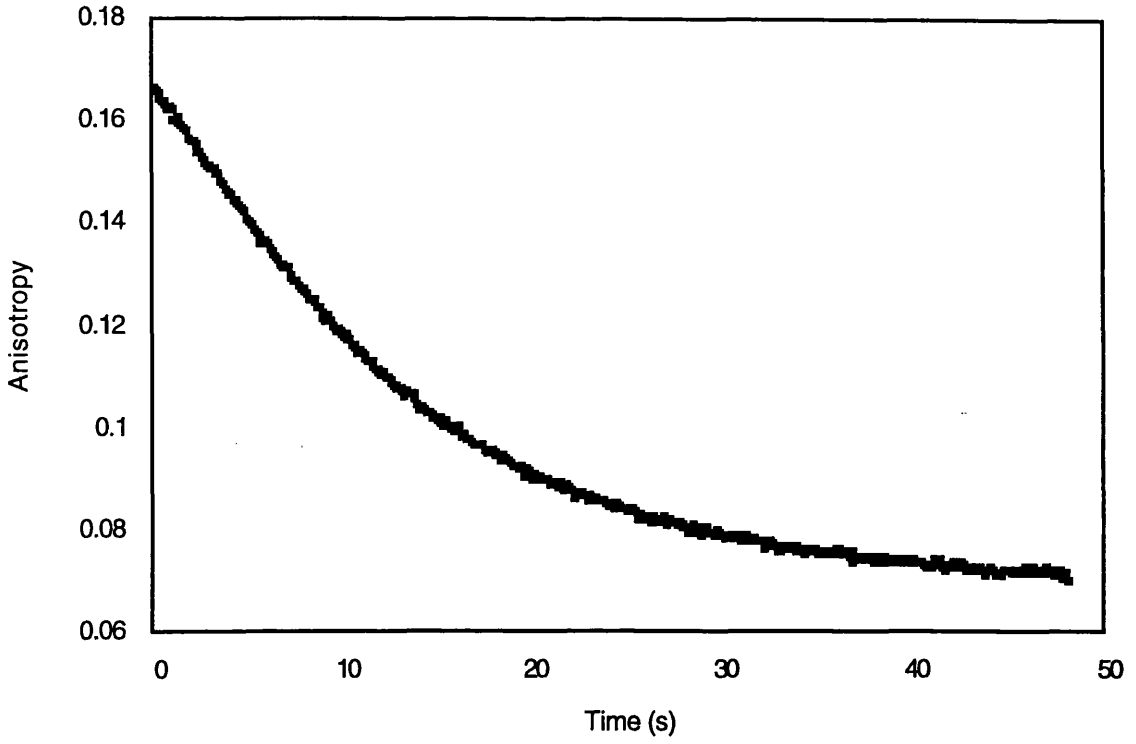

Figure 43a Changes in Anisotropy on Rac•MantGDP exchange in the absence of bound Mg^{2+}

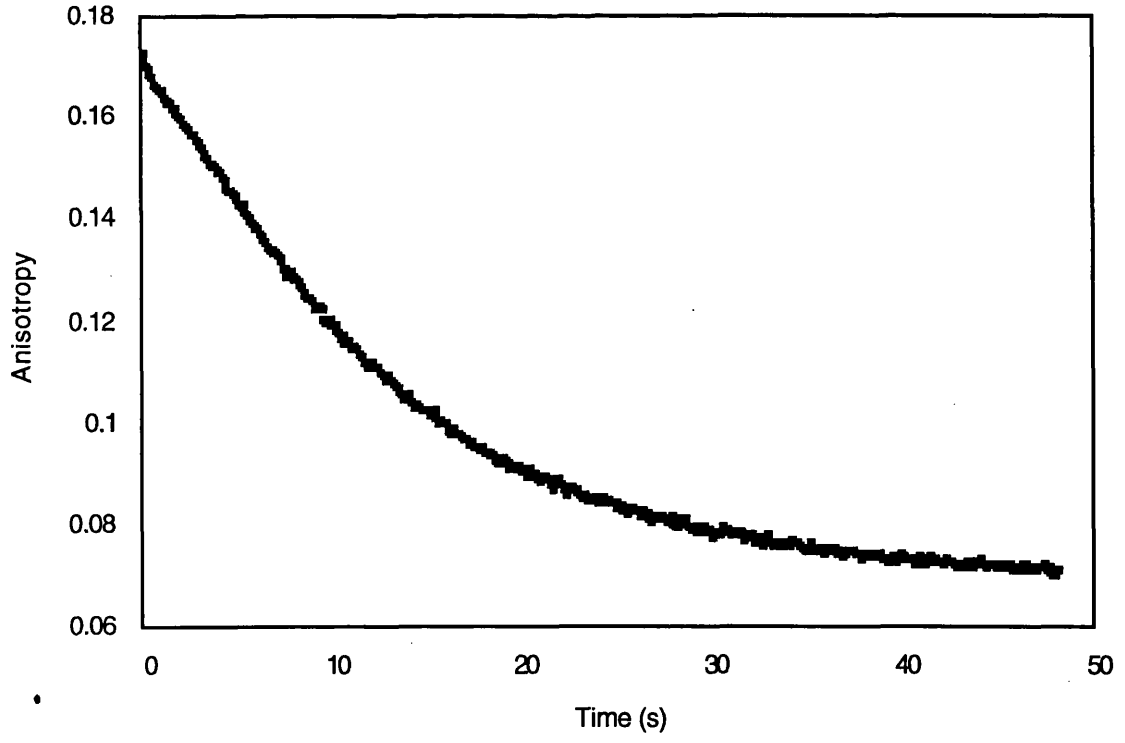

Figure 43a Changes in Anisotropy on Rac•MantGDP•Mg^{2+} exchange

Figure 35: Changes in Anisotropy on Rac•MantGMPPNP Exchange

The panels opposite show the changes in anisotropy on nucleotide exchange with Rac•MantGMPPNP in the presence and absence of Mg^{2+}.

The *upper panel*, 35a, which illustrates the changes of anisotropy of Mg^{2+}-free Rac•MantGMPPNP on nucleotide exchange, shows an immediate and rapid decrease in anisotropy, which can be fitted to a single exponential with a rate of 0.85 s^{-1}.

The *lower panel,* 35b, shows the changes in anisotropy on Rac•MantGMPPNP•Mg^{2+} exchange. The data shows a decrease in anisotropy, as in the *upper panel*, however there is a clear lag during the initial few seconds. The large decrease in anisotropy can be fitted to a single exponential with a rate of 0.007 s^{-1}.

These data suggest that in the presence of Mg^{2+}, the nucleotide is released slowly, although the cause of the initial lag is unclear. The data produced in the absence of Mg^{2+} suggests that the MantGMPPNP nucleotide is release rapidly into solution on GDP exchange.

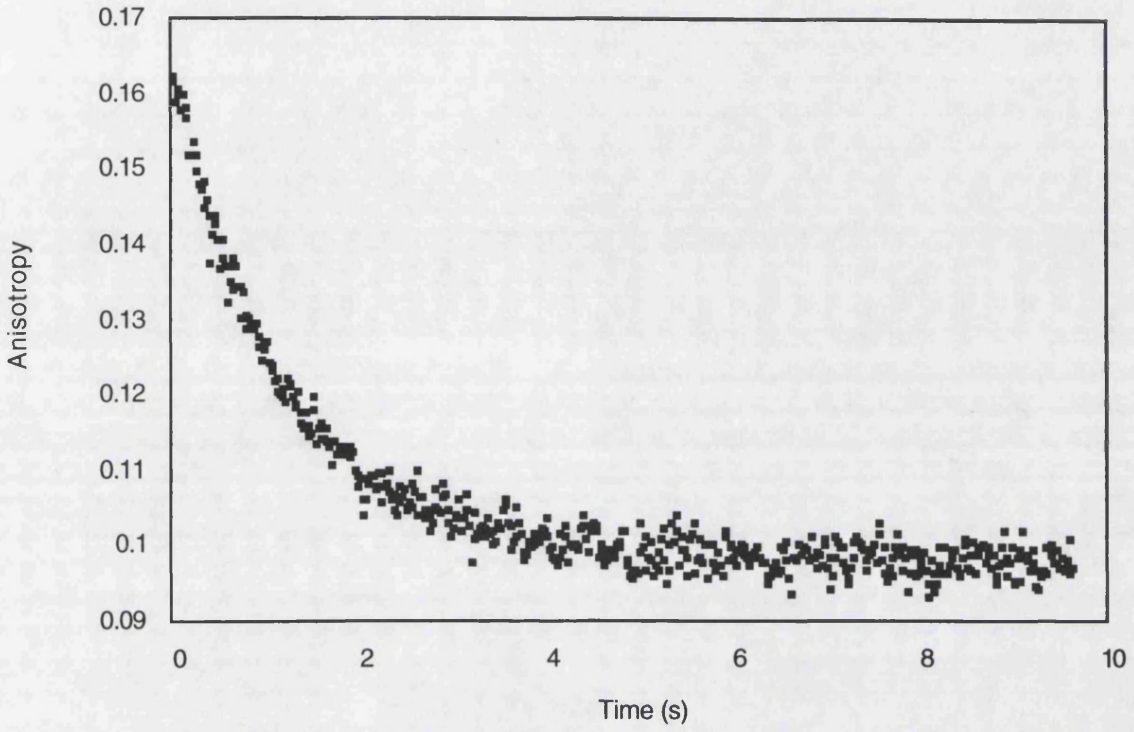

Figure 35a Changes in Anisotropy on Rac•MantGMPPNP exchange in the absence of bound Mg^{2+}

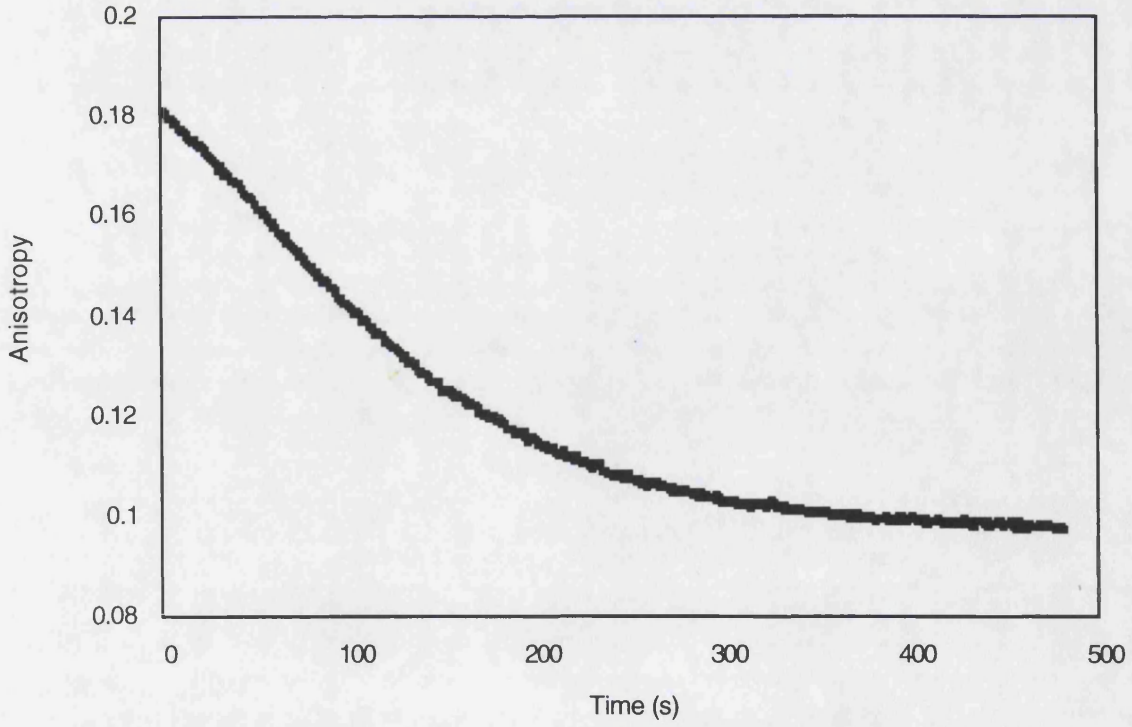

Figure 35b Changes in Anisotropy on Rac•MBCGMPPNP exchange in the presence of bound Mg^{2+}

Mg^{2+}, the rates of nucleotide release as measured by anisotropy and fluorescent intensity differ by approximately 10-fold.

These results suggest that in Rac•MantGDP complexes, the nucleotide is able to exchange freely but this requires initial release of Mg^{2+}, which may be reflected by the small initial lag in the anisotropy data. The release of Mg^{2+} is not rate limiting for nucleotide exchange, and the anisotropy data supports the two-step model. In Rac•MantGMPPNP complexes in the absence of Mg^{2+}, nucleotide release occurs at a faster rate than that of MantGDP, suggesting that the nucleotide is bound more weakly to Rac than MantGDP. However, its release in the presence of Mg^{2+} is slowed greatly by 100-fold, suggesting that Mg^{2+} release acts as the rate limiting step for the exchange process. The data of MBCGMPPNP release broadly agrees with the previous fluorescent intensity data and the two step model, although in the absence of Mg^{2+} some anomalous values are observed, which are discussed later.

4.2.5.2 MBC Nucleotide

Anisotropy measurements were made with both Rac•MBCGDP and Rac•MBCGMPPNP complexes providing information on the rate of nucleotide release of MBC nucleotides, Step Two in the proposed model (Figure 31). These measurements were made in the absence and presence of Mg^{2+} and Mn^{2+}, which allows a comparison of the effects that these two metal ions have on the exchange process. If the earlier two step model is correct, then the main changes in anisotropy will occur on nucleotide release, which will show differences

between the GMPPNP and GDP Rac forms, but not between Mg^{2+} or Mn^{2+} bound or free Rac forms.

On rapid mixing of Rac•MBCGDP (in the absence of associated-Mg^{2+}) with excess GDP and EDTA, anisotropy decreases exponentially, with a rate of 0.020 s^{-1} (Figure 36a). On rapid mixing of Rac•MBCGDP•Mg^{2+} with excess EDTA and GDP, a short lag, lasting approximately 2 seconds can be seen (Figure 36b), before an exponential decrease in anisotropy occurs, which is similar to that shown in Figure 36a, and with a rate of 0.020 s^{-1}.

These data can be compared with the data from the fluorescent intensity experiments earlier in the section. The rates of change in anisotropy measured here for Rac•MBCGDP complexes are in agreement with the rates for step two of the proposed model, as measured by fluorescence intensity.

These experiments were repeated with the MBCGMPPNP nucleotide complexed to Rac. On rapid mixing of Rac•MBCGMPPNP in the absence of Mg^{2+}, a rapid exponential decrease in anisotropy with a rate of 0.4 s^{-1} was observed (Figure 37a). In the presence of Mg^{2+} (Figure 37b) the exponential decrease in anisotropy on nucleotide exchange is very slow, a rate of 0.004 s^{-1}. There is also a very slight decreased rate during the first few seconds of the exchange.

The data for the MBCGMPPNP nucleotides as measured by fluorescent anisotropy is in broad

Figure 36: Changes in Anisotropy on Rac•MBCGDP Exchange

The panels opposite show the changes in anisotropy on nucleotide exchange with Rac•MBCGDP in the presence and absence of Mg^{2+} in the Rac•MBCGDP complex.

The *upper panel,* 36a, shows exchange in the absence of complex-associated Mg^{2+}. A decrease in anisotropy is observed, which can be fitted to a single exponential with a rate of 0.02 s^{-1}. No lag was observed preceding the decrease in anisotropy.

The *lower panel,* 36b, shows the first 50 seconds of nucleotide exchange with Rac•MBCGDP•Mg^{2+}. The remainder of the data shows a decrease in anisotropy, similar to that found in the *upper panel* (with a rate of 0.02 s^{-1}), however, the data shown opposite illustrates the short lag period observed under the exchange conditions.

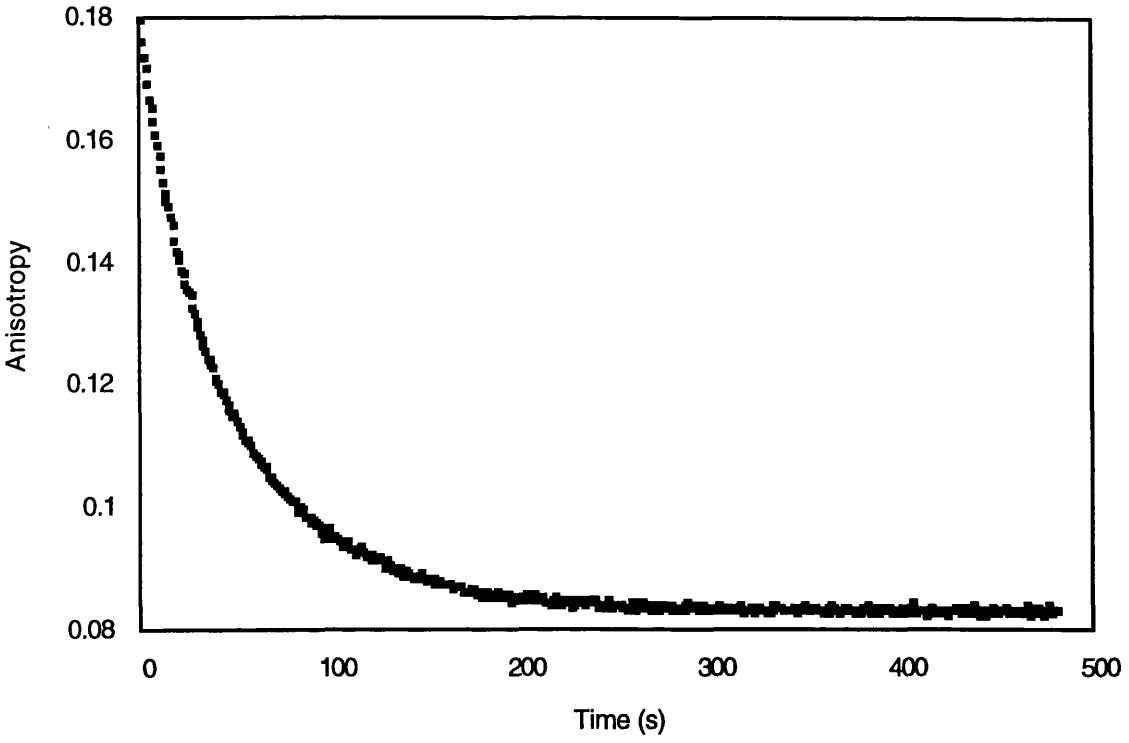

Figure 36a Changes in Anisotropy on Rac•MBCGDP exchange in the absence of bound Mg^{2+}

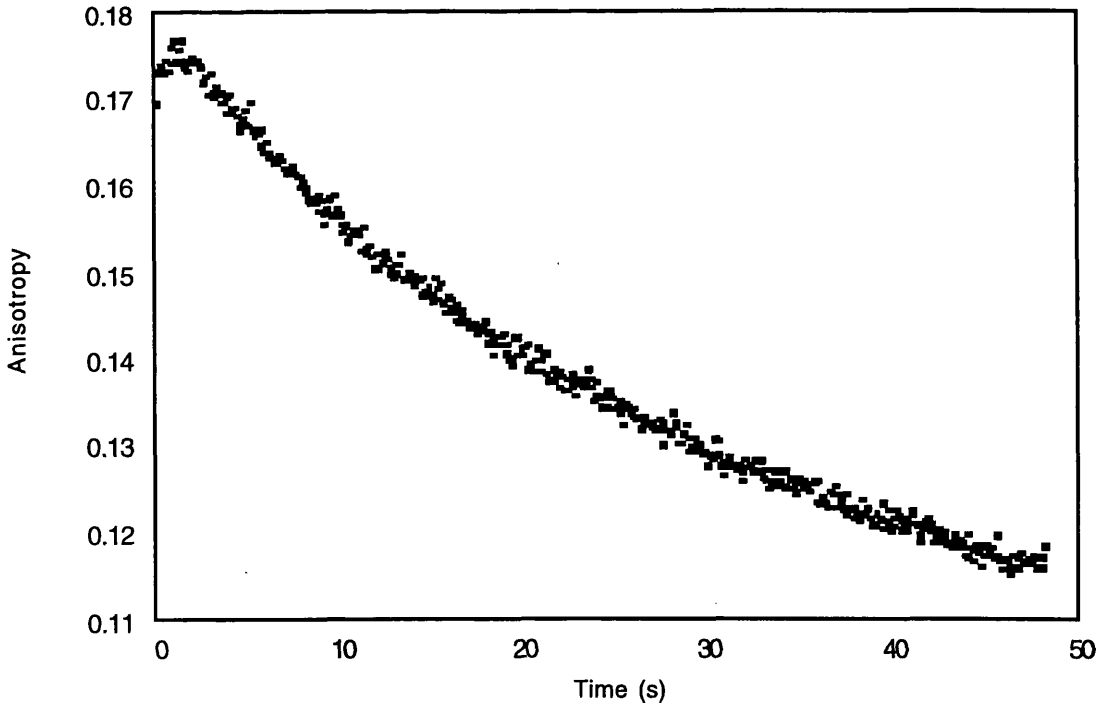

Figure 36b Changes in Anisotropy on Rac•MBCGDP exchange in the presence of bound Mg^{2+}

Figure 37: Changes in Anisotropy on Rac•MBCGMPPNP Exchange

The panels opposite show the changes in anisotropy on nucleotide exchange with Rac•MBCGMPPNP in the presence or absence of complexed Mg^{2+} in the Rac•MBCGMPPNP complex.

The *upper panel,* 37a, shows exchange in the absence of complex-associated Mg^{2+}. A decrease in anisotropy is observed, with a rate of 0.4 s^{-1}.

The exchange of GDP for MBCGMPPNP in the presence of Mg^{2+} is shown in the *lower panel,* 37b. A slow decrease in anisotropy is observed with rate of 0.004 s^{-1}.

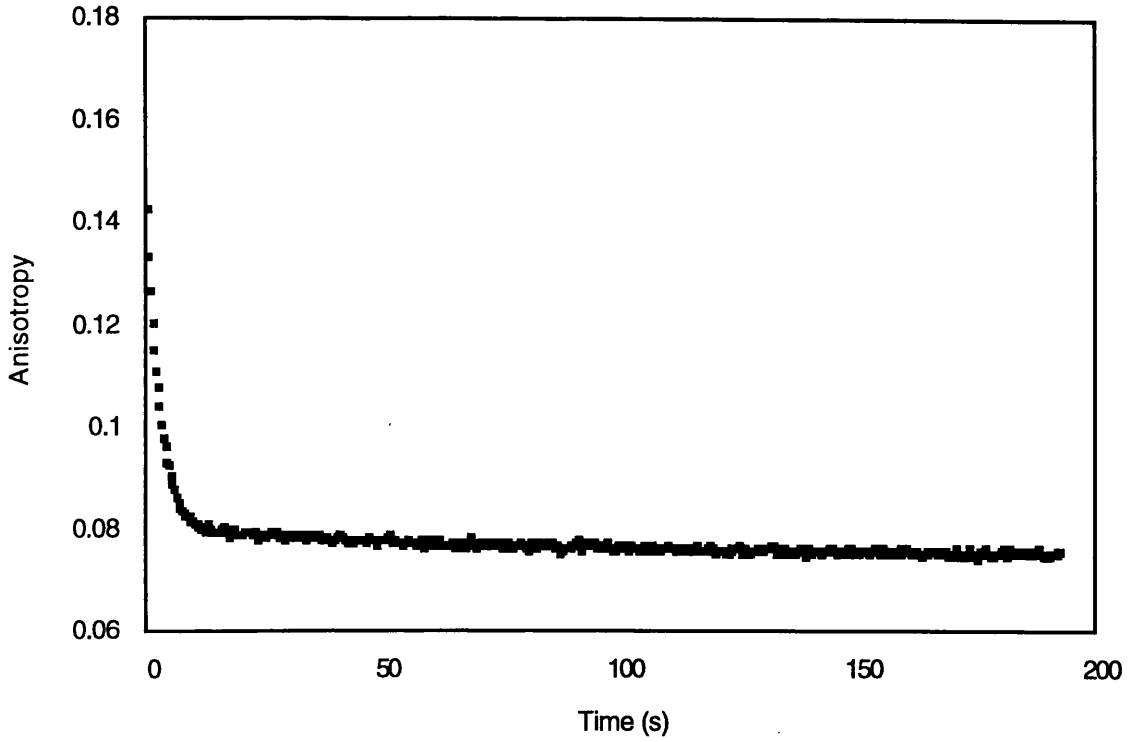

Figure 37a Changes in Anisotropy on Rac•MBCGMPPNP exchange in the absence of bound Mg^{2+}

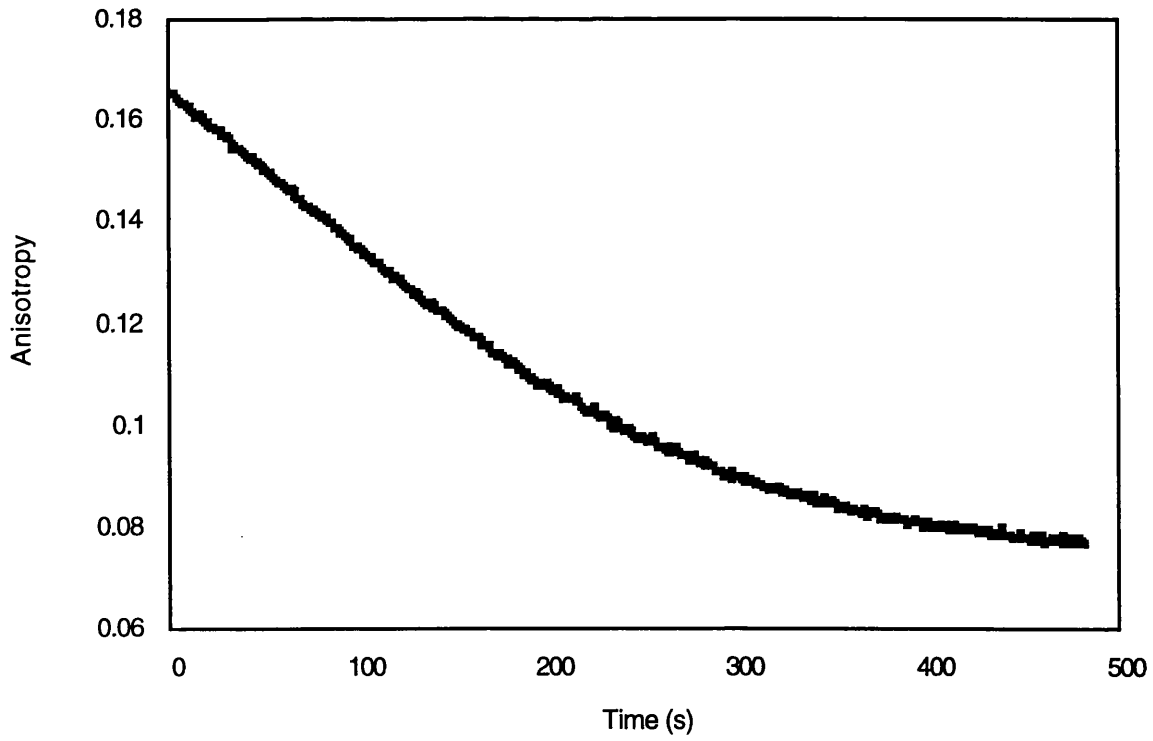

Figure 37b Changes in Anisotropy on Rac•MBCGMPPNP exchange in the presence of bound Mg^{2+}

agreement with the data measured previously by fluorescent intensity, although the data in the absence of Mg^{2+} differs between the intensity and anisotropy experiments. This is discussed later.

4.2.5.3 Substitution of Mg^{2+} with Mn^{2+}

Exchange experiments with Rac•MBCGDP were repeated with the substitution of Mg^{2+} with Mn^{2+}. The changes in anisotropy on nucleotide exchange (Figure 38) are similar to those with Mg^{2+}. In the absence of Mn^{2+} (Figure 38a), the exponential decrease in anisotropy shows a rate of 0.03 s^{-1}. In the presence of Mn^{2+} (Figure 38b), an exponential decrease in anisotropy is observed with a rate of 0.03 s^{-1}, and a very short (0.5 s) lag period is observed.

On substitution of Mn^{2+} for Mg^{2+} in the Rac•MBCGMPPNP complexes (Figure 39), in the absence of complex-associated Mn^{2+}, an exponential decrease in anisotropy is observed with a rate of 0.4 s^{-1} (Figure 39a). In the presence of Mn^{2+}, a slow exponential decrease in anisotropy was observed, which could be fitted to a single exponential with a rate of 0.03 s^{-1} (Figure 39b).

The use of Mn^{2+} provided a further test of the simple model and the effects of the metal ion on nucleotide release. The rates of change in anisotropy for Rac complexes in the presence of both Mg^{2+} and Mn^{2+} were similar, which supports that the metal ion is involved in the

Figure 38: Changes in Anisotropy on Rac•MBCGDP•Mn^{2+} Exchange

The panels opposite show the changes in anisotropy on nucleotide exchange with Rac•MBCGDP in the presence and absence of Mn^{2+}.

The *upper panel*, 38a, shows exchange in the absence of complex-associated Mn^{2+}. A decrease in anisotropy is observed, which can be fitted to a single exponential with a rate of 0.03 s^{-1}. No lag was observed preceding the decrease in anisotropy.

The *lower panel,* 38b, shows the decrease in anisotropy during nucleotide exchange with the Rac•MBCGDP•Mg^{2+}. This decrease in anisotropy could be fitted to a single exponential curve, with a rate of 0.03 s^{-1}. A slight lag, lasting no longer than 0.5 seconds was observed (data not shown).

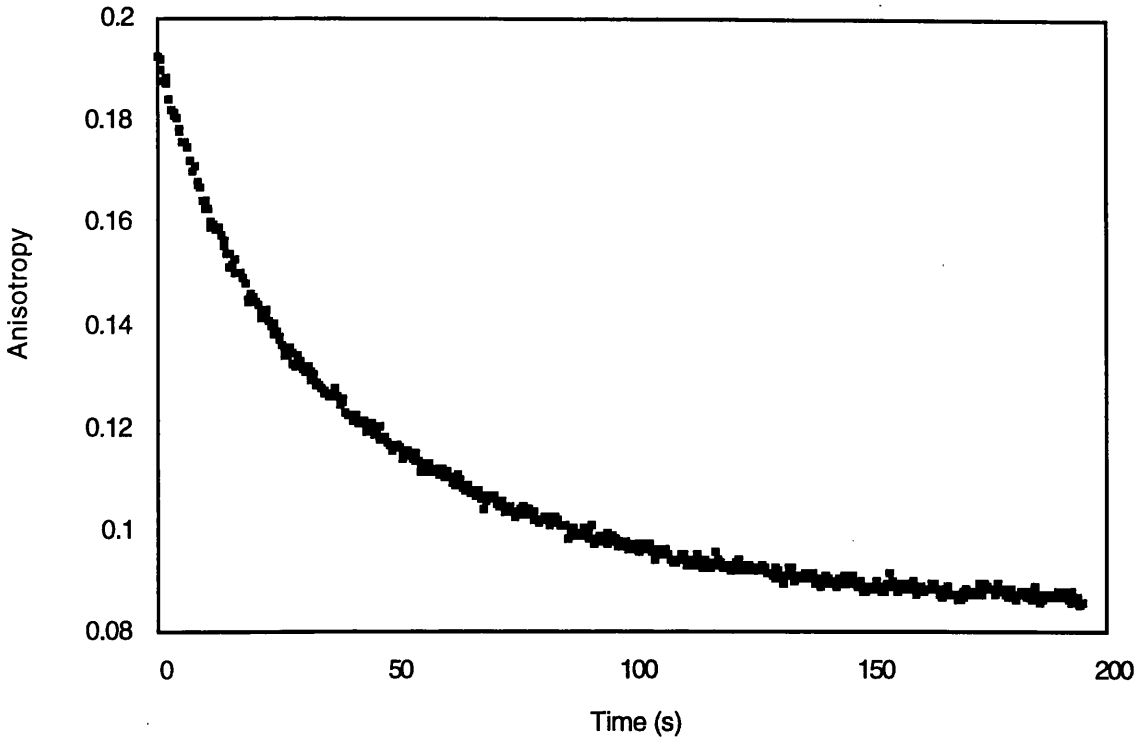

Figure 38a Changes in Anisotropy on Rac•MBCGDPexchange in the absence of bound Mn^{2+}

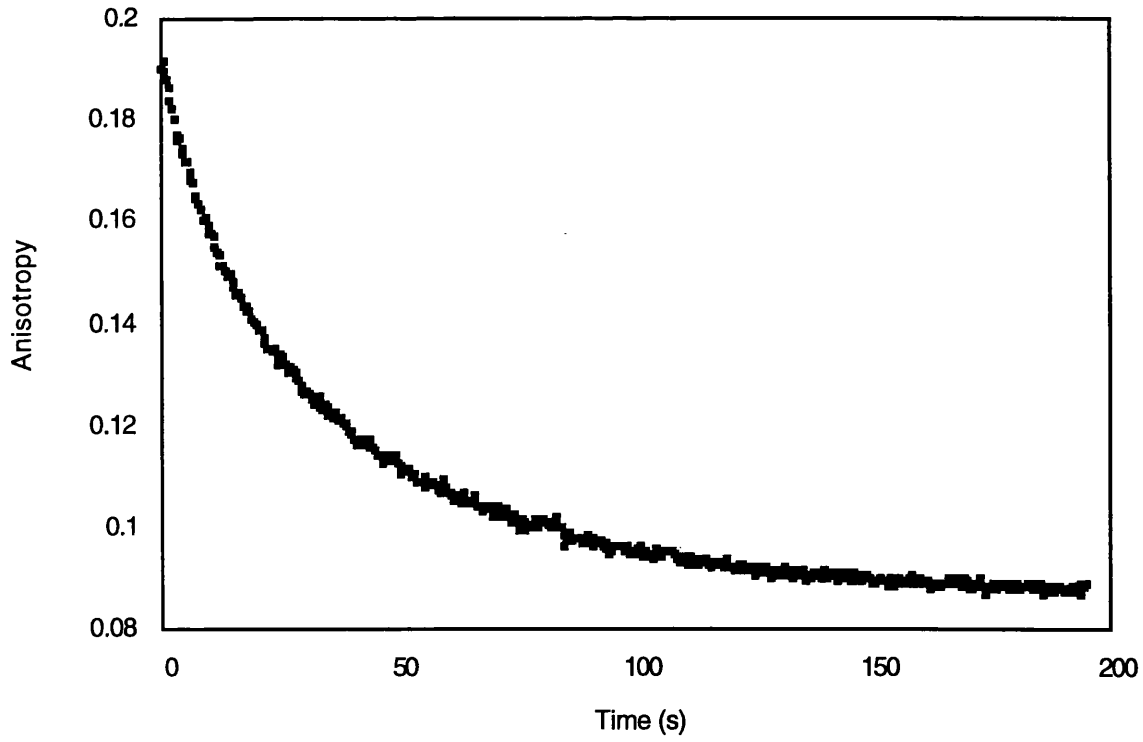

Figure 38b Changes in Anisotropy on Rac•MBCGDP exchange in the presence of bound Mn^{2+}

Figure 39: Changes in Anisotropy on Rac•MBCGMPPNP•Mn^{2+} Exchange

The panels opposite show the changes in anisotropy on nucleotide exchange with Rac•MBCGMPPNP in the absence and presence of bound Mg^{2+}.

The *upper panel, 39a,* shows exchange in the absence of complex-associated Mn^{2+}. An initial decrease in anisotropy is observed, which can be fitted to a single exponential with a rate of 0.4 s^{-1}.

The *lower panel, 39b,* illustrates the decrease in anisotropy on nucleotide exchange in the presence of Mn^{2+}. The release is slow, and can be fitted to a single exponential with a rate of 0.03 s^{-1}.

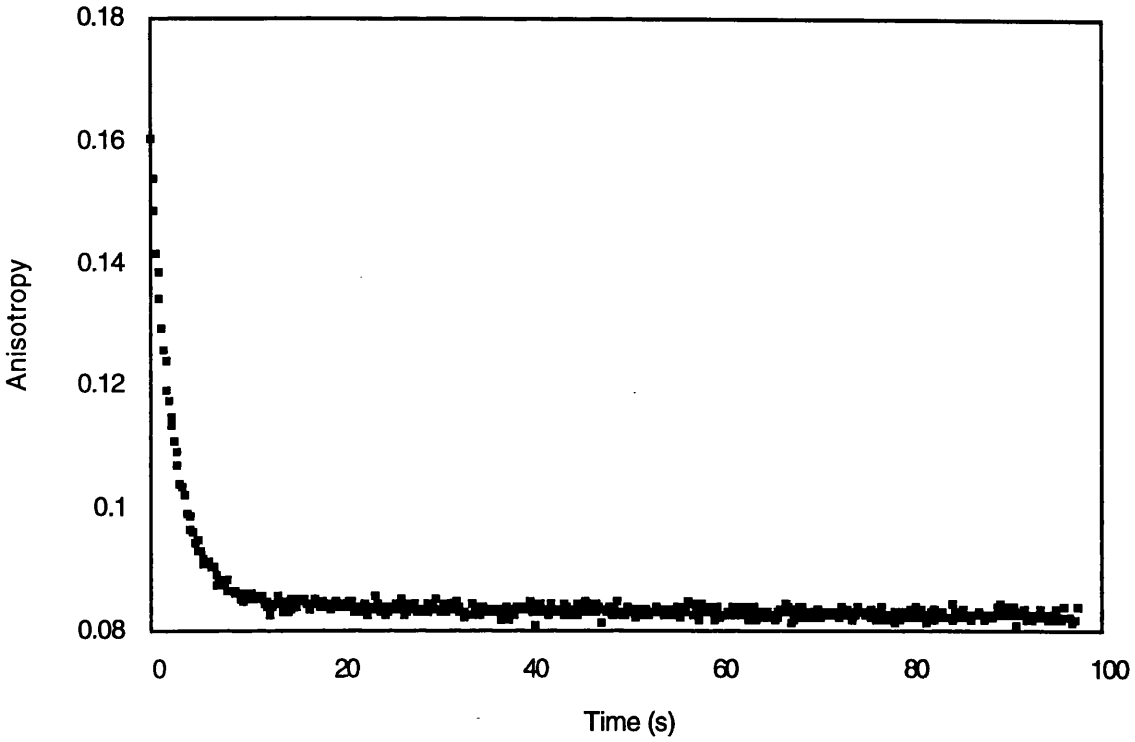

Figure 39a Changes in Anisotropy on Rac•MBCGMPPNP exchange in the absence of bound Mn^{2+}

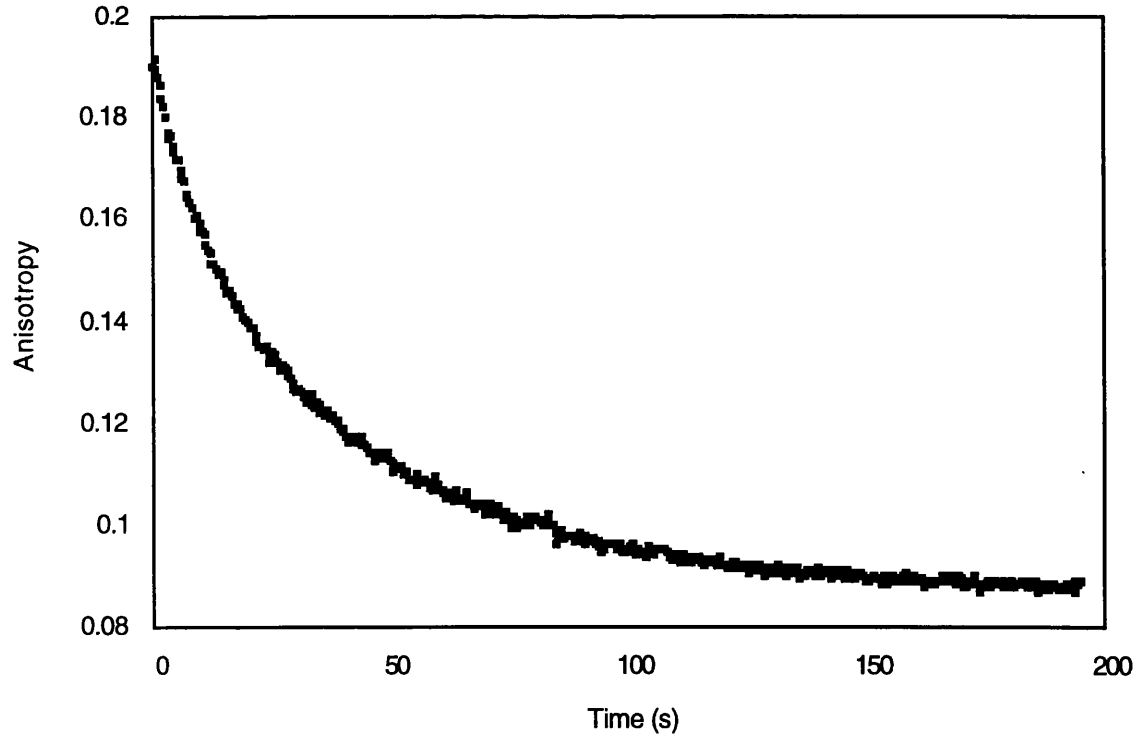

Figure 39b Changes in Anisotropy on Rac•MBCGMPPNP exchange in the presence of bound Mn^{2+}

first step of the proposed model.

Overall the anisotropy data shows little difference between the divalent cations, confirming that the anisotropy is providing information on the nucleotide. The only discrepancy between the fluorescent intensity data and anisotropy data is observed on release of MBCGMPPNP from Rac in the absence of metal ion. The Mant and MBC nucleotides both show similar rates for this change in anisotropy. The significance of this will be discussed later.

4.2.6 Mg^{2+} Binding to Rac MBC Nucleotide Complexes

This section examines binding of Mg^{2+} to Mg^{2+}-free Rac•MBCGDP and Rac•MBCGMPPNP. These complexes were rapidly mixed with excess Mg^{2+} at varying concentrations, in pseudo-first order conditions, using a variety of excess Mg^{2+} concentrations where the Mg^{2+} was in sufficient excess over the Rac complex so that the free Mg^{2+} concentration remained effectively constant throughout the binding process. The rates of fluorescent changes measured at these concentrations on the stopped flow instrument provide information on the binding events occurring. The Mg^{2+}-free complexes were created by incubation with excess concetrations of EDTA. For Rac•MBCGDP complexes, the concetration was sufficiently small (15 μM) to be negligble, but Rac•MBCGMPPNP required incubation with 0.5 mM EDTA. This produced an EDTA concetration in the mixing chamber of 0.25 mM. This may not be significant when rapidly mixed with higher concetrations of Mg^{2+}, although

its significance at lower concentrations of Mg^{2+} is unclear.

Two typical traces of Mg^{2+} binding to Rac•MBCGDP is shown in Figure 40a. The binding curves show an increase in fluorescence which can be fitted well to a single exponential, giving the rate for Mg^{2+} binding. A plot of Mg^{2+} concentration against observed rate is shown in Figure 40b. This demonstrates that the observed rate increases in a hyperbolic fashion with concentration and suggests a two-step process, which in this report is interpreted as rapid binding of Mg^{2+} followed by a change of protein conformation causing

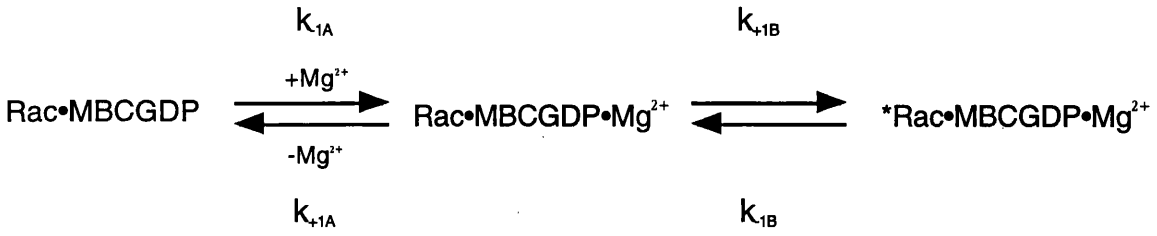

a change in MBC fluorescence (Figure 40b).

The data shown is fitted to a hyperbolic function, which gives a maximum binding rate (k_{-1B} + k_{+1B}) of 410 s^{-1}, and a value of $1/K_{1A}$ of 3.5 mM. Further analysis of these data can be found in the Discussion.

Similar Mg^{2+} binding experiments were performed using Rac•MBCGMPPNP. Typical traces can be seen in Figure 41 (Figure 41a short time scale, Figure 41b long time scale). This overall data is best fitted to two exponentials. The rate of the first phase increases with Mg^{2+} concentration and saturates at high Mg^{2+} levels. This suggests that this phase is directly related to Mg^{2+} binding. A second phase also is observed, whose rate is independent

Figure 40: Mg^{2+} Binding to Rac•MBCGDP

The *upper panel,* 40a, opposite shows typical data recorded from the binding of Mg^{2+} to Mg^{2+}-free Rac•MBCGDP. The data was produced by the rapid mixing of 2 mM $MgCl_2$ (*i*) or 100 µM $MgCl_2$ (*ii*) to 1 µM Rac•MBCGDP and 15 µM EDTA, as described in Chapter 2.8.2.2 (final concentrations 1 mM and 50 µM respectively). The rapid increase in fluorescence due to Mg^{2+} binding can be fitted to a single exponential, which in these examples, give initial rates of 82 s^{-1} and 5 s^{-1}.

The *lower panel,* 40b, shows the complete data of all the titration experiments. The final concentration of Mg^{2+} (mM) is plotted against the average initial rate at each particular Mg^{2+} concentration. The data is best fitted to a hyperbolic function, which give a (k_{+1} + k_{-1}) of 410 s^{-1}, and a K_{1A} of 3.5 mM.

The data described here suggests a two-step mechanism to Mg^{2+} binding, with one step in the mechanism causing a fluorescent change in the MBC fluorophore. Formally, this change in fluorescence can be caused by either the binding of Mg^{2+} to the protein, or a subsequent change in protein conformation on Mg^{2+} binding — however, using the data presented here, these two events would be indistinguishable.

It is known that Mg^{2+} binding is usually rapid, and so it is therefore more likely that in this report, the fluorescence change occurs on a protein conformational change subsequent to Mg^{2+} binding, rather than on actual Mg^{2+} binding.

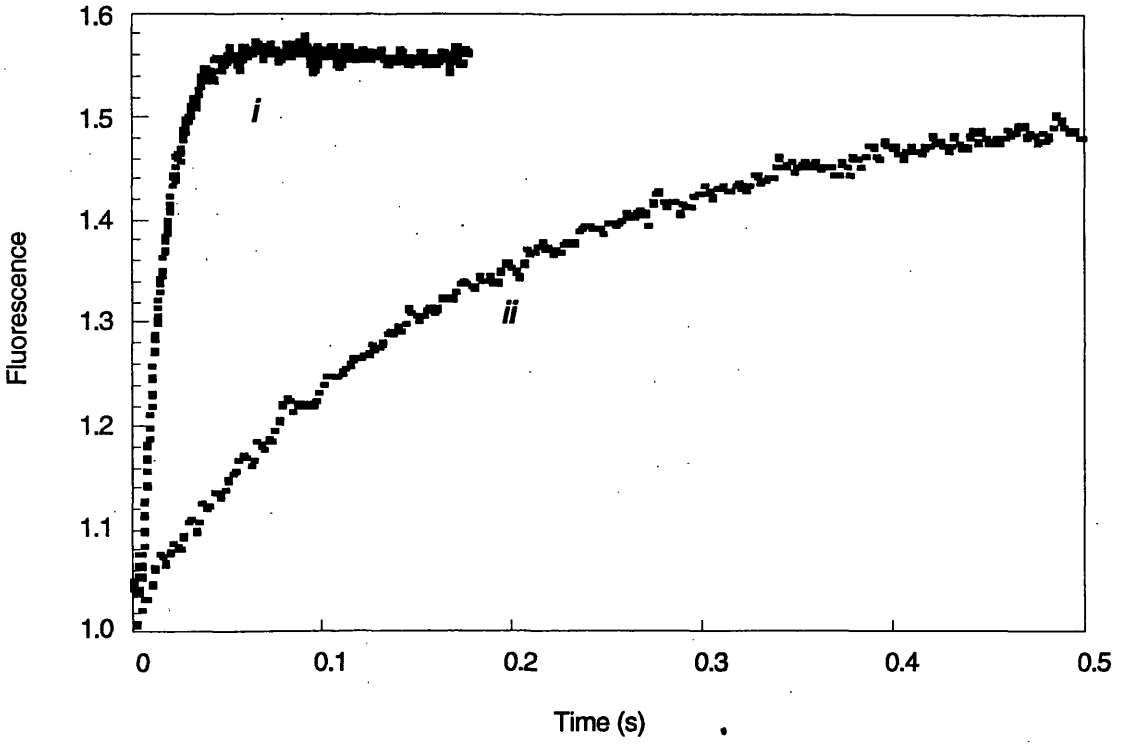

Figure 40a Changes in Fluorescent Intensity on Mg^{2+} binding to Rac•MBCGDP

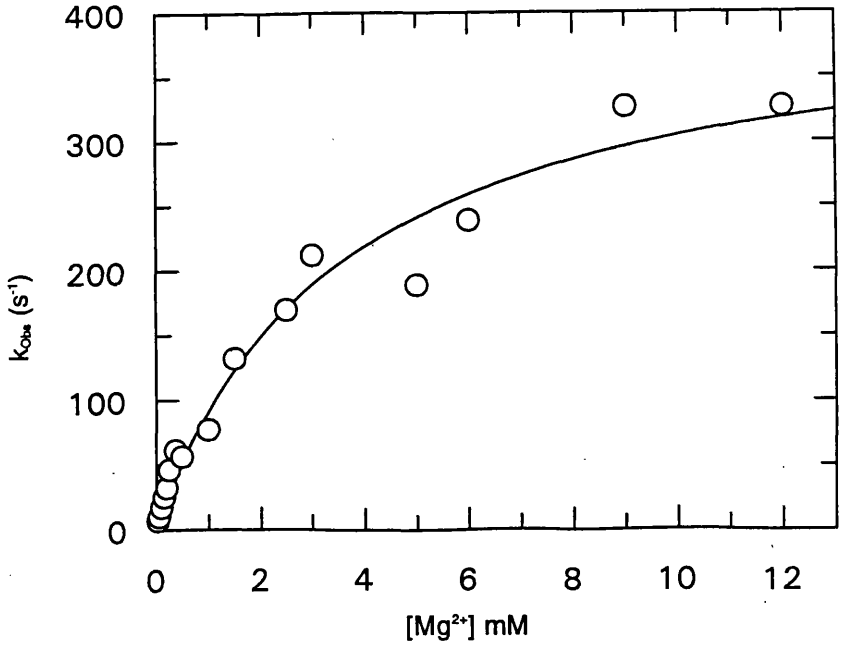

Figure 40b Observed Mg^{2+} to Rac•MBCGDP Binding Rate against Mg^{2+} Concentration

Figure 41: Mg^{2+} Binding to Rac•MBCGMPPNP

The *panels opposite* shows typical data recorded from the binding of Mg^{2+} to Mg^{2+}-free Rac•MBCGMPPNP.

The *upper panel* , 41a, shows a single binding reaction (1 μM Rac•MBCGMPPNP to 2 mM $MgCl_2$). A very rapid increase in fluorescence occurs within the first 0.2 seconds of the reaction, with a rate of (in this example) 165 s^{-1}. This initial increase is followed by a slower increase in fluorescence.

The *lower panel,* 41b, shows the secondary increase in fluorescence over a longer timescale. The secondary phase can clearly seen and the fluorescence increases in with a rate of 0.08 s^{-1}.

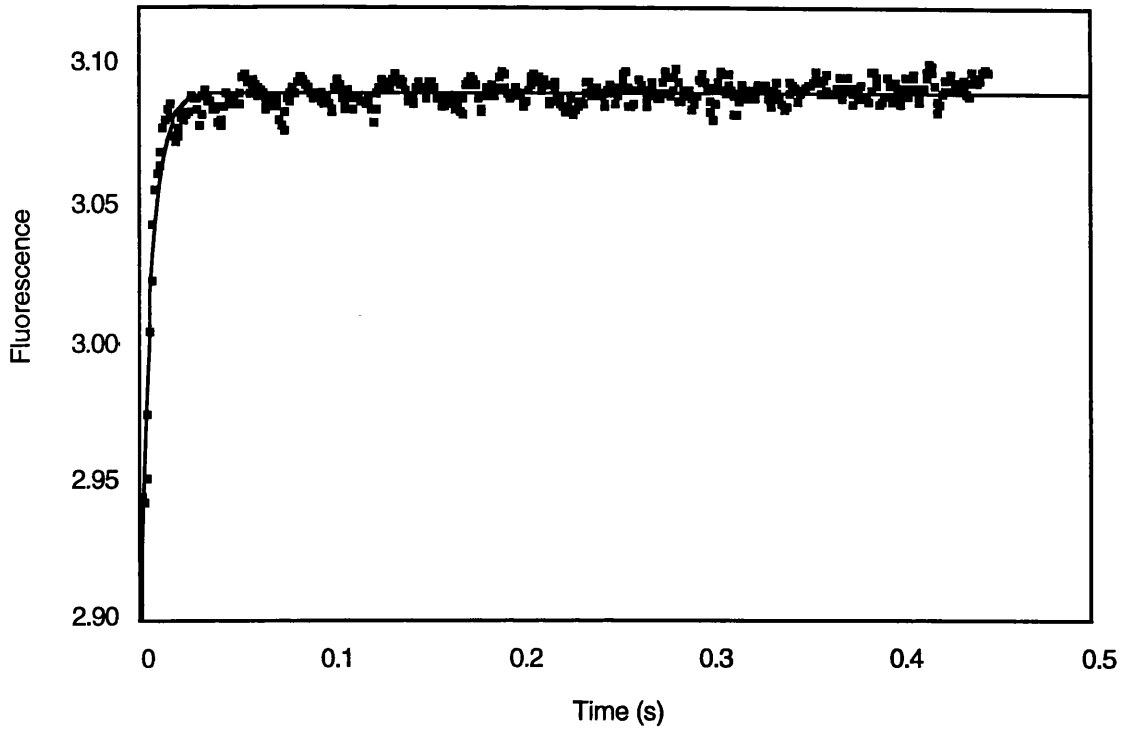

Figure 41a Changes in Fluorescent intensity on Mg^{2+} binding to Rac•MBCGMPPNP, over 0.5 second

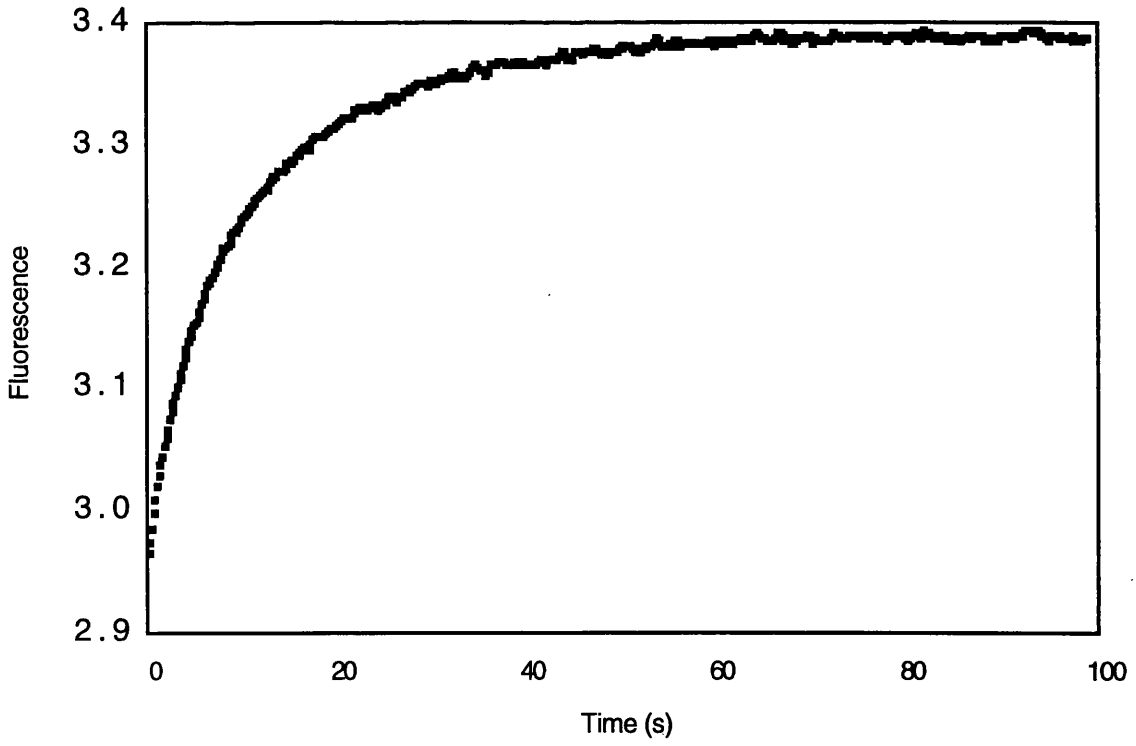

Figure 41b Changes in Fluorescent Intensity on Mg^{2+} binding to Rac•MBCGMPPNP, over 100 seconds

from Mg^{2+} concentration, which may suggest a slow conformational change. A plot of k_{obs} of the first phase against Mg^{2+} concentration (Figure 42) shows that the rate of Mg^{2+} binding, fitted to a hyperbolic binding curve gives a rate ($k_{-1B} + k_{-1B}$) of 237 s^{-1}, and a $1/K_{1A}$ value of 1.5 mM.

The fluorescent changes on Mg^{2+} binding to Rac•MBCGMPPNP suggests a model which has two steps similar to that found in Rac•MBCGDP (k_{-1A} and k_{-1B}), but may also have a further step (k_{-1C}) as indicated by the additional change in fluorescence, as shown in Figure 4· ъ. Further analysis of these data can be found in the Discussion.

4.3 Discussion

The previous sections have provided evidence for a two step model during exchange: Mg^{2+} release, followed by nucleotide release. The two fluorophores, Mant and MBC, each attached to GDP or GMPPNP nucleotides, provided information on the exchange process for both Rac•GDP and Rac•GMPPNP, and MBC in particular allowed observation of the two individual steps of the proposed model. The use of fluorescent anisotropy and Mn^{2+} as a Mg^{2+} substitute provide further support for the two step model.

This section of the Chapter will gather the data presented in the results section, and discuss the observations with respect to one another and the small G-protein field as a whole.

Figure 42: Mg^{2+} Binding to Rac•MBCGMPPNP

The *panel opposite* shows the complete titration data for Mg^{2+}-binding to Rac•MBCGMPPNP. Each point is an average of the initial rates at a particular Mg^{2+} concentration.

The data is fitted to a hyperbolic curve, with a $(k_{+1} + k_{-1})$ of 237 s^{-1}, and a K_{1A} of 1.5mM. The nature of the hyperbolic fit suggests that the act of Mg^{2+} binding is not itself the rate limiting step, rather another stage must be involved.

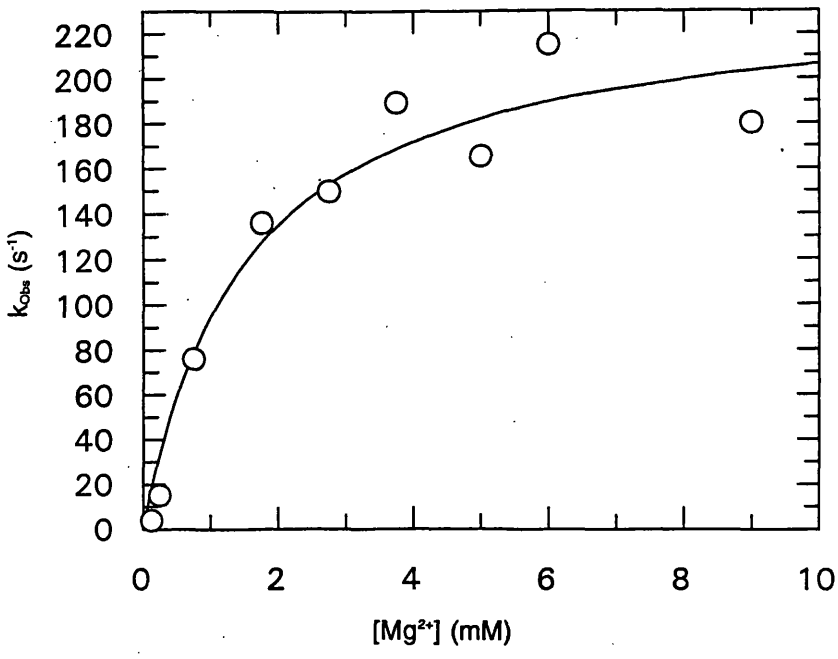

Figure 42 Observed Mg^{2+}-to-Rac•MBCGMPPNP Initial Rate against Mg^{2+} Concentration

The Two Step Model for Mg^{2+} and Nucleotide Release from Rac•GDP

The data from the Mg^{2+} and nucleotide release experiments with Rac•GDP (Table 3) suggest a two step model of nucleotide release (Figure 31), involving a fast step of Mg^{2+} release (Step 1) followed by a slower step of nucleotide release (Step 2). The subsequent experiments which examined the binding of Mg^{2+} to Rac•GDP showed two step binding for Step 1 itself. Step 1 can therefore be subdivided into Step 1A and Step 1B (Figure 43a).

The release of Mg^{2+} from Rac•GDP consists of the two steps, Step 1A and Step 1B. The rate of the change in fluorescence on Mg^{2+} release is also determined by the rates of these two steps. In the simplest model, Step 1A (the initial binding and release of Mg^{2+}) can be assumed to be very fast and not rate limiting, since it is possible to saturate Step 1B. The rate for Mg^{2+} release (k_{+1}) is therefore equal to the rate k_{+1B}, which has a measured value of 1.4 s^{-1}. Since Step 1B has a value of 410 s^{-1}, and equivalent to ($k_{-1B} + k_{+1B}$), k_{-1B} can be calculated as 409 s^{-1}. The association constant for Step 1B can be calculated, since K_{1B}, for this step:

$$K_{1B} = \frac{k_{+1B}}{k_{-1B}} = \frac{1.4}{409} = 3.4 \times 10^{-3}$$

K_{1A} is 3.5×10^{-3} M^{-1} (from Figure 40) , and it is therefore possible to calculate the overall dissociation constant of Mg^{2+} for Rac•MBCGDP, since:

$$K_d = \frac{1}{K_{1A} \times K_{1B}}$$

Figure 43: The Mg^{2+} Binding Models of Rac•MBCGDP and Rac•MBCGMPPNP

The *upper panel* shows a simple scheme for the binding and release of Mg^{2+} from Rac•GDP, using the binding data from the MBC fluorophore. The Mg^{2+} binding experiments to Rac•MBCGDP suggests that the binding process occurs in two steps. The ability to saturate Rac with increasing Mg^{2+} concentrations, suggests that the binding of Mg^{2+} to Rac (k_{-1A}) is a very fast (non-rate limiting step) which is not accompanied by a fluorescence change. The reverse step (k_{+1A}) is also assumed to be very rapid. The second step is both rate limiting and the step at which a fluorescence change occurs, and has a maximum rate of 410 s^{-1} ($k_{-1B} + k_{+1B}$). k_{+1B}, the release of Mg^{2+} is equivalent to k_{+1} (Figure 40), since it is this slow change in fluorescence that is observed during this process. This is measured at and average of 1.4 s^{-1}.

The *lower panel* illustrates the simple model suggested by the Mg^{2+} binding data for Rac•MBCGMPPNP. In a similar fashion to Rac•MBCGDP, the binding of Mg^{2+} to Rac•GMPPNP is assumed to be very fast (k_{-1A}) as is its release (k_{+1A}), with a K_{1A} of 1.5 mM. The saturated fluorescent change on Mg^{2+} binding is represented by k_{-1B}, and reflects a conformational change which is rate limiting. The maximum rate of this step is ($k_{-1B} + k_{+1B}$) and calculated to be 237 s^{-1}. During these binding experiments a further, slow change in fluorescence was observed, which may represent a further conformational change (k_{-1C}). However since so little information is known about this step, this is not included in the model.

Note that in Figure 31, the release rate constants were designated with '+' rates (k_{+1}), hence the use of '-' rate constants to represent the rate of Mg^{2+} binding.

Figure 43a The Two Step Mg^{2+} Binding Model for Rac•MBCGDP

Figure 43b The Multi-Step Mg^{2+} Binding Model for Rac•MBCGMPPNP

Then, $K_d = 12\ \mu M$.

An overall dissociation constant for MBCGDP release (Step Two) cannot be calculated, since only data concerning nucleotide release was measured ($k_{+2} = 0.01\ s^{-1}$) and to obtain a K_d, nucleotide binding data is also needed. The rate of release of GDP nucleotide is independent from that of Mg^{2+}, although it leaves subsequent to the Mg^{2+}, and that the rate is slow, $0.01\ s^{-1}$.

The overall scheme, including rate constants is shown in Figure 44 and Table 3.

The Two Step Model for Mg^{2+} and Nucleotide Release from Rac•GMPPNP

The Mg^{2+} and nucleotide release experiments with Rac•GMPPNP, as with Rac•GDP, suggest a simple model with two-steps (Figure 31). Step 1 involves Mg^{2+} release (k_{+1}), which occurs slowly, $0.01\ s^{-1}$, and is followed by Step 2, nucleotide release (k_{+2}), which in the absence of Mg^{2+} is a relatively fast $3\ s^{-1}$. This is the reverse of the case of Rac•GDP, in which the Mg^{2+} release is fast and the nucleotide release is comparatively slow.

The Mg^{2+} binding experiments with Rac•MBCGMPPNP showed that the process of Mg^{2+} binding and release is not a single step as described in Figure 31, rather the main fluorescent signals are consistent with a two step model (Figure 43b). In a similar fashion to the process observed in the case of Rac•GDP, Step 1 for Rac•MBCGMPPNP is a function of these individual steps (Step 1A and Step 1B). A further step (Step 1C) indicated by a small

Figure 44: The Mg^{2+} Kinetic Model of GDP Exchange

The *opposite panel* shows a simple scheme for the binding and release of Mg^{2+} from Rac•GDP, using the binding data from the MBC fluorophore.

The Mg^{2+} binding experiments to Rac•MBCGDP suggests that the binding process occurs in two steps. The ability to saturate Rac with increasing Mg^{2+} concentrations, suggests that the binding of Mg^{2+} to Rac (k_{-1A}) is a very fast (non-rate limiting step) which is not accompanied by a fluorescence change. The reverse step (k_{+1A}) is also assumed to be very rapid. The second step is both rate limiting and the step at which a fluorescence change occurs, and has a maximum rate of 410 s^{-1} ($k_{-1B} + k_{+1B}$).

The *lower panel* illustrates the simple model suggested by the Mg^{2+} binding data for Rac•MBCGMPPNP. In a similar fashion to Rac•MBCGDP, the binding of Mg^{2+} to Rac•GMPPNP is assumed to be very fast (k_{-1A}) as is its release (k_{+1A}). The fluorescent change which was saturated in the Mg^{2+} binding experiments is represented by k_{-1B}, and reflects a conformational change which is rate limiting. The maximum rate of this step is ($k_{-1B} + k_{+1B}$) and calculated to be 237 s^{-1}. During these binding experiments a further, slow, 0.08 s^{-1}, change in fluorescence was observed, and this is represented opposite by a further step (k_{-1C}), which may represent yet another conformational change, perhaps to one of higher affinity for Mg^{2+} and GMPPNP.

Note that in Figure 31, a simple model for Mg^{2+} and nucleotide release, the release rat constants were designated as the forward or '+' rates, hence the use of the '-' rate constants in the Mg^{2+} binding figures.

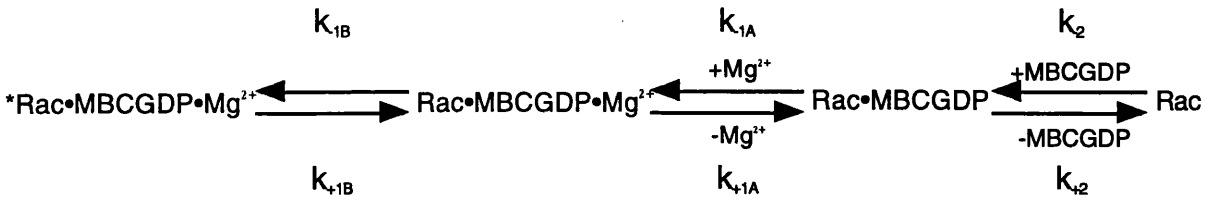

$$K_{1B} = \frac{k_{+1B}}{k_{1B}} \qquad K_{1A} = \frac{k_{+1A}}{k_{1A}} \qquad K_2 = \frac{k_{+2}}{k_2}$$

$K_{1B} = 3.4$ mM $\qquad K_{1A} = 3.5$ mM^{-1}

$$K_1 = (K_{1A})\ x\ (K_{1B})$$

$K_1 = 12$ µM

Mg^{2+} concentration-independent change in fluorescence suggests a further conformational change, however to simplify the kinetic analysis, this step can be excluded from the scheme (since little information has been observed about it). This extra step may be a further conformational change thus decreasing the dissociation rate even further.

The data can be analysed in a similar fashion to Rac•GDP. The rate constant for Step 1B, k_{1B} = (k_{+1B} + k_{-1B}) is equal to 237 s^{-1}. Step 1A (k_{-1A} and k_{+1A}) is assumed to be very fast, and therefore play no role as a rate limiting step. The rate of Mg^{2+} release (k_{+1}) is a function of k_{+1A} and k_{+1B}. Since k_{+1A} and k_{-1A} (the release and binding of Mg^{2+}) are assumed to be very fast, the overall rate of Mg^{2+} release, k_{+1}, is equal to k_{+1B}. k_{+1} has been measure as 0.01 s^{-1}, and so:

$$k_{+1B} = 0.01\ s^{-1}$$

Therefore:

$$k_{-1B} = 237\ s^{-1}$$

The equilibrium constant for Step 1B is equal to:

$$K_{1B} = \frac{k_{+1B}}{k_{-1B}} = \frac{0.01}{237} = 4.2 \times 10^{-6}$$

The equilibrium constant, K_{1A}, is 1.5 x 10^{-3} M, which allows calculation of the dissociation constant for Mg^{2+} from Rac•GMPPNP as, K_d = 63 nM. This value suggests tighter binding of

Mg^{2+} to Rac•GMPPNP than to Rac•GDP. The overall scheme including kinetic values is shown in Figure 45 and Table 3.

In the absence of Mg^{2+}, the GMPPNP is released from the Rac protein at a rate of on average 3 s^{-1} (k_{+2}). Data for the binding of GMPPNP to Rac (k_{-2}) was not gathered during this study, and so the dissociation constant for this step cannot be calculated. The release rate of GMPPNP from Rac is shown to be approximately equal to the release of GDP (although this is slowed by 100-fold in the presence of Mg^{2+}). Previous work has shown that GTP binds more tightly than GMPPNP which in turn binds with comparative tightness to GDP (John, J., *et al.* 1993; Neal, S., *et al.* 1988).

The binding affinity Mg^{2+} to Rac•MBCGMPPNP is approximately 1000-fold greater than that observed with Rac•MBCGDP. How can this be rationalised? The structures of Rac complexed with Mg^{2+} and GDP (Hirshberg, M., Shutes, A., Newcombe, T., Webb, M. unpublished data) or GMPPNP (Hirshberg, M., *et al.* 1997), show a notable difference between the Mg^{2+} coordination with the nucleotide and protein. In the GMPPNP form, Mg^{2+} interacts with both the β and γ phosphate of the nucleotide, whereas the GDP form interacts only with the β phosphate, the γ phosphate having been replaced by a water molecule. The stabilisation provided by this γ phosphate contact has therefore been lost. The Mg^{2+} is therefore likely to be less tightly bound to the GDP form than the GMPPNP form. This difference of γ-phosphate coordination may be responsible for the 1000-fold difference on the affinity for Mg^{2+}. It is also possible that the presence of both Mg^{2+} and

Figure 45: The Kinetic Model of Mg^{2+} and GMPPNP Exchange

The *opposite upper panel* shows a simple scheme for the binding and release of Mg^{2+} from Rac•GMPPNP, using the binding data from the MBC fluorophore.

The Mg^{2+} binding experiments to Rac•MBCGMPPNP suggests that the binding process occurs in two steps. Rac is saturated by a fluorescent change (k_{-1B}), suggesting that this step is separate to the actual Mg^{2+} binding (k_{-1A}). Since k_{+1B} and k_{+1} are known, k_{-1B} can be calculated. K_{1A} is already known from the Mg^{2+} binding data, which allows the calculation of K_1, assuming that K_1 consists of K_{1B} and K_{1A}. K_1, the dissociation constant for the process of Mg^{2+} release is equal to 63 nM. This reflects approximately 1000-fold tighter binding to Mg^{2+} than observed for Rac•GDP.

Although the presence of a further fluorescence change is observed (K_{1C}), there is insufficient data of this step which can contribute to the overall K_1 calculation.

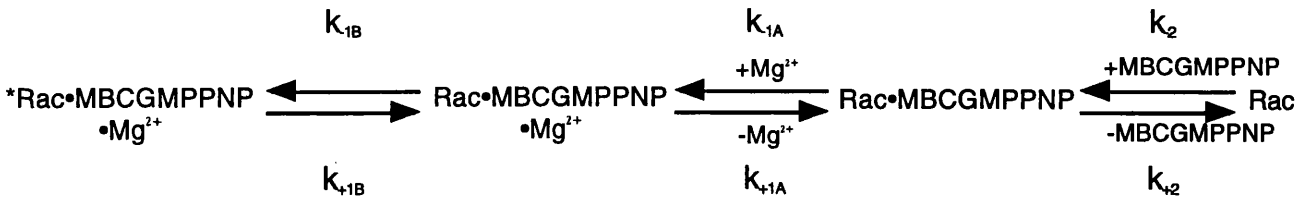

$$K_{1B} = \frac{k_{+1B}}{k_{1B}} \qquad K_{1A} = \frac{k_{+1A}}{k_{1A}} \qquad K_2 = \frac{k_{+2}}{k_2}$$

$K_{1B} = 42.2\ \mu M$ $\qquad$ $K_{1A} = 1.5\ mM^{-1}$

$$K_1 = (K_{1A})\ x\ (K_{1B})$$

$$K_1 = 63\ nM^{-1}$$

GMPPNP nucleotide causes a further conformational state in Rac. The extra step observed in the presence of Rac•GMPPNP (Step 1C) may represent this further conformation and may contribute to the tight binding of Mg^{2+}.

The release of GMPPNP (k_{+2}) occurs at a faster rate than the release of GDP in the absence of Mg^{2+}, but the presence of associated Mg^{2+} causes GMPPNP's release to be slowed. This suggests that for Rac•GDP complexes, GDP release is the rate limiting step, but for Rac•GMPPNP complexes, the release of Mg^{2+} is rate limiting. This supports the model that the tight binding of GMPPNP to Rac occurs in the presence of Mg^{2+}, and when the Mg^{2+} is lost, GMPPNP binds weaker. In the two step model, the release of nucleotide (k_{+2}) is a single step, although an extra very slow change (0.008 s^{-1}) in fluorescence is observed on GMPPNP nucleotide release (k_{+3}). It is possible that this slower rate of GMPPNP release is an alternative release pathway where Rac undergoes an additional slow conformational change. Perhaps this conformational change is related to the tight affinity state observed in the presence of Mg^{2+}, and the release of nucleotide from this state is particularly slow since it must undergo two conformational changes.

Differing Rates between Fluorescent Anisotropy and Intensity

As a test of the simple model of Mg^{2+} and nucleotide release and binding, fluorescent anisotropy was used to monitor the release rates of labelled nucleotide directly. The

majority of the anisotropy data, both with MBC nucleotides and Mant nucleotides, agreed with the intensity data, however one anomaly was observed. In the absence of Mg^{2+}, Rac•MantGMPPNP and Rac•MBCGMPPNP complexes show significant differences in their rates of fluorescent change when measured by fluorescent intensity and fluorescent anisotropy. For the step in the model, presumed to reflect nucleotide release, the anisotropy data demonstrated rates ($\sim 0.4\ s^{-1}$) which were $\sim$ 10-fold slower than the rates indicated by changes in fluorescent intensity ($\sim 3\ s^{-1}$). The reason for these differences is unclear, although it may lie in the intrinsic characteristics of the two methods used to measure these values. Anisotropy provides a measure of rotational rate of the fluorophore, which is related to the bound state of the nucleotide. Fluorescent intensity reflects the changes in environment around the fluorophore, which can often be related to conformational changes. It is therefore possible that the two methods have revealed two processes occurring during release that are subtly different. Perhaps a rapid change of protein conformation occurs allowing nucleotide release, which affects the intensity data, and is followed by a slower change as the nucleotide is actually released.

The determination of the crystal or NMR structures of Rac•MBCGMPPNP may provide a resolution to this situation.

The differences in the measured amplitudes of the MBC fluorescent changes (in particular on loss of nucleotide), between the fluorimetric and stopped-flow techniques, are notably significant (those measured by fluorimetry being smaller than by stopped-flow). The reason for these differences is unclear and may be inherent to the techniques themselves, perhaps reflecting the lower sensitivity of the fluorimeter, some other difference between the two techniques, or perhaps release of both Mg^{2+} and nucleotide, which cannot be resolved separately on the fluorimeter.

The Process of Nucleotide Exchange

Previous work has examined the process of nucleotide exchange in Ras and Rho proteins, both in the presence of specific GEFs, such as Sos and Dbl, as well as in the absence of such proteins. These studies have indicated that Mg^{2+} plays a central role mediated through its interactions with several key residues in the small G-protein's structure. Mg^{2+} has been shown to inhibit GDP release from Ras (John. J. *et al.* 1993), Rac (Neal, S., *et al.* 1990) and Rab (Pan, J., *et al.* 1996), although mutation of Serine 35 in Rab (equivalent to Threonine 35 in Rac) abolishes the Mg^{2+} mediated inhibition. Indeed these mutants have a higher affinity for their GEF protein than wild types, suggesting that they show some form of modified structure, which is ready to bind GEFs. An N-terminal region of the molecule is also suggested to play a role in controlling Mg^{2+} release, although whether this is due to a loss in structural integrity or some real inhibitory role is unclear. In contrast to Rab, the conserved Threonine 35 in Ras only affects the kinetics of the GTP state of the protein. Mutation of this residue causes a loss in Mg^{2+} coordination and a decrease in protein affinity for both Mg^{2+} and the GTP nucleotide (John, J. *et al.* 1993). Further work on Rab proteins (Simon, I., *et al.* 1996) using changes in intrinsic tryptophan fluorescence showed that Mg^{2+} bound 1000-fold more strongly to Rab•GTP than Rab•GDP, and also suggested that there were possibly two steps to nucleotide binding (in the presence of Mg^{2+}) — rapid initial binding followed by some conformational shift. Mg^{2+} acting to stabilise the interaction between the protein and nucleotide.

Rho proteins differ slightly in their ability to bind nucleotide and Mg^{2+} as compared to Ras

and Rab proteins. Both previous studies and this current study show that Rac can bind nucleotides in the absence of Mg^{2+}, as well as in its presence. The presence of Mg^{2+} causes a decrease in the dissociation rate of the nucleotide compared to the value for the nucleotide alone. This is particularly noticeable with the Rac•GMPPNP form, where the presence of Mg^{2+} decreases the rate of nucleotide dissociation by approximately 100-fold. This study has shown that the rate of GDP release is not affected by the presence or absence of Mg^{2+}, although other work (Zhang, B., *et al.* 2000) has shown that in the presence of a GEF, removal of Mg^{2+} increases the dissociation rate of GDP, suggesting that GEF-catalysed exchange may involve both a Mg^{2+}-dependent and Mg^{2+}-independent mechanism. The affinity of Rac1•GDP for Mg^{2+} has previously been estimated as 15 μM (Zhang, B., *et al.* 2000) — the value presented in this study of 12 μM is in close agreement with this value. The affinity of Rac•GMPPNP for Mg^{2+}, shown in this study to increase by 1000-fold over the value with GDP, has not been previously published. However, such similar data has been published with other Ras family proteins, such as Rab (Simon, I., *et al.* 1996) which also shows a 1000-fold increase in affinity. So, it appears that although Ras, Rab, Rac are different proteins which differ in their nucleotide binding in the absence of Mg^{2+}, they differ less in the presence of Mg^{2+} where the kinetics involved appear similar.

The work in this study supports the suggestion that Mg^{2+} appears to act as a gatekeeper to nucleotide release and further proposes that Mg^{2+} binding and release occurs in two stages. The presence of GMPPNP in the active site causes tight binding between the overall Rac, the GMPPNP nucleotide and Mg^{2+} ion, preventing GMPPNP dissociation. *In vivo*, this

decreased rate of GTP dissociation may cause GTP's retention in the active site until the process of hydrolysis has occurred. This study has shown that, once GDP is bound to Rac the affinity for Mg^{2+} is reduced by around 1000-fold (as compared to Rac•GTP). This reduction in Mg^{2+} affinity can be associated with an increased rate of Mg^{2+} release. This is likely due to a change in Rac conformation between the GTP and GDP forms and changes in Mg^{2+} coordination. Both of these processes may make the association of the small G-protein with a GEF more likely, and therefore increase the chances of nucleotide exchange. Studies on the mechanism of GEFs proposed that these molecules bind to small G-proteins in such a way as to destabilise the Mg^{2+} coordination, lowering the protein's affinity for Mg^{2+} even further (10-fold weaker (Zhang, B., *et al.* 2000)), thus promoting nucleotide (GDP) release. GEFs may therefore act in a way to bind a Rac•Mg^{2+} nucleotide complex (either GDP or GTP). When binding to Rac•GDP, where the Mg^{2+} binding is weak, the GEF is able disrupt the Mg^{2+} coordination and impose a modified structure on Rac•GDP — thus increasing the rate of nucleotide exchange. On binding to Rac•GTP•Mg^{2+}, where the Mg^{2+} is bound more tightly than in Rac•GDP (as shown in this study), the GEF is unable to disrupt the Mg^{2+} coordination, and therefore unable to impose a modified structure on Rac. The GEFs binding to Rac•GTP•Mg^{2+} would therefore be weaker than its binding to Rac•GDP•Mg^{2+}.

It has been recently suggested on the basis of the Mg^{2+}-free structure of RhoA (Shimizu, T. *et al.* 2000) that instead of imposing a form of destabilisation on the Mg^{2+} associated with Rac•GDP, GEFs may act to bind small G-proteins in a Mg^{2+} free state and stabilise this form instead. GEFs association with the small G-protein may destabilise or inhibit any further

Mg^{2+} binding. This does seem feasible, since the decreased affinity of Mg^{2+} for Rac•GDP complexes (as shown in this study) of Rac•GDP for Mg^{2+} will allow for a much faster release of Mg^{2+} into solution, thus providing GEFs sufficient opportunity to bind a Mg^{2+}-free Rac. Presumably, once GTP replaces the GDP, the fast Mg^{2+} equilibrium is drastically slowed as the Mg^{2+} and GTP bind tightly to Rac, the GEF interaction destabilised and a new G-protein conformational state is achieved. The conformation of Mg^{2+}-free RhoA (Shimizu, T. *et al.* 2000) has been shown to resemble that found in complexes with the GEFs, Dbl (Soisson, S., *et al.*, 1998) and Sos (Liu, X., *et al.*, 1998), so that a decrease in Mg^{2+} affinity found in the GDP Mg^{2+} state may also make the conformation of the small G-protein susceptible to GEF association. The conformation of Rac in the presence of Mg^{2+} and GTP is presumably not favourable for GEF association (but is for other effectors, such as IQGAP).

MBC as an Indicator of GTP Hydrolysis

The experiments described in this Chapter demonstrate that the fluorescence of the MBC fluorophore decreases on the hydrolysis of GTP to GDP. This rate of hydrolysis measured by this method, 0.002 s^{-1}, is similar to the rate of hydrolysis as measured by the release of P_i (using the P_i probe, MDCC-PBP, 0.002 s^{-1}) and by the increase in Rac•MBCGDP concentrations (using HPLC, 0.005 s^{-1}). The fluorescence of Rac-bound MBCGDP and MBCGMPPNP differ, so an observable change in fluorescence during hydrolysis is to be expected — assuming that the fluorescence of MBCGMPPNP is equivalent or similar to

MBCGTP. The process of GTP hydrolysis is shown in Figure 46.

The rate of the process measured by the production of P_i (MDCC-PBP) or by the accumulation of Rac•MBCGDP (HPLC) measures the rate of P_i release and product formation respectively (Rac•GDP). The change in MBC fluorescence presumably reports on a change in the protein conformation around the MBC fluorophore, most probably within Rac's active site. Previously MBC has been shown to be sensitive to processes involving Mg^{2+}, and so it is possible that the MBC fluorophore reports on changes in Mg^{2+} coordination on a Rac conformational change (from Rac•GTP to Rac•GDP) with the release of P_i and its replacement with H_2O. The similarity between the rates of hydrolysis, as measured by changes in MDCC-PBP and MBC fluorescence suggest that these methods may be measuring a similar process — the release of P_i causing a change in Rac conformation and Mg^{2+} coordination.

The rate measured by HPLC is slightly higher than that measured by MDCC-PBP and MBC. This may be due to the different processes measured, HPLC measuring the rate of β-γ phosphate bond cleavage, whereas the other methods measure the rate of P_i release. If this is the case then the release of P_i may be the rate-determining step in the overall hydrolysis process.

Another explanation to the higher HPLC rate is possible. The data consists of fewer time-points compared to the use of fluorescence, and the data shows more scatter around the

Figure 46: The Kinetic Model of GTP Hydrolysis

The *opposite panel* shows a simple scheme for the hydrolysis of GTP. The process is essentially unidirectional.

The fluorescent methods used to measure the process of GTP hydrolysis gave an approximately equivalent rate (0.002 s^{-1}), which suggests that they are each reporting on the same rate limiting process. The change in MBC fluorescence reflects a change in conformation on GTP hydrolysis, which may reflect a change in Mg^{2+} coordination. This rate is similar to that measured for P_i release (by MDCC-PBP). It is possible that the change in conformation indicated by the change in MBC fluorescence occurs on the release of P_i.

HPLC data shows a slightly increased rate, which may reflect a different process being measured — that of the cleavage of GTP to GDP, rather than product release.

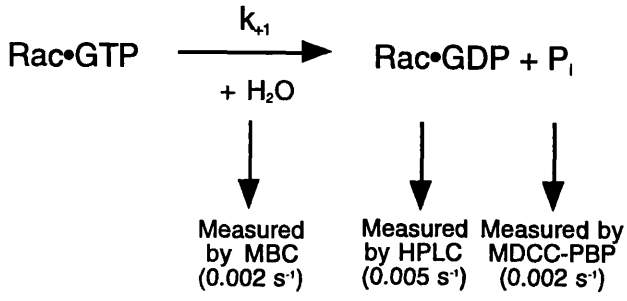
Rac•GTP
k_{+1}
+ H_2O
Rac•GDP + P_i
Measured by MBC (0.002 s^{-1})
Measured by HPLC (0.005 s^{-1})
Measured by MDCC-PBP (0.002 s^{-1})

best fit curve. More data points would provide an improved fit to the best fit curve. It is also possible that the quenching of hydrolysis in the acidic HPLC buffer was not immediate, and this would cause an increase in the apparent rate of GTP hydrolysis.

The ability of the MBC fluorophore to directly measure the conformational change occurring during GTP hydrolysis suggests that it may be a useful tool to examine changes in this process under different conditions, such as in the presence of effector proteins or with mutated small G-proteins.

Chapter 5

The Interaction of Rac1 with IQGAP

5.1 Introduction

The first member of the IQGAP family, IQGAP1, was identified in 1994 (Weissbach, L., *et al.* 1994), and since that period, more members of the family have been identified, yet the exact functions and mechanisms of IQGAP family proteins is still unclear. There is a great deal of evidence which suggests that IQGAP proteins play a central role in cytoskeletal arrangements, influencing cellular activities such as cell-to-cell adhesion and cytokinesis. IQGAP's role with the cytoskeleton is controlled by its interaction with Cdc42 and Rac1. The interaction between IQGAP and Cdc42 or Rac1 disrupts IQGAP's ability to associate with structures of the cytoskeleton, and therefore provides a direct molecular link between the Rho protein signalling pathway and cytoskeletal reorganisation. IQGAP is also able to associate with Ca^{2+}-binding proteins via its IQ domains, and interaction with such proteins causes it to release any bound Rho subfamily proteins. The interaction between the cytoskeleton, Rho subfamily proteins and Ca^{2+}-binding proteins, mediated through IQGAP, suggests that IQGAP may play an important role in connecting these signalling pathways *in vivo*.

Despite there being a growing amount of evidence for IQGAP's cellular roles, there have been few investigations into the kinetics and mechanism of IQGAP association with either Ca^{2+}-binding proteins, the cytoskeleton or Rho subfamily proteins.

IQGAP1 has been shown to associate with Cdc42 and Rac1 bound to nonhydrolysable GTP analogues (such as GMPPNP) (McCallum, S., *et al.*, 1996; Kuroda, S. *et al.*, 1996) and use of

mutants has narrowed the regions of interaction down to the Insert Loop and Effector Region (McCallum, S., *et al.*, 1996). Simultaneous labelling of both the nucleotide bound to Cdc42 and Cdc42 itself (on Lysine 150) also suggested that IQGAP associated with the Insert Loop and Effector Region of Cdc42 and that Insert Loop deletion reduced IQGAP interaction (Nomanbhoy, T. and Cerione, R., 1999). This investigation used fluorescent labelling of Cdc42 to show that IQGAP binds in a different manner than proteins which contain CRIB domains. CRIB-domain containing proteins, such as the p21-associated kinases and WASP proteins, associate through the distinct CRIB domain, whereas IQGAP proteins are thought to associate in a similar fashion to GTPase Activatory Proteins, such as p190GAP, using their GAP Related Domain. The GRD of IQGAP proteins is of similar sequence to the GAP domain found in active GAPs, although several residues (such as Arginines) which are critical in GAP function are mutated in IQGAP proteins. The GRD domain of IQGAP may therefore be both involved in Cdc42/Rac1 association and inhibition of the GTPase activity (Hart, M., *et al.* 1996). CRIB-containing proteins are also able to inhibit GTP hydrolysis, yet the absence of a CRIB domain in IQGAP and the presence of a subtly altered GRD suggest that IQGAP performs this inhibition through the GRD to interfere with the catalytic mechanism itself.

A limited amount of kinetic data of IQGAP's function and association with Cdc42 or Rac1 is available. The first of these studies (Zhang, B., Wang, Z.-X., Zheng, Y., 1997) used competition assays, in which non-hydrolysable Cdc42 analogues (Cdc42•GMPPNP and Cdc42•GDP) were used to inhibit the GAP-mediated hydrolysis of GTP bound to Cdc42. The concentration range in which Cdc42•GMPPNP or Cdc42•GDP could inhibit this hydrolysis

gave an indication of its affinity, for the associating protein. Cdc42•GMPPNP was able to inhibit the IQGAP-mediated inhibition of Cdc42•GTP hydrolysis, whereas Cdc42•GDP was unable to do this. This suggested that Cdc42•GDP was unable to bind to IQGAP. This study estimated that the affinity of IQGAP for Cdc42 is at least 10-fold greater than its affinity for CRIB-domain-containing proteins (IQGAP $\approx$ 80 μM, WASP $\approx$ 700 μM). A similar technique was applied to Rac1•GMPPNP (Zhang, B., Chernoff, J., Zheng, Y., 1998), indicating that the affinity for the fragment of IQGAP is 2.1 μM. The affinity of Cdc42•GMPPNP for IQGAP in this investigation was measured as 0.39 μM (significantly different from the previously measured value). In each of these studies, the IQGAP used was a C-terminal fragment (864-1657) expressed in *E.coli*. The fragment used in this investigation represents residues 862-1657.

There has not be a previous study describing the direct measurement of the interaction between IQGAP and Rac1. This Chapter describes the first results of such a measurement, using fluorescent anisotropy, between the C-terminal fragment of IQGAP1 and Rac1. It also assesses the contribution of the Insert Loop and Effector Regions in the interaction by using a panel of Rac mutants. These results suggest that the IQGAP fragment binds tightly to Rac1 through both the Insert Loop and Effector Region.

5.2 Results

5.2.1 Creation of Novel pGIT2 Clone

The C-terminal fragment of IQGAP was initially provided in a GST-fusion protein expression system which allowed its purification to a limited level (by competition of the fusion protein from a GST-affinity column using glutathione) (Figure 47a). The purity of such protein preparations was not sufficient for *in vitro* analysis, and so the gene fragment was inserted into a pGEX 2T expression system which contained a GST-fusion tag as well as a Thrombin cleavage site.

Using the procedure described in Chapter 2, initial manipulation of the gene fragment into a pGEX 2T vector was successful, however, protein preparations using such clones produced no IQGAP protein. Analysis of the gene construct showed that ligation of the gene fragment and new vector caused a loss of sense in the gene fragment at the point of ligation (Figure 48). Site-directed mutagenesis at the point of ligation, introduced two cytosines which restored the Open Reading Frame and maintained both the Bam HI cleavage site and the Thrombin cleavage site. The resulting plasmid, named pGIT2 (plasmid GAP-IQ-Thrombin-2) (Figure 49) was tested for correct protein expression, correct restriction enzyme digestion patterns and correct DNA sequence.

Figure 50 shows protein expression of the plasmid pGIT2 and the previous uncorrected plasmid. pGIT2 shows a band on the gel with an approximate mass of 120 kDa which is approximately equal to the predicted molecular weight of the GST-IQGAP fusion protein

Figure 47 : Expression & Purification of IQGAP

The IQGAP preparation procedure was modified from that used for Rac1. Cells were grown and induced for 4 hours in each period. After a low speed centrifugation, the cells were sonicated thoroughly before being subjected to a high speed centrifugation. Resuspension in a high salt buffer followed by either a Glutathione wash or a Thrombin digestion.

The *upper panel* represents the final outcome of expression and induction (as described above) followed by glutathione competition of the column-bound GST-IQGAP protein. Induction produced a single band (not shown), yet two proteins can be seen of similar apparent molecular weights — approximately 120 kDa and 110 kDa (*i*). There is a small degree of contamination by proteins of a lower apparent molecular weight.

The *lower panel* represents expression and induction followed by Thrombin digestion of column-bound GST-IQGAP. Induction of the cells showed only one main protein band (*ii*), yet after thrombin cleavage two main bands with apparent molecular weights of approximately 105 kDa and 96 kDa (*ii*) can be seen.

From these expression and purification experiments, it appears that IQGAP is being expressed as two main proteins, both of which are binding to the Glutathione-Sepharose column, and can be cleaved by thrombin. It is likely that the truncation occurring in the expressed protein is at the C-terminus — far from the GAP Related Domain.

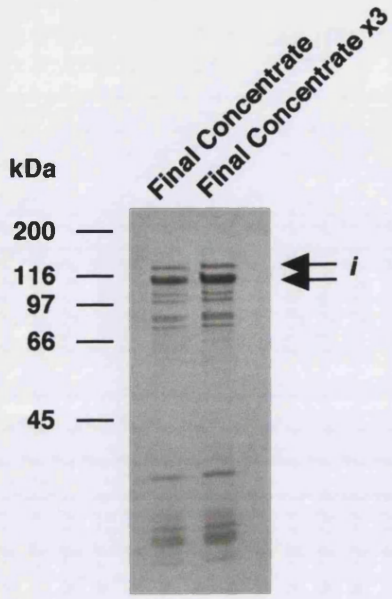

Figure 47a GST-IQGAP preparation with Glutathione competition

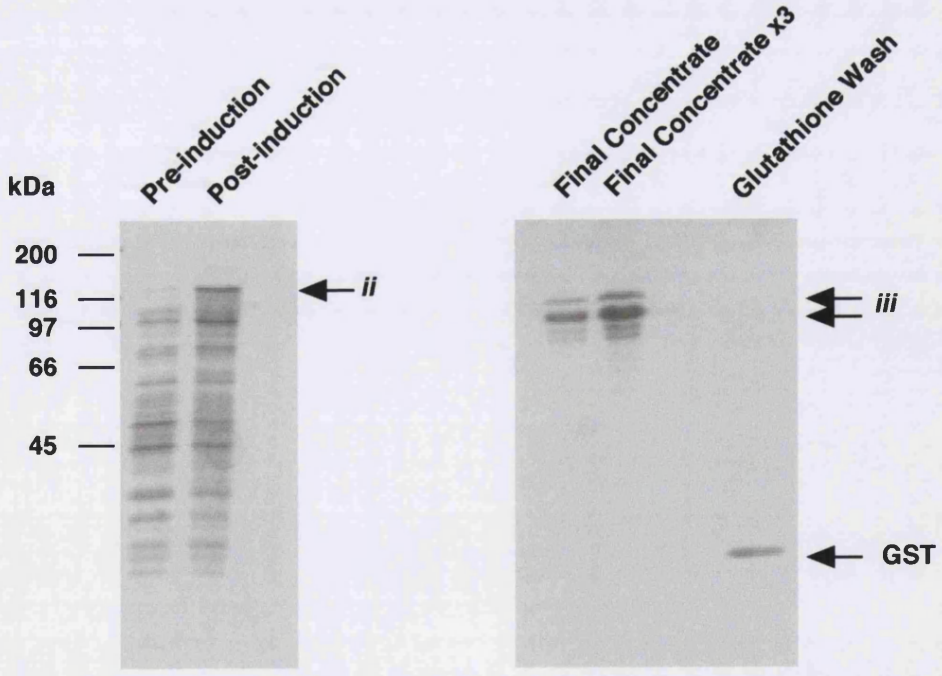

Figure 47b IQGAP preparation with Thrombin cleavage

Figure 48 : Misalignment of the Open Reading Frames

The *panels opposite* demonstrate the problem which occurred after the excision and ligation of the gene fragment into a pGEX2T vector. The Bam HI enzyme cleavage site and the GST expression open reading frames (ORF) were not in correct alignment. The GST ORF can be seen in frame 3 and the IQGAP ORF in frame 1 (48a *opposite*). This resulted in no IQGAP protein being produced since the two open reading frames were out of sequence alignment. The GST gene could be translated correctly, but the IQGAP gene became nonsense.

The insertion of two cytosine residues brought the two sequences into the same reading frame, as well as maintaining the Thrombin cleavage site and the Bam HI cleavage site. The final complete ORF can be seen *opposite* in frame 3 (48b).

This is further illustrated by the sequences *below*. The top sequence shows the GST sequence ligated to the IQGAP gene insert sequence, however the reading frame of the insert is lost at by the Bam HI ligation site (red). The insertion of two cytosines (underlined) corrects the reading frame, maintains the Thrombin site (VPRG) and causes the addition of a single Proline residue at the site (lower sequence). This extra residue does not affect the cleavage of the protein and is highly unlikely to affect the activity of the cleaved IQGAP fragment.

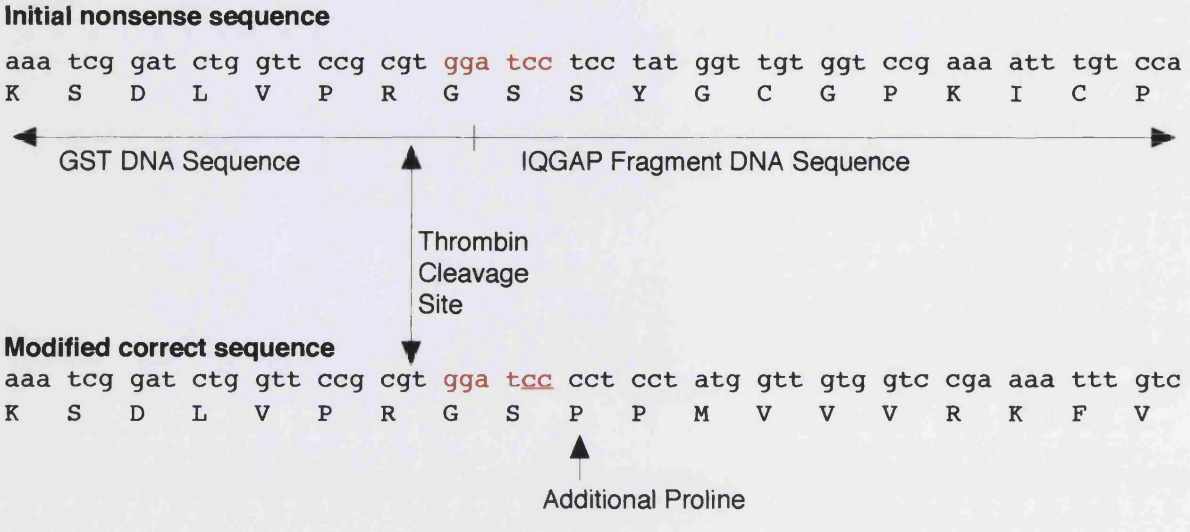

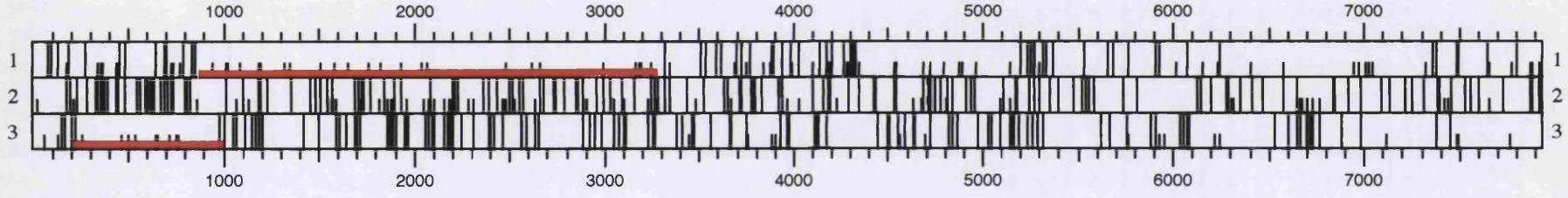

Figure 48a The uncorrected Open Reading Frame

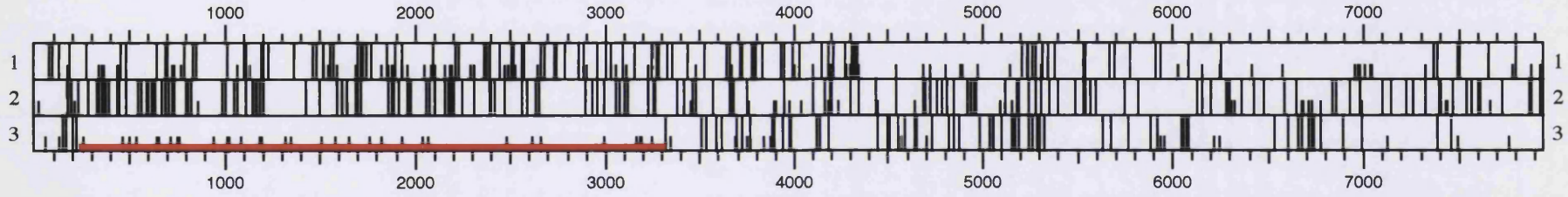

Figure 48b The Corrected Open Reading Frame

Figure 49 : The pGIT 2 Construct

The original IQGAP clone received contained the IQGAP1 gene fragment as a GST-fusion protein. However, the fusion protein lacked a Thrombin site which prevented its purification to a satisfactory level. Introduction of a Thrombin cleavage site was therefore necessary. This was achieved by cloning the fragment into a new vector (pGEX-2T).

The *panel opposite* shows the unique restriction enzyme sites in the plasmid, as well as the beginning and end of the GST-IQGAP1 gene fragment , which contains the Thrombin site as well as retaining the cloning enzyme sites (Bam HI, Eco RI and Xba I).

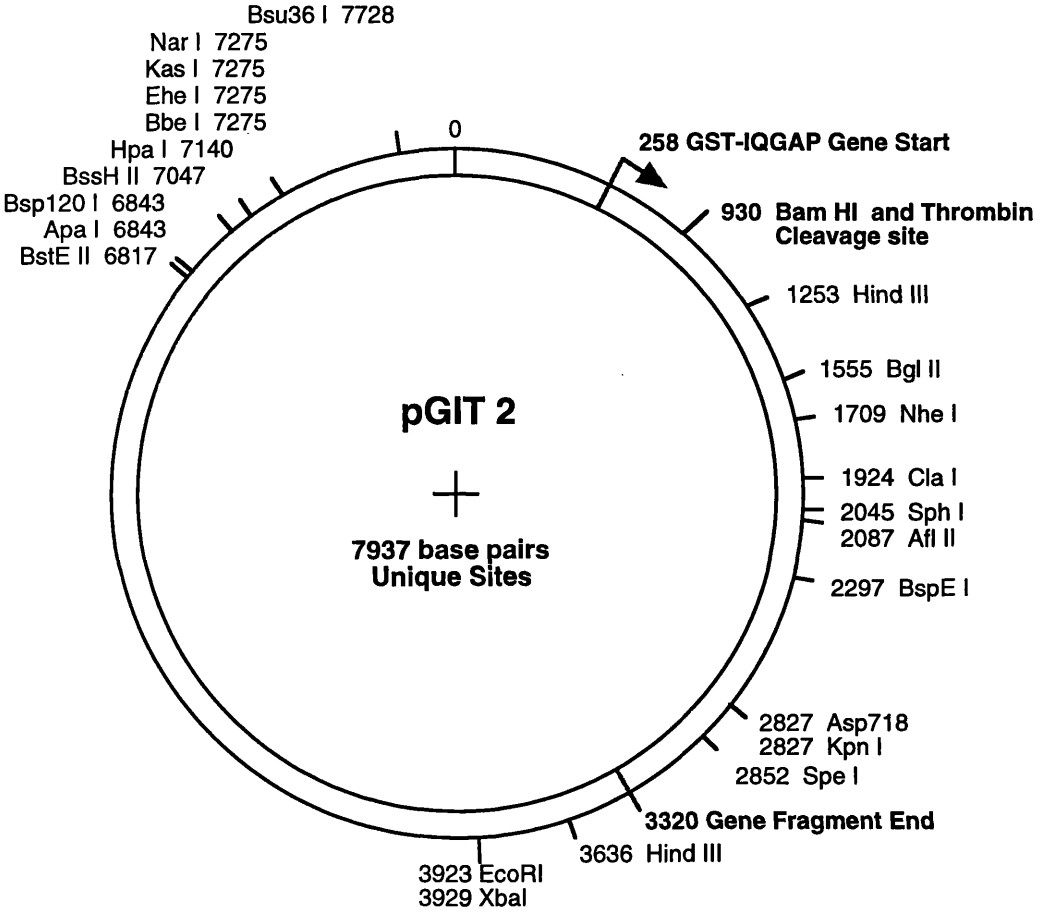
Bsu36 I 7728
Nar I 7275
Kas I 7275
Ehe I 7275
Bbe I 7275
Hpa I 7140
BssH II 7047
Bsp120 I 6843
Apa I 6843
BstE II 6817
0
258 GST-IQGAP Gene Start
930 Bam HI and Thrombin Cleavage site
1253 Hind III
1555 Bgl II
1709 Nhe I
1924 Cla I
2045 Sph I
2087 Afl II
2297 BspE I
2827 Asp718
2827 Kpn I
2852 Spe I
3320 Gene Fragment End
3636 Hind III
3923 EcoRI
3929 XbaI
pGIT 2
7937 base pairs
Unique Sites

(117 kDa). This band is absent in the uncorrected plasmid, where there is a band around 25 kDa, which may represent expressed GST protein, without the fused C-terminal IQGAP fragment (since it is out of reading frame).

Using the construct sequence to predict restriction enzyme digestion patterns (Figure 49), the plasmid was subjected to restriction digests to confirm that the gene fragment was present and inserted in the correct orientation (Figure 51). Restriction enzyme digests with Bam HI and Nhe I produced fragments with weights of approximately 7.1 kb and 779 b, as expected from the predicted pattern. Similarly, a digest with Hind III, produced 2 fragments of approximately 5.5 kb and 2.3 kb, which suggested that the gene insert was present and in the correct orientation. Digestion with the enzyme Bst XI produced fragments of 3.2 kb, 2.5 kb and 1.8 kb, which also agreed with the predicted pattern. This confirmed correct gene insertion. The three smallest fragments were not resolved on the agarose gel, due to their extremely low molecular weight.

DNA sequencing of the plasmid was performed by the PCR dye-terminated method, to confirm the presence of the gene fragment, in the correct orientation. These sequences also showed that it contained no mutations from the original gene fragment (Appendix 1).

5.2.2 IQGAP Protein Expression and Purification

The previous section describes the successful transfer of the C-terminal IQGAP DNA fragment into a vector allowing Thrombin purification of the expressed GST-IQGAP fusion protein.

Figure 51 : Restriction Enzyme Digests

The *panels opposite* show restriction enzyme digest tests on the plasmid containing the IQGAP C-terminal gene fragment, after its ligation into a pGEX2T vector and reading frame modification.

The *upper panel* (51a) shows an agarose gel with various restriction digestions. **Lane a**, shows the native, uncut plasmid DNA.
Lane b, shows the digestion pattern of the Hind III enzyme. Two fragments are produced of 5.5 kDa and 2.3 kDa. These correlate with their predicted sizes from the digest construct (Figure 49).
Lane c, shows the digest pattern in the presence of the enzymes Bam HI and Nhe I, both of which cut the DNA at a single point on the plasmid. The fragment sizes produced are in agreement with those predicted for the digestion: 7.1 kb and 779 bp.

The *lower panel* (51b) shows the digestion pattern of pGIT2 with the restriction enzyme, Bst XI. This enzyme has a digestion pattern of 3 large and 3 small fragments, spread throughout the vector, and thus correct digestion will confirm correct vector/insert combination. The largest three fragments can be seen opposite (3.2 kb, 2.5 kb and 1.8 kb), whereas the three smaller fragments (129 kb, 123 kb and 48 kb) were not resolved due to their low molecular weight.

These digests confirm that the gene insert is present in the vector and that it is in the correct orientation.

DNA sequencing was also performed on the plasmid, and this further confirms the presence and correct orientation of the gene (see Appendix 1 for sequence).

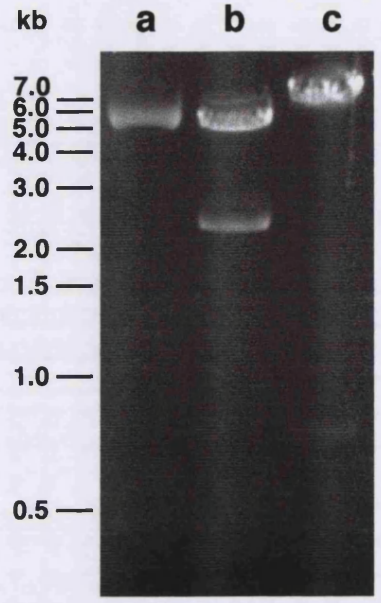

Figure 51a Agarose Gel Showing Uncut, Hind III Cut, and Bam HI/Nhe I Cut pGIT2 Plasmid

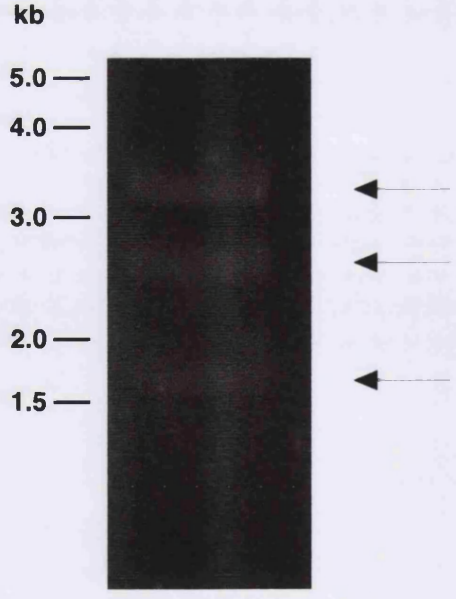

Figure 51b Agarose Gel Bst XI Cleaved pGIT2 Plasmid

This was performed so as to provide a greater level of purity protein preparation for biochemical investigations. The level of purification achieved can be seen in Figure 47b.

By comparison with Figure 47a, the level of purification on preparation of the cleaved protein is much improved with Thrombin cleavage over the use of Glutathione competition. The appearance of a protein band on the SDS-PAGE gel at 120 kDa after induction of the vector (47b) suggests expression of the GST-IQGAP fusion protein. This can be compared with a protein band in a similar position in the concentrate of the uncleavable GST-IQGAP (47a). Cleavage of this expressed protein when bound to a column produces two major protein bands of approximately 105 kDa and 96 kDa. These are likely to be cleaved forms of IQGAP without GST. A similar pattern of protein is observed with Glutathione competition (47b), and therefore it is unlikely that these proteins are formed by extra Thrombin cleavage of the fusion protein. It is possible that they are artefacts from the gene due to premature termination of translation or transcription, although the presence of a single induced band in the cell lysate would suggest otherwise. It is most likely that the protein is being slightly degraded at the C-terminal end by a bacterial protease, although protein preparation in the presence of bacterial protease inhibitors, and protein expression in protease-deficient bacteria, had no effect on the protein expression pattern.

After thrombin cleavage of the proteins from the column, the GST-affinity columns were washed with glutathione, and the protein eluate collected. For the cleaved protein preparation (47b) the eluate from this process is shown, and the presence of a single band of the correct molecular weight for GST suggests that the expressed GST-IQGAP proteins are

cleaved correctly at a single position at their N-terminus.

Increased purification of IQGAP is successful, however the amount of protein produced in the final concentration stage is comparatively low. A 4 litre IQGAP preparation produces, on average, 60 nmol of IQGAP protein in the final concentrate. This can be compared to a Rac1 preparation, in which the amount of protein produced is around 10-fold higher. Possible causes and solutions to this problem can be found in the Discussion section of this chapter.

5.2.3 IQGAP Inhibits the Intrinsic GTP Hydrolysis Rate of Rac1

Previously published studies of IQGAP have assessed its ability to inhibit GTP hydrolysis by Rho subfamily G-proteins, and used this to estimate the affinity between the IQGAP and Rho subfamily proteins (in their GTP bound state). This study assesses the activity of the IQGAP C-terminal fragment produced in the previous section, by examining its ability to inhibit Rac1's GTP hydrolysis under single turnover conditions. The measurement of the rate of single turnover GTP hydrolysis is performed by the use of the phosphate probe MDCC-PBP, as described in Chapter 2, and used previously in Chapters 3 and 4.

Figure 52 shows example traces of Rac•GTP hydrolysis in the absence and presence of IQGAP. The increase in fluorescence is due to the MDCC-PBP binding free P_i as it is released from GTP hydrolysis. In the absence of IQGAP, 0.2 μM Rac•GTP shows a rate of GTP hydrolysis of 2.6×10^{-3} s^{-1}. The traces in the presence of IQGAP show an inhibition of Rac's GTPase activity by IQGAP, and that the C-terminal fragment is active.

Figure 52: Inhibition of Single Turnover GTP Hydrolysis by IQGAP

The *panel opposite* shows representative traces produced during the Rac single turnover GTP hydrolysis assay, which was used to examine the activity of the C-terminal IQGAP fragment.

0.2 μM Rac•GTP was incubated in the presence of 20 mM Tris.HCl pH 7.6, 1 mM $MgCl_2$, 15 μM MDCC-PBP and varying amounts of the IQGAP C-terminal fragment at 20 °C. On initiation of Rac•GTP hydrolysis (by the addition of the Rac•GTP), the increase in P_i levels were monitored by observation of the fluorescence increase of MDCC-PBP as it bound the P_i released from GTP hydrolysis. The rate of this fluorescence increase is equivalent to the rate of GTP hydrolysis. Calibration of the increase in fluorescence of MDCC-PBP was achieved by adding known amounts of P_i to 15 μM PBP.

The *traces opposite* show an increase in P_i levels against time, demonstrating Rac•GTP hydrolysis. On the addition of IQGAP, the rate of GTP hydrolysis (as measured by MDCC-PBP fluorescence) decreases. Each of the data sets could be fitted well to an exponential curve, giving the rate of GTP hydrolysis. Rac•GTP demonstrated a rate of 2.6 x 10^{-3} s^{-1}, which was reduced to 1.8 x 10^{-3} s^{-1} in the presence of 0.1 μM IQGAP, which was further reduced to 1.0 x 10^{-3} s^{-1} in the presence of 0.2 μM IQGAP.

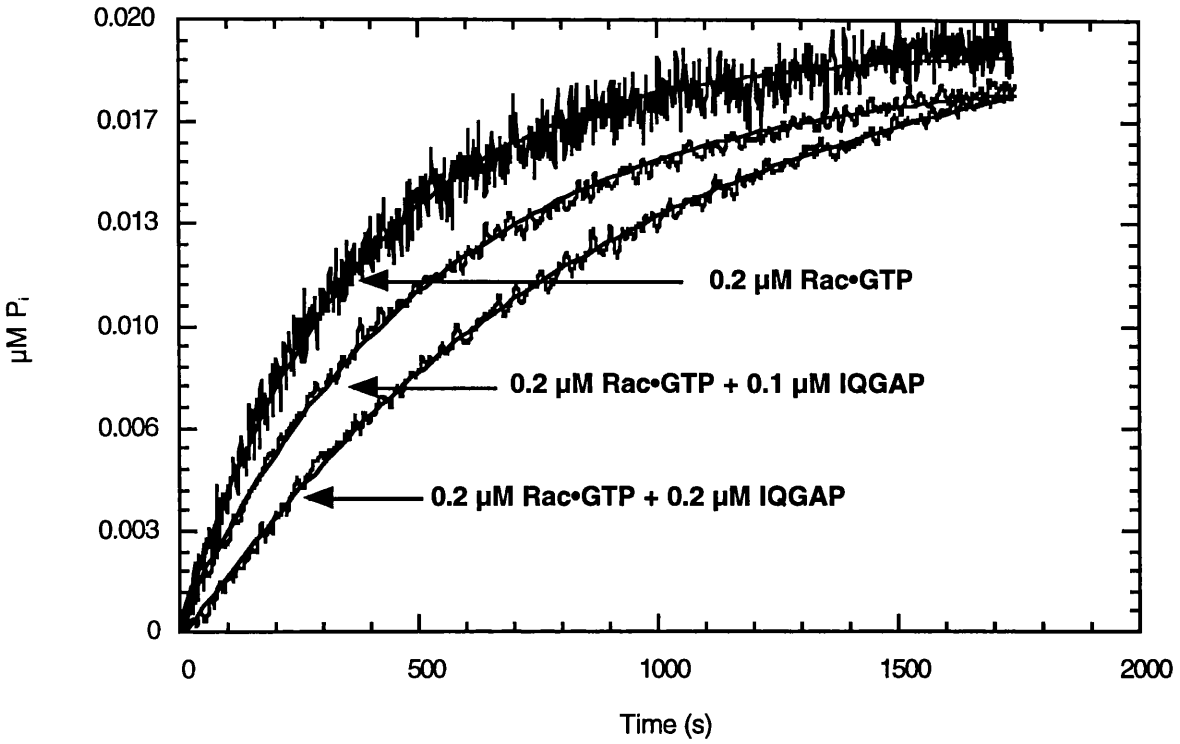

Figure 52 Inhibition of Rac-mediated GTP hydrolysis by the C-terminal Fragment of IQGAP

This method of determining the inhibition of Rac's GTPase rate was used to determine an approximate limit for the K_d of the IQGAP/Rac•GTP interaction. Varying concentrations of the C-terminal fragment of IQGAP were incubated with constant concentrations of Rac•GTP (0.2 μM) (Figure 53). The resulting rates at IQGAP concentrations could then be plotted and fitted to a quadratic curve (derived in Appendix 2) to provide an estimate of the K_d.

This method provided an estimate for the interaction between IQGAP and Rac•GTP of ~ 50 nM. The Rac•GTP concentration used (0.2 μM) to calculate this value demonstrated a low fluorescent signal intensity, so that measurement of the changes in the fluorescence was difficult. Increasing the concentration of Rac•GTP to 1 μM improved the signal, but could not provide an estimate of the K_d value.

5.2.4 Measurement of Rac and IQGAP Interaction by Changes in Fluorescent Intensity

The previous section demonstrated that the C-terminal fragment of IQGAP is active and able to inhibit the GTPase activity of Rac, as well as indicating that the K_d between the two proteins is in the nanomolar range, suggesting relatively tight binding.

The use of environmental fluorescent probes to monitor interaction between two proteins has been successfully used in many previous studies, and this method of analysis may be useful to monitor the IQGAP/Rac interaction. The observation of the interaction between

Figure 53: IQGAP Inhibition against IQGAP Concentration

The *panel opposite* represents a plot of the rate of 0.2 μM Rac•GTP hydrolysis in 20 mM Tris.HCl pH 7.6, 1 mM $MgCl_2$ and in presence of various concentrations of IQGAP.

The curve is fitted to the equation (derived in Appendix 2), and this provides an estimate of the limit of the K_d between IQGAP and Rac•GTP of 50 nM. This provides an estimate of the K_d = 50 nM. Each point is an average of at least 3 separate measurements of the rate of GTP hydrolysis.

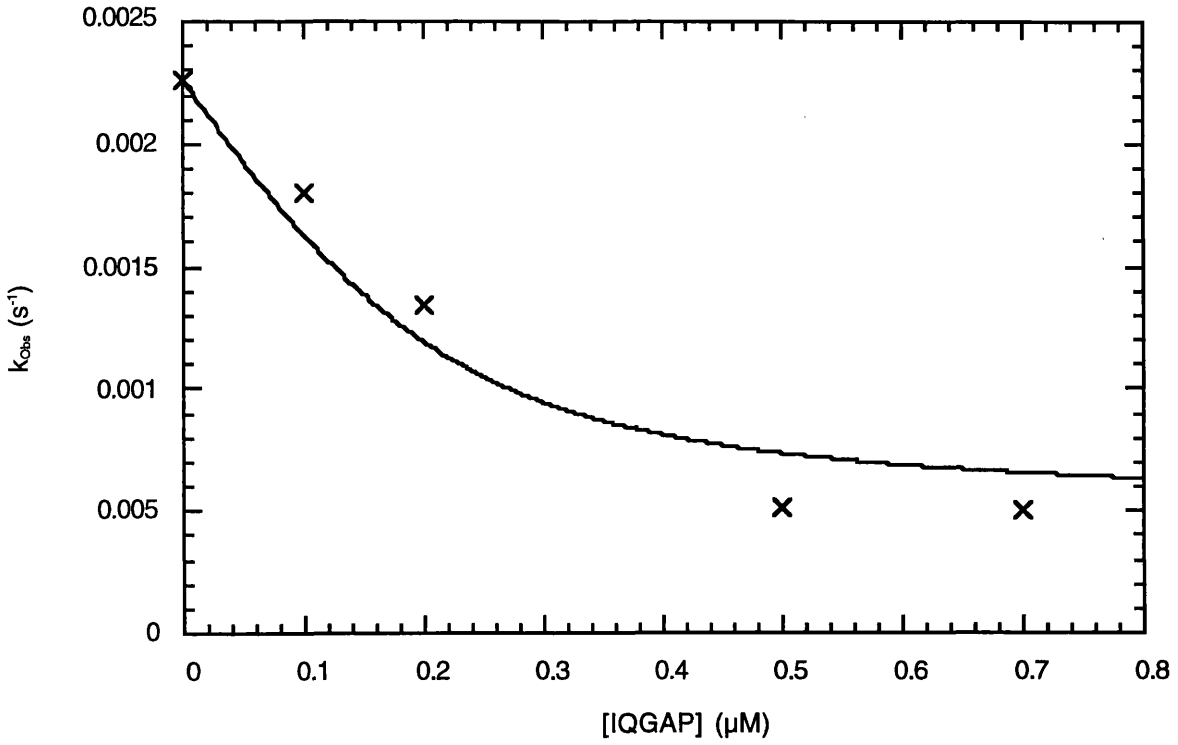

Figure 53 Plot of Observed Rate of Rac•GTP hydrolysis (k_{obs}) v [IQGAP]

IQGAP and Rac was attempted using both fluorescently labelled nucleotides and by fluorescently labelling the IQGAP fragment itself.

The interaction of IQGAP with fluorescently labelled Rac•GMPPNP proteins was attempted, using direct fluorescent measurement of the interaction between IQGAP and the GTP state of Rac. The labelled nucleotides, MantGMPPNP and the coumarin but-edaGMPPNP were used. An attempt to monitor the interaction between IQGAP and Rac•GMPPNP was also tried by labelling IQGAP itself with the two different coumarins, MDCC and IDCC. For both fluorescently labelled nucleotide and fluorescently labelled IQGAP, the fluorophores act as an environmental sensor, where an increasingly hydrophobic environment (such as by exclusion of solvent) causes an increase in Mant or coumarin fluorescence. If these fluorophores are proximal to the area of protein-protein interaction then a change in fluorescence might be expected on binding.

The changes in fluorescence on addition of IQGAP to Rac•MantGMPPNP were measured as described in Chapter 2. The use of the MantGMPPNP fluorophore provide different potential ways of detecting the interaction, either by direct Mant group excitation (360 nm) or through FRET by excitation of tryptophan residues (290 nm) proximal to the Mant group, which transferred their excitation energy to Mant and emitted light at 440 nm. Both of these methods were tried to assess the best method for monitoring the Rac/IQGAP interaction but gave very small changes in fluorescence. Figure 54 shows the changes in fluorescence of Rac•MantGMPPNP against the concentration IQGAP. The graph shows an initial increase in

Figure 54: Fluorescent Changes on Interaction of Rac•GMPPNP with IQGAP

The *upper panel opposite* represents the percentage increases in fluorescence (over the value in the absence of any IQGAP) on the addition of IQGAP, corrected for dilution, monitored by FRET of the Mant fluorophore. The additions of IQGAp were made into 1 μM Rac•MantGMPPNP 20 mM Tris.HCl pH 7.6 1 mM $MgCl_2$ at 20 °C.

An initial addition of IQGAP (final 1μM) causes a fluorescence increase an increase of 23% of the original fluorescence. Subsequent additions of 1 μM IQGAP show a small increase or small decrease in fluorescence.

The table *opposite* shows the magnitude of the initial increase in fluorescence on the addition of IQGAP for each of the fluorescent nucleotides used.

The magnitude of the change in fluorescence observed by any of the three methods is not sufficiently large to be useful in estimating the K_d of the interaction between IQGAP and Rac.

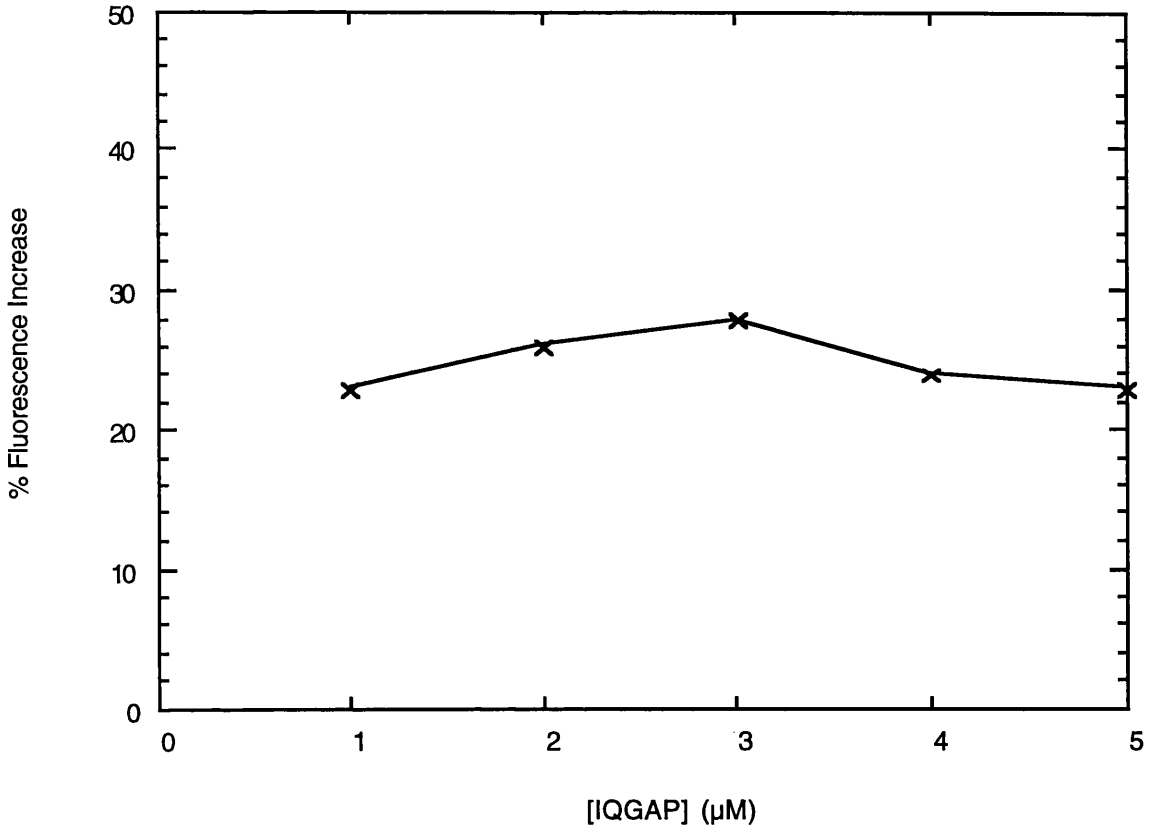

Figure 54 Increases in fluorescence on addition of1μM IQGAP to 1μM Rac•MantGMPPNP Measured by FRET (Ex. 290 nm, Em. 440 nm)

Fluorophore	% Fluorescence Change
Mant (Ex. 360 nm)	+ 15%
Mant (Ex. 290 nm)	+ 23%
but-eda Coumarin (Ex. 425 nm)	+ 11%

fluorescence, followed by no further increases. These changes in fluorescence were similar for Rac•MantGMPPNP (excited at either 360 nm or 290 nm) or Rac•but-edaGMPPNP. Direct excitation of Mant produced an average initial increase in fluorescence of 15%, whereas indirect excitation by FRET produced an average initial increase in fluorescence of 23%. The average initial increase on Rac•but-edaGMPPNP was 11%.

The initial increases in fluorescence observed are due to the interaction of IQGAP with the various labelled forms of Rac•GMPPNP, however, none of the different labels produced a particularly large increase in fluorescence on IQGAP binding. When the Rac•GMPPNP in each case was saturated, and no more binding could take place, the maximum increase in fluorescence is 23% (with Mant excited indirectly). The sensitivity of this method for measuring the binding between Rac and IQGAP is therefore quite low.

The use of the different fluorescent forms of Rac•GMPPNP have shown that each fluorophore produces a small change in intensity on the interaction of IQGAP with Rac•GMPPNP, but that this method is not sufficiently sensitive to provide accurate data with which to estimate a K_d for the interaction.

The second approach taken to monitoring the interaction between IQGAP and Rac•GMPPNP was by the labelling of IQGAP itself with a fluorescent label. A useful method for attaching fluorescent labels to proteins is through reactive cysteine residues, which are able to react irreversibly with a particular class of coumarin fluorophores. From its sequence,

the C-terminal fragment of IQGAP contains only two Cys residues, one proximal to the GRD in the primary sequence and one proximal to the C-terminal end of the fragment. Nothing is known of the IQGAP structure, and so the situation of these Cysteines could be either: buried within the molecule; S-S bonded together; unreactive; potentially reactive and only in that case, receptive for labelling. The use of the DTNB assay, as described in Chapter 2, demonstrated that only one of the two potential Cysteines in the C-terminal fragment of IQGAP is active, although not which one.

The indication that IQGAP contained a reactive Cysteine residue permitted labelling of IQGAP with the coumarins MDCC and IDCC, and subsequent attempts to observe any changes in fluorescence on addition of Rac•GMPPNP, as described in Chapter 2. After labelling of IQGAP with MDCC or IDCC, a wavelength absorbance scan confirmed that the label and protein were in a 1:1 concentration ratio.

Addition of 1 μM Rac•GMPPNP aliquots into 2 μM MDCC-IQGAP or 2 μM IDCC-IQGAP showed no increases in fluorescence.

The presence of a Cysteine proximal to the GRD suggested that this approach had potential, but the lack of any noticeable fluorescent change demonstrated that this Cys was either not labelled, or that the fluorophore was not in a position susceptible to the IQGAP/Rac interaction. This method was not pursued, although future prospects would include labelling with different coumarin fluorophores and mutagenesis of a cysteine residue into a potential

site of Rac/IQGAP interaction.

5.2.5 Interaction of Rac and IQGAP as Measured by Fluorescent Anisotropy

The attempts to monitor the interaction between IQGAP and Rac•GMPPNP using changes in fluorescent intensity, as previously described, were unsuccessful. However, the use of fluorescent anisotropy was successful in measuring the interaction. Anisotropy is likely to be reflect a change in the rotational correlation time of the fluorophore and therefore represents the size of the complex to which the fluorophore is attached (assuming local fluorophore rotation is zero). In the case of IQGAP, if Rac•MantGMPPNP becomes complexed with IQGAP, then the entire size of the complex will increased. This increased complex size may cause a decrease in its rotation rate, which in turn would cause an increase in the anisotropy value.

IQGAP was titrated into a solution of Rac•MantGMPPNP, and the increase in anisotropy measured after each addition (as described in Chapter 2). Titration experiments were performed in the presence of both 0.2 μM Rac•MantGMPPNP and 0.2 μM Rac•GDP (Figure 55). The titration data for 0.2 μM Rac•MantGMPPNP fitted well to a simple binding curve, and produced an average K_d value of 0.34 μM. The use of Rac•MantGDP in the titration experiments showed little change in anisotropy. The data for Rac•MantGDP could be fitted to a linear fit, which gave an estimated $K_d > 60$ μM. This suggests that IQGAP shows an approximately 200-fold higher affinity towards the activated form of Rac than the inactive

Figure 55: Titrations of IQGAP into Rac•MantGMPPNP

The *panel opposite* are representative of titrations of the C-terminal fragment of IQGAP into a solution of 0.2 μM Rac•MantGMPPNP. The anisotropy change on addition of IQGAP to a 0.2 μM Rac•MantGDP solution is also shown. Each titration experiment was performed at 20 °C, in the presence of 1 mM $MgCl_2$, 20 mM Tris.HCl pH 7.6, and each measurement taken 60 seconds after the addition occured, to allow complex formation and temperature equilibration.

The data for Rac•MantGMPPNP is fitted to a simple binding curve:

$$[\text{Rac•IQGAP}] = \frac{[\text{IQGAP}]_{\text{total}}.[\text{Rac}]}{[\text{Rac}] + K_d}$$

which estimates the K_d of the interaction to be 0.3 μM.

The increase in anisotropy on addition of IQGAP to Rac•MantGDP can be fitted to a linear fit. From this fit, the K_d can be estimated > 60 μM.

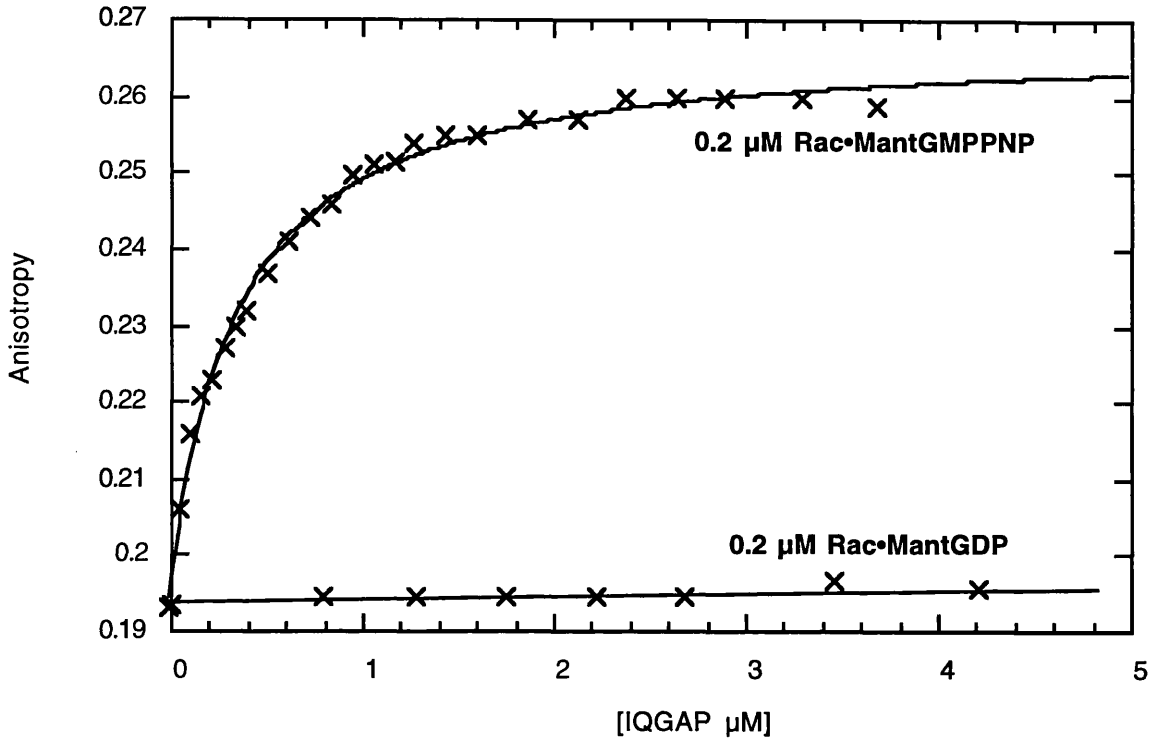

Figure 55 Simple Binding Curve of 0.2 µM Rac•MantGMPPNP and 0.2 µM Rac•MantGDP with IQGAP additions

form.

The titration experiments indicate that the use of fluorescent anisotropy is a successful method to measure the interaction between Rac and IQGAP. They show that the interaction between IQGAP and Rac requires the GTP form of Rac, since little binding is observed between the GDP state, and this interaction appears to be relatively tight, on average K_d of 0.34 μM. The previous section 5.3.2. used the inhibitory activity of IQGAP to provide an estimate of the K_d between for the Rac and IQGAP interaction (Figure 56) of 50 nM. These two values are sufficiently similar to be consistent.

To provide information on the kinetics of the association and dissociation between the two proteins, fluorescent anisotropy was measured in stopped flow experiments.

Association experiments, as described in Chapter 2, were performed using increasing concentrations of IQGAP against a constant concentration of 1 μM Rac•MantGMPPNP under pseudo first order conditions where the concentration of free IQGAP is effectively constant. A representative trace of the association data is shown in Figure 57a. After fitting the data to a single exponential, a k_{Obs} is obtained for each IQGAP concentration. The k_{Obs} values measured at increasing concentrations of IQGAP increased linearly with concentration (Figure 57b) which reflects the binding of IQGAP to Rac. In this linear fit, the gradient of the line represents the association rate constant (k_{+1}) for the process (Figure 56) and has a value of 0.7×10^6 M^{-1} s^{-1}. The y-intercept represents an estimation of the dissociation rate constant (k_{-}

Figure 56: The Rac•GMPPNP & IQGAP Interaction Process

The scheme opposite represents the interaction between IQGAP and Rac•MantGMPPNP as a simple single process.

The K_d for the process, estimated by titration binding expereiments, is 0.34 μM. By measuring the rates of association between Rac and various concentrations of IQGAP, the association rate constant (k_{+1}), can be calculated: 0.7 $s^{-1}M^{-1}$. k_{-1}, the dissociation rate constant can be calculated as 0.8 s^{-1}, using the same data (see Figure 57).

Direct measurement of the dissociation rate using unlabelled Rac•GMPPNP rapidly mixed with IQGAP•Rac•MantGMPPNP (Figure 58), showed that the dissociation rate was approximately constant (average value 1.6 s^{-1}), which suggests that the dissociation of the two proteins may be a simple single process.

The equilibrium constant, K_1, for this process is = k_{+1}/k_{-1} = 0.44 x 10^6 M^{-1}, and from this a K_d value ($1/K_1$) can be calculated of 2.2 μM.

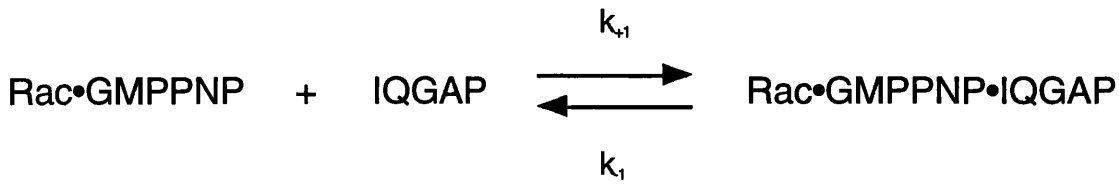
k+1
Rac•GMPPNP + IQGAP
Rac•GMPPNP•IQGAP
k-1

Figure 57: Rac•GMPPNP & IQGAP Association

The *upper panel* is a representative experiment of the change in anisotropy on the association of IQGAP and Rac•MantGMPPNP. Final Concentrations of 10 μM IQGAP and 0.2 μM Rac•MantGMPPNP were rapidly mixed in the presence of 20 mM Tris.HCl pH 7.6, 1 mM $MgCl_2$ at 20 °C. The increase in anisotropy represents an increase in complex formation. The data fitted well to a single exponential curve, with a rate of 6.5 s^{-1}.

The *lower panel* is a plot of rate of association against the concentration of IQGAP. The plot is fitted to a linear fit. The gradient of the line is the association rate constant (k_{+1}), 0.7 x 10^{-6} M^{-1} s^{-1}. The y-intercept represents the dissociation rate constant (k_{-1}), 0.8 s^{-1}. Each point on the graph is an average of at least three points at the relevant concetrations.

From these values an equilibrium constant can be calculated, $K_1 = k_{+1}/k_{-1}$ = 0.88 x 10^6 M^{-1}.

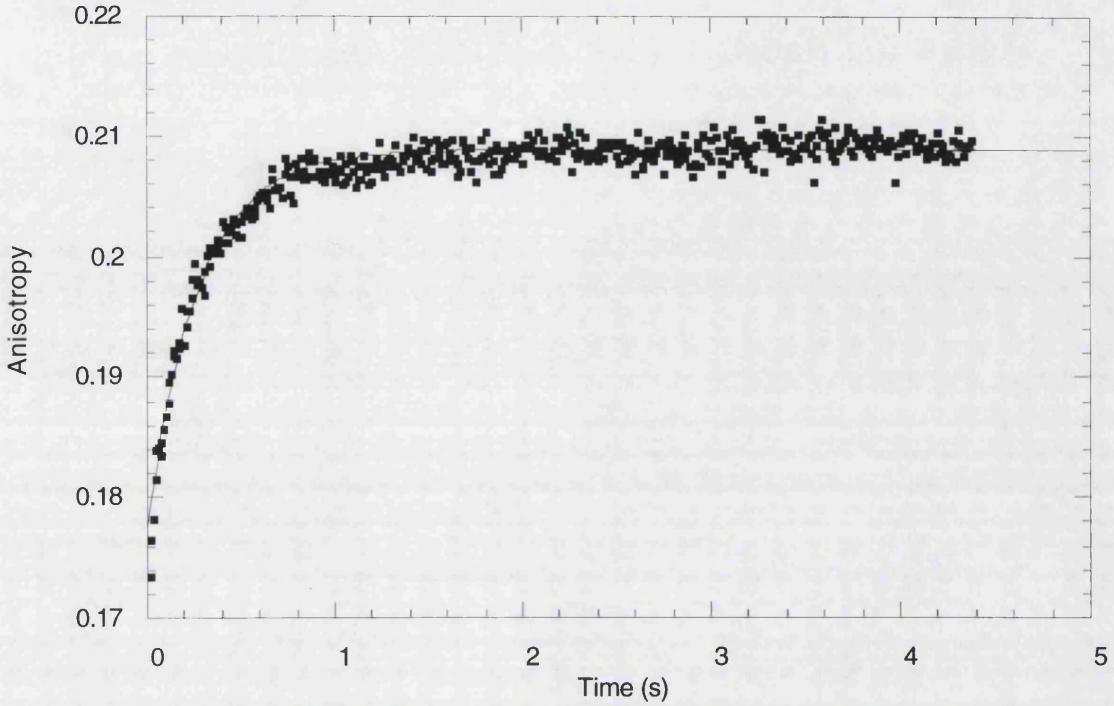

Figure 57a Rapid Mixing of 10 µM IQGAP with 0.2 µM Rac•MantGMPPNP shows an Increase in Anisotropy

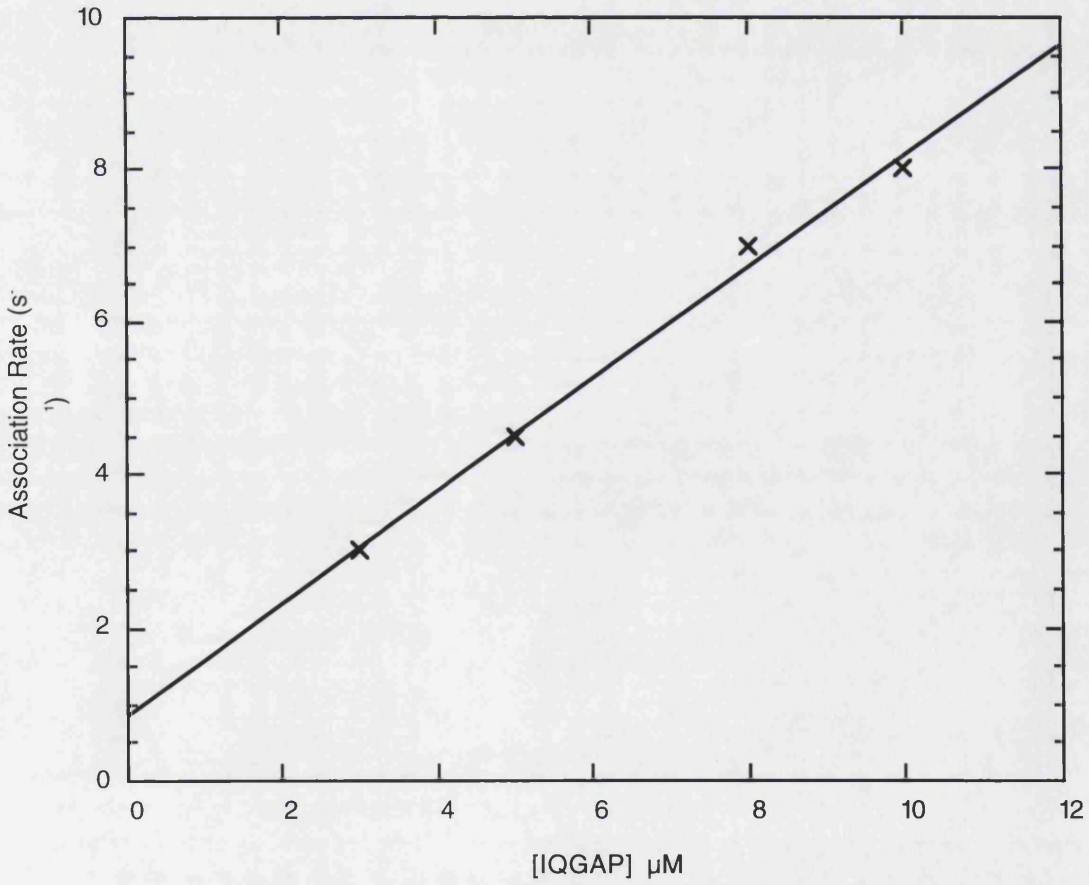

Figure 57b The Rate of Association of IQGAP with 0.2 µM of Rac•MantGMPPNP increases with IQGAP Concentration

$_1$), and in this graph is close to zero.

The dissociation rate of IQGAP from Rac•MantGMPPNP was measured as described in Chapter 2, IQGAP was premixed with Rac•MantGMPPNP, and then rapidly mixed with varying excess concentrations of unlabelled Rac•GMPPNP. The changes in anisotropy were monitored on the stopped flow instrument. An example trace and summarised overall data is shown in Figure 58. The single exponential nature of each curve suggests that the dissociation may be a single process. The dissociation rate between Rac•MantGMPPNP and IQGAP is approximately constant over the concentrations of Rac•GMPPNP used. The average dissociate rate constant is 1.6 s^{-1}, which is a more accurate estimation of the dissociation rate than the value calculated from the association data.

The dissociation constant (K_d) can now be calculated, since:

$$K_d = \frac{k_{-1}}{k_{+1}}$$

Using $k_{+1} = 0.7 \times 10^6\ M^{-1}\ s^{-1}$, and $k_{-1} = 1.6\ s^{-1}$, then the K_d is equal to 2.2 μM. This K_d value is approximately 6-fold greater than that measured from the binding titration experiments. These two values are consistent with each other, although the binding experiments may represent a more accurate value since they measure the actual binding process.

Figure 58: Rac•GMPPNP•IQGAP Dissociation

The *panels opposite* represent data from the dissociation of the C-terminal fragment of IQGAP from Rac•MantGMPPNP, caused by the rapid mixing of excess Rac•GMPPNP (varying concentrations).

The *upper panel* is a representative experiment of the change in anisotropy. Final concentrations of 1 μM Rac•MantGMPPNP•IQGAP and 2 μM Rac•GMPPNP were rapidly mixed in the presence of 20 mM Tris.HCl pH 7.6, 1 mM $MgCl_2$ at 20 °C. The data fitted well to a single exponential curve, with a decrease in rate of 1.9 s^{-1}.

The *lower table* represents the dissociation rates, as measured using varying concentrations of unlabelled Rac•GMPPNP. The average rate is 1.6 s^{-1}. The similarity between the rates suggests that the release of IQGAP from Rac involves a single process.

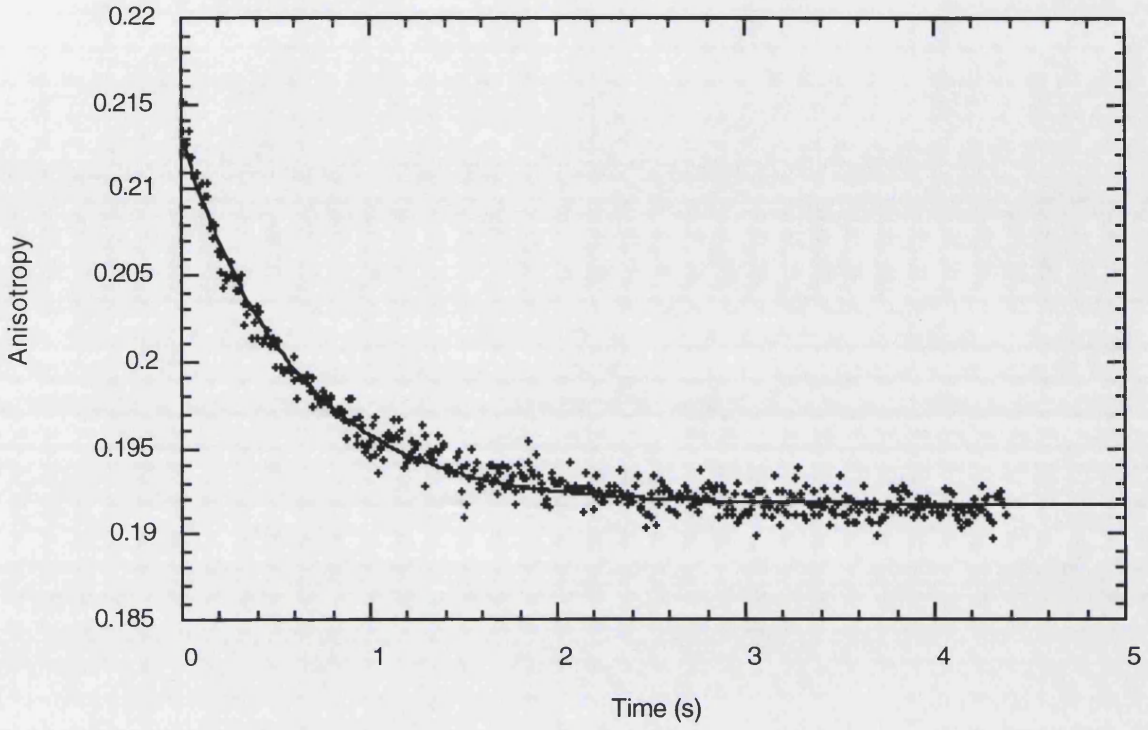

Figure 58a The Dissociation of IQGAP from Rac•MantGMPPNP Causes a Decrease in Anisotropy

Final [Rac•GMPPNP] (μM)	k_{-1} s^{-1}
14	1.3
10	1.8
8	1.0
5.5	1.4
4	1.7
2	1.9

5.2.6 Interaction of Rac Mutants with IQGAP

Various Effector Region and Insert Loop Rac mutants were used in binding titration experiments in order to asses the importance of these regions within Rac, with respect to IQGAP association (Figure 59). The increases in anisotropy on association of the mutant with IQGAP can be fitted to a simple binding curve, which provides an assessment of each of Rac's regions affect on the K_d of the overall IQGAP/Rac interaction. The Rac mutants used were, Effector Region: A27K, I33D, T35A and F37E; Insert Loop: D124S, E131K and K133A. These mutants have been used in other studies to examine changes in Rac/Effector interaction, and so can be compared to other such studies.

The average K_d values for the interaction between the C-terminal fragment of IQGAP and the various mutants, can be seen in Table 4. Out of the seven mutants used, five (A27K, F37E, D124S, E131K, and K133A) had no significant effect (less than 3-fold change) on the K_d compared to the wild type. These mutants were from both the Effector Region and Insert Loop. The mutations in the Effector Region (I33D, T35A) did have a significant effect on the K_d of interaction between Rac and IQGAP. I33D demonstrated a K_d of 3.5 μM, an approximately 10-fold decrease in the affinity for IQGAP. T35A, which like I33D is found in the Effector Region, showed almost no binding to IQGAP at all: from the data produced the K_d was estimated > 27 μM. No mutated residues from the Insert Loop demonstrated a significant change in the K_d for the interaction. D124S caused a 3-fold decrease in affinity, and E131K caused a 10% increase affinity, however neither of these are significantly different from the wild type and therefore the data suggests that the Insert Loop plays no role in the interaction.

Figure 59: Rac Mutant Residues Positions

The panel opposite shows The Rac•GDP structure illustrating the positions of the various mutants used in this study to probe the regions of Rac which interact with the C-terminal fragment of IQGAP. The mutations are marked by red areas on the purple backbone structure. The green sphere in the centre of the molecule represents the associated Mg^{2+} ion and the blue structure is the bound GDP.

The mutants are divided into two regional structures: the Effector Loop (A27K, I33D, T35A and F37E), the Insert Loop (D124S, E131K and K133A).

The affect each mutation had on the wild type K_d of IQGAP/Rac interaction can be seen in Table 4.

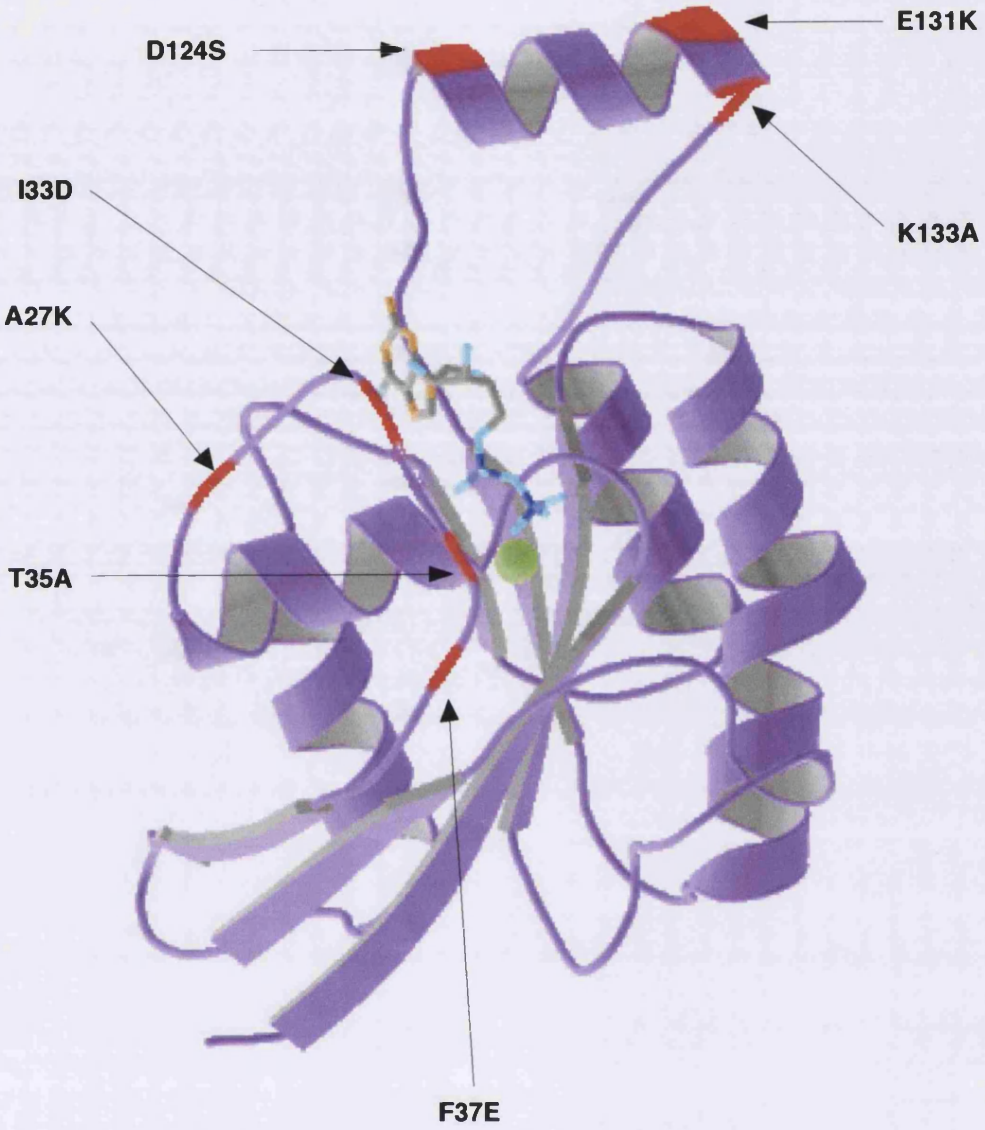

Figure 59 The Position of the Rac Mutations used to analyse IQGAP Interaction

Table 4: Rac Mutant Interaction with IQGAP

	Rac Mutant	K_d (μM)
Effector Loop	**A27K**	0.58
	I33D	3.5
	T35A	> 27*
	F37E	0.44
Insert Loop	**D124S**	1.0
	E131K	0.20
	K133A	0.48
	Wild Type	0.34

* Data for T35A was plotted and fitted to a linear fit, from which the concentration of IQGAP necessary to reach the maximum change in anisotropy could be calculated.

These results suggest that the C-terminal IQGAP fragment interacts with the Effector Region of Rac, although the specific amino acid requirements for the interaction seem to be somewhat flexible, since some non-conservative mutations do not perturb the K_d greatly. The reasons for the mutations effect on the K_d will be discussed in the next section.

5.3 Discussion

The progress of this Chapter has reflected a study beginning with the genetic manipulation of the IQGAP gene fragment and vector into a modified form, resulting in increased purity of IQGAP fragment expression. This IQGAP fragment was shown to be active, through its inhibition of Rac's GTPase activity, which also allowed an estimation for the limit of affinity (K_d) between the C-terminal fragment of IQGAP and Rac•GTP. This value (0.05 μM) suggested that the binding between the two proteins was of high affinity. In an attempt to measure the K_d by a more direct method, the changes in fluorescent intensity were observed on interaction between the two proteins, using either labelled Rac-bound nucleotide (Mant or Coumarin 343), or labelled IQGAP (MDCC or IDCC). Neither of these methods proved to be sufficiently sensitive to monitor the interaction process.

C-terminal Fragment IQGAP Expression Problems

The DNA sequence of the gene fragment in the newly created pGIT2, showed the correct

sequence, yet the final protein preparation of the C-terminal fragment of IQGAP showed two major protein bands on an SDS-PAGE gel. The presence of equivalent protein bands (of a higher molecular weight) can also be seen in the preparations of the original clone (without a Thrombin site), and these are likely due to some form of limited proteolysis by a protease expressed in bacteria. The large size of the fragment (8 kb is a large plasmid for an *E.coli* cell) may cause expression problems, including premature termination of transcription or translation or loss of the plasmid from the growing bacterial population. The IQGAP gene fragment also contains a number of eukaryotic codons, in particular Arginines, whose tRNA counterparts are not as frequent in *E.coli* cells as they are in eukaryotic cells. The low number of these correct tRNAs may impose a limit on the production of the IQGAP protein, or even cause its premature truncation. Preparations were attempted in a strain of *E.coli*, which contained a plasmid incorporating genes for such tRNAs, however, the transformation of these bacteria and subsequent protein preparation showed no improvement over the previous *E.coli* strains used.

The region of the fragment which this study is particularly interested in is the GRD. This domain is located close (141 residues) to the N-terminus of the fragment and GST fusion protein, and is also relatively short (270 residues) in comparison to the overall length of the fragment (820 residues). It may therefore be the case, that the GRD itself is complete in the two major protein bands observed, and only a short amount of sequence is lost from the C-terminal end. The expression of the IQGAP fragment in protease deficient cells, and its purification in the presence of a protease inhibitor cocktail suggested that the IQGAP

protein fragment was clipped by some uninhibited bacterial protease, most likely near the C-terminus.

A way around this problem may be to truncate the gene fragment further within the vector, such as by the introduction of STOP codons directly after the GRD, or by excising the DNA sequence between the GRD and the existing STOP codon. This would not only hopefully lead to even greater level of preparation purity, but may also increase the amount of expressed protein, due to the lower transcription load required of the *E.coli* host. It may also provide information as to the role of the sequence immediately C-terminal of the GRD, with respect to Rac interaction or inhibition of GTP hydrolysis.

Investigation of the Rac/IQGAP Interaction

The use of fluorescent anisotropy of MantGMPPNP labelled nucleotides in both binding titration experiments and time-resolved stopped flow experiments, provided an estimation of a K_d, as well as the rate of association and dissociation between the two proteins. These methods gave a K_d of 0.34 μM, an association rate constant of 0.7 x 10^6 M^{-1} s^{-1}, and dissociation rate constants of 0.8 s^{-1} and 1.5 s^{-1}, the latter value being derived from dissociation experiments, and therefore more accurate. The C-terminal IQGAP fragment did not associate with Rac•MantGDP. This technique was then used to probe the nature of IQGAP/Rac interaction: a panel of Rac mutants (in both the Effector Region and Insert Loop) were used to assess which regions of Rac were important in the interaction with IQGAP. Only the Effector Region contained mutated residues that demonstrated a significant effect on

the K_d, although the exact residue contribution to the association remains unclear. From this data, it is impossible to suggest any interaction between IQGAP and Rac's Insert Loop, unlike previous studies.

The study of IQGAP's association with Rac, utilising changes in fluorescent intensity of fluorescent nucleotides (MantGMPPNP and but-edaGMPPNP), and fluorescently labelled IQGAP (MDCC and IDCC) was unsuccessful. It is unclear why this was the case. The Mant- and but-edaGMPPNP nucleotide analogues would be expected to report on any interaction affecting the nucleotide binding site, however only small changes in fluorescent intensity were observed on IQGAP binding which were not sufficient for confident K_d determination. It is unclear as to why the change in fluorescence was so small. It may be that the change in environment around the fluorophore, caused by the binding of IQGAP, was not sufficient to cause a change in fluorescence. It is possible that the Rac•MantGMPPNP and Rac•but-edaGMPPNP complex cause a steric hindrance factor, preventing the association with IQGAP.

The absence of a change of fluorescent intensity with the MDCC- and IDCC-labelled IQGAP is understandable, since only the primary structure of the C-terminal IQGAP fragment is known, the position of the two Cysteine residues in the tertiary structure, with respect to the GRD of the fragment, is unclear. Furthermore, only one of these Cysteines is reactive, which suggests that the likelihood of the reactive Cys being proximal to the GRD and the attached label being in such a position as to be affected by Rac•GMPPNP binding, is relatively small. If this method of monitoring the interaction between the two proteins was

to be pursued, then engineering of Cysteines into various positions around the GRD may prove successful.

Measurement of the changes in fluorescent anisotropy of Rac-bound Mant nucleotides acted as a successful reporter for the association of IQGAP and Rac. Titration binding experiments, gave an average K_d value of 0.34 μM, which suggests relatively tight binding between the two proteins, and is consistent with the value calculated using the inhibitory studies of 50 nM. The K_d established through the titration experiments suggests slightly weaker binding than that measured via the inhibition experiments. The difference between these two values, may well represent the differences between the two techniques — the inhibitory studies were technically more difficult to perform, and therefore potentially more prone to sources of error, indeed the fit of the curve to the data is not perfect. The nature of the titration experiments required the use of the non-hydrolysable Rac•MantGMPPNP, whereas the inhibition studies used Rac•GTP. GTP, not MantGMPPNP, is the *in vivo* substrate for Rac, and the differences between these two nucleotides may be an explanation for part of these differences. Mant, which lies at the mouth of the nucleotide binding site, may cause a small amount of steric hindrance. Additionally the GMPPNP nucleotide may not replicate the exact GTP conformation which is optimally recognised by IQGAP, although this effect may be minimal.

The K_d value calculated using the association and dissociation rate constants is 2.2 μM, approximately 6-fold greater than that measured during binding experiments. Again, the

value calculated is much greater than the lower limit suggested by the inhibition studies, and this may reflect differences caused by the Mant group or GMPPNP nucleotide. Repeating these experiments with the Rac mutant Q61L, which is defective in GTP hydrolysis and can be purified bound to GTP may clarify these issues. This will provide a natural nucleotide control for MantGMPPNP bound Rac (although the exchange of MantGTP into the active site is technically difficult).

The value measured from the titration experiments may represent the most accurate K_d value, since it represents a direct measure of the binding process. The differences observed between the two K_d values may indicate a form of complicated multistep process, where the K_d as measured by the titration experiments may differ from that calculated by k_{-1}/k_{+1}. Since the IQGAP fragment is relatively large it is conceivable that a number of conformational changes are required for binding to occur between the two proteins.

Previous kinetic studies on IQGAP fragment association and GTPase inhibition have been performed using Cdc42 and Rac1 (Zhang, B., Wang, Z-X., Zheng, Y., 1997; Zhang, B., Chernoff, J., Zheng, Y., 1998). The initial published work suggested that the K_d for Cdc42 and IQGAP interaction was 0.08 μM (using similar inhibition studies as described in this study). The subsequent work with Rac1 and Cdc42 using the same methods suggested that the K_d for the interaction between Rac1 and IQGAP was 2.13 μM, and that with Cdc42 was now 0.39 μM. These studies showed that the C-terminal fragment of IQGAP1 could bind tightly to both Rac1 and Cdc42 and may therefore be an *in vivo* effector for both (supported

by the large amount of functional studies). This present study has confirmed that the binding between the GTP state of Rac1 and the IQGAP fragment is relatively tight, although slightly more tight than suggested in the previously published study, which may reflect the ability to measure the K_d directly by use of fluorescent anisotropy. IQGAP's specificity for Rac•MantGMPPNP (and by analogy, Rac•GTP) over Rac•GDP forms is also confirmed, although there may be a slight difference between the affinity of IQGAP for Rac•GTP and Rac•MantGMPPNP.

What cellular significance can be attributed to the kinetic properties of IQGAP and Rac1? This study has used only a C-terminal fragment of IQGAP, yet it is still able to demonstrate tight binding and effective inhibition of Rac's GTPase activity. This suggests that the C-terminal domain of IQGAP provides a significant contribution to the interaction with Rac, whereas the N-terminal domain may provide a smaller contribution, if at all. Some form of communication between the two domains is to be expected, since such communication is required for the release of Rac or Cdc42 on Ca^{2+} binding, and vice versa. It maybe that a number of IQGAP's domains are important for this communication: it has been shown that activation of the GEF, Ras-GRF, by Ca^{2+} requires the co-operation of its pleckstrin domain, coiled-coil domain and IQ domain (Buchsbaum, R. *et al.* 1996). Such concerted multi-domain action may also occur in IQGAP. Similar experimentation, as described in this study, with the whole of the IQGAP molecule or in the presence of the N-terminal fragment may provide details of the importance of the N-terminal domain, with respect to small G-protein inhibition and binding.

It is possible to envisage IQGAP acting in a similar fashion to RhoGDI proteins (although with GTP-bound form rather than GDP-bound form), where IQGAP maintains the bound small G-protein in an active state before releasing it into an area of activity on an activating signal. The evidence presented in this and other studies suggests that IQGAP associates tightly with Rac's Effector Region (in particular).. The tightness of their association may resist Rac association with other effector proteins. In this case, it makes sense to consider that IQGAP's maintenance of Rac in its GTP-bound state is to prolong IQGAP's active lifetime. The role of IQGAP may not be one of small G-protein regulation, rather small G-proteins may regulate IQGAP's function.

The presence of bound Rac•GTP or Cdc42•GTP bound to IQGAP has been shown to cause activation of its cytoskeletal functions, such as actin bundling. Indeed, it may be, that the selective binding of IQGAP to Rac and Cdc42, two small G-proteins intricately involved in cytoskeleton organisation, is a reflection of one of the main pathways through which these two proteins mediate their cytoskeletal function. The potent inhibitory effect of IQGAP may provide a mechanism by which the active states of Rac or Cdc42 are able to activate IQGAP-mediated rearrangements of the cytoskeleton in a relevant timeframe that such rearrangements requires, rather than the relatively rapid, GAP-accelerated rate that the hydrolysis would occur under, *in vivo*. Recent work on the CRIB-domain containing protein, WAsP, has revealed how WASP affects cytoskeletal arrangements in response to activated Cdc42 (Mullins, D., 2000). Active, GTP-bound Cdc42 is localised to the membrane, and there

recruits WASP. WASP is then able to recruit both actin filaments and a further protein involved in actin polymerisation to this complex. The complex is able to stay intact until Cdc42 hydrolyses the bound GTP (WASP inhibits of the GTPase activity). It is easy to imagine IQGAP acting in a very similar fashion with Cdc42 and Rac, allowing recruitment of the cytoskeleton to the membrane. The lifetime of such a complex being dependent on the inhibitory activity of IQGAP.

This discussion of IQGAP function, with respect to its kinetic properties, poses the question of how IQGAP is activated. Previous work has suggested that the two regulatory pathways which feed into the IQGAP protein are the Rac/Cdc42 and Ca^{2+}/Calmodulin pathways, each having an antagonistic effect on the other. The mechanism and kinetics of the interplay between these two pathways, using IQGAP as the central element, would further our understanding of IQGAP's activity and function. No study has yet provided kinetic information on the affinity of Ca^{2+} for IQGAP, but for a complete understanding of how the two pathways influence IQGAP this would be essential. Are the affinities such that the equilibrium between Ca^{2+} binding and small G-protein binding provides a mechanism by which a small change in either pathway causes a large change in the opposing element? It may be that IQGAP sits at an equilibrium point with both the Ca^{2+} and small G-protein pathways in a resting cell. A small change in activity of either component is rapidly able to influence IQGAP's function fulfilling cellular demand, before returning to its resting state. Perhaps if IQGAP's main role is cytoskeletal organisation, activation of Rac or Cdc42 is a positive signal, whereas a Ca^{2+} increase is a negative signal on cytoskeleton polymerisation.

The mutational studies described in this study used a number of mutants from the Insert Loop and Effector Region of Rac. Previous work has suggested that both of these regions of Rac and Cdc42 are involved in IQGAP association. Replacement of the Insert Loop with residues from Ras (effectively deleting it) caused a 2- to 3-fold decrease in the affinity of IQGAP for Cdc42 (Wu, W-J., *et al.* 1997). Individual mutations of Cdc42 residues illustrated the importance of the Effector Region in binding (McCallum, S., *et al.* 1996). D38E showed little effect on binding, Y32K caused a small decrease in the affinity of binding, but T35A showed a complete loss of any binding. Figure 59 illustrates the positions of the mutants on the Rac structure used in this current study.

The Insert Loop mutations, D124S, E131K and K133A each changed the K_d by an insignificant amount. D124S, the change from a negatively charged Aspartate to a neutral Serine caused a slight increase in the K_d between the two proteins. The mutation of the negatively charged Glutamate 131 to a positively charged Lysine residue is the only mutation that showed a slight decrease in the K_d for the interaction. The replacement of the positively charged Lysine 133 with an Alanine slightly increased the K_d for the interaction. Previous studies have shown that the Insert Loop appears to be important for the interaction between IQGAP and Rac or Cdc42, however the data presented here shows no significant change of K_d on mutation of certain Insert Loop residues, and therefore is unable to suggest any interaction between IQGAP and Rac's Insert Loop.

It is unclear as to the reason between the differences in Insert Loop effect, between this study and previous work. The mutation E133K is quite peripheral to the Insert Loop, and the mutation may therefore not influence any interaction. The lack of effect on the K_d with both the D124S and K133A mutations may suggest that these mutations are not sufficient to interfere with any interaction, or that IQGAP does not interact through these residues. It is possible that the interaction between IQGAP and Rac's Insert Loop is not mediated by the residues investigated in this report — mutations of other residues in the Insert Loop may show a more significant effect on the K_d.

The mutations of Effector Region residues also indicate that this area of Rac is involved in the interaction with IQGAP. On mutation of the neutral Alanine 27 to positively charged Lysine, and the neutral Phenylalanine 37 to negatively charged Glutamate, the K_d of the interaction is not significantly affected. Both of these residues are found in the periphery of the Effector Region, so the small change in K_d is perhaps understandable. Their small effects can perhaps be compared with the D38E mutant which is also quite peripheral (McCallum *et al.* 1996). The change of Isoleucine to the negatively charged Aspartate, results in a 10-fold decrease in affinity, suggesting that the introduction of the larger, charged group into the central region of the Effector Domain causes a reasonable amount of disruption of the interaction.

The T35A mutation, the change of Threonine 35 to Alanine, has an effect which causes the a drastic loss of binding between Rac and IQGAP ($K_d > 27\ \mu M$) (comparable to the reduced binding observed for Rac•GDP, $K_d > 60\ \mu M$). A similar result has also been observed in a

previous study (McCallum, S., *et al.*, 1996), where it was suggested that the loss of binding, caused by the mutation of T35A (in Cdc42 rather than Rac1) implicated the Threonine side chain in a direct binding role with IQGAP. However, it is possible that the mutation of Threonine 35 causes such a major effect of Rac due to further effects the mutation has on the Rac protein, potentially involving Mg^{2+} coordination. Threonine 35, located in the Effector Region (Switch I) and is essentially involved in Mg^{2+} coordination. In the structure of Rac•GDP this coordination is mediated through its main chain carbonyl group, with the side chain pointing out into the solvent body, whereas in the Rac•GMPPNP structure the side chain is used in the coordination of the Mg^{2+}. The Threonine 35 residue is therefore crucially involved in the switching between active and inactive states of Rac.

The presence of an Alanine methyl side chain in the Effector Region may cause aberrant packing of the region, which may directly prevent IQGAP interaction with the Effector Region directly due to an altered conformation, or it may mediate its effects through aberrant Mg^{2+} coordination. Since correct Mg^{2+} coordination is important in maintaining both the correct Effector Region switching and conformation, a change in the Mg^{2+} coordination may prevent IQGAP binding. It has already been shown in this, and other studies that IQGAP is unable to associate with Rac•GDP forms, which suggests that the interaction is sensitive to changes in the Effector and Switch Regions. It is therefore possible to see how a change in Mg^{2+} coordination preventing the switching of Rac to an active state or modifying Effector Region conformation could abolish binding of IQGAP to Rac.

The sensitivity of the binding between IQGAP and Rac may be due to the nature of the interaction with respect to the overall Rac structure. This study has shown that IQGAP interacts with the Effector Region, and other studies with the Insert Loop. It is therefore conceivable that there are spatial demands for IQGAP's binding to Rac, perhaps specified by the distances between the Insert Loop and the Effector Region — Rac•GTP being the correct, optimal overall conformation, whereas Rac•GDP and the T35A mutant reflect a conformation to which IQGAP is unable to bind due to a change in the relative conformations of the Insert Loop and Effector Region.

Use of the T35A mutant in interaction studies between Rac1 and RhoGDI demonstrated only a small decrease in binding affinity between the two proteins. The structure of the Cdc42•RhoGDI complex (Hoffman, G., *et al.* 2000) showed that GDI associates with the Effector Region (including Threonine 35) but not the Insert Region. GDI may therefore, not require such a rigid target Rac conformation — indeed it is able to bind both GTP-bound and GDP-bound forms, inhibiting the GTPase activity and GDP dissociation activity, respectively.

IQGAP's sensitivity to correct overall Rac conformation may also explain any differences in the K_d measured by Anisotropy titrations (MantGMPPNP) and inhibition studies (GTP). If IQGAP is highly sensitive to slight conformational differences around the Effector Region, then even the analogous labelled nucleotides may have an effect. This may also be the cause of the low sensitivity for the Coumarin labelled nucleotide used in an attempt to measure changes in fluorescent intensity on IQGAP/Rac association.

Chapter 6

Summary

6. Summary

This Thesis has described an examination of three separate aspects of the small G-protein, Rac1.

In *Chapter 3*, Rac's intrinsic GTP hydrolysis rate was studied. Previous reports had suggested that the intrinsic rates of several Rho subfamily proteins, including Rac1, exhibited particularly high rates due to a self-stimulatory factor in the C-terminal tail. This suggested determinant was an Arginine residue, and its presence appeared to allow homodimerisation of Rac molecules in similar nucleotide bound states, which conferred the self-stimulatory activity onto proteins, such as Rac1. Experiments described in this thesis could not find any evidence of self-stimulatory activity. Truncated and full length forms of Rac1 were used complexed to GTP or GMPPNP (a GTP analogue) as well as peptides mimicking the C-terminal tails., but at no time was a stimulated GTPase rate observed of the same magnitude as that found in previous studies.

Chapter 4 relates a study of the role of Mg^{2+} in nucleotide exchange with Rac1. This was studied using two fluorophores, the well characterised Mant and the novel MBC. MBC was shown to have potential in the study of small G-proteins, since it was shown to be sensitive to the state of nucleotide bound (GDP or GMPPNP/GTP) and the presence or absence of Mg^{2+}. Both release and binding experiments were performed on both GDP and GMPPNP nucleotides, and these experiments showed that the process of nucleotide release involved at least two main steps involving: 1. Mg^{2+} release/binding; 2. Nucleotide release/binding.

The kinetics of these steps could be monitored separately by the MBC fluorophore, and thus allowed the construction of a simple model of the process. This simple model for Mg^{2+} and nucleotide release was tested by using fluorescent anisotropy to monitor the involvement of the nucleotide alone, and the substitution of Mg^{2+} with Mn^{2+} to confirm the role of the metal ion. These further confirmed that the simple model was valid, although there were some discrepancies with the anisotropy data, the reasons for which are not completely clear. Structural determination of the MBC fluorophore bound to Rac may help to explain some of these differences.

Observed changes in MBC fluorescence during the process of Mg^{2+} binding showed that for Rac•GDP, the Mg^{2+} step could be further separated into two steps: the rapid binding of Mg^{2+} followed by some form of conformational change. Similar experiments with Rac•GMPPNP showed that this process could also be separated into two representing rapid Mg^{2+} binding, and a conformational change. The MBC fluorophore allowed the kinetics of the steps in Mg^{2+} binding to be measured, and therefore allowed calculation of the overall equilibrium constants for the Mg^{2+} exchange for both Rac•GDP and Rac•GMPPNP nucleotides. Mg^{2+} was shown to bind approximately 1000-fold more tightly to GMPPNP nucleotides than to GDP nucleotides. This does make sense with respect to the mechanism of GEF-mediated nucleotide exchange, where in the presence of GDP, Mg^{2+} does not obstruct GDP release, whereas in the presence of GMPPNP (GTP) nucleotides, Mg^{2+} release is slowed which prevents the GMPPNP nucleotide release. The increased affinity of Mg^{2+} for the GMPPNP of Rac (and vice versa) is probably due to some conformational change caused

by the coincident binding of the Mg^{2+} and nucleotide.

The study of the association of Rac with a C-terminal fragment of IQGAP was studied in *Chapter 5*. Preparation of usable IQGAP required a large amount of time-consuming genetic manipulation. The gene was moved into a pGEX 2T vector, allowing IQGAP's purification via Thrombin cleavage, although this also required modification of the construct to correct a reading frame shift. The IQGAP fragment was shown to inhibit Rac's GTPase activity quite effectively, and from these experiments, a limit of the K_d for the interaction could be calculated, 50 nM, suggesting the association was tight.

The next step was to attempt to measure the interaction between the two proteins directly by fluorescence. Use of fluorescently labelled GTP analogues, such as MantGMPPNP, showed a small change in fluorescence on interaction, but the change was not sufficiently large to allow a reasonable K_d estimation. Labelling of IQGAP with Coumarins was successful, although they showed no change in fluorescence on interaction with IQGAP. It was the use of fluorescent anisotropy of the MantGMPPNP which provided a direct measure of the K_d. This method showed that the association was tight (0.3 μM). IQGAP was unable to bind to Rac•GDP. Anisotropy also allowed functional investigation into the interaction of Rac with IQGAP via a panel of Rac mutants.

The interaction was affected by mutations in the Effector Region of Rac, suggesting that IQGAP associates through the Effector Region. The use of the T35A

mutant, which is thought to show aberrant Mg^{2+} coordination, showed no IQGAP binding. This suggested that IQGAP may have rigid structural requirements for distances between the Insert Loop and Effector Region. A change, such as that found with Rac•GDP causes loss of binding. This indicated that the loss of Mg^{2+} coordination in T35A may cause a drastic change in Effector Region conformation and thus prevent IQGAP association.

This result provides support for the important role of Mg^{2+} found in Chapter 4. Not only is Mg^{2+} important in maintaining a correct small G-protein activation inactivation cycle by regulating exchange and hydrolysis, but it also appears to be important in maintaining correct small G-protein structure, allowing sensitivity to a number of different effector proteins.

Acknowledgements

I would like to thank my laboratory: Dr. Martin Webb for his insightful and persistent supervision and guidance; Martin Brune for many hours of entertainment and his expertise in Molecular Biology; Colin Davis for his tales of Ralph McTell and assorted folk musicians; and Jackie Hunter for priceless general assistance everyday throughout my PhD. I would also like to thank the players of NIMROD F.C. who have survived my goalkeeping over the past three years.

This Thesis was written to the music of: George Russell '*Electronic Sonata for Souls Loved by Nature*' & '*Jazz in the Space Age*'. John Cage '*Piano Concertos*'. Bikini Kill '*Singles Collection*'. Bob Dylan '*Blood on the Tracks*', '*Blonde on Blonde*', '*The Freewheelin' Bob Dylan*', '*The Basement Tapes*' and '*The Bootleg Series*'. Elvis Presley '*Millenium Collection*'. Bang Bang '*Je t'Aime*'. Stanford Prison Experiment '*Stanford Prison Experiment*'. Fleetwood Mac '*Rumours*'. The Cardigans '*Gran Turismo*'. Stereolab '*Aluminium Tunes*'. Axelle Red '*Toujours Moi*'. Sarah Dougher '*Day One*' and '*The Walls Ablaze*'. The Orb '*Live 93*'. The Aislers Set '*The Last Match*' and '*The Aislers Set*'. Sleater Kinney '*The Hot Rock*', '*All Hands on the Bad One*' and '*Call the Doctor*'. Laptop '*Opening Credits*'. Geno Washington '*60 Minutes Live*'. James Taylor '*Walking Man*'. Neil Young '*Harvest*', '*After the Gold Rush*', '*Mirrorball*' and '*Harvest Moon*'..... to name but a few.

References

Abo, A. *et al.* (1998) PAK4, a novel effector for Cdc42Hs, is implicated in the reorganisation of the actin cytoskeleton and in the formation of filipodia. *EMBO J.* **17**, 6527-6540.

Adachi, H. *et al.* (1997) Dictyostelium IQGAP-related Protein Specifically Involved in the Completion of Cytokinesis. *J. Cell Biol.* **137**, 891-898.

Adamson, P., Marshall, C., Hall, A., Tilbrook, P. (1992) Post-translational Modifications of p21rho Proteins. *J. Biol. Chem.* **267**, 20033-20038.

Aghazadeh, B. *et al.* (1998) Structure and Mutagenesis of the Dbl Homology Domain. *Nat. Struct. Biol.* **5**, 1098-1107.

Allen, W., Jones, G., Pollard, J., Ridley, A. (1997) Rho, Rac and Cdc42 regulate actin organisation and cell adhesion in macrophages. *J. Cell Sci.* **110**, 707-720.

Apolloni, A. *et al.* (2000) H-ras but Not K-ras Traffics through the Exocytic Pathway. *Mol. Cell. Biol.* **20**, 2475-2487.

Ayme-Southgate, A., Lasko, P., French, C., Pardue, M. (1989) Characterisation of the gene for mp20: a Drosophila muscle protein that is not found in asynchronous oscillatory flight muscle. *J. Biol. Chem.* **108**, 521-531.

Barrett, T. *et al.* (1997) The structure of the GTPase-activating domain from p50rhoGAP. *Nature* **385**, 458-460.

Bashour, A.-M., Fullerton, A., Hart, M., Bloom, G. (1997) IQGAP1, a Rac- and Cdc42-binding Protein, Directly Binds and Cross-links Microfilaments. *J. Cell Biol.* **137**, 1555-1566.

Buchsbaum, R., Telliez, J.-B., Goonesekera, S., Feig, L. (1996) The N-terminal Pleckstrin, Coiled-Coil, and IQ Domains of the Exchange Factor Ras-GRF Act Cooperatively to Facilitate Activation by Calcium. *Mol. Cell. Biol.* **16**, 4888-4896.

Baudier, J. *et al.* (1991) Purification and characterization of a brain-specific protein kinase C substrate, neurogranin (p17). *J. Biol. Chem.* **266**, 229-237.

Berghuis, A. *et al.* (1996) Structure of the GDP-P_i complex of Gly203-> Ala $G_{i\alpha1}$: a mimc of the ternary product complex of G_α-catalyzed GTP hydrolysis. *Structure* **4**, 1277-1290.

Bourne, H., Sanders, D., McCormick, F. (1991) The GTPase superfamily: conserved structure

and molecular mechanism. *Nature* **349**, 117-127.

Brill, S. *et al.* (2000) The Ras GTPase-Activating-Protein-Related Human Protein IQGAP2 Harbours a Potential Actin Binding Domain and Interacts with Calmodulin and Rho Family GTPases. *Mol. Cell. Biol.* **16**, 4869-4878.

Brownbridge, G. *et al.* (1993) Interaction of GTPase Activating Proteins (GAPs) with p21Ras Measured by a Novel Fluorescence Anisotropy Method. *J. Biol. Chem.* **268**, 10914-10919.

Brune, M., Hunter, J., Corrie, J., Webb, M. (1994) Direct, Real-Time Measurement of Rapid Inorganic Phosphate Release Using a Novel Fluorescent Probe and It's Application to Actomyosin Subfragment 1 ATPase. *Biochem.* **33**, 8262-8271.

Cepus, V., Scheidig, A. J., Goody, R., Gerwert, K. (1998) Time-resolved FTIR Studies of the GTPase Reaction of H-Ras p21 Reveal a Key Role for the β-Phosphate. *Biochem.* **37**, 10263-10271.

Chapman, E. R. *et al.* (1991) Characterisation of the calmodulin binding domain of neuromodulin. Functional significance of serine 41 and phenylalanine 42. *J. Biol. Chem.* **266**, 207-213.

Cheney, R. E., Mooseker, M. S. (1992) Unconventional myosins. *Curr. Opin. cell Biol.* **4**, 27-35.

Corbalan-Garcia, S. *et al.* (1998) Regulation of Sos Activity by Intramolecular Interactions. *Mol. Cell. Biol.* **18**, 880-886.

Corrie, J., Munasinghe, R., Rettig, W. (2000) Synthesis and fluorescence properties of substituted 7-aminocoumarin-3-carboxylate derivatives. *J. Hetero. Chem.*, In Press.

Der, C., Finkel, T., Cooper, G. (1986) Biological and Biochemical Properties of Human rasH genes Mutated at Codon 61. *Cell* **44**, 167-176.

Diaz, J. F., Wroblowski, B., Schlitter, J., Engelborghs, Y. (1997) Calculation of Pathways for the Conformational Transition Between the GTP- and GDP- Bound States of the Ha-ras-p21 Protein: Calculations With Explicit Solvent Simulations and Comparison with Calculations in Vacuum. *Prot. Str. Fun. Genet.* **28**, 434-451.

Du, X., Frei, H., Kim, S.-H. (2000) The Mechanism of GTP Hydrolysis by Ras Probed by Fourier Transform Infrared Spectroscopy. *J. Biol. Chem.* **275**, 8492-8500.

Ermekova, K. *et al.* (1997) The WW Domain of Neural Protein FE65 Interacts with Proline-rich

Motifs in Mena, the Mammalian Homolog of Drosophila Enabled. *J. Biol. Chem.* **272**, 32869-32877.

Erickson, J., Cerione, R., Hart, M. (1997) Identification of an Actin Cytoskeletal Complex That Includes IQGAP and the Cdc42 GTPase. *J. Biol. Chem.* **272**, 24443-24447.

Farnsworth, C. *et al.* (1995) Calcium activation of Ras mediated by the neuronal exchange factor Ras-GRF. *Nature* **376**, 524-527.

Faix, J. *et al.* (1998) The IQGAP-related protein DGAP1 interacts with Rac and is involved in the modulation of the F-actin cytoskeleton and control of cell motility. *J. Cell Sci.* **111**, 3059-3071.

Feuerstein, J., Goody, R., Webb, M. (1989) The Mechanism of Guanosine Nucleotide Hydrolysis by p21 c-Ha-ras. *J. Biol. Chem.* **264**, 6188-6190.

Freeman, J., Abo, A., Lambeth, D. (1996) Rac "Insert Region" Is a Novel Effector Region That Is Implicated in the Activation of NADPH Oxidase, but Not PAK65. *J. Biol. Chem.* **271**, 19794-19801.

Fritz, G., Kaina, B., Aktories, K. (1995) The Ras-related Small GTP-binding Protein RhoB Is Immediate-early Inducible by DNA Damaging Treatments. *J. Biol. Chem.* **270**, 25172-25177.

Fukata, M. *et al.* (1999) Cdc42 and Rac1 regulate the Interaction of IQGAP1 with β-catenin. *J. Biol. Chem.* **274**, 26044-26050.

Gerald, N., Dai, J., Ting-Beall, P., De Lozanne, A. (1998) A role for Dictyostelium RacE in Cortical Tension and Cleavage Furrow Progression. *J. Cell Biol.* **141**, 483-492.

Goetinck, S. and Waterston, R. (1994) The Caenorhabditis elegans muscle-affecting gene unc-87 encodes a novel thin filament-associated protein. *J. Biol. Chem.* **127**, 79-93.

Goldberg, J. (1999) Structural and Functional Analysis of the ARF1-ARFGAP Complex Reveals a Role for Coatomer in GTP hydrolysis. *Cell* **96**, 893-902.

Gulbins, E. *et al.* (1996) Fas-induced Apoptosis Is Mediated by Activation of a Ras and Rac Protein-regulated Signaling Pathway. *J. Biol. Chem.* **271**, 26389-26394.

Haataja, L., Groffen, J., Heisterkamp, N. (1997) Characterisation of Rac3 a Novel Member of the Rho Family. *J. Biol. Chem.* **272**, 20384-20388.

Hart, M., Callow, M., Souza, B., Polakis, P. (1996) IQGAP1, a calmodulin-binding protein with a rasGAP-related domain, is a potential effector for cdc42Hs. *EMBO J.* **15**, 2997-3005.

Heyworth, P. *et al.* (1993) Regulation of NADPH Oxidase Activity by Rac GTPase Activating Protein(s). *Mol. Biol. Cell* **4**, 1217-1223.

Hirshberg, M., Stockley, R., Dodson, G., Webb, M. (1997) The crystal structure of human rac1, a member of the rho-family complexed with a GTP analogue. *Nat. Struct. Biol.* **4**, 147-152.

Ho, Y.-D., Joyal, J., Li, Z., Sacks, D. (1999) IQGAP1 Integrates Ca^{2+}/Calmodulin and Cdc42 Signaling. *J. Biol. Chem.* **274**, 464-470.

Hoffman, G., Nassar, N., Cerione, R. (2000) Structure of the Rho Family GTP-Binding Protein Cdc42 in Complex with the Multifunctional Regulator RhoGDI. *Cell* **100**, 345-356.

Houdusse, A. and Cohen, C. (1995) Target sequence recognition by the Calmodulin superfamily: Implications from light chain binding to the regulatory domain of scallop myosin. *Proc. Natl. Acad. Sci.* **92**, 10644-10647.

Hunter, T. and Jähner, D. (1991) The ras-related Gene rhoB is an Immediate-Early Gene Inducible by v-Fps, Epidermal Growth Factor, and Platelet-Derived Growth Factor in Rat Fibroblasts. *Mol. Cell. Biol.* **11**, 3682-3690.

Ihara, K. *et al.* (1998) Crystal Structure of Human RhoA in a Dominantly Active Form Complexed with a GTP Analogue. *J. Biol. Chem.* **273**, 9656-9666.

Ivell, R., Sander, G., Parmeggiani, A. (1981) Modulation by monovalent and divalent cations of the guanosine-5'-triphosphatase activity dependent on elongation factor Tu. *Biochem.* **20**, 6852-6859.

Jin Wu, W., Leonard, D., Cerione, R., Manor, D. (1997) Interaction between Cdc42Hs and RhoGDI is mediated through the Rho Insert Region. *J. Biol. Chem.* **272**, 26153-26158.

John, J. *et al.* (1990) Kinetics of Interaction of Nucleotides with Nucleotide-Free H-ras p21. *Biochem.* **29**, 6058-6065.

John, J. *et al.* (1993) Kinetic and Structural Analysis of the Mg^{2+}-binding Site of the Guanine Nucleotide-binding Protein p21H-ras. *J. Biol. Chem.* **268**, 923-929.

Joyal, J. *et al.* (1997) Calmodulin Modulates the Interaction between IQGAP1 and Cdc42. *J. Biol. Chem.* **272**, 15419-15425.

Kay, B., Williamson, M., Sudol, M. (2000) The importance of being proline: the interaction of proline-rich motifs in signaling proteins with their cognate domains. *FASEB J.* **14**, 231-241.

Khosravi-Far, R. *et al.* (1995) Activation of Rac1, RhoA and Mitogen-Activated Protein Kinase is Required for Ras Transformation. *Mol. Cell. Biol.* **15**, 6443-6453.

Kraulis, P. *et al.* (1994) Solution structure and dynamics of ras p21.GDP determined by heteronuclear three- and four-dimensional NMR spectroscopy. *Biochem.* **33**, 3515-3531.

Krengel, U. *et al.* (1990) Three-Dimensional Structures of H-ras p21 Mutants: Molecular Basis for their Inability to Function as Signal Switch Molecules. *Cell* **62**, 539-548.

Kuroda, S. *et al.* (1996) Identification of IQGAP as a Putative Target for the Small GTPases Cdc42 and Rac1. *J. Biol. Chem.* **271**, 23363-23367.

Kuroda, S. *et al.* (1998) Role of IQGAP1, a Target of the Small GTPases Cdc42 and Rac1, in Regulation of E-cadherin-Mediated Cell-Cell Adhesion. *Science* **281**, 832-835.

La Cour, T., Nyborg, J., Thirup, S., Clark, B. (1985) Structural details of the binding of guanosine diphosphate to elongation factor Tu from E.coli as studied by X-Ray crystallography. *EMBO J.* **4**, 2385-2388.

Lebowitz, P., Davide, J., Prendergast, G. (1995) Evidence that Farnesyltransferase Inhibitors Suppress Ras Transformation by Interfering with Rho Activity. *Mol. Cell. Biol.* **15**, 6613-6622.

Lee, S., Escalante, R., Firtel, R. (1998) A Ras GAP is essential for cytokinesis and spatial patterning in Dictyostelium. *Develop.* **124**, 983-996.

Leonard, D., Lin, R., Cerione, R., Manor, D. (1998) Biochemical Studies of the Mechanism of Action of the Cdc42-GTPase-activating Protein. *J. Biol. Chem.* **273**, 16210-16215.

Leung, T., Manser, E., Tan, L., Lim, L. (1995) A Novel Serine/Threonine Kinase Binding the Ras-related RhoA GTPase Which Translocates the Kinase to Peripheral Membranes. *J. Biol. Chem.* **270**, 29051-29054.

Leupold, C., Goody, R., Wittinghofer, A. (1983) Stereochemistry of the elongation factor Tu-GTP complex. *Eur. J. Biochem.* **135**, 237-241.

Longenecker, K. *et al.* (1999) How RhoGDI binds Rho. *Acta Crysta.* **55**, 1503-1515.

Li, S. *et al.* (2000) Gastric Hyperplasia in Mice Lacking the Putative Cdc42 Effector IQGAP1. *Mol. Cell. Biol.* **20**, 697-701.

Liu, X. *et al.* (1998) NMR Structure and Mutagenesis of the N-Terminal Dbl Homology Domain of the Nucleotide Exchange Facto Trio. *Cell* **95**, 269-277.

Macias, M. *et al.* (1996) Structure of the WW Domain of a kinase-associated protein complexed with a proline-rich peptide. *Nature* **382**, 646-649.

McCallum, S., Jin Wu, W., Cerione, R. (1996) Identification of a Putative Effector for Cdc42Hs with High Sequence Similarity to the RasGAP-related Protein IQGAP1 and a Cdc42Hs Binding Partner with Similarity to IQGAP2. *J. Biol. Chem.* **271**, 21732-21737.

Ménard, L. and Snyderman, R. (1993) Role of Phosphate-Magnesium-Binding regions in the High GTPase Activity if Rac1 Protein. *Biochem.* **32**, 13357-13361.

Milburn, M. *et al.* (1990) Molecular Switch for Signal Transduction: Structural Differences Between Active and Inactive Forms of the Protooncogenic ras Proteins. *Science* **247**, 939-945.

Mittal, R., Reza Ahmadian, M., Goody, R., Wittinghofer, A. (1996) Formation of a Tranistion State Analog of the Ras GTPase Reaction by Ras•GDP, Tetrafluoroaluminate, and GTPase-Activating Proteins. *Science* **273**, 115-117.

Mullins, D. (2000) How WASP-family proteins and the ARP2/3 complex convert intracellular signals into cytoskeletal structures. *Curr. Op. Cell Biol.* **12**, 91-96.

Munshi, H. *et al.* (1996) Ca^{2+} regulates calmodulin binding to IQ motifs in IRS-1. *Biochem.* **35**, 15883-15889.

Murayama, T. and Ui, M. (1984) [3H]GDP release from rat and hamster adipocyte membranes independently linked to receptors invovled in activation or inhibition of adenylate cyclase. Differential susceptibility to two bacterial toxins. *J. Biol. Chem.* **259**, 761-769.

Neal, S., Eccleston, J., Hall, A., Webb, M. (1988) Kinetic analysis of the hydrolysis of GTP by p21N-ras. The basal GTPase mechanism. *J. Biol. Chem.* **263**, 19718-19722.

Nimnual, A., Yatsula, B., Bar-Sagi, D. (1998) Coupling of Ras and Rac Guanosine Triphosphatatses Through the Ras Exchanger Sos. *Science* **279**, 560-563.

Nobes, C. and Hall, A. (1995) Rho, Rac and Cdc42 GTPases Regulate the Assembly of Multimolecular Focal Complexes Associated with Actin Stress Fibres, Lamellipodia, and

Filopodia. *Cell* **81**, 53-62.

Nomanbhoy, T. and Cerione, R. (1999) Fluorescence Assays of Cdc42 Interaction with Target/Effector Proteins. *Biochem.* **38**, 15878-15884.

Pai, E. *et al.* (1989) Structure of the guanine-nucleotide binding domain of the Ha-ras oncogene product p21 in the triphospahte conformation. *Nature* **341**, 209-214.

Pan, J. and Wessling-Resnick, M. (1998) GEF-mediated GDP/GTP exchange by monomeric GTPases: a regulatory role for Mg^{2+}? *BioEssays* **20**, 516-521.

Pan, J., Sanford, J., Wessling-Resnick, M. (1996) Influence of Mg^{2+} on the Structure and Function of Rab5. *J. Biol. Chem.* **271**, 1322-1328.

Poe, M., Scolnick, E. M., Stein, R. B. (1985) Viral Harvey ras p21 expressed in Escherichia coli purifies as a binary one-to-one complex with GDP. *J. Biol. Chem.* **260**, 3906-3909.

Pokutta, S. and Weis, W. (2000) Structure of the Dimerization and β-Catenin-Binding Region of α-Catenin. *Mol Cell* **5**, 533-543.

Prendergast, G. (2000) Farnesyltransferase inhibitors: antineoplastic mechanism and clinical prospects. *Curr. Op. Cell Biol.* **12**, 166-173.

Privé, G. *et al.* (1992) X-ray crystal structures of transforming p21 ras mutants suggest a transition-state stabilisation mechanism for GTP hydrolysis. *Proc. Natl. Acad. Sci.* **89**, 3649-3653.

Qiu, R.-G. *et al.* (1995) An essential role for Rac in Ras transformation. *Nature* **374**, 457-459.

Ridley, A. *et al.* (1992) The Small GTP-binding Protein rac regulates Growth Factor-Induced Membrane Ruffling. *Cell* **70**, 401-410.

Ridley, A. and Hall, A. (1992) The Small GTP-binding Protein Rho regulates the Assembly of Focal Adhesions and Actin Stress Fibers in Response to Growth Factors. *Cell* **70**, 389-399.

Ridley, A. (1995) Rac and Bcr regulate phagocytic phoxes. *Curr. Biol.* **5**, 710-712.
Scheffzek, K. *et al.* (1996) Crystal structure of GTPase-activating domain of human p120GAP and implications for the interaction with Rac. *Nature* **384**, 591-596.

Rittinger, K. *et al.* (1997) Crystal Structure of a G Protein Complex with the GTPase-activating protein rhoGAP. *Nature* **388**, 693-697.

Rhoads, A. and Friedberg, F. (1997) Sequence motifs for calmodulin recognition. *FASEB J.* **11**, 331-340.

Scheffzek, K. *et al.* (1997) The Ras-RasGAP Complex: Structural Basis for GTPase Activation and It's Loss in Oncogenic Ras Mutants. *Science* **277**, 333-338.

Scheffzek, K. *et al.* (2000) The rac-rhoGDI complex and the structural basis for the regulation of rho proteins by rhogdi. *Nat. Struct. Biol.* **7**, 122-126.

Scheidig, A. J., Burmester, C., Goody, R. (1999) The pre-hydrolysis state of p21 ras in complex with GTP: new insights into the role of water molecules in the GTP hydrolysis reaction of ras-like proteins. *Structure* **7**, 1311-1324.

Schweins, T., Scheffzek, K., Aßheuer, R., Wittinghofer, A. (1997) The Role of the Metal Ion in the p21ras Catalysed GTP-hydrolysis: Mn^{2+} versus Mg^{2+}. *J. Mol. Biol.* **266**, 847-856.

Self, A. and Hall, A. (1986) The Effect of Mg^{2+} on the Guanine Nucleotide Exchange Rate of p21 N-Ras. *J. Biol. Chem.* **261**, 10963-10965.

Shimizu, T. *et al.* (2000) An open conformation of Switch I revealed by the crystal structure of a Mg^{2+}-free form of RhoA complexed with GDP: Implications for the GDP/GTP exchange mechanism. *J. Biol. Chem.* **275**, 18311-18317.

Simon, I., Zerial, M., Goody, R. (1996) Kinetics of Interaction of Rab5 and Rab7 with Nucleotides and Magnesium Ions. *J. Biol. Chem.* **271**, 20470-20478.

Soisson, S. *et al.* (1998) Crystal Structure of the Dbl and Pleckstrin Homology Domains from the Human Son of Sevenless Protein. *Cell* **95**, 259-268.

Symons, M. (1996) Rho family GTPases: the cytoskeleton and beyond. *T.I.B.S.* **21**, 178-181.

Takaishi, K. *et al.* (1997) Regulation of Cell-Cell Adhesion by Rac and Rho Small G Prtoeins in MDCK Cells. *J. Cell Biol.* **139**, 1047-1059.

Tong, L., Milburn, M., de Vos, A., Kim, S.-H. (1989) Structure of Ras Protein. *Science* **245**, 244-244.

Tong, L., de Vos, A., Milburn, M., Kim, S.-H. (1991) Crystal Structures at 2.2Å Resolution of the Catalytic Domains of Normal ras Protein and an Oncogenic Mutant Complexed with GDP. *J. Mol. Biol.* **217**, 503-516.

de Vos, A. *et al.* (1988) Three-Dimensional Structure of an Oncogene Protein: Catalytic Domain of Human c-H-ras p21. *Science* **239**, 888-893.

Wang, J. H. *et al.* (1998) Raman Difference Studies of GDP and GTP Binding to c-Harvey ras. *Biochem.* **37**, 11106-11116.

Webb, M. and Hunter, J. (1992) Interaction of GTPase-activating protein with p21ras, measured using a continuous assay for inorganic phosphate release. *Biochem. J.* **287**, 555-559.

Webb, M. (1992) A continuous spectrophotometric assay for inorganic phosphate and for measuring phosphate release kinetics in biological systems. *Proc. Natl. Acad. Sci.* **89**, 4884-4887.

Weissbach, L. *et al.* (1994) Identification of a Human RasGAP-related Protein Containing Calmodulin-binding Motifs. *J. Biol. Chem.* **269**, 20517-20521.

Weissbach, L., Bernards, A., Herion, D. (1998) Binding of Myosin Essential Light Chain Kinase to the Cytoskeleton-Associated Protein IQGAP 1. *Biochem. Biophys. Res. Comm.* **251**, 269-276.

Wójciak-Stothard, B., Entwhistle, A., Garg, R., Ridley, A. (1998) Regulation of TNF-α-Induced Reorganisation of the Actin Cytoskeleton and Cell-Cell Junctions by Rho, Rac, and Cdc42 in Human Endothelial Cells. *J. Cell. Physiol.* **176**, 150-165.

Zhang, B., Wang, Z.-X., Zheng, Y. (1997) Characterisation of the Interactions between the Small GTPase Cdc42 and Its GTPase-activating Proteins and Putative Effectors. *J. Biol. Chem.* **272**, 21999-22007.

Zhang, B., Chernoff, J., Zheng, Y. (1998) Interaction of Rac1 with GTPase-activating Proteins and Putative Effectors. *J. Biol. Chem.* **273**, 8776-8782.

Zhang, B. and Zheng, Y. (1998) Negative Regulation of Rho Family GTPases Cdc42 and Rac2 by Homodimer Formation. *J. Biol. Chem.* **273**, 25728-25733.

Zhang, B. and Zheng, Y. (1998a) Regulation of RhoA GTP Hydrolysis by the GTPase-Activating Protein p190, p50RhoGAP, Bcr and 3BP-1. *Biochem.* **37**, 5249-5257.

Zhang, B. *et al.* (1999) A Built in Arginine Finger Triggers the Self-Stimulatory GTPase-activating Activity of Rho Family GTPases. *J. Biol. Chem.* **274**, 2609-2612.

Zhang, B., Zhang, Y., Wang, Z.-X., Zheng, Y. (2000) The role of Mg^{2+} cofactor in the guanine nucloetide exchange and GTP-hydrolysis reactions of Rho family GTP binding proteins. *J. Biol. Chem.* **275**, 25299-25307.

Zheng, Y. *et al.* (1995) Direct involvement of the Small GTP-binding Protein Rho in lbc Oncogene Function. *J. Biol. Chem.* **270**, 9031-9034.

Appendix 1 - DNA Sequence of the pGIT2 Plasmid Containing C-terminal IQGAP

```
1/1                                         31/11                                       61/21                                       91/31
ATG TCC CCT ATA CTA GGT TAT TGG AAA ATT AAG GGC CTT GTG CAA CCC ACT CGA CTT CTT TTG GAA TAT CTT GAA GAA AAA TAT GAA GAG CAT TTG TAT GAG CGC GAT GAA GGT GAT AAA
Met ser pro ile leu gly tyr trp lys ile lys gly leu val gln pro thr arg leu leu leu glu tyr leu glu glu lys tyr glu glu his leu tyr glu arg asp glu gly asp lys
121/41                                      151/51                                      181/61                                      211/71
TGG CGA AAC AAA AAG TTT GAA TTG GGT TTG GAG TTT CCC AAT CTT CCT TAT TAT ATT GAT GGT GAT GTT AAA TTA ACA CAG TCT ATG GCC ATC ATA CGT TAT ATA GCT GAC AAG CAC AAC
trp arg asn lys lys phe glu leu gly leu glu phe pro asn leu pro tyr tyr ile asp gly asp val lys leu thr gln ser met ala ile ile arg tyr ile ala asp lys his asn
241/81                                      271/91                                      301/101                                     331/111
ATG TTG GGT GGT TGT CCA AAA GAG CGT GCA GAG ATT TCA ATG CTT GAA GGA GCG GTT TTG GAT ATT AGA TAC GGT GTT TCG AGA ATT GCA TAT AGT AAA GAC TTT GAA ACT CTC AAA GTT
met leu gly gly cys pro lys glu arg ala glu ile ser met leu glu gly ala val leu asp ile arg tyr gly val ser arg ile ala tyr ser lys asp phe glu thr leu lys val
361/121                                     391/131                                     421/141                                     451/151
GAT TTT CTT AGC AAG CTA CCT GAA ATG CTG AAA ATG TTC GAA GAT CGT TTA TGT CAT AAA ACA TAT TTA AAT GGT GAT CAT GTA ACC CAT CCT GAC TTC ATG TTG TAT GAC GCT CTT GAT
asp phe leu ser lys leu pro glu met leu lys met phe glu asp arg leu cys his lys thr tyr leu asn gly asp his val thr his pro asp phe met leu tyr asp ala leu asp
481/161                                     511/171                                     541/181                                     571/191
GTT GTT TTA TAC ATG GAC CCA ATG TGC CTG GAT GCG TTC CCA AAA TTA GTT TGT TTT AAA AAA CGT ATT GAA GCT ATC CCA CAA ATT GAT AAG TAC TTG AAA TCC AGC AAG TAT ATA GCA
val val leu tyr met asp pro met cys leu asp ala phe pro lys leu val cys phe lys lys arg ile glu ala ile pro gln ile asp lys tyr leu lys ser ser lys tyr ile ala
601/201                                     631/211                                     661/221                                     691/231
TGG CCT TTG CAG GGC TGG CAA GCC ACG TTT GGT GGT GGC GAC CAT CCT CCA AAA TCG GAT CTG GTT CCG CGT GGA TCC CCT CCT ATG GTT GTG GTC CGA AAA TTT GTC CAC CTG CTG GAC
trp pro leu gln gly trp gln ala thr phe gly gly gly asp his pro pro lys ser asp leu val pro arg gly ser pro pro met val val val arg lys phe val his leu leu asp
721/241                                     751/251                                     781/261                                     811/271
CAA AGT GAC CAG GAT TTT CAG GAG GAG CTT GAC CTT ATG AAG ATG CGG GAA GAG GTT ATC ACC CTC ATT CGT TCT AAC CAG CAG CTG GAG AAT GAC CTC AAT CTC ATG GAT ATC AAA ATT
gln ser asp gln asp phe gln glu glu leu asp leu met lys met arg glu glu val ile thr leu ile arg ser asn gln gln leu glu asn asp leu asn leu met asp ile lys ile
841/281                                     871/291                                     901/301                                     931/311
GGA CTG CTA GTG AAA AAT AAG ATT ACG TTG CAG GAT GTG GTT TCC CAC AGT AAA AAA CTT ACC AAA AAA AAT AAG GAA CAG TTG TCT GAT ATG ATG ATG ATA AAT AAA CAG AAG GGA GGT
gly leu leu val lys asn lys ile thr leu gln asp val val ser his ser lys lys leu thr lys lys asn lys glu gln leu ser asp met met met ile asn lys gln lys gly gly
961/321                                     991/331                                     1021/341                                    1051/351
CTC AAG GCT TTG AGC AAG GAG AAG AGA GAG AAG TTG GAA GCT TAC CAG CAC CTG TTT TAT TTA TTG CAA ACC AAT CCC ACC TAT CTG GCC AAG CTC ATT TTT CAG ATG CCC CAG AAC AAG
leu lys ala leu ser lys glu lys arg glu lys leu glu ala tyr gln his leu phe tyr leu leu gln thr asn pro thr tyr leu ala lys leu ile phe gln met pro gln asn lys
1081/361                                    1111/371                                    1141/381                                    1171/391
TCC ACC AAG TTC ATG GAC TCT GTA ATC TTC ACA CTC TAC AAC TAC GCG TCC AAC CAG CGA GAG GAG TAC CTG CTC CTG CGG CTC TTT AAG ACA GCA CTC CAA GAG GAA ATC AAG TCG AAG
ser thr lys phe met asp ser val ile phe thr leu tyr asn tyr ala ser asn gln arg glu glu tyr leu leu leu arg leu phe lys thr ala leu gln glu glu ile lys ser lys
1201/401                                    1231/411                                    1261/421                                    1291/431
GTA GAT CAG ATT CAA GAG ATT GTG ACA GGA AAT CCT ACG GTT ATT AAA ATG GTT GTA AGT TTC AAC CGT GGT GCC CGT GGC CAG AAT GCC CTG AGA CAG ATC TTG GCC CCA GTC GTG AAG
val asp gln ile gln glu ile val thr gly asn pro thr val ile lys met val val ser phe asn arg gly ala arg gly gln asn ala leu arg gln ile leu ala pro val val lys
1321/441                                    1351/451                                    1381/461                                    1411/471
GAA ATT ATG GAT GAC AAA TCT CTC AAC ATC AAA ACT GAC CCT GTG GAT ATT TAC AAA TCT TGG GTT AAT CAG ATG GAG TCT CAG ACA GGA GAG GCA AGC AAA CTG CCC TAT GAT GTG ACC
glu ile met asp asp lys ser leu asn ile lys thr asp pro val asp ile tyr lys ser trp val asn gln met glu ser gln thr gly glu ala ser lys leu pro tyr asp val thr
1441/481                                    1471/491                                    1501/501                                    1531/511
CCT GAG CAG GCG CTA GCT CAT GAA GAA GTG AAG ACA CGG CTA GAC AGC TCC ATC AGG AAC ATG CGG GCT GTG ACA GAC AAG TTT CTC TCA GCC ATT GTC AGC TCT GTG GAC AAA ATC CCT
pro glu gln ala leu ala his glu glu val lys thr arg leu asp ser ser ile arg asn met arg ala val thr asp lys phe leu ser ala ile val ser ser val asp lys ile pro
1561/521                                    1591/531                                    1621/541                                    1651/551
TAT GGG ATG CGC TTC ATT GCC AAA GTG CTG AAG GAC TCG TTG CAT GAG AAG TTC CCT GAT GCT GGT GAG GAT GAG CTG CTG AAG ATT ATT GGT AAC TTG CTT TAT TAT CGA TAC ATG AAT
tyr gly met arg phe ile ala lys val leu lys asp ser leu his glu lys phe pro asp ala gly glu asp glu leu leu lys ile ile gly asn leu leu tyr tyr arg tyr met asn
1681/561                                    1711/571                                    1741/581                                    1771/591
CCA GCC ATT GTT GCT CCT GAT GCC TTT GAC ATC ATT GAC CTG TCA GCA GGA GGC CAG CTT ACC ACA GAC CAA CGC CGA AAT CTG GGC TCC ATT GCA AAA ATG CTT CAG CAT GCT GCT TCC
pro ala ile val ala pro asp ala phe asp ile ile asp leu ser ala gly gly gln leu thr thr asp gln arg arg asn leu gly ser ile ala lys met leu gln his ala ala ser
1801/601                                    1831/611                                    1861/621                                    1891/631
AAT AAG ATG TTT CTG GGA GAT AAT GCC CAC TTA AGC ATC ATT AAT GAA TAT CTT TCC CAG TCC TAC CAG AAA TTC AGA CGG TTT TTC CAA ACT GCT TGT GAT GTC CCA GAG CTT CAG GAT
asn lys met phe leu gly asp asn ala his leu ser ile ile asn glu tyr leu ser gln ser tyr gln lys phe arg arg phe phe gln thr ala cys asp val pro glu leu gln asp
1921/641                                    1951/651                                    1981/661                                    2011/671
AAA TTT AAT GTG GAT GAG TAC TCT GAT TTA GTA ACC CTC ACC AAA CCA GTA ATC TAC ATT TCC ATT GGT GAA ATC ATC AAC ACC CAC ACT CTC CTG TTG GAT CAC CAG GAT GCC ATT GCT
lys phe asn val asp glu tyr ser asp leu val thr leu thr lys pro val ile tyr ile ser ile gly glu ile ile asn thr his thr leu leu leu asp his gln asp ala ile ala
2041/681                                    2071/691                                    2101/701                                    2131/711
CCG GAG CAC AAT GAT CCA ATC CAC GAA CTG CTG GAC GAC CTC GGC GAG GTG CCC ACC ATC GAG TCC CTG ATA GGG GAA AGC TCT GGC AAT TTA AAT GAC CCA AAT AAG GAG GCA CTG GCT
pro glu his asn asp pro ile his glu leu leu asp asp leu gly glu val pro thr ile glu ser leu ile gly glu ser ser gly asn leu asn asp pro asn lys glu ala leu ala
2161/721                                    2191/731                                    2221/741                                    2251/751
AAG ACG GAA GTG TCT CTC ACC CTG ACC AAC AAG TTC GAC GTG CCT GGA GAT GAG AAT GCA GAA ATG GAT GCT CGA ACC ATC TTA CTG AAT ACA AAA CGT TTA ATT GTG GAT GTC ATC CGG
lys thr glu val ser leu thr leu thr asn lys phe asp val pro gly asp glu asn ala glu met asp ala arg thr ile leu leu asn thr lys arg leu ile val asp val ile arg
2281/761                                    2311/771                                    2341/781                                    2371/791
TTC CAG CCA GGA GAG ACC TTG ACT GAA ATC CTA GAA ACA CCA GCC ACC AGT GAA CAG GAA GCA GAA CAT CAG AGA GCC ATG CAG AGA CGT GCT ATC CGT GAT GCC AAA ACA CCT GAC AAG
phe gln pro gly glu thr leu thr glu ile leu glu thr pro ala thr ser glu gln glu ala glu his gln arg ala met gln arg arg ala ile arg asp ala lys thr pro asp lys
2401/801                                    2431/811                                    2461/821                                    2491/831
ATG AAA AAG TCA AAA TCT GTA AAG GAA GAC AGC AAC CTC ACT CTT CAA GAG AAG AAA GAG AAG ATC CAG ACA GGT TTA AAG AAG CTA ACA GAG CTT GGA ACC GTG GAC CCA AAG AAC AAA
met lys lys ser lys ser val lys glu asp ser asn leu thr leu gln glu lys lys glu lys ile gln thr gly leu lys lys leu thr glu leu gly thr val asp pro lys asn lys
2521/841                                    2551/851                                    2581/861                                    2611/871
TAC CAG GAA CTG ATC AAC GAC ATT GCC AGG GAT ATT CGG AAT CAG CGG AGG TAC CGA CAG AGG AGA AAG GCC GAA CTA GTG AAA CTG CAA CAG ACA TAC GCT GCT CTG AAC TCT AAG GCC
tyr gln glu leu ile asn asp ile ala arg asp ile arg asn gln arg arg tyr arg gln arg arg lys ala glu leu val lys leu gln gln thr tyr ala ala leu asn ser lys ala
2641/881                                    2671/891                                    2701/901                                    2731/911
ACC TTT TAT GGG GAG CAG GTG GAT TAC TAT AAA AGC TAT ATC AAA ACC TGC TTG GAT AAC TTA GCC AGC AAG GGC AAA GTC TCC AAA AAG CCT AGG GAA ATG AAA GGA AAG AAA AGC AAA
thr phe tyr gly glu gln val asp tyr tyr lys ser tyr ile lys thr cys leu asp asn leu ala ser lys gly lys val ser lys lys pro arg glu met lys gly lys lys ser lys
2761/921                                    2791/931                                    2821/941                                    2851/951
AAG ATT TCT CTG AAA TAT ACA GCA GCA AGA CTA CAT GAA AAA GGA GTT CTT CTG GAA ATT GAG GAC CTG CAA GTG AAT CAG TTT AAA AAT GTT ATA TTT GAA ATC AGT CCA ACA GAA GAA
lys ile ser leu lys tyr thr ala ala arg leu his glu lys gly val leu leu glu ile glu asp leu gln val asn gln phe lys asn val ile phe glu ile ser pro thr glu glu
2881/961                                    2911/971                                    2941/981                                    2971/991
GTT GGA GAC TTC GAA GTG AAA GCC AAA TTC ATG GGA GTT CAA ATG GAG ACT TTT ATG TTA CAT TAT CAG GAC CTG CTG CAG CTA CAG TAT GAA GGA GTT GCA GTC ATG AAA TTA TTT GAT
val gly asp phe glu val lys ala lys phe met gly val gln met glu thr phe met leu his tyr gln asp leu leu gln leu gln tyr glu gly val ala val met lys leu phe asp
3001/1001                                   3031/1011                                   3061/1021
AGA GCT AAA GTA AAT GTC AAC CTC CTG ATC TTC CTT CTC AAC AAA AAG TTC TAC GGG AAG TAA
```

Appendix 2 - Derivation of the Quadratic Fit to Estimate the K_d from Inhibitory Data

The hydrolysis of Rac•GTP, and production of P_i can be regarded as a simple 1st order reaction:

$$Rac \bullet GTP \xrightarrow{k_{hydrolysis}} Rac \bullet GDP + P_i \qquad (1)$$

Where $k_{hydrolysis}$ is the rate constant. The measurement of the rate of P_i production is equivalent to the rate of GTP hydrolysis. The observed rate, $k_{hydrolysis}$, can be determined by fitting the data recorded to a single exponential function for single turnover reactions. An estimate for the Kd of IQGAP binding to Rac•GTP can be calculated using a quadratic function derived from the following equilibrium:

$$Rac \bullet GTP + IQGAP \rightleftharpoons Rac \bullet GTP \bullet IQGAP \qquad (2)$$

$$K_d = \frac{[Rac \bullet GTP]\,[IQGAP]}{[Rac \bullet GTP \bullet IQGAP]} \qquad (3)$$

Where Rac•GTP represents free Rac•GTP (Rac_{free}), IQGAP represents free IQGAP and Rac•GTP•IQGAP represents the bound complex. Since:

$$[Rac_{free}] = [Rac_{total}] - [Rac \bullet GTP \bullet IQGAP] \qquad (4)$$

and

$$[IQGAP_{free}] = [IQGAP_{total}] - [Rac \bullet GTP \bullet IQGAP] \qquad (5)$$

The substituting [4] and [5] into [3]:

$$K_d = \frac{([Rac_{total}] - [Rac \bullet GTP \bullet IQGAP])([IQGAP_{total}] - [Rac \bullet GTP \bullet IQGAP])}{[Rac \bullet GTP \bullet IQGAP]} \quad (6)$$

Expanding [6] gives [7]:

$$\underset{a}{([Rac \bullet GTP \bullet IQGAP])^2} - \underset{b}{([IQGAP_{total}]+[Rac_{total}]+K_d)([Rac \bullet GTP \bullet IQGAP])} + \underset{c}{([Rac_{total}][IQGAP_{total}])} = 0$$

From this quadratic, [Rac•GTP•IQGAP] can be calculated using the quadratic formula:

$$\frac{-b \pm \sqrt{(b^2-4ac)}}{2a}$$

Where from (6):

$$a = 1$$

$$b = ([IQGAP_{total}]+[Rac_{total}]+K_d)$$

$$c = ([Rac_{total}][IQGAP_{total}])$$

This derivation assumes that:

i) The rate of GTP hydrolysis for the Rac•GTP•IQGAP complex is zero, otherwise the dissociation of IQGAP from the complex (after hydrolysis) will alter the amount of Rac•GTP•IQGAP present.

ii) The exchange between free and IQGAP-bound Rac is faster than the rate of GTP hydrolysis, otherwise the rate of this exchange will affect the rate of hydrolysis measured.

iii) As GTP is hydrolysed by Rac, $[Rac \bullet GTP]_{total}$ changes, although the change in $[Rac \bullet GTP]_{free}/[Rac]_{total}$ is small.

From equation (1), the unidirectional hydrolysis of Rac•GTP, the observed hydrolysis rate is:

$$\frac{([Rac \bullet GTP_{free}])(k_{hydrolysis})}{[Rac \bullet GTP_{total}]} \qquad (7)$$

Where $k_{hydrolysis}$ is equal to the rate of hydrolysis when [IQGAP] is zero — the uninhibited rate.

Experimental data can then be fitted to this curve, and an approximate K_d can be calculated.